FABRICATION AND PERFORMANCE EVALUATION OF LOW TO MEDIUM POROSITY CLOSED-CELL POROUS ALUMINUM VIA POWDER METALLURGY TECHNIQUE

NUR AYUNI BINTI JAMAL

FACULTY OF ENGINEERING
UNIVERSITY OF MALAYA
KUALA LUMPUR

2016

FABRICATION AND PERFORMANCE EVALUATION OF LOW TO MEDIUM POROSITY CLOSED-CELL POROUS ALUMINUM VIA POWDER METALLURGY TECHNIQUE

NUR AYUNI BINTI JAMAL

THESIS SUBMITTED IN FULFILMENT OF THE
REQUIREMENTS FOR THE DEGREE OF DOCTOR OF
PHILOSOPHY

FACULTY OF ENGINEERING
UNIVERSITY OF MALAYA
KUALA LUMPUR

2016

UNIVERSITI MALAYA

ORIGINAL LITERARY WORK DECLARATION

Name of Candidate: Nur Ayuni binti Jamal

Registration/Matric Number: KHA 120018

Name of Degree: Doctor of Philosophy

Title of Project Research/Research Report/Dissertation/thesis ("this work"): Fabrication and Performance Evaluation of Low to Medium Porosity Closed-Cell Porous Aluminum via Powder Metallurgy Technique

Field of Study: Design Engineering

I do solemnly and sincerely declare that:

(1) I am the sole author or writer of this Work;
(2) This Work is original;
(3) Any use of any work in which copyright exists was done by fair dealing and for permitted purposes and any excerpt and extract form or reference to or reproduction of any copyright work has been disclosed expressly and sufficiently and the title of the Work and its authorship have been acknowledge in this Work;
(4) I do not have any actual knowledge nor do I ought reasonably to know that the making of this work constitutes of an infringement of any copyright work;
(5) I hereby assign all and every rights in the copyright to this Work to the University of Malaya ("UM"), who henceforth shall be owner of the copyright in this Work and that any reproduction or use in any form or by any means whatsoever is prohibited without the written consent of UM having been first had and obtained;
(6) I am fully aware that in the course of making this Work I have infringed any copyright whether intentionally or otherwise, I may be subject to legal action or any other action as may be determined by UM

Candidate's Signature: Date:

Subscribed and solemnly declared before,

Witness's Signature: Date:

Name:
Designation:

ABSTRACT

In recent years, closed-cell porous Aluminum (Al) have drawn increasing attention, particularly in the applications that require reduced weight and energy absorption capability such as in the automotive and aerospace industries. In the present research, porous Al with closed-cell structure was successfully fabricated by powder metallurgy technique using polymethylmetacrylate (PMMA) as a space holder. The effects of different processing parameters such as PMMA content, compaction pressure and sintering time on the porosity, density, microstructure and compressive behaviors of the porous specimens were systematically evaluated. Under this powder metallurgy technique, similar compaction method but different processing conditions such as mixing equipments, binder types, sintering profiles and optimization techniques were utilized in the preparation of closed-cell porous Al. Specifically, this research was divided into two phases namely as Phase 1 and Phase 2. The porous specimens were characterized through density measurement, X-ray diffraction (XRD), thermogravimetric/differential thermal (TG/DT) analyzer and compressive behavior determination. In addition, the microstructural evolutions of the sintered porous structure were also examined by field emission scanning electron microscopy (FESEM) equipped with energy dispersive spectroscopy (EDS). Based on the findings in Phase 1, different processing parameters such as space holder content and sintering time were selected for further study in Phase 2. The results showed that closed-cell porous Al having different porosities and densities could be produced by varying the amount of PMMA. The addition of PMMA particle as the space holder material during fabrication reduced the density of the porous Al and consequently increased the porosity of the porous specimen. FESEM images revealed successful formation of closed macro-pores structure that replicated the initial morphology of the spherical PMMA particle especially in the case of 25 wt. % and 30 wt. % of PMMA. On the other hand, the highest density and compressive strength of porous specimen were achieved with 300 MPa compaction pressure and 1.5 hr sintering. Prolong sintering to 2.5 hr however was found to deteriorate the sintered density and porosity of the resultant porous Al with no clear effect on their porosity level. In contrast, highest porosity was obtained at 2 hr sintering and 250 MPa compaction pressure at any given PMMA content. Based on the maximum porosity (essential in energy absorption capacity) obtained with the abovementioned processing conditions, the energy absorption values were calculated from the area under the stress-strain curves of porous specimen with different PMMA content. The stress-strain curves demonstrated that the plateau stress decreased and the energy absorption capacity increased with increasing amount of PMMA. However, the maximum energy absorption capacity was achieved in the closed-cell porous Al with the addition of 25 wt. % PMMA. Therefore, fabrication of closed-cell porous Al using 25 wt. % PMMA, 2 hr sintering and 250 MPa compaction pressure are considered as the optimal condition in the present study since the resultant closed-cell porous Al possessed good combinations of porosity, density and plateau stress, as well as energy absorption capacity.

ABSTRAK

Sejak akhir-akhir ini, Aluminium (Al) berliang dengan struktur sel tertutup telah menarik perhatian terutamanya di dalam applikasi yang memerlukan berat bahan yang minimum serta tenaga penyerapan keupayaan yang optimum seperti di dalam industri automotif dan aeroangkasa. Dalam kajian ini, Al berliang dengan struktur sel tertutup telah berjaya direka dengan teknik metalurgi serbuk dengan menggunakan partikel polymethylmetacrylate (PMMA) sebagai bahan pemegang ruang. Di bawah teknik ini, teknik pemampatan yang sama tetapi pembolehubah pemprosesan yang berbeza seperti mesin pencampuran, jenis pelekatan, profil pembakaran dan teknik pengoptimum pembolehubah pemprosesan telah dieksploitasi di dalam penyediaan bahan Al berliang dengan struktur sel tertutup. Kesan parameter pemprosesan yang berbeza seperti kandungan PMMA, tekanan pemadatan dan masa pensinteran pada keliangan, ketumpatan, struktur mikro dan tingkah laku mampatan spesimen berliang dinilai secara sistematik. Secara khususnya, penyelidakan ini telah dibahagikan kepada dua fasa iaitu Fasa 1 and Fasa 2. Spesimen berliang dicirikan melalui pengukuran ketumpatan, ketumpatan pukal, sinar-X pembelauan, penganalisis haba serentak, dan ujian mampatan. Di samping itu, evolusi mikrostruktur struktur berliang tersinter juga telah diperiksa oleh pelepasan bidang imbasan mikroskop elektron (FESEM) yang dilengkapi dengan tenaga spektroskopi serakan (EDS).

Berdasarkan keputusan yang diprolehi di dalam Fasa 1, parameter pemprosesan yang berbeza seperti kandungan partikel PMMA dan masa pensinteran telah dipilih untuk kajian lanjut dalam Fasa 2. Hasil kajian menunjukkan bahawa Al berliang dengan struktur sel tertutup dengan tahap keporosan dan ketumpatan yang berbeza boleh dihasilkan dengan mengubah jumlah kandungan partikel PMMA. Penambahan partikel

PMMA sebagai bahan pemegang ruang semasa fabrikasi mengurangkan ketumpatan berliang Al dan seterusnya meningkatkan tahap keliangan spesimen Al berliang. Imej-imej FESEM pula menunjukkan kejayaan pembentukan struktur makro-liang tertutup yang menyerupai morfologi partikel PMMA yang berbentuk sfera terutamanya dengan penggunaan 25 wt. % dan 30 wt. % PMMA. Di dalam kajian ini, kepadatan yang tinggi dan kekuatan mampatan yang maksimum diperolehi pada spesimen berliang yang melalui 1.5 jam masa pensinteran dan 300 MPa tekanan pemadatan. Selain daripada itu, kajian ini mendapati bahawa ketumpatan bahan tersinter merosot dengan memanjangkan masa pensinteran kepada 2.5 jam tanpa kesan yang jelas pada tahap keliangan bahan Al tersinter. Sebaliknya, tahap keliangan yang tertinggi diperolehi pada bahan berliang yang melalui 2 jam masa pensinteran dan 250 MPa tekanan pemadatan tanpa mengambil kira jumlah kandungan PMMA. Berdasarkan tahap keliangan maksimum (penting dalam mencapai kapasiti penyerapan tenaga yang optimum) yang diperolehi dengan keadaan pemprosesan seperti yang dinyatakan di atas, nilai penyerapan tenaga di dalam kajian ini telah dikira dari kawasan di bawah lengkung tegasan-terikan spesimen berliang pada kandungan PMMA berbeza. Lengkung tegasan-terikan menunjukkan bahawa tekanan dataran tinggi menurun dan kapasiti penyerapan tenaga meningkat dengan peningkatan jumlah PMMA. Walau bagaimanapun, kapasiti penyerapan tenaga maksimum telah dicapai dengan penggunaan bahan Al berliang dengan struktur sel tertutup dengan penggunaan 25 wt. % PMMA. Oleh itu, fabrikasi bahan Al berliang dengan struktur sel tertutup dengan menggunakan 25 wt. % PMMA, 2 jam masa pensinteran dan 250 MPa tekanan pemadatan dianggap sebagai keadaan optimum di dalam kajian ini memandangkan bahan berliang yang terhasil mempunyai gabungan tahap keliangan, ketumpatan, tekanan dataran tinggi dan juga kapasiti penyerapan tenaga yang baik.

ACKNOWLEDGEMENTS

Firstly, I would like to express my heartfelt gratitude to my supervisor, Dr. Farazila Yusof and Professor Ir. Dr. Ramesh Singh, for their ever-lasting enthusiasm, encouragement, excellent advice and great concern to my work. I am also wish to register my deep appreciation and sincere thanks to my field supervisor, Assoc. Prof. Dr. Hazleen Anuar for her help, guidance, motivation and invaluable advices. I would also wish to convey my deep appreciation to Professor Dr. Katsuyoshi Kondoh and Associate Professor Dr. Hisashi Imai under Joining and Welding Research Institute Research Institute (JWRI) of Osaka University, Japan (Kondoh Laboratory) for the great technical assistance and valuable advice that contributed to the successful of the current research. Also, I would like to thank all the technicians and members of powder metallurgy laboratory, surface laboratory and advanced materials laboratory of University Malaya for helping and making the lab an enjoyable place to work. I am gratefully acknowledged to the financial assistance provided by the University Malaya under the grants of High Impact Research (HIR), Postgraduate Research (PPP) and University Malaya Research (UMRC) (RP017/2012-B, UM/MOHEUM.C/625/1/HIR/MOHE/H16001-D000001 and PG128-2012B) as well as Ministry of Higher Education, Malaysia (MOHE) and International Islamic University of Malaysia (IIUM) under the academic training scheme (SLAI) to carry out the research. Last but not least I would like to express my gratitude to my parents, husband, children as well as the entire lecturer from the department of mechanical engineering and those who have directly or individually assisted me in the preparation of this thesis.

Thank You.

TABLE OF CONTENTS

CHAPTER 1: INTRODUCTION

CHAPTER 2: LITERATURE REVIEW

CHAPTER 3: MATERIALS AND METHODS

CHAPTER 4: RESULTS AND DISCUSSION

CHAPTER 5: CONCLUSIONS AND RECOMMENDATION

LIST OF FIGURES

LIST OF TABLES

LIST OF SYMBOLS AND ABBREVIATIONS

LIST OF SYMBOLS

%	Percentage
µm	Micrometer
vol. %	Volume percentage
wt. %	Weight percentage
MPa	Mega pascal
hr	Hour
°C	Degree celcius
mm	Milimeter
nm	Nanometer
<	Less than
>	More than
2ϴ	2theta
ρ^*/ρ_s	Relative density
ρ^*	Density of porous specimen
ρ_s	Density of solid specimen
MJ/m^3	Megajoule/meter^3
ml	Mililitre
g	Gram
°C/min	Celcius/minute
g/ml	gram/milimeter
kN	Kilonewton
mm/min	milimeter/min
σ_c	Compressive strength (sigma)

F	Force
A	Area
W	Energy absorption capacity
σ	Compression stress
ε	Compression strain
$^{\circ}$	Degree
g/cm^3	Gram/centimetre^3

LIST OF ABBREVIATIONS

Al	Aluminum
Al_2O_3	Alumina
Sn	Tin
Mg	Magnesium
Polymethyl metacrylate	PMMA
TiH_2	Titanium hydride
$CaCO_3$	Calcium carbonate
NaCl	Sodium chloride
XRD	X-ray diffraction
PEG	Polyethylene glycol
Ar	Argon
L_9	Inner array
CLE	Crude oil of low sulfur content
$MgAl_2O_4$	Magnesium aluminate
Polyvinyl alcohol	PVA
HDPE	High density polyethylene
MA	Mechanical alloying

Process control agents	PCA’s
rpm	Revolutions per minute
Zr	Zirconium
BPR	Ball to powder weight ratio
Chromium	Cr
Copper	Cu
Iron	Fe
Nickel	Ni
Zinc	Zn
Ti	Titanium
WC	Tungsten carbide
Co	Cobalt
PAD	Pressure assisted sintering
Cr	Chromium
Si	Silicon
Mo	Molybdenum
O	Oxygen
C	Carbon
N_2	Nitrogen
UTS	Ultimate tensile strength
TD	Theoretical density
OAs	Orthogonal arrays
DOE	Design of experiment
S/N	Signal to noise
ANOVA	Analysis of variance

FESEM	Field emission scanning electron microscopy
EDS	Energy dispersive x-ray spectroscopy
Mw	Molecular weight
PP	Polypropylene
3D	Three dimensional
d_g	Diameter of green compact
d_d	Diameter of die opening
d_s	Diameter of sintered compact
ASTM	American Society for Testing and Materials
W_d	Unsaturated (dry) weight of sample
W_s	Weight of saturated sample when submerged in liquid
W_{ss}	Saturated weight (assumed that all pores were filled with liquid)
ρ_l	Density of liquid (water)
TG/DTA	Thermogravimetric/Differential thermal analysis
CuKα	Radiation
T_s	Starting temperature
T_f	Final temperature
FCC	Face centered cubic
MMA	methyl methacrylate
H^2	Hydrogen gas
H	Hydrogen

CO	Carbon oxide
CO2	Carbon dioxide
CH4	Methane
C_2H_4	Ethene
CH_3COOH	Acetic acid

LIST OF APPENDICES

CHAPTER 1: INTRODUCTION

GENERAL BACKGROUND

Porous materials play an important role in every aspect of human activity. Porous materials are extracted either naturally from the environment like bone, coral, cork and wood or through human made (synthetic) including porous materials made of ceramics, polymers and metals. Unlike other porous materials, porous metals possess greater interest in terms of higher mechanical properties and thermal properties as well as excellent stability in harsh environment. In general, porous metals and metallic foams can be defined as a solid material enclosed by a three dimensional network of voids (Roswell and Yaghi, 2004). Porous metals refer to the metallic materials having low level of porosity (<70 wt. %) whereas metallic foams represent metallic materials that fabricated by using foaming processes having minimum 50 wt. % of total porosity (Wang & Zhang, 2008). In the past, porosity used to be considered as a drawback in designing dense metals. However, as research in this area evolved, porous structure has become important due to their lightweight, low density and unique combination of physical and mechanical characteristics such as high strength-to-weight ratio, high stiffness, excellent impact energy absorption, high damping capacity, and good sound absorption properties (Dewidar, 2012; Astaraie et al., 2015; Kato et al., 2012; Kevorkijan, 2010; Koizumi et al., 2011; Yu et al., 2007). Owing to their excellent properties, they are widely applied in circumstances where high strength and stiffness to weight ratio are concerned, as well as in the areas where energy absorption and permeability are appreciated (Smith et al., 2012). For examples, they have found increasing applications in various fields such as in the structural fields as heat exchanger, filters, flame retardant and silencers, as well as in the functional fields as crash energy absorption, sandwich panels and noise control (Astaraie et al., 2015; Kevorkijan et al., 2010; Koizumi et al., 2011; Yu et al., 2007).

Theoretically, porous metals can be classified into two groups, which are open-celled and closed-cell, depending on the connectivity of the cells (Ashby at al., 2000). Open-celled porous metals consist of interconnected pores whereas closed-cell porous metals are made of sealed pores that are surrounded by thin metallic cell walls (Ashby et al., 2000). These open-celled are originally assembled from the consolidated of space holder particles due to compacting effect while closed-cell are generated from the segregated space holder particles in the mixture (Arifvianto & Zhou, 2014; Ruperez et al., 2015). Closed-cell porous metals possess high bulk density, high modulus and high strength and thus commonly applied for structural applications including energy absorption capability, cores in sandwich panels and blast resistant (Astaraie et al., 2015; Jiang et al., 2005; Smith et al., 2012). In contrast, open–celled porous metals are extremely light weight with adjustable elastic modulus thus cost effective and mostly utilized in functional applications such as heat exchangers, filters, sound and energy absorbers (Jiang et al., 2005; Bin et al., 2007; Wang & Zhang, 2008).

Various types of metallic material have been used to fabricate closed-cell porous metals, in particular aluminum (Al). Closed-cell porous Al is unique in terms of ultra-lightweight with combination of high specific strength, stiffness, good sound absorption properties as well as excellent energy absorption (Banhart, 2001; Simancik, 2001). It is important to note that Al is also known as sintering-resistant material due to the presence of a stable 1 to 2 nm of alumina (Al_2O_3) coating formed on its surface (Gokce & Findik, 2011; Katsuyoshi et al., 2007; Sukiman et al., 2014). The Al_2O_3 coating is usually disrupts by adding sintering aids such as tin (Sn) or magnesium (Mg) or combination of these two materials (Gokce & Findik, 2011; Katsuyoshi et al., 2007; Sukiman et al., 2014).

To date, different fabrication methods of producing closed-cell porous metals including closed-cell porous Al have been exploited i.e., powder sintering, expansion of pressurized gas bubbles, powder deposition, rapid prototyping and powder metallurgy method (Arifvianto & Zhou, 2014). The powder metallurgy method is widely used to manufacture closed-cell porous metals due to many advantages especially greater control of pore characteristics including pore size, pore structure and level of porosity. Powder metallurgy technique exploits the use of space holder materials or pore foaming agents to develop porous metals. These space holder materials are temporary particles added to the metallic matrix powder that act as a pore former (Arifvianto & Zhou, 2014). Many types of space holder material have been proposed as pore creator potential such as ceramics, metals, polymers, hydrides and carbonates (Koizumi et al., 2011; Mustapha et al., 2011; Xie et al., 2006; Zhao et al., 2005).

Powder metallurgy technique involves basic processes of mixing, compacting and sintering. Various processing conditions have been manipulated in fabrication of closed-cell porous Al via powder metallurgy technique including conditions of mixing (time, speed, equipments, different binders introduction and so on), compaction (pressure, holding time, environment (hot or cold), equipment and so on) as well as sintering (temperature, time, atmosphere (protected or normal environment), sintering profiles, with or without pressure and so on). Moreover, optimization of these processing parameters can be performed using variety of techniques such as Taguchi orthogonal array design, response surface, mixture design, crossed design and so on (Surace et al., 2009; Surace et al., 2010). These techniques are widely applied due to lesser number of experiments, simplification of experimental design and feasibility of interaction study between various parameters (Kamaruddin et al., 2004). In contrast, full set of experimental design are also commonly practiced that involves complete number of experiment between different parameters.

In the present study, the practical feasibility of polymethyl metacrylate (PMMA) particle as a suitable space holder material in the fabrication of closed-cell porous Al with low to medium porosity using powder metallurgy method was investigated. Moreover, the effects of PMMA content, compaction pressure and sintering time on the porosity, density, microstructure and compressive behavior of the porous Al were examined.

1.2 PROBLEM STATEMENT

Greater attention has been given to closed-cell porous metals fabrication due to emerging demand for lightweight, compact and economical materials. Closed-cell porous metals with high stability and required porosity often made of titanium, copper, tin, bronze, iron and steel. These metals however suffer from higher density, low thermal conductivity, higher cost of starting metal powder and low to medium capability of corrosion resistance. Therefore, aluminum (Al) is proposed in the current study as closed-cell porous metal potential due to low density (ultra-lightweight), higher functionality, lower cost of starting material, higher thermal conductivity and good corrosion resistance (least noble metal).

Over the years, studies of open-celled porous Al in terms of their fabrication techniques, characterizations and mechanical performances have been extensively performed (Kavei, 2015; Chen et al., 2014; Jiang et al., 2005). In contrast, there have been little investigations on the closed-cell porous Al, especially on those with low to medium porosity (Zhang et al., 2015; Manonukul et al., 2010; Gulsoy and German, 2008). In recent years, closed-cell porous Al have drawn increasing attention, particularly in the applications requiring reduced weight and energy absorption capabilities such as in the automotive and aerospace industries (Astaraie et al., 2015; Kevorkijan, 2010; Koizumi et al., 2011; Yu et al., 2007). Due to their ability to undergo large deformation with relatively constant stress, closed-cell porous Al with low to medium porosity level possess higher moduli, strength and impact energy absorbing ability than their open-celled counterparts, as well as the closed-cell porous Al with higher porosity (Zhang et al., 2015; Astaraie et al., 2015; Yu et al., 2007). Although they have been eliciting much interest in many applications, literature on the production methods and mechanical performance of these closed-cell porous Al, particularly involving low to medium porosity, is still limited and the current paper addresses that. Hence, better understanding in this area can be gained in terms of processing conditions, physical properties and compressive behavior as well as energy absorption ability.

In general, closed-cell porous Al can be produced via two processing routes, known as liquid state processing (melt route) and solid state processing (powder metallurgy) (Yu et al., 2007; Astaraie et al., 2015; Manonukul et al., 2010; Gulsoy and German, 2008). Liquid state processing route is a direct foaming method starting from slurry of molten Al and gases are introduced into the melt through foaming agents or external gas sources to create bubbles, followed by subsequent solidification to produce a close-pored microstructure (Yu et al., 2007; Astaraie et al., 2015; Li et al., 2012). In contrast, solid state processing route, often collectively called space-holder method, is an indirect foaming method starting from mixing of metallic powder and foaming agents (also known as space holder), followed by compacting and sintering processes to obtain the resultant porous metal (Manonukul et al., 2010; Gulsoy and German, 2008; Wang and Zhang, 2008). Although liquid state processing route has been extensively practiced due to the simplicity of the processing, the as-produced porous metals are usually of low quality, characterized by non-uniform distribution of pore sizes and porosity. Moreover, additional material such as ceramic particle (typically silicon carbide (SiC) or alumina (Al_2O_3)) is generally added along with foaming agent to stabilize the molten Al, and thereby incurring additional processing cost (Yu et al., 2007; Astaraie et al., 2015; Manonukul et al., 2010; Liu et al., 2008). Therefore, powder metallurgy technique that exploits the use of space holder or foaming agent particle have been utilized in the current research to prepare closed-cell porous Al with low to medium porosity (<50 wt. %).

On the other hand, space holder materials including titanium hydride (TiH_2), calcium carbonate ($CaCO_3$) and sodium chloride (NaCl) have been widely employed as the space holder materials for the successful fabrication porous Al by powder metallurgy route (Kevorkijan, 2010; Koizumi et al., 2011; Mustapha et al., 2010; Bafti and Habibolahzadeh, 2010; Jha et al., 2013). However, there are certain drawbacks in the use of these space holder materials. For example, economical limitation in terms of manufacturing cost arises when the expensive TiH_2 is employed as the foaming agent and the decomposition of TiH_2 leads to the formation of chemically inert hydrogen gas (Paulin et al., 2011; Matijasevic and Banhart; 2006). In contrast, although $CaCO_3$ is an inexpensive alternative to TiH_2, the decomposition temperature of $CaCO_3$ is relatively higher (between 700-900°C), which is significantly above the melting point of the Al

(Kevorkijan, 2010; Koizumi et al., 2011). One of the most important steps in the production of porous Al is the porous body stabilization. The high decomposition temperature of $CaCO_3$ makes porous Al stabilization become more demanding and costly, thereby it is not cost effective. Moreover, the use of cheaper NaCl often required subsequent process either before or after sintering prior to their decomposition thus it is time consuming. In addition, incomplete NaCl removal often corroded the base material. Therefore, further studies concerning the selection of a cost effective space holder material that can be well performed in the porous Al stabilization would be valuable.

Recently, polymethyl metacrylate (PMMA) has been proposed as one of the suitable space holder materials due to some outstanding characteristics such as excellent formability, good biocompatibility, and most importantly, it has a low decomposition temperature of around 360-400 °C, which causes almost no contamination on the resultant porous metal due to the ease in thorough decomposition. Moreover, it has a perfectly spherical shape, which is reported to have significant effects in affecting the mechanical properties of the resultant porous metal. Indeed, the successful fabrication of closed-cell porous metal by powder metallurgy route using PMMA as the space holder has been reported in some recent studies. Li et al. (2010) have successfully produced porous titanium with an average pore size of 200-400 μm and porosity in the range of 10-65 % by varying the amount and size of the PMMA particle. In another study by Jeon et al. (2015), they found that porous titanium with closed pore structure can only be obtained with 20 vol. % PMMA, whereas porous titanium with 70 vol. % PMMA showed the open cellular structure, suggesting that the pore structure of the resultant porous metal is dependent on the size and content of PMMA. In a more recent study, Bi et al. (2015) fabricated porous magnesium with porosities between 1% and

40% by powder metallurgy using PMMA as the space holder and they found that the corresponding porosity of the resultant porous magnesium increased with increasing content of PMMA from 0 wt. % to 30 wt. %. Although there has been progressive research in the fabrication of closed-cell porous metals using PMMA as the space holder, little efforts have been directed towards the fabrication of closed-cell porous Al with low to medium porosity (<50 wt. %).

Finally, considering successful fabrication of closed-cell porous metals using combination of higher melting point metallic materials such as titanium, copper and stainless steel with PMMA space holder have been abundantly documented in the literatures (Wang and Zhang, 2008; Manonukul et al., 2010; Li et al., 2010; Jeon et al., 2015; Bi et al., 2015), the current research emphasized on the use of lower melting point metallic matrix that is Al. Moreover, the current research has also been undertaken to study the flexibility of powder metallurgy technique in processing lower melting point metallic material with PMMA space holder in obtaining closed-cell structure with low to medium porosity (<50 wt. %). Therefore, the novelty of the current research relies on the introduction of low melting point of metallic matrix (Al) and PMMA as space holder material with the combination of different processing conditions (PMMA content, compaction pressure and sintering time) to fabricate porous Al with low to medium porosity (<50 wt. %).

1.3 RESEARCH OBJECTIVES

The objectives of the present research are:

1) To fabricate closed-cell porous Al with low to medium porosity (<50 wt. %) via powder metallurgy technique by utilizing PMMA as space holder material

2) To evaluate the effects of processing parameters such as space holder content, compaction pressure and sintering time on the overall density, porosity and compressive property of closed-cell porous Al

3) To determine the optimum processing parameters to produce a closed-cell porous Al suitable for energy absorption application

1.4 SCOPE OF RESEARCH

In the present research, powder metallurgy technique was implemented to fabricate closed-cell porous Al with low to medium porosity (<50 wt. %). Under this technique, similar compaction method but different processing conditions such as mixing equipments, binder types, sintering profiles and optimization techniques were utilized in the preparation of closed-cell porous Al. Specifically, this research has been divided into two phases that are Phase 1 and Phase 2. In Phase 1, high energy mixing by planetary ball milling equipment, ethanol binder, single step sintering profile and Taguchi robust design for optimization of processing parameters were exploited for porous Al fabrication. Processing parameters such as space holder content (40 wt. %, 45 wt. % and 50 wt. %), compaction pressure (200 MPa, 250 MPa and 300 MPa), sintering time (1.5 hr, 2 hr and 2.5 hr) and sintering temperature (450 °C, 475 °C and 500 °C) were varied to evaluate the flexibility of porous Al fabricated in Phase 1. Based on the findings in Phase 1, different range of space holder content (20 wt. %, 25 wt. % and 30 wt. %) were selected whereas ranges of compaction pressure and sintering time remained as in Phase 1. In addition, different approach of powder preparation prior to closed-cell porous Al fabrication was implemented in Phase 2 by utilizing low energy mixing equipments such as table-top ball mill and turbular shaker, oil binder, two steps sintering profile and full set of experimental design for optimization of processing parameters. On the other hand, supplementary studies on the variation of Sn content and sintering temperature were also performed in Phase 2 to investigate the sintering quality of passive Al material. The selection of optimum sintering temperature was made based on the physical body examination (oxidation level, slumping, cracking, bloating and collapse of porous body), morphology and oxidation level of the resultant porous Al at 30 wt. % of PMMA. In contrast, the optimization Sn content was made based on the physical body assessment, densities and morphology of sintered Al and porous Al at 30 wt. % of PMMA. Moreover, the resultant porous Al specimen that exhibited the highest porosity level with considerable physical and compressive properties was selected for further study as energy absorber potential. Finally, the effects of processing parameters on the porosity level, densities, morphology and compressive behavior of closed-cell porous Al fabricated in Phase 1 and Phase 2 were also examined.

1.5 STRUCTURE OF THESIS

There are five main chapters in this thesis. In Chapter 1, general background, research problem along with its significant, research objectives and research scope are briefly discussed. A concise explanation on Phase 1 and Phase 2 introduced in this research was also mentioned.

Chapter 2 presents a brief overview on the past studies that have been performed on both open-celled and closed-cell porous metals including porous Al. Different parameters that determine the properties of porous metals such as mixing conditions, compaction techniques, sintering methods, pores structure, binders usage and space holder types are also discussed. Moreover, this chapter also reviews the literatures related to theories that have an impact on the physical and mechanical properties of open-celled and closed-cell porous Al. The implementation of Taguchi orthogonal array for processing parameters optimization for Phase 1 and potential applications particularly in energy absorption field are also discussed in this chapter.

Chapter 3 explains the experimental procedure for closed-cell porous Al fabrication along with the various characterization techniques and equipments introduced in this study. This chapter was separated into two sections for better understanding in terms of powder preparation technique for Phase 1 and Phase 2. Characterizations of porous specimen were documented under one section for both Phase 1 and Phase 2. Details on the processing parameters for Phase 1 and Phase 2 are also clarified.

Chapter 4 emphasizes on the results obtained for closed-cell porous Al in terms of starting materials properties, physical evaluation of porous body specimen, densities, compressive behavior, porosity level as well as pores morphology. This chapter is divided into two sections in which the first section discussed on the results obtained for Phase 1. The second section discussed on the results obtained for Phase 2. A discussion with justifications on closed-cell porous Al as energy absorption ability potential is only made in Phase 2 for porous specimen that exhibited the highest porosity level with considerable physical and compressive behavior.

Finally, chapter 5 summarizes on the findings reported in this thesis. Some suggestions for future work are also presented in this chapter.

CHAPTER 2: LITERATURE REVIEW

2.1 INTRODUCTION

Porous metals often display unique mechanical properties and thermal properties initiating from cells or pores structure. Because of these exceptional properties, porous metals find a lot of interest in various applications such as automotive, catalyses, electrodes, and constructions. Fabrication techniques, selection of materials as porous metals potential, selection of potential space holder particles or spacers and processing parameters are critical criteria in developing porous metals. Moreover, types of porosity either having open-celled or closed-celled structure also play important role in developing porous metals in which later will determine the final properties and potential applications. Gibson and Ashby (1997) mentioned that, relative density, the degree of anisotropy of porous material and the material properties of the ligaments are also among the important characteristics that affect the properties of porous materials potential. Therefore, rigorous tests and analysis play important role to characterize the properties of porous Al.

The first attempt to produce metal foam or porous metal was pioneered by Benjamin Sosnick in 1943 via mercury addition into molten aluminum (Al) (Dawood and Nazirudeen, 2010). This technique was invented to produce Al foam having open-celled structure, uniform pore distribution and consistent length of passage. In brief, Hardt et al. (2002) described porosity as the percentage of void space in a solid and it is morphological property independent of the material. According to Babcsan et al. (2003), porous metallic systems can be divided into a few categories as follow:

- Materials with high volume fraction of voids that being connected by network of walls and membranes are defined as cellular metals
- Materials with low levels of porosity which is usually less than 70% with isolated spherical pores are referred to as porous metals
- Materials with closed or open-celled structure having the same property as cellular metals are often defined as metal foams

On the other hand, porous metals are often classified as either having closed-cell or open- celled (reticulated) structure. Generally, closed-cell structure referred to the pores that are not connected and consist of distribution of pores that are totally segregated from one another and completely enclosed by the membrane or cell wall of the material (Mour et al., 2010) as seen in Figure 2.1. Moreover, Gokhale et al. (2011) described the closed pore as the structures resembling of a network of soap bubbles with higher compressive strength. This closed-cell structure is beneficial in term of its bulk density, mechanical strength and thermal conductivity.

Porous metals with closed-cell are mainly used in structural applications such as impact absorbers, cores in sandwich panels, blast resistant material and so on (Arenas and Crocker, 2010; Gokhale et al., 2011). In contrast, open-celled structure refers to large channels of interconnected cells with flow-through capability and access to the internal surface. Open-celled structure can have either connected or interconnected pores (pores are open at both end) or unconnected pores (pores are only at one end). Open-celled structure has advantageous such as high heat exchange and radiation ability, excellent permeability and good absorption of electromagnetic waves (Mour et al., 2010; Arenas and Crocker, 2010; Gokhale et al., 2011). The fabrication of porous metals having open-celled structure is used for functional applications including as sound absorbing material, filters, heat exchangers, thermal management material and many more (Gokhale et al., 2011; Arenas and Cracker, 2010; Aqida et al., 2004). An example of open-celled structure is presented in Figure 2.2.

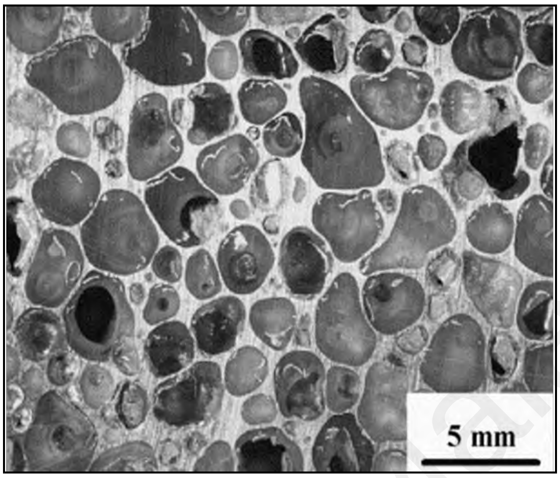

Figure 2.1 : Closed-cell structure (Mukai et al., 2006)

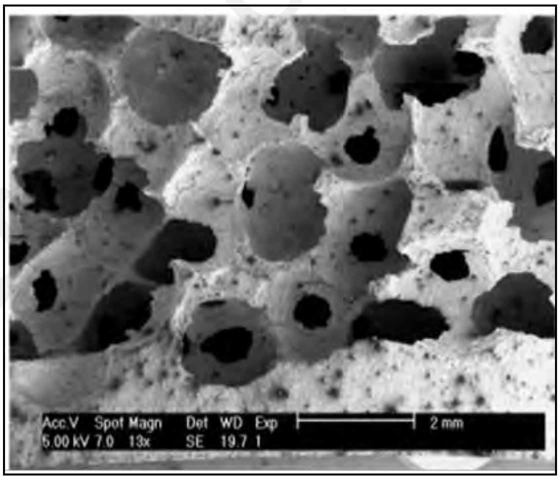

Figure 2.2 : Open-celled structure (Bafti and Habibolahzadeh, 2010)

2.2 FABRICATION OF POROUS METALS

Porous metal can be manufactured by several ways including solid-state processes, liquid-state processes, chemical and electrochemical (metal ion deposition) deposition and physical vapor deposition processes (Banhart, 2001; Mour et al., 2010; Sobczak, 2003). Banhart (2001) described the liquid-state processes as space holder particles or polymeric foams that are filled with liquid refractory metals which are then cured followed by decomposition, dissolution or chemical treatment processes. The removal processes of space holder particles will result in metallic foam or porous metal production.

Contrary, solid-state processes is a process of mixing metal powders and space holder particles or sacrificial fillers in solid or powder form followed by compacting and later heat treatments. In this process, the metal powder form remains solid during the entire process. This technique often results in open foam structure. Powder metallurgy route is classified under solid-state process. This process is beneficial in term of easy control of materials properties through mixing different materials in various fractions (Dobrzanski et al., 2008). On the other hand, chemical and electrochemical deposition process involves the fabrication of porous metals from the ionic state of metals (solution of ions in an electrolyte). The metal is then electrically deposited onto polymeric foam with open-celled structure in which being removed in later stage.

Finally, physical vapor deposition process refers to the porous metal made from gaseous metal or gaseous metallic compounds. In this process, a solid precursor structure is required which defines the geometry of the foam or cellular material to be produced (Banhart, 2001). In manufacturing of porous metals, different processing methods will result in different type of porous materials. The properties of porous metals greatly depend on the relative density, metal properties and cell topology (open-celled, closed-celled, cell size, cell shape, anisotropic and so on). Various fabrication methods of porous metals are given in Figure 2.3.

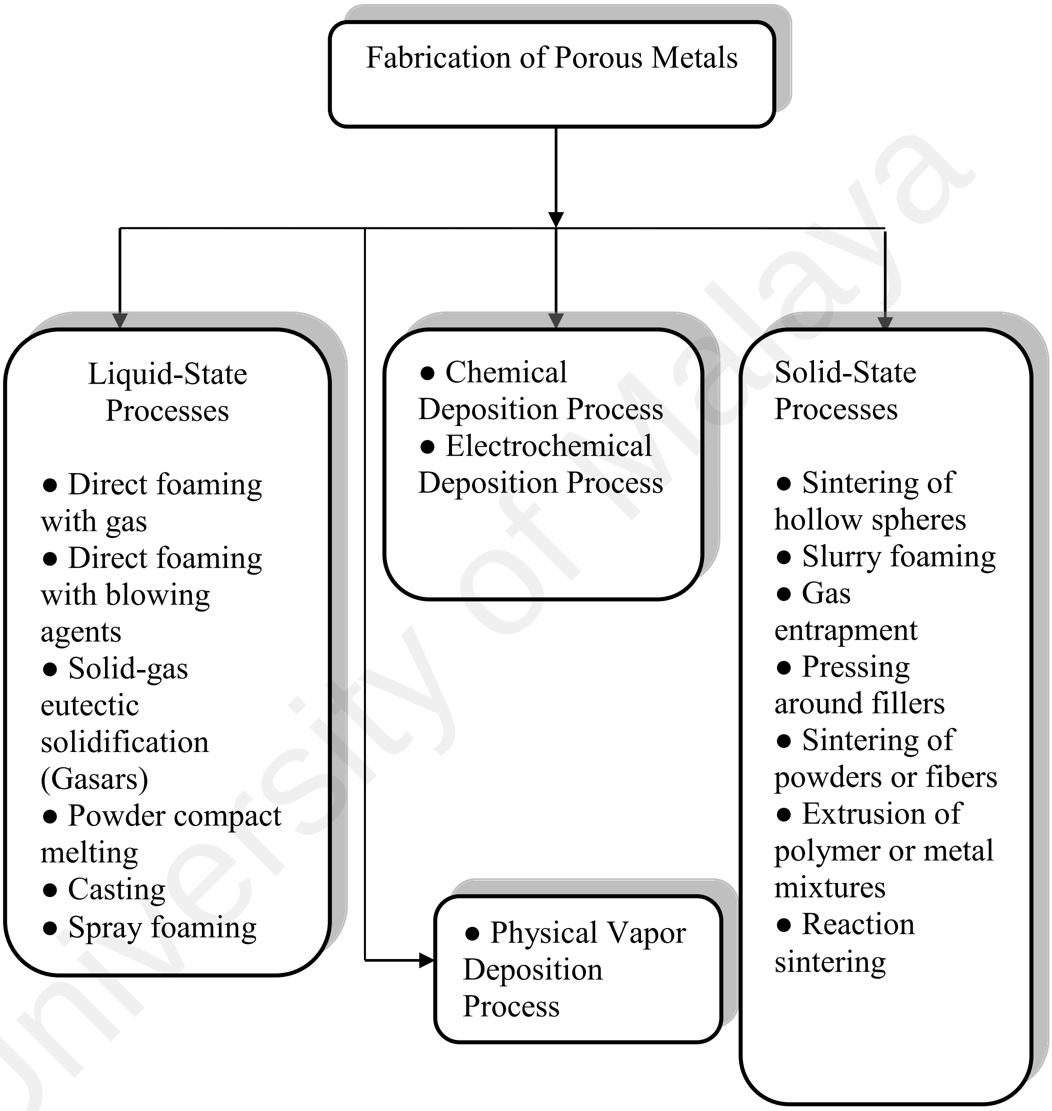

Figure 2.3 : Fabrication methods for porous metals

In the early development of porous metals, the porosity obtained did not exceed 30% with pore size smaller than 0.3 mm (Liu and Liang, 2001). Nonetheless, rapid growth in porous metal fields requires the porosity to be produced more than 30%. By far, all these processes are capable of producing porous metals either having open foam structure or closed foam structure depending on the applications. Nevertheless, powder metallurgy technique is usually applied to avoid segregation effects and brittle reaction product formation that are more likely to occur in liquid state processes. In this section, powder metallurgy technique was discussed in detail due to simplicity of fabrication process and widely applied in the production of porous metals (Surace et al., 2009; Jiang et al., 2005; Wang and Zhang, 2008; Hassani et al., 2012).

In powder metallurgy process, there are five basic steps involved including a) selection of metallic powders, b) mixing of metallic powders and space holder particle c) compacting, and d) sintering (Yusoff and Jamaludin, 2011).

2.3 SELECTION OF METALLIC MATRIX POWDER

Various types of metal powders can be proposed as metallic matrix powder. The selection of metallic matrix powder depends on the desired application as well as it should be cost effective. The choice of metal powders properties are made based on the potential applications. Bronze, stainless steel, nickel and nickel based alloys are among the preferred choices of available metal powders especially in the powder metallurgy process. These metal powders are classified as ferrous metal powders, but other non-ferrous metal powders such as aluminum, copper, gold, niobium, silver, tantalum, titanium and zirconium are also widely used as starting material for porous metal potential (Aqida et al., 2004; Wang et al., 2012; Kheder et al., 2011; Dewidar, 2012). In the current study, aluminum (Al) was used as a base material due to many advantages. These include lightweight (a third as heavy as copper or steel), greater corrosion resistance, excellent conductor (heat and electrical), non-magnetic, better cryogenic properties, good machine ability, good response to a variety of finishing processes and completely recyclable (energy efficient) (Banhart, 2001; Simancik, 2001).

It is known that alumina oxide (Al_2O_3) constantly covers Al powder (Schaffer et al., 2001; Mittal and Singh, 2012; Pieczonka et al., 2008, Sukiman et al., 2014) and that the temperature as well as atmosphere in which Al powder is stored, mainly the humidity influences the thickness of this oxide layer. The thickness of this oxide layer can differ from 5 to 15 nm thus preventing solid state sintering of low melting point metals, in particular Al (Dunnett et al., 2008; Gokce et al., 2011; Sercombe and Schaffer, 1999; Lumley and Schaffer, 1996). Because of this, a combination of tin (Sn) powder and magnesium (Mg) powder as sintering aids are necessary in sintering process of Al powder.

The addition of Sn powder facilitates the liquid phase sintering of Al particles. The use of Sn as sintering additive is effective as it has low melting point than the base Al material. Moreover, no inter-metallic phases are formed during the liquid phase sintering process for Al material. In addition, German (1985) also reported that an ideal liquid phase sintering also relies on the low solubility of additive in the base material as well as complete solubility of the base material in the liquid sintering additive with no formation of immiscible liquids. For this reason, Sn powder is an ideal sintering aid for Al particle as it is scarcely soluble in solid Al with entirely solubility of Al in liquid Sn. In order to enhance the efficiency in liquid phase sintering of Al, Mg powder is needed to disrupt the oxide layers on Al powder particles through formation of spinel ($MgAl_2O_4$) (Scahffer et al., 2001; Gokce and Findik, 2008; Dunnet et al., 2008; Sukiman et al., 2014). The formation of magnesium aluminate ($MgAl_2O_4$) spinel ruptures the oxide layers on Al particle during sintering in which reveals the underlying metal and assists sintering (Schaffer et al., 2001). As a result, Mg powder enhances the liquid phase sintering for Al with the addition of Sn powder due to the disruption of Al_2O_3 layer. It should be noted that only small amount of Sn and Mg powders are usually added in which between 0.5% and 2% of total powder volume (Schaffer et al., 2001; Mittal and Singh, 2012; Pieczonka et al., 2008; Gokce et al., 2008; Dunnet et al., 2008).

The properties of porous metals are governed by the matrix powder particles sizes and morphology of matrix powder particles. There are two types of matrix powder morphologies commonly introduced including compacted spherical powder and angular powder (Figure 2.4 and Figure 2.5). In comparison with a compacted spherical powder, larger pore sizes and higher porosity were obtained with the sintering of a compacted angular powder (Guden et al., 2008). This results in lower compressive strength and elastic modulus as compared to those of the sintered spherical powder. Guden et al. (2008) reported that better mechanical properties for the sintered spherical powder were due to the higher deformation capability of spherical particles than those angular particles under the same compacting pressure thus resulted in lower porosity.

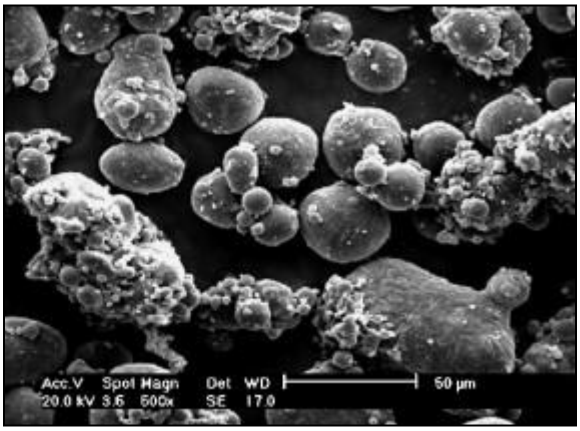

Figure 2.4: Spherical shape of metallic matrix powder (Jiang et al., 2005)

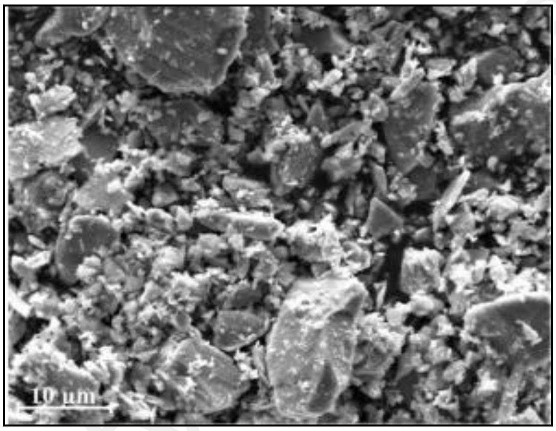

Figure 2.5: Angular shape of metallic matrix powder (Guden et al., 2008)

On the other hand, Tuncer et al. (2011) mentioned that the use of compacted spherical powder particle often resulted in lower green strength as compared to the angular powder particles in which led to the collapsing of porous body during the debinding process of space holding particles. This is believed to be due to the less mechanical interlocking between initially compacted of spherical powder particles. Asavavisithchai et al. (2014) also reported similar findings where silver particles as matrix powder having spherical and cylindrical particles shape exhibited larger surface area and higher density as compared to the silver particles of octahedral shape. As a result, the compressive strength for the silver particles of octahedral shape was lower than silver particles of spherical and cylindrical shape. Table 2.1 summarizes the effect of different metallic powder shapes on the physical and mechanical properties of metallic foam.

Table 2.1: The effect of using different metallic powder shape on the physical and mechanical properties of metallic foam (Arifvianto and Zhou, 2014)

Angular shape of metallic powder	Spherical shape of metallic powder
High green density	Low green density
Low compressive strength	High compressive strength
Low elastic modulus	High elastic modulus

The sizes of matrix powder particles also determine the quality of a sintered porous metal as well as densification property. Fully densified porous framework can be obtained from sintering of powder particles having sizes finer than 16 µm (Bram et al., 2000). In contrast, porous framework with voids and sintering neck were likely to occur with the sintering of powder particles having larger sizes than 16 µm (Bram et al., 2000). Moreover, Wang and Zhang (2005) mentioned that the yield strength for finer powder particles (5 µm) of sintered porous body was found to be higher than those coarse powder particles (45 µm). According to Lund (1982), this enhancement might be due to the increase in the number of bonds among the partic1es that leads to efficient solid-state diffusion process. Furthermore, Sanchez et al. (2003) found that small pores distributed throughout the entire compact with the use of small powder particles whereas larger particle powder gives small number of heterogeneously pores distributed in the sample. Although the use of smaller powder particles possess greater advantages as compared to larger powder particles sizes, Wang and Zhang (2005) reported that open pores with interconnected structure were successfully fabricated with the use of larger powder particle size (45 µm) whereas smaller powder particle size (5 µm) resulted in closed pores.

2.4 MIXING OF METALLIC MATRIX POWDER AND SPACE HOLDER PARTICLE

Mixing of metallic matrix powder and space holder particle is considered as a critical process in order to achieve a homogeneous distribution between these two materials. Obtaining a homogeneous distribution between metallic matrix powder and space holder particle is important because it will determine the final properties of porous metals.

Inhomogeneous distribution of space holder particles in metallic matrix powders usually lead to the inhomogeneous distribution of macro pores in porous body. Such non-uniform dispersion of space holder particle in metallic matrix powders is often attributed to powder segregation that commonly arises during the mixing process. There are two types of powder segregation known as buoyancy and percolation (Arifvianto and Zhou, 2014; Jain et al., 2005; Tang and Puri, 2004). Different types of powder segregation during mixing are illustrated in Figure 2.6.

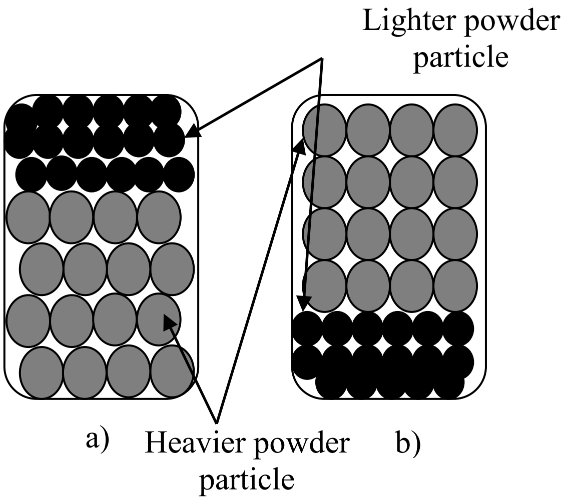

Figure 2.6 : a) Buoyancy type of powder segregation and b) percolation type of powder segregation

The buoyancy type is classified as a difference in powder density that leads to powder segregation. In this buoyancy type, the heavier powder particles submerged to a lower level of the mixture whereas the lighter powder particles are located at the higher level in the mixture. In contrast, powder segregation with the percolation type arises due to the difference in particle size and particle size distribution. In this type, smaller particle sizes fall through the gap of larger particles and settle at the bottom level of a mixing container (Arifvianto and Zhou, 2014). These two types of powder segregation often occur simultaneously during mixing as it involves the use of both smaller but heavier metallic matrix particles and larger but lighter space holder particles. A few studies claimed that the matrix particles should be several times smaller than space holder particle to improve the sinterability of metallic matrix powders (Surace et al., 2009; Tuncer et al., 2011; Bram et al., 2000). In contrast, there are a few studies also reported that an average size of metallic matrix powders and space holder particles with particles size slightly greater than the metallic matrix particle size is desirable for porous metals fabrication (Sharma et al., 2011; Xie et al., 2006; Al-Grafi 2014).

In order to minimize powder segregation during mixing process, binders are commonly added into the mixture. The use of binders produce granular materials consist of space holder particle’s coated with smaller metal matrix particles (Bram et al., 2000; Bekoz et al., 2012; Bakan, 2006; Mutlu and Oktay, 2011). Binders are preferably in liquid form and should be completely removed during sintering process. Moreover, binders are introduced to provide an adequate binding strength between metallic matrix powder and space holder particles by providing sufficient green density prior to sintering. In addition, careful selection of binders is necessary to avoid any chemical and physical reaction between binders and metallic powders during mixing as well as during sintering process. For example, water-soluble binder like water is not desirable for water-soluble space holder particles including carbamide, saccharide, sodium chloride and ammonium hydrogen carbonate due to the reaction between these powders and thus distorts the shape and size of space holder particle. The amount of binders to be added into the mixture should be carefully selected to avoid any changes in overall integrity of porous body. Bloating, slumping, cracking and even collapsing of porous body are among the possible distortion of porous body associated with the use of binders. Table 2.2 shows a few examples of commonly used binder and their advantage.

Table 2.2 : Commonly used binders and their advantage

Binder	Advantage
Ethanol	Low decomposition temperature (Hassani et al., 2012)
Paraffin wax	Non-toxic (Manonukul et al., 2010)
Water	Non-toxic, easy decompose (Michailidis and Stergioudi, 2011)
Polyester resin	High stability thus does not react with parent material (Golabgir et al., 2014)
Polymethyl metacrylate (PMMA)	Good mechanical properties (Bakan, 2006)

The amount of binders is usually added between 1 wt. % to 5 wt. % of total powder content (Zhang and Wang, 2005; Jiang et al., 2005; Arifvianto and Zhou, 2014; Hassani et al., 2012). It is important to note that excessive binders might result in deformation of porous body during debinding stage as well as larger dimensional changes during sintering. Appropriate amount and concentration of binders are critical factors in achieving homogenous dispersion between metal matrix powders and space holder particle. To date, various binders have been introduced during mixing process including ethanol (Xie et al., 2006; Hassani et al., 2012; Zhao et al., 2005), PEG (Niu et al., 2009), polyvinyl alcohol (PVA) (Al-Grafi, 2014; Esen and Bor, 2011; Esen and Bor, 2007; Bekoz and Oktay, 2012), paraffin (Dabrowski et al., 2010; Mutlu and Oktay, 2011; Hao et al., 2008), polymethylmetacrylate (PMMA) (Bakan, 2006) and polyester resin (Golabgir et al., 2014). On the contrary, fabrication of porous metals via powder injection molding exploits the use of multi component binders consisting of stearic acid, paraffin wax, high density polyethylene (HDPE) and PEG (Manonukul et al., 2010).

The mixing technique between metallic matrix powders and space holder particles is commonly performed by using various equipments including vertical mixer, rotary mixer, three dimensional mixer, turbular mixer, rolling container, sigma blade mixer and so on. Table 2.3 concludes the reports on the mixing process for metal matrix powder and space holder particles in the preparation of porous metals.

Table 2.3 : Various mixer type used for mixing of metal matrix powder and space holder particle

Metal matrix powder	**Space holder**	**Mixer type**	**Duration**	**References**
Aluminum	NaCl	Turbular	30 minutes	Mustapha et al. (2010)
Aluminum	Carbamide	Rotary	2 hour	Hassani et al. (2012)
Stainless steel 316L	Carbamide	Turbular	3 hour	Bakan (2006)
Aluminum	NaCl and Carbamide	Planetary ball mill	20 hour	Kavei (2015)
Magnesium	Carbamide	Agate mortar	Not defined	Wen et al. (2004)
Copper	PMMA	Horizontal mixer	Not defined	Wang and Zhang (2008)

Appropriate mixing technique is necessary to obtain porous body having balance properties in mechanical and thermal. In the current study, mixing of metallic powders and space holder particle was done in two different ways including in a high speed planetary ball milling equipment under a process known as mechanical alloying (MA). The second mixing technique exploited the use of low energy mixing process via table-top milling equipment. For both techniques, the use of tungsten carbide and zirconia ball was applied as mixing medium to obtain homogenous mixing. It is important to note that MA has attracted considerable attention for manufacturing complex materials including amorphous alloys, inter-metallic compounds, quasi-crystalline materials, nanocomposite and composite materials (Zhang and Ying, 2000; Travessa et al., 2012; Senthil-Kumar and Ahamed, 2011; Adamiak, 2008).

As part of powder metallurgy technique, MA involves a simple and low cost fabrication method that cannot be obtained by other conventional melting or casting techniques. John Benjamin originally invented MA, which later has been widely utilized to produce powders with controlled microstructure (Benjamin, 1976). The basic mechanism of MA process involves the ball to powder collision. During MA process, repeated process namely as deformation, cold-welding and fracturing continuously occurs. According to Suryanarayana (2001), deformation leads to a change in particle shape, cold-welding leads to an increase in particle size and fracture leads to decrease in particle size resulting in the formation of fine dispersed alloying particles in the grain-refined soft matrix. The powder particles are repeatedly flattened, cold-welded, fractured and re-welded until a steady state equilibrium condition is reached. Such condition refers to a balance reaction between the rate of welding (average particle size tends to increase) and the rate of fracturing (average particle size tends to decrease). Benjamin (1976) mentioned that smaller starting powder materials could resist deformation without fracturing and tend to be welded into larger pieces, with an overall tendency to drive both very fine and very large particles towards an intermediate size. In the early stage of MA, at least 15% of a ductile material is needed during MA process to act as a host or binder.

However, as many studies have been done on MA process, this requirement is no longer necessary as MA of employing fully brittle materials have been successfully performed

(Koch, 1991). The raw powders for MA process are usually commercially available pure powders having particle size in between 1-200 µm. The particle size of the starting powders is not a critical factor except that it should be smaller than the diameter of the grinding balls. This is due to the decreasing particle size of starting powders during MA with time and reaches a small value of a few microns only after a few minutes of milling process (Suryanarayana, 2001). There are three basic mechanism occurs during MA process of metallic powders including ductile-brittle system, brittle-brittle system and ductile-ductile system. A brief explanation regarding mechanical alloying mechanisms is discussed in subsequent section.

2.4.1 DUCTILE-DUCTILE SYSTEM

According to Benjamin (1976), true alloying only occurs with the presence of at least one component of ductile material (15%). This is because mechanical alloying represents repeated process of cold welding and fracturing in which cold welding process only proceeds with the existence of ductile material. The MA process involving ductile-ductile system is presented in the flowchart shown in Figure 2.7 (Suryanarayana, 2001).

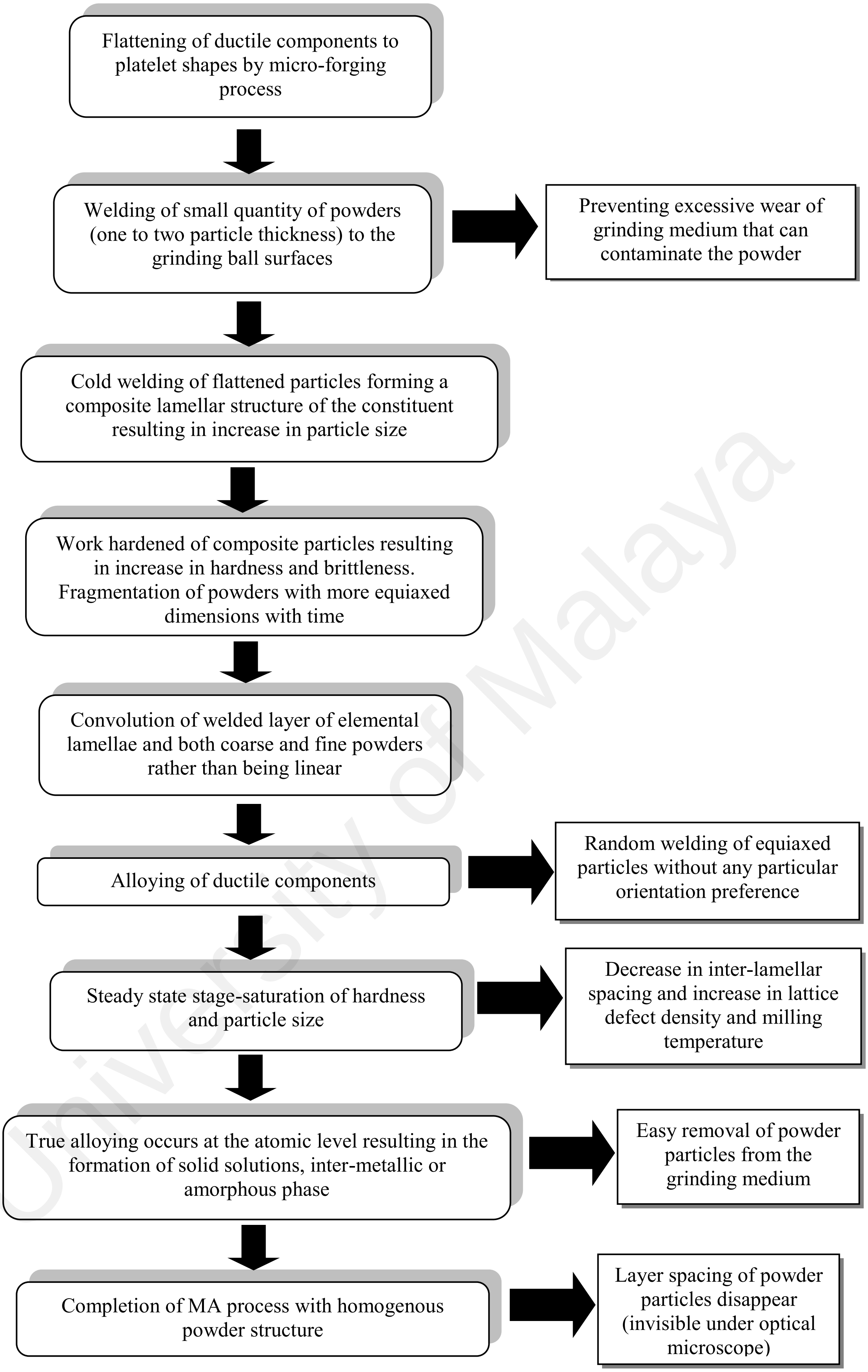

Figure 2.7 : Mechanical alloying mechanism of ductile-ductile component (Suryanarayana, 2001)

2.4.2 DUCTILE-BRITTLE SYSTEM

Initial stage of MA of ductile-brittle components involves deformation process of ductile particles and fragmentation of brittle particles by the ball to powder to ball collisions. Then, the ductile particles are flattened and welded together while brittle particles are trapped and embedded in the layer of ductile particles. With increasing milling time, layers of ductile particles become closer and finally become unresolved, with brittle phases were uniformly distributed as fine particles in the matrix of ductile phase. At this stage, the composition of the individual particles combine and cover the overall composition of the starting powder blend. After that, the lamellae get further refined resulting in the decrease in the inter-lamellar spacing. If brittle particles are insoluble in the ductile particles, the brittle particles remain disperse in these ductile powders. This could be attributed to the difference in the equilibrium solubility of brittle phase in the matrix phase.

In contrast, if the brittle phase is soluble, alloying occurs between both ductile and brittle components resulting in chemical homogeneity. Therefore, in order to achieve alloying during MA, the brittle component not only need to be fragmented to a small size to facilitate short-range diffusion, but also should acquire reasonable solid solubility in the ductile matrix component (Suryanarayana, 2001).

2.4.3 BRITTLE-BRITTLE SYSTEM

MA process of brittle-brittle components often resulted in amorphous composite material. As explained before, fragmentation of the brittle components occurs during the early process of MA resulting in decrease in the powder particle size. During MA of brittle-brittle components, the harder (more brittle) particles will undergo fragmentation process and are embedded in the softer (less brittle) particles. Although diffusion is an essential process in most MA systems, alloying did not proceed in brittle-brittle system at very low temperatures (liquid nitrogen medium). This is due to the longer diffusion distances required in the brittle-brittle granular compared to ductile-ductile lamellar geometry, and the enhanced diffusion paths provided due to plastic deformation in ductile-ductile system (Suryanarayana, 2001). Koch (1991) mentioned that possible mechanisms that may contribute to material transfer during milling of brittle components may include plastic deformation due to local temperature rise, micro-deformation in defect-free volumes, surface deformation, and (d) hydrostatic stress state in the powders during milling. Finally, instead of producing homogenous brittle powders particles, the MA powders appear to be composed of smaller particles cold-welded together (Davis and Koch, 1987).

Process variables or parameters involved during MA process are important in order to achieve the desired final product properties. Murthy and Ranganathan (1998) mentioned that the kinetics of alloying and other phase transformations resulted from MA process depend on the energy transferred from the balls to the powder during milling. The energy transfer is governed by many parameters such as milling speed, milling time, powder to ball ratio, milling atmosphere and process control agents (PCA's). It should be noted that these MA parameters are not completely independent and thus it is necessary to optimize the milling conditions. The effects of these MA parameters are explained in the subsequent sections.

2.4.4 MILLING SPEED

Milling speed is often associated with the energy input into the powders. Higher milling speed will result in higher input of energy and leads to the increase in the temperature of the vial. Homogenization or alloying of powders, acceleration of MA process, contamination of powders, decompositions of super saturated solutions or other meta-stable phases, increasing crystal size, and decreasing internal strain are among the effects of higher vial temperature due to higher milling speed of 300 rpm and above (Suryanarayana, 2001). Zi-Li et al. (2010) found that the milling speed affects the particle size, shape and distribution during MA of magnesium (Mg) and zirconium (Zr) powders. The authors reported that coarse microstructure with uneven powders distribution and higher porosity of Mg and Zr mixing was found at low milling speed of 280 rpm whereas these properties along with micro-hardness and bending strength were improved with increase in milling speed of 310 rpm.

However, as milling speed was further increased to 300 rpm, the microstructure was found to be coarser but still maintaining homogenous powder distribution with little porosity. On the other hand, Calka and Radlinski (1991) mentioned that mixing of Zr-Ni powders at higher milling speed (300 rpm and above) resulted in fully amorphous phases whereas a mixture of crystalline and amorphous phases were introduced during milling at low speed (<100 rpm) and intermediate speed (170 rpm to 260 rpm). Moreover, Khakbiz (2008) reported that finer Al particles (80 nm) were achieved with increasing milling speed (420 rpm) at any specific milling time. The author added that the minimum particle size (<60 μm) was obtained within shorter time of milling process at higher milling speed (420 rpm) compared to longer time (>10 hr) taken at lower speed (320 rpm). This indicates that a faster fragmentation-welding-fragmentation event in powders has occurred and the equilibrium has attained within shorter milling time at higher milling speed.

On the other hand, Zhang et al. (1993) stated that the temperature of the mixed powders increased at higher milling speed of 300 rpm resulting in even softer and more ductile behavior during mixing of different ductile powders due to excessive cold welding. This resulted in bigger particle size (0.5 mm) of ductile powders with larger amounts of the coarser size fraction. However, the author claimed that as milling speed was reduced to 150 rpm, the mixed powder particle size gradually decreased between 10 μm to 45 μm with uniform powder distribution.

2.4.5 MILLING TIME

Milling time is one of the important processing parameters during MA process to reach a balance reaction between fracturing and cold welding processes. The effects of milling time on powder mixing vary depending on the milling speed, the ball to powder ratio and the milling temperature. Crystallite size and lattice strain are often associated with milling time. A study done by Senthil-Kumar and Ahamed (2011) found that crystallite size decreased while lattice or internal strain increased with increasing milling time of 40 hr. Moreover, Shaw et al. (2003) supported that the reduction of grain size (14 nm) result in an increase in lattice strain. The authors added that the XRD peak also shifted to higher 2θ angle that indicates the formation of solid solutions and increase in the solute concentration. Moreover, Xiong et al. (2010) stated that the grain size of powder particles decreased with milling time (<10 hr) and leveled off at prolonged milling time (>30 hr) with increase in lattice strain. The authors also mentioned that the micro-hardness is enhanced with increased in milling time (48 hr) with equiaxed structure compared to laminar structure (severe agglomeration) at an early stage of milling.

2.4.6 MILLING ATMOSPHERE

Milling atmosphere is usually prepared to avoid or reduce contamination or oxidation of powders during MA process. Argon and helium gaseous are often used as milling atmospheres that have been evacuated or filled inside the milling medium. Regardless of this advantage, the use of inert gaseous as milling atmosphere often associated with trapping of inert gaseous inside the powder particles. This resulted in the production of defects known as interstitial atoms and bubbles that can degrade the mechanical properties (embrittlement) and density of the powders (Ohtaguchi et al., 2005). Nitrogen gas is also used as a milling atmosphere but it has an adverse reaction during milling of metal powders and leads to contamination of the mixed powders. Therefore, nitrogen gas is usually applied with intention to produce nitrides (Suryanarayana, 2001).

Siebeck et al. (2011) mentioned that similar effect as PCA’s can be observed with application of milling atmosphere in which cold welding, powder coarsening and excessive adhesion on the milling tools were greatly reduced with milling atmosphere. However, the use of milling atmosphere was found to contribute to the higher oxidation content of the powders. Furthermore, Ohtaguchi et al. (2005) stated that the use of milling atmospheres such as argon, helium, hydrogen, nitrogen, and vacuum were found to contaminate the powders mixing during MA in which later reduced the impact strength of the powders due to swelling at elevated temperature. The gaseous entrapment inside the powders was found difficult to be remove even with heat treatment process.

2.4.7 BALL TO POWDER WEIGHT RATIO

Ball to powder weight ratio (BPR) between 5:1 to 10:1 is generally used during MA process due to its effectiveness in promoting MA process (Xiong et al., 2010). BPR plays an important role in achieving a particular phase of milled powder with respect to milling time. The higher the BPR, the shorter the time needed for completing MA process (Xiong et al., 2010). This is believed due to the higher energy transfer between the collisions of balls on the powder thus accelerating the alloying process. The higher energy transfer indicates an increase in the formation of heat and affects the powder phases (resulting in mixture of amorphous and crystalline phases). At combination of low BPR and low milling speed, meta-stable phases might be formed. On the other hand, high BPA with combination of high speed often resulted in the formation of equilibrium phase (Suryanarayana, 2001). Xiong et al. (2010) discussed the effect of applying various BPR in which the average particle size of powders was found to decrease with increased in BPR. As BPR was further elevated, contamination of powders was significant with low powder yield due to the increase in times of collision of powders. A schematic view of motion of the ball and powder mixture during mixing is presented in Figure 2.8.

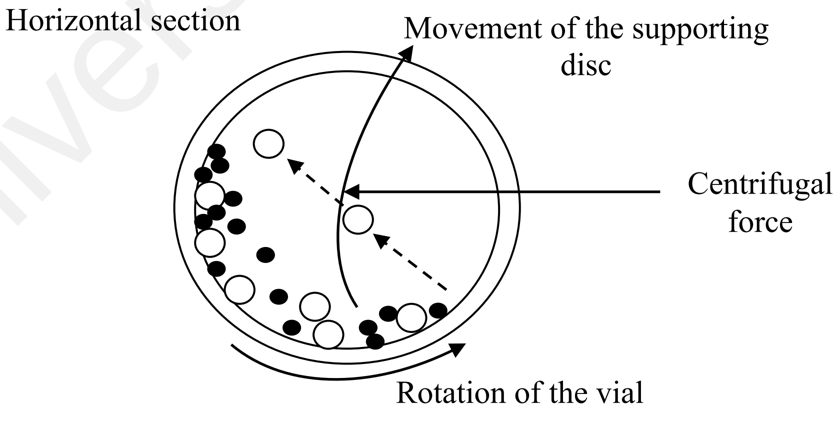

Figure 2.8 : Schematic view of motion of the ball and powder mixture (Suryanarayana, 2011)

Moreover, Zuyan et al. (1996) reported that during MA of metallic powders, broadening of XRD peak with decreasing intensity, grain size reduction, plastic strain enhancement and faster refinement of microstructure were evidenced with increasing value of BPR. They added that at higher BPR, the fine microstructures shorten the distance of inter-diffusion whereas low activation energy of powders due to the coupling effects of grain boundary and defects accelerated the alloying rate thus homogenous distribution of powders could be achieved at shorter time.

2.4.8 PROCESS CONTROL AGENTS (PCA's)

Milling of metallic powders or pre-alloyed powders can be carried out either in a dry or wet milling medium. Wet milling is referred to the milling process that involves a liquid medium whereas dry milling does not involve any use of liquid medium (Ramezani et al., 2012; Dehaqani and Akbari, 2010; Pei-heng et al., 2005). Many studies claimed that wet milling is more desirable to produce finer-ground products. This is associated to better absorption of solvent molecules on the newly formed surfaces of the particles (lower surface energy) that hinder agglomeration, homogenous powder particles distribution, higher powder yield, and faster amorphization rate (Ahn et al., 2008; Suryanarayana, 2001; Heng et al., 2005; Dehaqani and Akbari, 2010; Ramezani et al., 2012). Nevertheless, some studies also claimed that wet grinding contributed to the increase in the contamination of the powders mixing, slowing down the MA process, and changing the nature of the final milling products (Suryanarayana, 2001; Heng et al., 2005).

Wet milling is often associated with the use of surface-active substances or also known as process control agent (PCA's). In MA process involving soft materials or ductile materials like Al, chromium (Cr), copper (Cu), iron (Fe), Nickel (Ni), zinc (Zn) and Sn or combination of any these materials, PCA's are often introduced to avoid excessive cold welding of powder particles due to heavy plastic deformation (Ramezani et al., 2012; Dehaqani and Akbari, 2010; Heng et al., 2005; Suryanarayana, 2001). PCA's are added to achieve a balance process between cold welding and fracturing during MA to prevent agglomeration of ductile powders that lead to the increase in powder particle size. Dehaqani and Akbari (2010) reported that the absence of PCA's during MA of ductile powders resulted in alloying of larger powder particle size (0.5 cm). As ethanol is introduced as PCA's, the particle size of ductile powders greatly reduced even at longer milling time.

The PCA's can be in the form of solids, liquids and gaseous but in most cases PCA's are organic compounds. The amount of PCA's needed is one of the critical factor that will affect the MA process. Usually, PCA's content is applied between 1-5% of the total powder composition. The use of higher content of PCA's (>5%) generally leads to the pyrophoric reaction of metallic powders (self-ignition after MA process) and thus retard the overall milling process. On the other hand, the absence or insufficient content of PCA's often resulted in larger particle size of milled powder that indicates the absence of fracturing process (Zhang et al., 1999; Dehaqani and Akbari, 2010; Ramezani et al., 2012). Moreover, generally the PCA's will decompose during milling, interact with the powder and form compounds, and finally incorporated into the powder particles forming inclusions or dispersoids. Thus hydrocarbons containing hydrogen and carbon, and carbohydrates containing hydrogen, carbon, and oxygen are likely to introduce carbon or oxygen into the powder particles, resulting in the formation of carbides and oxides which are uniformly dispersed in the matrix (Suryanarayana, 2001). Ethanol. methanol and stearic acid are among the widely used of PCA's but polyethylene glycol, dodecane, ethyl acetate, toluene, oxalic acid, boric acid, borax, alumina, and aluminum nitrate have also been used (Dehaqani and Akbari, 2010; Heng et al., 2005; Ramezani et al., 2012).

On the other hand, dry milling is also often introduced during MA process (Blaskov et al., 1994). During milling under dry condition, mixing of two or more different powder elements often resulted in alloying of these materials forming composite material. Heng et al. (2005) discussed that during mixing of Fe and Ni powders under dry condition, alloying of these two elements are evidenced through disappearance of Ni peaks under XRD analysis. Therefore, it can be concluded that the use or absence of PCA's depends on the properties of the milled powders such as the cold welding characteristics, the powders final properties (particle size and shape) and composite powders fabrication in achieving a balance MA process.

In the fabrication of porous metals via powder metallurgy technique, space holder materials exploited to create porous structure in the metallic matrix. This technique depends on the temporary particles added to metallic matrix powder known as space holder particle or spacer that act as a pore former. The particles size and particle shape of space holder particle play an important role in developing porous structure. Macro pore sizes between 300 μm to 400 μm are usually produced by using space holder particle having particle sizes of 100 μm to 500 μm. According to Tuncer et al. (2011), larger particles sizes of space holder particle resulted in increase in macro pore interconnected size, greater percentage of total open porosity and greater pore wall thickness. These conditions could be attributed to larger packing coordination of bigger size space holder particles. In term of space holder particle shape, irregular shape of space holder often contribute to the decrease in compressive strength and elastic modulus of porous metals (Mutlu and Oktay, 2011; Bafti and Habibolahzadeh, 2010; Bakan, 2006).

Moreover, Wen et al. (2001) found that the use of carbamide particles having irregular (polygonal) shape resulted in different compressive flow stresses as compared to the spherical or rounded shape of carbamide particles even at the same porosity content. The authors suggested that it might be attributed to the remaining defects in the porous body after sintering. Jiang et al. (2005) also reported similar finding in which the use of irregular (strip) shape of space holder particle resulted in lower compressive strength and elastic modulus. Furthermore, the authors added that many defects and protuberances on the surface of the cell walls were observed with the use of irregular shape of space holder particle due to the rough surfaces of this material. Therefore, the cell walls collapsed easily prior to compaction. In addition, Zhang et al. (2005) discussed that higher ordered array of macro pores and interconnections in porous structure were obtained with the use of spherical space holder particle particularly at higher level of space holder particle amount. The authors also mentioned that the use of irregular (cubical) shape of space holder particle often resulted in an irregular porous structure due to inefficient geometrical packing structure.

There are different space holder particles being utilized in porous metal fabrication including sodium chloride (NaCl), PMMA, carbamide particle, titanium hydride particle, Mg powder, calcium carbonate ($CaCO_3$), ammonium bicarbonate and so on (Capek and Vojtech, 2013; Li and Lu, 2011; Ozan and Bilhan, 2008; Yu et al., 2007; Hussain and Suffin, 2011; Vendra et al., 2006). Among these space holder particles, carbamide, titanium hydride and ammonium bicarbonate particles are known to release harmful gases and residue to the environment during thermal decomposition. Because of this reason, decomposition of these space holder particles are usually carried out before or after sintering treatment via leaching in liquid (Bakan, 2006; Mutlu and Oktay; 2011; Bafti and Habibolahzadeh, 2010; Hussain and Suffin, 2011). Similar process applies to porous metal fabrication using NaCl spacer. In order to eliminate additional process to manufacture porous metal, PMMA spacer has been introduced in the current study. By utilizing PMMA spacer, subsequent process can be discarded due to easy thermal degradation of PMMA spacer as well as clean environmental sintering process can be obtained as PMMA material does not produces toxic gases and residues. On the other hand, the introduction of PMMA material as space holder particle can be beneficial as to date, only a few studies on porous Al fabrication using PMMA spacer via ball milling mixing technique have been reported. Therefore, different steps on porous metals fabrication with addition of PMMA as space holder potential can be explored. In brief, Table 2.4 concludes different factors affecting the mixing process between metallic matrix powders and space holder particle in fabrication of porous metal particularly for porous Al fabrication.

Table 2.4 : Various processing factors that affecting the mixing condition between metallic matrix powders and space holder particle

Metallic matrix powder	Space holder particle	Mixing equipment	Mixing duration	Binder	References
Aluminum	Carbamide	Rolling container	1 hr	Ethanol	Jiang et al., (2005)
Aluminum	NaCl	Three dimensional mixer	30 min	Not defined	Mustapha et al. (2011)
Aluminum, 0.15% Mg	NaCl	Manual	Not defined	Ethanol	Surace et al. (2009)
Aluminum	PMMA	V-blender	Not defined	Not defined	Xie et al. (2006)
Copper	Carbonate	Manual	Not defined	Ethanol	Zhao et al. (2005)
Aluminum, 1% Sn, 1% Mg	Carbamide	Rotary	2 hr	Ethanol	Hassani et al. (2012)
Iron, 10% Aluminum	NaCl	Manual	Not defined	Polyester Resin	Golabgir et al. (2014)
Aluminum	Polyvinylchloride	Manual	Not defined	Ethanol	Al-Grafi (2014)
Aluminum	NaCl	Ball Milling	1 hr	Ethanol	Hussain and Suffin (2011)

2.5 COMPACTION PROCESS OF METALLIC MATRIX POWDER AND SPACE HOLDER PARTICLE MIXTURE

Compaction process is done after mixing process to provide sufficient strength of green body in order to retain shape prior to sintering. An enhancement in sinter-ability of porous body is likely to occur after powder compaction due the absence of oxide film on the powder particle surface. According to Hao et al. (2008), compaction process disrupts this oxide film due to large shear strains, stress concentrations, scratching and jabbing by pressing the metallic matrix powder and space holder particles against one another under a given compacting pressure. This is important to ensure effective metallurgical bonding between metallic powder particles. In general, compaction process is defined as filling of controlled amount of powder into a die cavity with top and bottom pressing move to press the powder and followed by ejection of compacted powder from the die (Verma et al., 2012). During compaction process, a lubricant is commonly added to enhance the compact-ability, minimize tools damage and wear to reduce adverse effect of friction (Verma et al., 2012). In the current study, zinc stearate is applied at various compaction tools including its body, puncher and base material.

There are three stages of powder particles compaction in fabricating green compacts. The first stage of powder compaction involves rearrangement of powder particles. The rearrangement of powder particle is greatly affected by the particle size and particle shape (Verma et al., 2012; Sanchez et al., 2001; Chen et al., 2007). For instance, Sanchez et al. (2001) stated that small particle size powder (44 µm) usually contribute problems as compared to larger particle size powder (150 µm). According to the authors, this is due to higher surface area of smaller size powders in which resulted in longer times to fill the matrix, wear in die and tooling elements and decrease in productivity. In contrast, maximum green strength of 13 MPa was obtained with medium particle size of 74 µm due to the combination of particle morphology and number of bonds effects in the compacted samples (Sanchez et al., 2001). Moreover, Lund (1982) stated that the use of larger particle size powder is desired for mixing and compacting of powders due to increase in surface contact between powder particles, high level of density packing particles and higher micro-porosity. An increase in powder density is believed due to the elimination of spaces, bridges and gaps between powder particles (Lund 1982).

Compaction pressure also plays important role that affects the properties of porous metals. It is known that green density and green strength increased with increasing compacting pressures (Ozan and Bilhan, 2008; Bafti and Habibolahzadeh, 2010; Uzun and Turker, 2014). Wisutmethangoon et al. (2008) mentioned that increased in compaction pressures led to decreased in porosity and higher compressive strength of porous titanium (Ti) due to better packing density of mixed powders. Moreover, Ozan and Bilhan (2008) mentioned that higher compaction pressures often resulted in a decreased in porosity of porous Al. Dewidar et al. (2012) were in agreement with the findings of Ozan and Bilhan (2008). They found that higher compaction pressures (250 MPa and above) increased the relative density of both green and sintered compacts due to the decreased in particle space that inhibits the deformation of particle shape.

Furthermore, a study on porous Al3Ti-Al composite done by Inoguchi et al. (2009) found that uniform pore characteristics including porous structure and pore sizes were enhanced at higher compaction pressure of 165 MPa. Jabur (2013) found an important correlation between variation in compaction pressures with green density, bulk density, apparent porosity as well as water absorption on porous bronze fabrication. The author reported that the green density and bulk density of porous bronze increased with higher compacting pressure of 500 MPa. Such increase in green density could be attributed to the continuing and rearrangement of particles movement without reaching a steady state condition whereas an increase in bulk density might be due to the pores reduction with increasing contact regions that enhanced necking and diffusion between particles during sintering (Jabur 2013).

On the other hand, excessive compaction pressure is not desirable as it often contributed in changing of space holder particle sizes and shapes (Laptev et al., 2004; Kim et al., 2013; Arifvianto and Zhou, 2014). Laptev et al. (2004) described that fracture of ammonium hydrogen carbonate as space holder particle in a mixture of titanium matrix particles was observed under a compaction pressure above 350 MPa. This could be attributed to the critical stresses to fracture are surpassed by the compacting pressures in which locally transferred to the space holding particles (Laptev, 2004; Kim et al., 2013). Furthermore, Golabgir et al. (2014) revealed that NaCl space holder particles were collapsed at high compaction pressure. In addition, Jamaludin et al. (2013) claimed that total porosity decreased with increasing compaction pressures. The authors added that at higher compaction pressures, metallic matrix powders are in contact with each other and joined together in the subsequent sintering process. Therefore the formation of voids in the sintered powder is suppressed and thus reduced the porosity.

Arifvianto and Zhou (2014) mentioned that space holder particles act as bridge that separate metal matrix particles under a given compacting pressure. As compacting pressure increased, the metal matrix particles tend to compress space holder particles more strongly thus resulted in deformation of space holder particles. In other words, such condition occurred due to the compaction stress exceeding the elastic limit and critical strength of space holder particles. A study done by Jabur (2013) found that apparent density and water absorption of porous bronze decreased with increasing compacting pressures (200 MPa, 300 MPa, 400 MPa and 500 MPa) due to the reduction in the number and size of pores in green compacts and consequently in sintered compacted samples. The author added that a linear drop in water absorption level was found with increasing compacting pressures (200 MPa, 300 MPa, 400 MPa and 500 MPa) thus indicating that the volume fraction of pores may have reached a steady state condition.

Contrary, low compacting pressure (<300 MPa) are also detrimental as it may result in the collapse of porous body during sintering process (Jabur, 2013; Kim et al., 2013; Kotan and Bor, 2007; Golabgir et al., 2014). For example, Kotan and Bor (2007) stated that porous body could not remain intact after carbamide spacer removal below compaction pressure of 300 MPa. Moreover, Golabgir et al. (2014) mentioned that lower compaction pressure that is under 70 MPa resulted in a collapsed and spalling of metallic matrix powder during leaching process. Additionally, Zhao et al. (2008) reported that significant damage to the space holder particles occurred at higher compaction pressure of 150 MPa prior to sintering.

Different compaction techniques have been applied for porous metal fabrication including uniaxial compaction, isotacic compaction and injection molding (Jamaludin et al., 2013; Golabgir et al., 2014; Zhao et al., 2008; Umashankar et al., 2011; Mustapha et al., 2011; Manonukul et al., 2010; Michailidis et al., 2011; Rafter et al., 2014). Moreover, the compaction process of metallic matrix particles and space holder particles can be conducted at either room temperature (cold compaction) or elevated temperatures (hot pressing) (Umashankar et al., 2011; Mustapha et al., 2011; Manonukul et al., 2010). Uniaxial compaction is performed by the action of an upper punch at a constant velocity, while the lower punch does not move within the mechanical assembly (Figure 2.9) (Verma et al., 2012; German, 2005). Once the compaction is accomplished, the compacted powders or granular materials are ejected from the die. The compressibility and compact-ability effects of powder particles are two important characteristics associated with uniaxial compaction (Verma et al., 2012; German et al., 2005). Compressibility refers to the ability to reduce volume, while compact-ability is the ability to form particle bonding. Furthermore, uniaxial compaction is often applied for fabrication of simple shape components with limited length to diameter ratio of 5 to 1.

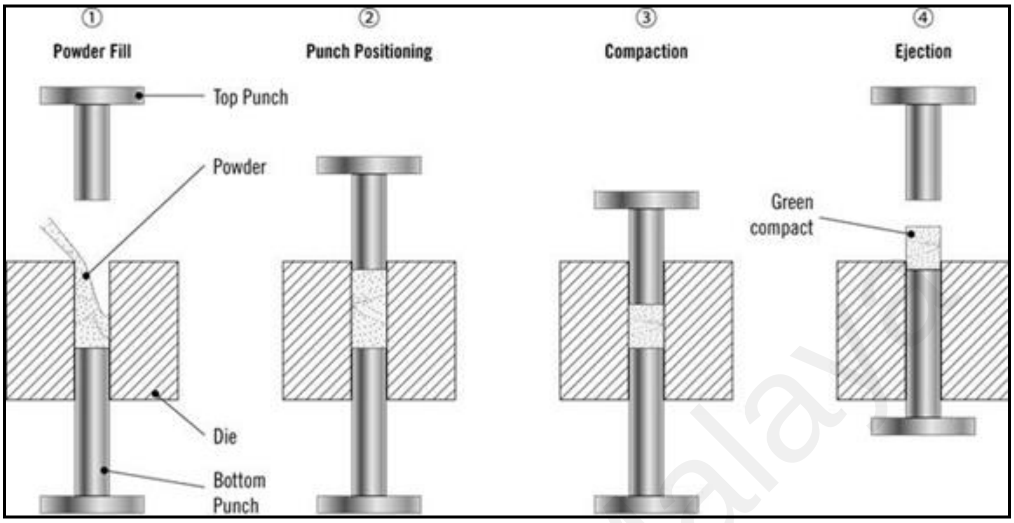

Figure 2.9 : Schematic diagram for stages in uniaxial powder compaction process (German, 2005)

Moreover, inter-particle friction and the friction between powder particles and die wall are the constraints corresponded to the uniaxial compaction in which led to variation in pressures and green density in powder compacts (Arifvianto and Zhou, 2014; Kwon et al., 1997; Kim et al., 1997). These limitations often resulted in the inhomogeneity of pore distribution in porous structure (Zhao et al., 2009; Li et al., 2005). Gilani et al. (2012) documented that cracking of porous samples at upper and lower section of cylindrical compacts occurred at higher compaction pressures prior to sintering. This phenomenon could be attributed to the effective stress at the upper and lower zones of the green compacts as compared to the middle zone in which resulted in the variations in density of these different zones (Wu et al., 2005). In other words, the upper and lower sections are denser than the middle section where cracking of porous samples are more pronounce at these sections particularly at higher compaction pressure. Therefore, the powder particles located in the zone with the lowest green density tend to collapse since the green strength is proportional to green density (Arifvianto and Zhou, 2014). In order to reduce the variations in pressure and green density, double action die compaction has been introduced in porous metals fabrication (Bakan, 2006; Bonaccorsi and Proverbio, 2006; Paulin, 2014). Two moving punches are used in double action die compaction from the end of the die to compact powder or granular materials from upper and bottom sides (Figure 2.10). This is done to achieve uniform densification over cylindrical powder compacts (Bonaccorsi and Proverbio, 2006; Kwon et al., 1997; Kim et al., 1997).

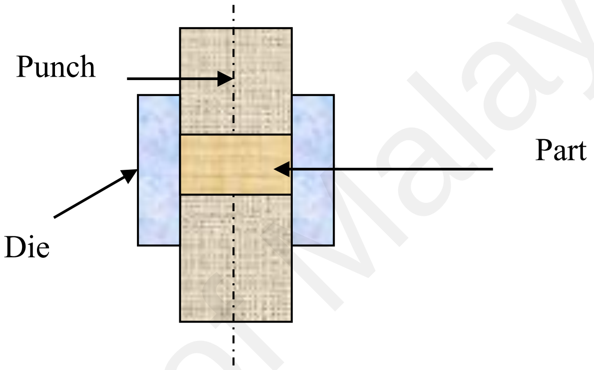

Figure 2.10 : Schematic diagram of double action die compaction

On the other hand, accomplishment of uniform distribution of pressure and green density can also be done under isostatic powder compaction (Umashankar et al., 2011). In this method, uniform pressure is applied simultaneously to all the external surfaces of flexible mold containing powder or granular materials with the presence of fluids (water or oil) to establish a powder compacts (Eksi and Saritas, 2002). Figure 2.11 demonstrates the schematic diagram of cold isostatic press (CIP) process. In addition, shape forming and densification involving powders and granular materials are combined in a single step with hot isostatic pressure (Mustapha et al., 2011) (Figure 2.12). This process therefore eliminates the need for higher sintering temperature to obtain fully densified porous body. Contrary, mass production of porous metals with complex shapes can be produced by using injection-molding process (Manonukul et al., 2010; Muhamad et al., 2012; Weise et al., 2013). This technique combines the conventional powder metallurgy and metal injection molding for the fabrications of components from powders.

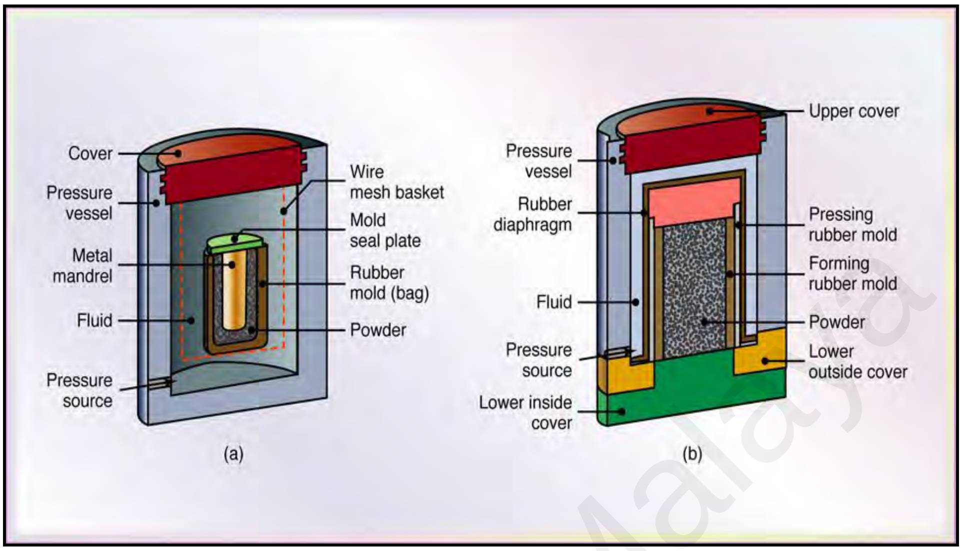

Figure 2.11 : Schematic diagram of CIP process for a) wet bag method and b) dry bag method (German, 2005)

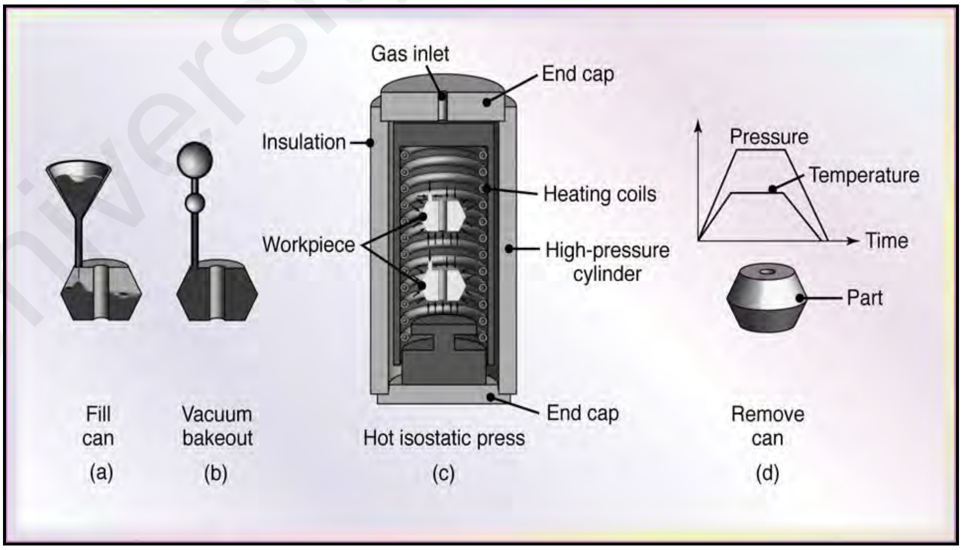

Figure 2.12 : Schematic illustration of HIP process (German, 2005)

2.6 REMOVAL OF SPACE HOLDER PARTICLE

To date, there are two common techniques applied to remove space holder particles known as sintering process and leaching in liquid process (Ozan and Bilhan, 2008; Xie at al., 2006; Hussain and Suffin, 2011; Jabur, 2013; Uzun and Turker, 2014). The current study utilizes the sintering process to remove space holder particles to develop porous body. Complete removal of space holder particles is necessary to achieve the required porosity as well as to avoid contamination of the space holder particles in the porous structure. The removal process for space holder particles is critical to ensure purity and structural reliability of porous body as well as to determine the geometry of macro pores in the porous network. The main problem associated with removal of space holder particles often contributed to the deviation in porosity from the design value due to entrapped particles of space holder residue in the porous body and collapsing of matrix particles during removal of space holder particles. Moreover, distortions of porous body including bloating, slumping and swelling often occur during space holder particles removal owing to the low structural integrity of porous network (Arifvianto and Zhou, 2014).

2.7 SPACE HOLDER PARTICLE REMOVAL BY SINTERING PROCESS

Sintering is defined as a thermal treatment for bonding particles into a coherent, predominantly solid structure via mass transport events that often occur on the atomic scale under the influence of an elevated temperature. The bonding of matrix particles leads in improving strength of green compacts. The framework of the porous structure is assembled through these bonded matrix particles. Moreover, densification of matrix particles occurs during sintering process in which resulted in increase of micro-hardness of porous body cell wall (Ozan and Bilhan, 2008; Hussain and Suffin, 2011). Thus, the mechanical properties of porous body are enhanced along with densification of matrix particles.

There are two types of sintering process known as solid state sintering and liquid phase sintering. In general, solid state sintering is defined as the densification of powder compact in a solid state at the sintering temperature while liquid phase sintering is referred to as the presence of liquid phase in the powder compact during sintering. On the other hand, Olevsky et al. (2004) defined solid state sintering as a thermally activated process of the matter transport driven by high surface energies of the aggregates of fine particles. This resulted in the decrease in the area of internal surfaces of powder compacts due to the redistribution of diffusion matter that leads to consolidation. In contrast, according to German et al. (2009), liquid phase sintering involves sintering under conditions where solid grains coexist with a wetting liquid.

2.7.1 SOLID STATE SINTERING

There three stages involve during solid state sintering including initial, intermediate and final stages. It should be noted that no grain growth could be observed during initial stage of sintering process. At first, necks formation between particles occurs until equilibrium or steady state condition is reached. It means that the contact area between particles increases from zero. At this stage, the compact shrinkage is between 2-3% at most. The second or intermediate stage of sintering involves densification from isolated pore state. As opposed to initial stage, grain growth begins to occur during intermediate stage.

Wide development of grain boundaries occurs at this stage with inter-connected and continuous pore networks. This indicates that grain boundaries are still isolated with no formation of continuous grain boundary networks even pore channels are exist. The intermediate stage completed once pores become isolated and grain boundaries form a continuous network. As isolated pores are located at grain boundaries or entrapped in grains, the final stage of sintering begins to develop. At this point, an increase in density can be observed along with rapid development in microstructure (grains growth) (Coble, 1961). A schematic illustration of stages in solid-state sintering is given in Figure 2.13.

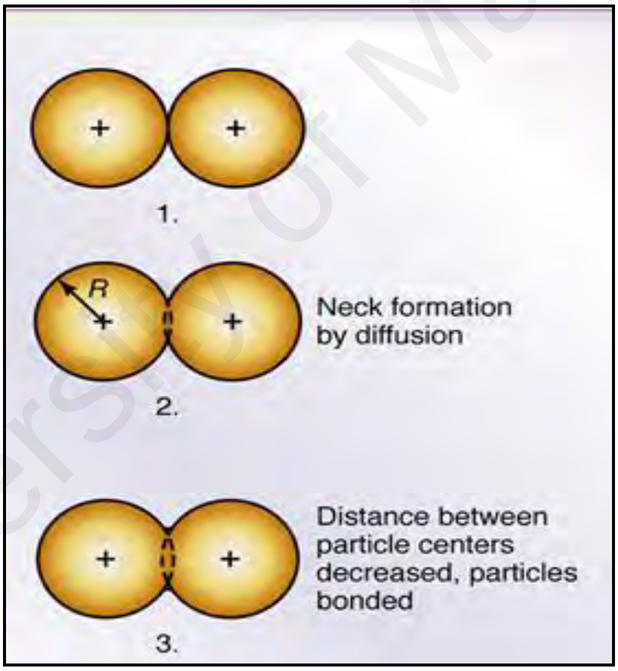

Figure 2.13 : Schematic illustration of stages in solid state sintering (Kalpakjian and Schmid, 2006)

2.7.2 LIQUID PHASE SINTERING

Liquid phase sintering is often associated with mixing of different powders in which the melting temperature of the primary constituent might be above the melting point of other constituent. Because of this condition, the sintering process takes place in the presence of a liquid phase. According to German et al. (2005), the mechanism involves during liquid phase sintering begins with solid-state sintering of solid grains upon heating. Different grain growth pathways are possible depending on the solid–liquid solubility relations. The common situation is for the liquid to wet the solid. In this case, penetration of newly formed liquid between the solid grains occurs followed by dissolution of sintered bonds and thus initiates rearrangement of grains during sintering.

As the liquid improves the transport rates due to the solid solubility in the liquid, grain coarsening and densification proceeded. An increase in surface energy due to the formation of pores leads to the destruction of pores itself with rapid coarsening and bonding of microstructure that resulted in increase in rigidity. Schematic diagram of liquid phase sintering mechanism is shown in Figure 2.14. Liquid phase sintering is advantageous as compared to solid state sintering in terms of better control of microstructure, low cost processing and ideal for sintering hard materials that cannot be manufactured by using other approaches like densification of tungsten carbide (WC) and cobalt (Co) cemented carbides, Cu and Sn and Fe and Cu (German, 2005).

In fabricating porous body, micro pores are not desired as they deteriorate the mechanical properties of porous body including decreasing in load bearing cross sectional area of cell wall in which reducing the compressive strength of porous body (Dabrowski et al., 2010; Laptev et al., 2004). This is believed to be due to the insufficient diffusion in the inter particle contact area and thus leading to incomplete sintering process. Therefore, careful control of sintering parameters like sintering time, sintering temperature and sintering atmosphere are important to overcome such problems. Details on the effects of sintering parameters on porous metal fabrication are discussed as below.

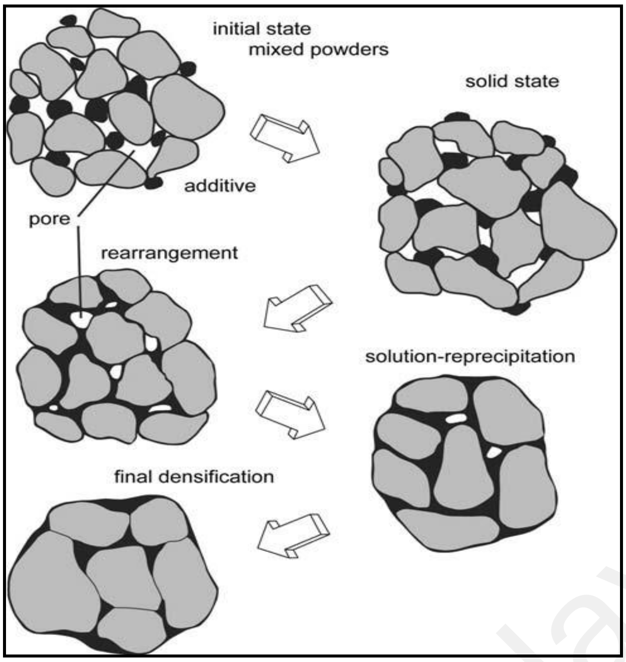

Figure 2.14 : Overview of liquid phase sintering mechanism involving two mixed powders (German, 2005)

It is important to note that as Al material was chosen as the base material for porous metal fabrication, the addition of additives or sintering aids are necessary as Al particle is always covered with Al_2O_3 coating. The Al_2O_3 coating is usually disrupted by adding sintering aids such as Sn or Mg or combination of these two materials (Katsuyoshi et al., 2007; Gokce and Findik, 2008; Sukiman et al., 2014). According to Sukiman et al., the presence of Sn can interrupt the oxide layers covered on the surface of Al particle by increasing the fluidity during sintering whereas Mg powder promotes segregation of Sn particles on the Al surface (Sukiman et al., 2014). Furthermore, acceleration of breaking the oxide layers can be realized with the addition of 0.1 to 1 wt. % of Mg (Gokce and Findik, 2008; Sukiman et al., 2014). Similar findings were reported by Katsuyoshi et al. (2007) where an enhancement in the sintered density was observed with the addition of 1 wt. % Mg thus enhancing the mechanical characteristics. In contrast, pressure assisted sintering (PAD) technique has also being applied to achieve fully sintered body of Al material without the need of sintering aid material (Mustapha et al., 2010 & 2011). However, this technique is not commonly used, as it is restricted to the type of space holder material that can be completely decomposed before or after sintering treatment. Accordingly, small content of Mg and Sn powders were applied in this study to promote liquid phase sintering of Al material.

2.7.3 SINTERING TEMPERATURE

The sintering temperature is normally set 100 °C below the melting point of metallic matrix powder (60-90% of melting temperature) (Wang and Zhang, 2008). It should be noted that excessive sintering temperature is undesirable as it may initiate partial melting and evaporation of certain elements including main, alloying or additive powders in the metallic matrix powders (Arifvianto and Zhou, 2014; Jiang et al., 2005). Surace et al. (2009) reported that at excessively high sintering temperature, globules formation were detected as some molten Al often oozes out from the surface of the compact. In developing porous structure, porosity usually decreases with increasing sintering temperature.

According to Esen and Bor (2011) and Oh et al. (2002), porosity of titanium, Ti alloy foam decreased linearly with increasing in sintering temperature. This might be due to the increases in the number of inter-particle contacts as well as enhancement in growth of particles necks in which led to the reduction of micro pore sizes and densification of Ti foam (Oh et al., 2002; Oh et al., 2003). Furthermore, a study done by Dewidar (2012) on porous 316 stainless steel also found that the density of sintered porous bodies increased with increasing sintering temperature. The author suggested that liquid phase sintering assisted densification prior to increasing sintering temperature. According to Jiang et al. (2005), compressive strength of Al foam was found to increase with increasing sintering temperature due to the better binding among Al particles.

2.7.4 SINTERING TIME

Similar findings as sintering temperature were reported with sintering time. According to Bafti and Habibolahzadeh (2010), the compressive strength of Al foam improved with increasing sintering time. Such increase could be attributed to the better diffusion and bonding between different constituents in the system. Moreover, Sharma et al. (2011) mentioned that micro-hardness of the cell wall was found to increase with reduction in pore sizes at prolong sintering time. In other word, densification of porous body occurs at longer sintering time. Moreover, Capek and Vojtech (2013) also reported that flexural strength of porous Mg improved at longer sintering period. Furthermore, Mutlu and Oktay (2011) discussed that the compressive strength and Young modulus of chromium (Cr) / silicon (Si)/ Ni/molybdenum (Mo) steel foam enhanced with increasing sintering time. This is believed to be due to the densification of the cell walls. It is important to note that less sintering time is required in liquid phase sintering as compared to conventional solid state sintering due to the faster diffusion of sintering additives in the metallic matrix particles during sintering (Bafti and Habibolahzadeh, 2010).

2.7.5 SINTERING ATMOSPHERE

Sintering process for most of porous metals commonly carried out under protective sintering atmospheres. Protective sintering atmospheres is important due to the involvement of large surface area, involvement of temperature between 60-90% of melting temperature, preventing oxidation and promoting reduction of surface oxides (Kang, 2005). In addition, contamination in the sintering furnace and exposure to atmospheric always occur air during sintering. Contamination is critical as it reduces the properties of porous body. This contamination could be from the presence of oxygen (O), carbon (C) and nitrogen (N_2) after sintering process. Moreover, the selection of appropriate sintering atmospheres has been reported to enhanced density, strength of metallic bonds between particles, rounding pores as well as reduces porosity, defects and homogenizes the structure (Marcus et al., 2003).

Dewidar (2010) mentioned that an increased in sample density was observed for all various sintering atmospheres including nitrogen, argon and vacuum. This finding however contradicted with the findings reported by Ardakani et al. (2013). The authors stated that shrinkage or densification with significant dimensional changes of sintered porous samples was found to increase under nitrogen atmosphere along with increasing sintering temperature while minimum shrinkage was obtained under vacuum atmosphere. They also added that higher strength, wear resistance and hardness of sintered porous samples were observed under nitrogen atmosphere as compared to argon and vacuum atmospheres. Krug and Zachman (2009) also reported similar results in which higher tensile strength but lower ductility of injection molded 316L stainless steel powders sintered were achieved under N_2 atmosphere as compared to argon and hydrogen atmospheres.

Despite the importance of sintering process variables, materials properties such as particle size, particle shape, particle structure, particle composition and green density also play significant role in determining the final properties of sintered products. Particle size affects the sintering rate mechanism in which larger driving force is trigged by smaller particle size powder due to smaller pore. This often resulted in greater surface area (higher surface diffusion), small grain size (greater grain boundary diffusion) and larger inter-particle contact area to volume diffusion. A study done by Paul et al. (2012) stated that smaller particle size of cobalt powder decomposed at much lower temperature resulted in low sintered density. It means that, smaller particle size initiates faster sintering rate compared to larger particle size. This is due to the oxidation resulted from high surface area that covers the particles thus reducing the diffusivity and in turn sinter-ability.

On the other hand, particle shape affects the sintering process by providing greater intimate contact between particles and increased internal surface area. This led to the increase in macro or micro surface roughness. Lin and Hwang (2009) stated that spherical powder yielded the highest permeability and sintered density, followed by the dendritic-shaped powder and the irregular-shaped powder. In term of particle distribution point of view, a fine grain structure can promote sintering due to its desirable effects on several material transport mechanisms. Spierings et al. (2011) reported that fine particles (55.54 μm) of stainless steel powder are easy to be melted at lower temperature and resulted in higher density and mechanical strength. In contrast, bigger particles gave higher elongation at fracture under tensile mode.

Nevertheless, Liu et al. (2011) stated that larger range of powder particle size (0 to 45 μm) generated higher density while narrower range of powder particle size (15 to 45 μm) gave better flow-ability, higher ultimate tensile strength (UTS) and larger hardness. Moreover, particle composition can affect the sintering kinetics in which dispersed phases within the matrix may promote sintering by inhibiting grain boundary motion whereas impurities and base metal or alloying elements reaction at relatively high sintering temperature (near the melting point) may result in undesirable sintered properties. Lindsley et al. (2005) discussed that the addition of 0.6% of graphite into the base Fe resulted in the smallest shrinkage whereas further addition of graphite content (1%) increased the shrinkage level. Moreover, the addition of Cu into Fe and graphite alloy only resulted in little shrinkage but with further addition of Cu amount

(2%), the shrinkage was found to decrease. The interaction between Cu and carbon in graphite was identified to affect the shrinkage of Fe alloy due to the inhibiting effect of C content on copper distribution.

Finally, green density and sintered density also affected the driving force during sintering According to Upadhyaya (2002), higher green density material often associated with higher sintered density. Chhillar et al. (2008) mentioned that higher green density (58% of theoretical density (TD)) often resulted in a higher sintered density (96% of TD) particularly at higher sintering temperature of 1400 °C. This is believed to be due to the higher diffusion rates at higher temperatures that allow large inter-agglomerate pores to be removed. In contrast, at lower temperatures, the diffusion kinetics is much slower, thus result in difficulty in removing large pores even when sintered for several hours.

In overall, to give better understanding regarding the abovementioned fabrication process in porous metals development using space holder material, schematic flow diagram of porous metals processing is presented in Figure 2.15.

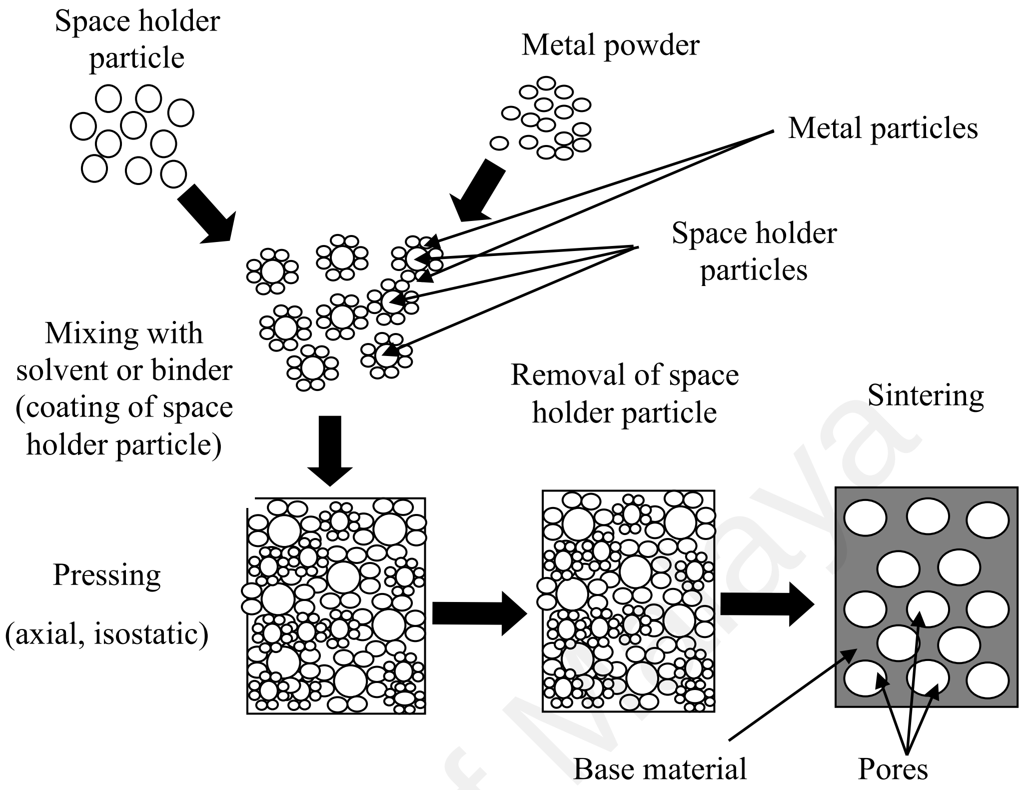

Figure 2.15 : Schematic flow diagram of porous metals fabrication involving space holder particle (Bram et al., 2000)

2.8 OPTIMIZATION OF PROCESSING PARAMETERS

To date, there are many potential techniques to optimize the processing parameters for fabrication of porous materials as well as non-porous materials including factorial design, response surface, mixture design, crossed design and so on (Surace et al., 2009 & 2010). Among these techniques, factorial design particularly Taguchi robust design has been widely implemented for the selection of optimum processing parameters (Surace et al., 2009 & 2010). In brief, Dr Genichi Taguchi proposed the Taguchi design to improve the quality of manufactured goods and extensively applied in the fields of engineering, chemicals, pharmaceuticals, marketing and advertising (Surace et al., 2010). The Taguchi design is unique in terms of cost and time saving (Pachal and

Bagesar, 2013). In this technique, lesser number of experiments is required prior to optimization of processing parameters due to simplification of experimental design and feasibility of interaction study between various parameters (Kamaruddin et al., 2004). It is important to note that, before an experiment is conducted using Taguchi robust design, an experimental design needs to follow the following steps:

1) Independent variables selection
2) Number of level settings for each independent variable selection
3) Orthogonal array selection
4) Assigning the independent variables to each column
5) Conducting the experiments
6) Analyzing the data
7) Inference

In this Taguchi design, orthogonal arrays (OAs) have been employed in experimental plan to study the effects of the entire processing parameters through the small number of experiments (Cicek et al., 2012). This OAs are highly fractionated factorial design having a special set of design consists of tables of numbers to determine the least number of experiments needed for a given set of factor (Roy, 2010). In other words, OAs are a matrix design consists of numbers arranged in rows and columns in which each row symbolizes a specific factor that can be changed from each other. This Taguchi matrix is actually originated from the classical full factorial arrays. The factors in OAs can be evaluated independently as the OAs is balanced to ensure that all levels of all factors are considered equally. Moreover, Taguchi robust designed have been developed to investigate factors at two level, three level, four level and even mixed level (Roy, 2010). Considering many choices of OAs, each of these arrays are destined for a specific number of independent design variables and levels. For example, L_9 OAs can be applied for four different independent variables having three set values (level values). In this context, the letter L symbolizes the OAs in Latin square (Kacker et al., 1991). Table 2.5 illustrates an L_9 orthogonal array (OA).

Table 2.5 : Layout example of L_9 orthogonal array

L_9 (3^4) Orthogonal array					
	Independent Variables				**Performance parameter value**
Experiment Number	Variable 1	Variable 2	Variable 3	Variable 4	
1	1	1	1	1	p1
2	1	2	2	2	p2
3	1	3	3	3	p3
4	2	1	2	3	p4
5	2	2	3	1	p5
6	2	3	1	2	p6
7	3	1	3	2	p7
8	3	2	1	3	p8
9	3	3	2	1	p9

In this OA, there is total number of nine experiments to be conducted and each experiment is based on the combination of level values as shown in Table 2.5. In general, OAs can be categorized into standard OAs, extended OAs, mixed OAs and column-merged OAs. Moreover, this design also emphasizes on the multiple factors to determine the most influential factor, the least influential as well as the average influential factors that affect the performance of experimental design (Unal and Dean, 1991). It should be noted that the technique of defining and investigating all possible conditions in an experimental plan involving multiple factors is known as the design of experiments (DOE) or factorial design (Roy,2010). The analysis of the main effect is performed based on the average output value of quality characteristic at each parameter level (Kamaruddin et al., 2004).

In short, it can be said that Taguchi robust design aimed to adjust the processing parameters (control factors) to the optimum levels such that the system response is robust that is, insensitive to noise factors (Pachal and Bagesar, 2013). These noise factors are defined as the factors that influence the response of a process but cannot be or impossible to control (Roy, 2010). Weather conditions, machinery wear, human interference or imperfection are among the possible prime sources for the variations (Roy, 2010). In order to study the influence of these noise factors with the least number of repetitions, a signal to noise (S/N) value has been introduced prior to obtain the end-result that is minimally affected by noise factors. Different ways to compute the (S/N) value for different conditions are listed as follow:

1) Smaller-the-better characteristic

$$S/N_i = -10\log\left[\frac{1}{n}\sum_{j=1}^{n} y_{ij}^2\right] \tag{2.1}$$

2) Larger-the-better characteristic

$$S/N_i = -10\log\left[\frac{1}{n}\sum_{j=1}^{n} 1/y_{ij}^2\right] \tag{2.2}$$

3) Nominal-the-best characteristic

$$S/N_i = -10\log\left[\frac{1}{n}(S_{ni} - V_i)/V_i\right] \tag{2.3}$$

Analysis of variance (ANOVA) using Pareto ANOVA is then utilized to investigate the relative influence of the factors as well as possible interactions between these factors (Roy, 2010). In this analysis, Pareto principles are introduced based on the simplification of ANOVA method (Rajesh and Venkatesh, 2014). The results of the parameter design can be analyzed in a quick and easy method with absence of ANOVA table. The important factors and interactions are then studied by Pareto-type analysis. This analysis selects the optimal levels of the control factors within the test range of levels for specific targeted functions without affecting any constraint on the other functions. An advanced optimization technique should be applied in the case of any level beyond the test range variables.

2.9 POTENTIAL APPLICATION FOR POROUS ALUMINUM

Depending on the level of porosity as well as structure (open –celled or closed-cell), porous Al can be potentially applied in structural fields such as heat exchanger, filters, flame retardant and silencers as well as in functional fields including crash energy absorption, sandwich panels and noise control (Banhart, 2001; Byakova et al., 2012; Kavei, 2015). Porous metals in general can absorb more energy compared to dense metals due to their capability on maintaining peak stress while absorbing kinetic energy (Tingvall, 2010). Additional advantage of porous metals relies on its irreversible capability in converting absorbed energy into plastic deformation energy. On the contrary, dense Al usually converts the stored energy in the regime of reversible linear elastic stresses under the same stress level as porous metals after the removal of the applied loads (Baumesiter et al., 1997). It is important to note that the typical deformation pattern for closed-cell porous metals can be divided into three distinct stages including: (1) a linear elastic region at the beginning of the deformation where cell wall bending and face stretching occur; (2) a plateau region that is characterized by a plastic deformation at a nearly constant flow stress and (3) a final densification region where the flow stress abruptly increased (Amsterdem et al., 2006; Yu et al., 2007; Liu et al., 2008; Li et al., 2013; Nesic et al., 2014). An example of compressive stress-strain curve for porous metals as previously reported in the literature is presented in Figure 2.16 (Goel et al., 2014).

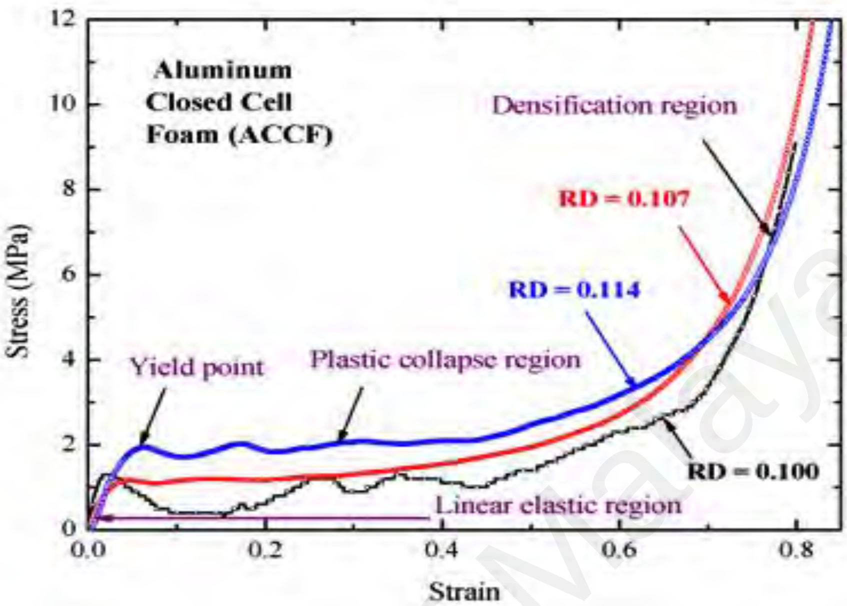

Figure 2.16 : Stress-strain curve of porous Al (Goel et al., 2014)

According to Alizadeh and Aliabadi (2012), the energy absorption ability of porous metals during compressive deformation is described as the energy required for deformation of porous specimen up to a specific strain. It has been reported that porosity and relative density (ρ^{*}/ρ_{s}), which is the ratio of the density of the porous specimen (ρ^{*}) to that of the solid (ρ_{s}), are important factors in determining energy absorption capacity of porous metals due to the fact that higher porosity of porous specimen provides porous metals with greater ability to maintain a constant plateau stress during plastic deformation of porous metals (Baumeister et al., 1997; Ashby et al., 2000; Yu et al., 2007; Qiao et al., 2008). In a study of Grilec et al. (2012), they mentioned that Al foams with higher porosity level that consequently contributes to longer plateau region (>40% strain) can result in higher amount of energy absorption capacity. In addition, Ashby et al. (2000) reported that porous metals with an ideal energy absorption capacity possess the longest plateau deformation up to a limiting nominal strain due to higher porosity level that can absorb most energy before reaching the densification stage.

On the contrary, higher energy absorption capacity of porous metals associated with higher relative density at comparable porosity level can be attributed to higher plateau stress as a result of higher relative density (Yu et al., 2007; Luo et al., 2007; Alizadeh and Aliabadi; 2012). This phenomenon has been reported in the studies of Yu et al. (2007), Qiao et al. (2008), Luo et al. (2010) and Alizadeh and Aliabadi, (2012). According to Yu et al. (2007), higher energy absorption capacity of porous metals with respect to higher relative density can be attributed to higher content of the parent metal that resulted in higher yield and fracture strength during deformation stage (Yu et al., 2007). The authors also added that sufficient amount of porosity is however necessary to achieve higher energy absorption capacity. An increased in energy absorption capacity of porous metals is also documented in the study of Qiao et al. (2008) in which energy absorption capacity of porous sintered fiber metals increased from 7.17 to 25.75 MJ/m^3 with increasing relative density from 0.177 to 0.355 under similar porosity level. Based on these facts, it is reasonable to deduce that porous metals with higher porosity and relative density (higher plateau stress) can dissipate more energy during compression. Therefore, an investigation on the energy absorption capacity of porous Al in the current research has been done by evaluating the area under the compressive stress-strain curve of the resultant porous Al mainly for porous specimen having the highest porosity level with considerable physical and compressive properties. Moreover, the relationship between the energy capacity, porosity, relative density (ρ^*/ρ_s) and plateau stress has also being studied in the present research.

SUMMARY

An overview of the porous metals background had been presented in this chapter. Depending on the connectivity of the cells, porous metals could be classified as either having open-celled or closed cell. In line with this, porous metals could be applied in the functional and structural applications as either energy absorber, sound absorber, filters or heat exchanger. Processing of porous metals involved mainly either solid state or liquid state in which details background on the solid state process (powder metallurgy) was discussed in this chapter. Processing conditions including equipment, binder as well as conditions of mixing, compaction and sintering that play important contribution in obtaining good quality of porous metals were also discussed in this chapter. In addition, porous metals as energy absorber potential was also described in details along with the factors that influence their potential as energy absorber. It had been found that most studies had been successfully developed porous metals using high melting point of metallic materials such as titanium, copper and stainless steel with combination of low decomposition temperature of space holder materials mainly PMMA to minimize any possible reaction with the parent material. In contrary, low melting point of metallic material that was Al had been introduced in the current study as a base metal with the utilization of PMMA spacer to produce closed-cell porous structure with low to medium porosity level (<50 wt. %) that can be applied in the field of energy absorption.

CHAPTER 3: MATERIALS AND METHODS

3.1 INTRODUCTION

This section introduces the experimental procedures, equipment used and characterization techniques for porous Al specimen. In general, porous Al was fabricated via powder metallurgy technique. This technique involves mixing of metallic matrix powder and space holder particle followed by compaction process and finally sintering of compacted specimen. Under this powder metallurgy technique, similar compaction method but different processing conditions such as mixing equipment, binder types, sintering profiles and optimization techniques were utilized in the preparation of closed-cell porous Al. Specifically, this research has been divided into two phases that are Phase 1 and Phase 2. In Phase 1, high energy mixing by planetary ball milling equipment, ethanol binder, single step sintering profile and Taguchi robust design for optimization of processing parameters were exploited for porous Al fabrication. Processing parameters such as space holder content (40 wt. %, 45 wt. % and 50 wt. %), compaction pressure (200 MPa, 250 MPa and 300 MPa), sintering time (1.5 hr, 2 hr and 2.5 hr) and sintering temperature (450 °C, 475 °C and 500 °C) were varied to evaluate the flexibility of porous Al fabricated in Phase 1. Based on the findings in Phase 1, different range of space holder content (20 wt. %, 25 wt. % and 30 wt. %) were selected whereas ranges of compaction pressure and sintering time remained as in Phase 1.

In addition, different approach of powder preparation prior to closed-cell porous Al fabrication was implemented in Phase 2 by utilizing low energy mixing equipment such as table-top ball mill and turbular shaker, oil binder, two steps sintering profile and full set of experimental design for optimization of processing parameters. On the other hand, supplementary studies on the variation of Sn content and sintering temperature were also performed in Phase 2 to investigate the sintering quality of passive Al material prior to fabrication of porous Al. The selection of optimum sintering temperature was made based on the physical characteristic (oxidation level, slumping, cracking, bloating and collapse of porous body), morphology and oxidation level of the resultant porous Al at 30 wt. % of PMMA. The optimum sintering temperature obtained was then set constant followed by optimization of other processing parameters such as PMMA content, compaction pressure and sintering time. In contrast, the optimization Sn content was made based on the physical body assessment, densities and morphology of sintered Al and porous Al at 30 wt. % of PMMA. Moreover, the resultant porous Al specimen that exhibited the highest porosity level with considerable physical and compressive properties was selected for further study as energy absorber potential.

Characterizations of porous Al specimen fabricated in Phase 1 and Phase 2 were performed by utilizing density measurement (Archimedes principle), X-ray diffraction (XRD) analysis, field emission scanning electron microscopy (FESEM) equipped with energy dispersive x-ray spectroscopy (EDS) and compression test. Details on the fabrication process, equipment used and characterization techniques of porous Al fabricated using Phase 1 and Phase 2 is presented in the following sections. Finally, the effects of processing parameters on the porosity level, densities, morphology and compressive behavior of closed-cell porous Al fabricated in Phase 1 and Phase 2 were also examined.

3.2 MATERIALS SELECTION

Similar starting materials were used for the fabrication of porous Al in Phase 1 and Phase 2 and the details are listed as below.

All the materials unless otherwise stated were purchased from NovaScientific resources (M) Sdn Bhd (Malaysia). Aluminum (Al) (99.9% purity, ~45 μm particle size), magnesium (Mg) (99.9%purity,~10 μm particle size) and tin (Sn) (99.5% purity, ~45 μm particle size, Sigma Aldrich, Malaysia) powders were used as the starting powders whereas polymethyl metacrylate (PMMA) micro-bead (99.9% purity, ~150 μm particle size) was served as the space holder material. The topography of metallic matrix powders and space holder particle used in this study was observed under FESEM. In the present research, small content of Mg powder and Sn powder were used as the sintering aids to assist Al in liquid phase sintering. Small content polyethylene glycol (PEG) having 400 molecular weight (Mw) used in Phase 1 and crude oil of low sulfur content called CLE-safe oil used in Phase 2 were introduced as binder to lessen powder mixture segregation in the mixing stage. Table 3.1 summarizes the starting materials used in this study.

Table 3.1 : The starting materials and its properties based on the manufacturer data

Material	**Particle Size (μm)**	**Density (g/cm^3)**	**Particle Shape**	**Melting point (°C)**	**Supplier**
Al	~45	2.7	Spherical and irregular	660	Nova Scientific Resources (M) Sdn Bhd Purity: 99.9%
Mg	~10	1.74	Spherical	650	Nova Scientific Resources (M) Sdn Bhd Purity: 99.9%
Sn	~45	7.31	Irregular	232	Sigma-Aldrich Incorporation Purity: 99.5%
PMMA	~150	1.19	Spherical	160	Nova Scientific Resources (M) Sdn Bhd Purity: 99.9%
PEG-400 (Mw)	Liquid	-	-	8	Sigma Aldrich (M) Sdn Bhd
CLE-safe oil	Liquid	-	-	80	JX Nippon Oil and Energy, Japan

3.3 FABRICATION PROCESS OF POROUS ALUMINUM USING PHASE 1 ROUTE

Porous Al with porosity level between 30 wt. % and 50 wt. % has been fabricated in Phase 1. Details on the fabrication process that involved mixing, compaction and sintering are discussed in the following sections. For better understanding, a flowchart diagram showing the fabrication of porous Al in Phase 1 is presented in Figure 3.1.

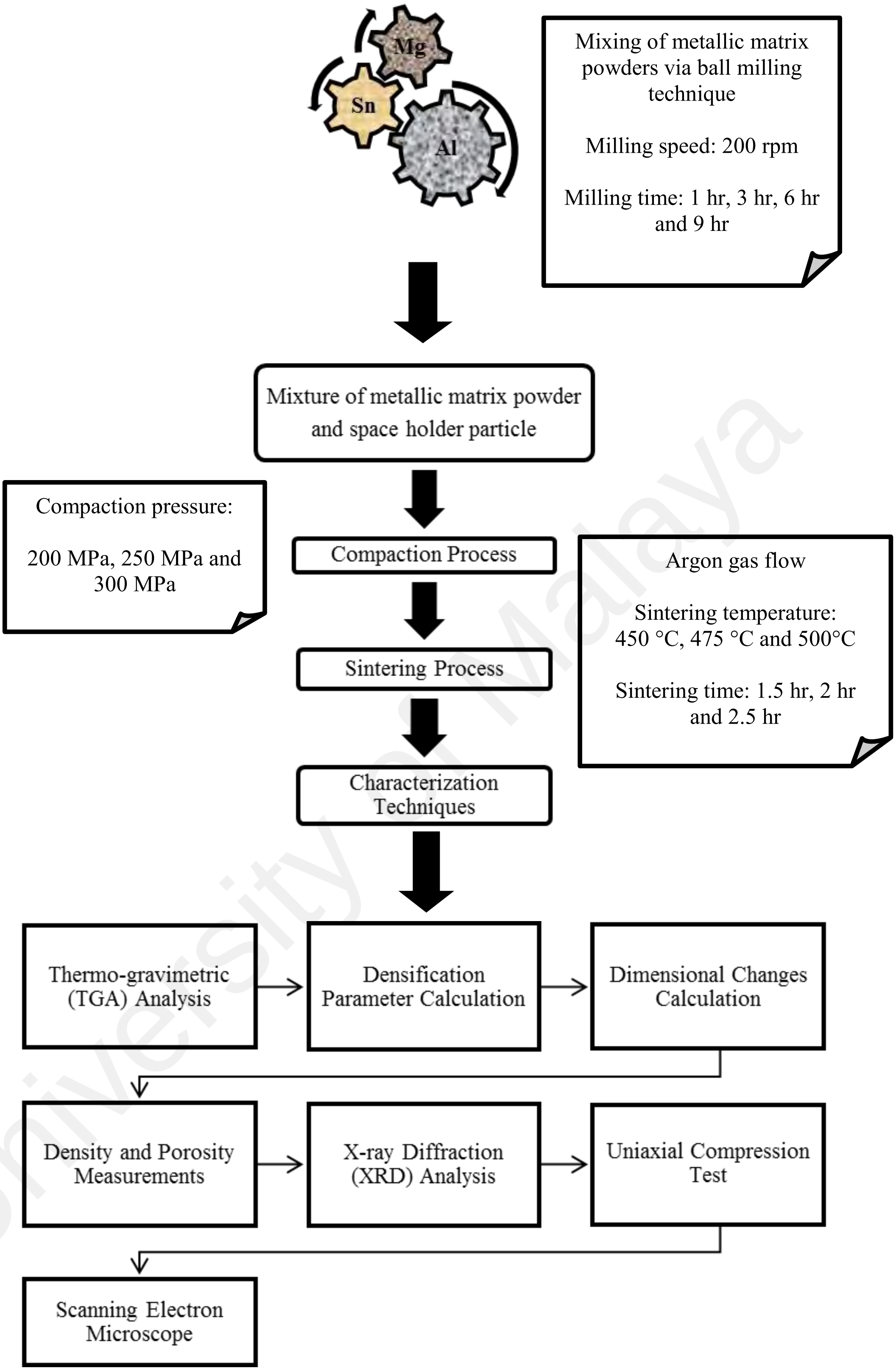

Figure 3.1: A flowchart diagram of porous Al fabrication in Phase 1

3.3.1 PROCESSING PARAMETERS

Processing parameters play an important role in determining the quality of porous Al specimen. In Phase 1, the amount of Mg and Sn powders were fixed at 0.5 wt. % and 1 wt. %. The variations in processing parameters rely on the space holder particle content, compaction pressure, sintering time and sintering temperature. In Phase 1, in situ mixing between metallic matrix powder and space holder particle was adopted with variation in mixing time (1 hr, 3 hr, 6 hr and 9 hr) while the mixing speed was set constant at 200 rpm. The optimum mixing time needed to obtain homogenous mixing between metallic matrix powder and space holder particle was selected based on FESEM analysis and XRD analysis and set constant for other various processing parameters including PMMA content, compaction pressure, sintering time and sintering temperature. Details on the optimum mixing time for porous Al fabrication were discussed in the next section. The variety of processing parameters applied in this phase is tabulated in Table 3.2.

Table 3.2 : Processing parameters for fabrication of porous Al in Phase 1

Processing Parameters **Number**	**PMMA Content (wt. %)**	**Compaction Pressure (MPa)**	**Sintering Time (hr)**	**Sintering Temperature (°C)**
1	40	200	1.5	450
2	45	250	2	475
3	50	300	2.5	500

3.3.2 MIXING PROCESS

Metallic matrix powder consisted of Al, Mg and Sn were mixed with space holder particle via high-energy planetary ball milling equipment (Fritsch, Alemania) (see Appendix A). At this stage, the amount of space holder particle was varied between 40 wt. %, 45 wt. % and 50 wt. % as given in Table 3.2, whereas the mixing time varied between 1 hr, 3 hr, 6 hr and 9hr. Before the mixing process proceeded, the amount of metallic matrix powder and space holder particle was weighed using electronic digital balance. The amount of metallic matrix powder and space holder particle needed for the mixing process was based on the ball to powder ratio. At this mixing stage, ball to powder ratio of 3:1, ball diameter of 20 mm, ball material of tungsten carbide and 250 ml capacity of stainless steel vial were fixed throughout the experiment. In order to prevent overheating, the high-energy ball milling is stopped periodically for every 30 minutes and resumed after 30 minutes. A total of 2 wt % of PEG-400 was added as binder to prevent segregation of metallic matrix powder and space holder particle during the mixing process. Argon (Ar) gas was supplied to the vials for about 10 minutes before the ball mill takes place to minimize contamination of metallic matrix powder and space holder particle mixture from O_2 and C gases. Finally, once the milling process ended, the mixture of metallic matrix powder and space holder particle was obtained in the form of paste due to the presence of PEG binder.

3.3.3 COMPACTION PROCESS

Conventional uniaxial powder compaction was selected for compaction purpose between metallic matrix powder and space holder particle mixture. The compaction process proceeded once the mixing process between metallic matrix powders and space holder particle completed. In this part, a rigid cylindrical die was used under an applied pressure along one axis at maximum substantial load of 25 tons. About 1.6 g of metallic matrix powders and space holder particle mixture was then poured into cylindrical die having dimensional diameter of 10 mm. Zinc stearate material was applied as lubricant during compaction process to minimize friction between the punch and die wall as well as between powder mixture particles and die wall to facilitate ejection of compacted specimen. Then, the metallic matrix powder and space holder particle mixture was compacted to the desired pressure using hydraulic hand press (Specac, United Kingdom) (see Appendix A). The compacted specimen was then held inside the die for 5 minutes before the compacted green body ejected out of the die. The measurement for diameter and thickness were taken using digital vernier caliper and the weight of the compacted specimen was taken using electronic balance for density measurement reason. The same compaction process was repeated for various compaction pressures as mentioned in Table 3.2. Furthermore, for each processing parameter, at least three compacted samples were prepared.

3.3.4 SINTERING PROCESS

Sintering process was the final step in fabrication of porous Al specimen. Sintering of compacted specimen was performed in a tube furnace (LT Furnace, Malaysia) under an inert atmosphere using argon gas flowing throughout the furnace during the entire sintering process (see Appendix A). In this process, the heating rate was fixed at 1 °C/min while the sintering temperature and sintering time were varied as illustrated in Table 3.2. In the current study, single step sintering profile was selected for sintering of compacted specimen. The compacted specimen was heated at various sintering temperature (450 °C, 475 °C and 500°C) which is above the degradation temperature of space holder particle to ensure complete removal of these space holder particles. After that, the specimen was held constant at different sintering time (1.5 hr, 2 hr and 2.5 hr) followed by cooling process in the tube furnace under an argon atmosphere. The schematic diagram for single step sintering profile is shown in Figure 3.2. On the other hand, a schematic diagram showing the fabrication of porous Al in this study is presented in Figure 3.3.

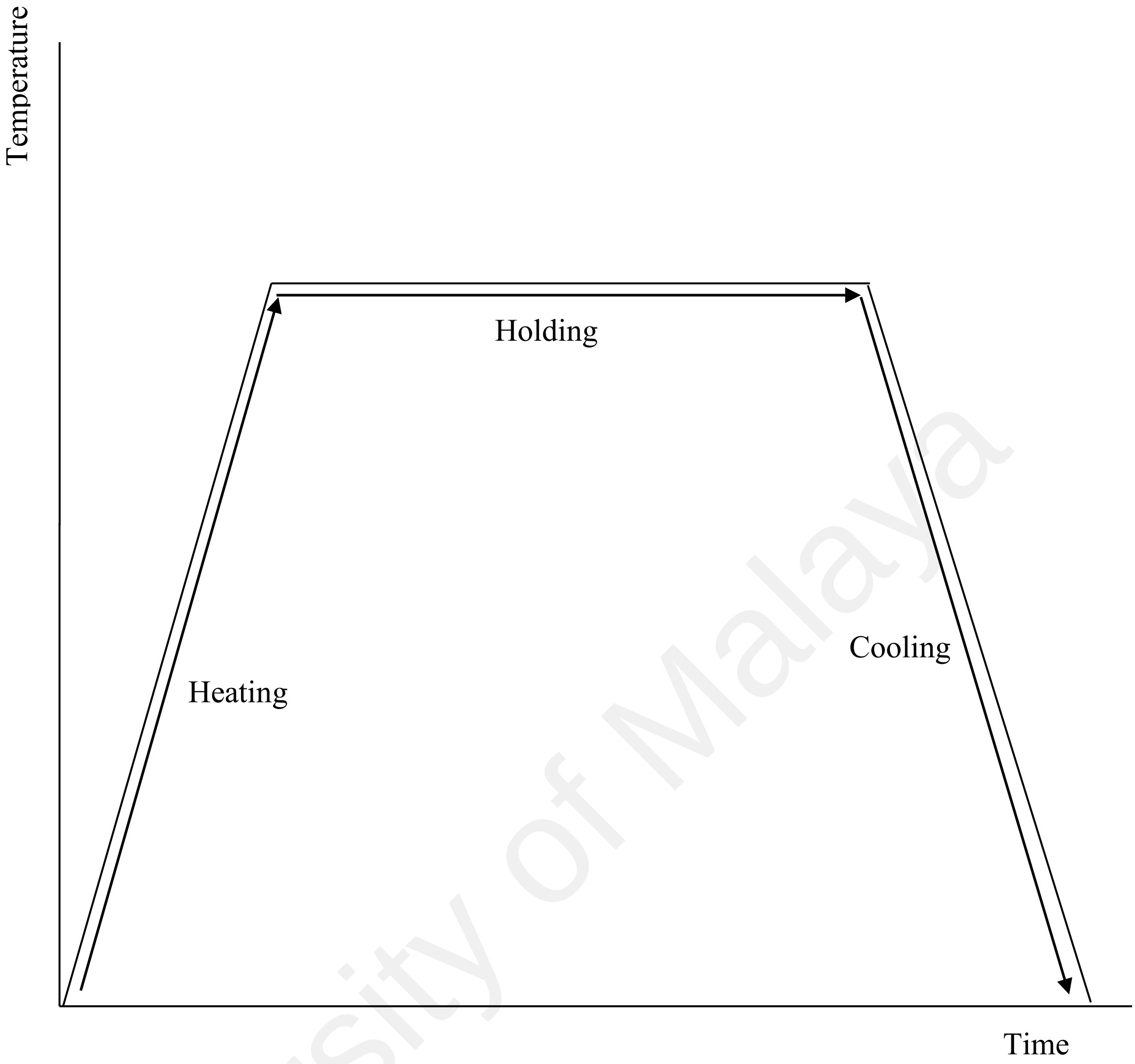

Figure 3.2 : Single step sintering profile adopted in Phase 1 for porous Al fabrication

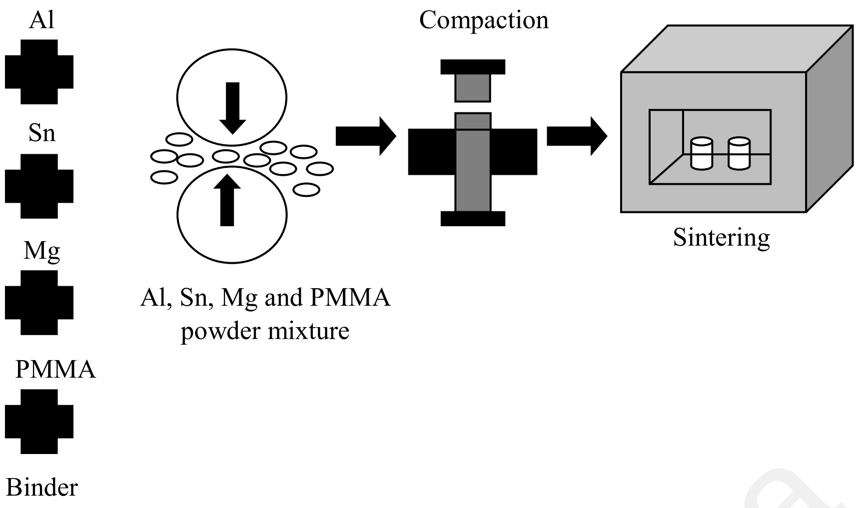

Figure 3.3 : Schematic representation of porous Al preparation in Phase 1

3.3.5 OPTIMIZATION OF PROCESSING PARAMETERS

Taguchi's robust design was applied to obtain optimum experimental condition in Phase 1 for porous Al fabrication. The main goal of utilizing Taguchi's parameters design was to obtain higher porosity with a balance in physical and compressive properties. The diagram for factor-characteristic relationship is illustrated in Figure 3.4. There are four control parameters and one interaction that were considered under this phase. The list of control parameters is shown in Table 3.3. In this Taguchi's parameters design, L_9 (3^4) orthogonal array was implemented in the current study as depicted in Table 3.4. Other than control parameters, there are other important parameters of factors known as noise factors. According to Wysk et al. (2000), noise factors are difficult, impossible, or too costly to control. Therefore, three replications were used for each set of experimental conditions to minimize the effect of noise factors. The potential noise factors that discovered to influence porous Al fabrication is revealed in Table 3.5. Moreover, the actual design using Taguchi orthogonal array in this study is demonstrated in Table 3.6. Finally three output parameters namely as porosity, overall density and compressive strength were classified to identify the optimum processing parameters. The outline of these output parameters is shown in Table 3.7.

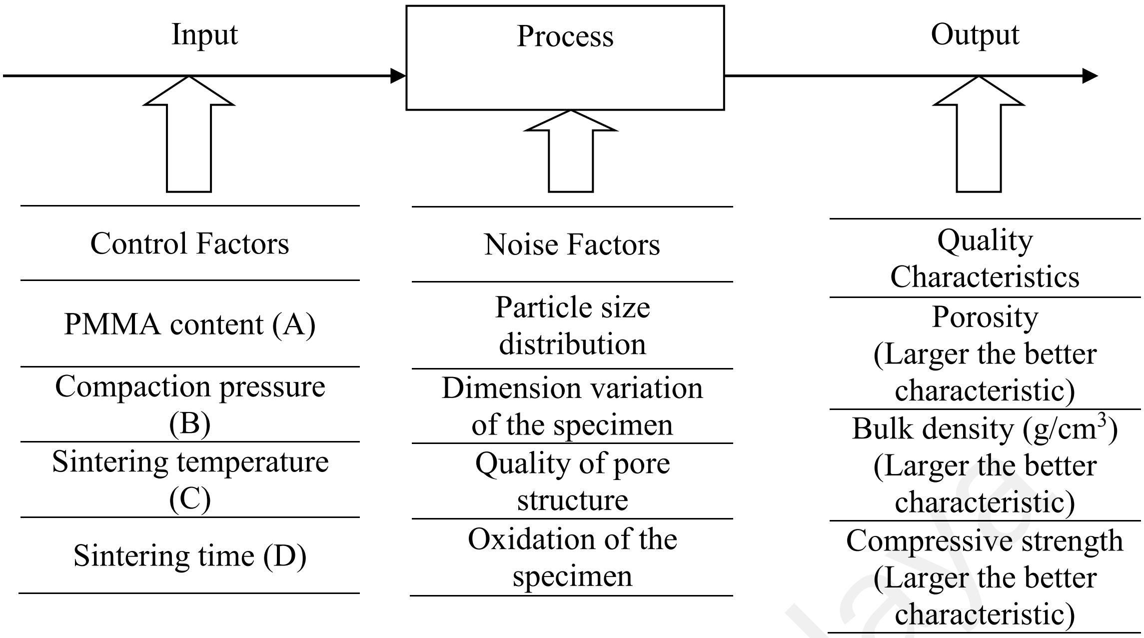

Figure 3.4 : Factor characteristic relationship diagram

Table 3.3 : List of level setting for control parameters

No	**Processing parameters**	**Level 1**	**Level 2**	**Level 3**
1	A : PMMA content (wt. %)	40	45	50
2	B : Compaction pressure (MPa)	200	250	300
3	C : Sintering temperature (°C)	450	475	500
4	D : Sintering time (hr)	1.5	2	2.5

Table 3.4 : Orthogonal array for $L_9\,(3^4)$

		Control Parameters				**Responses (Repetitions)**			
Number	**Sequence of Experiment Run**	**A(1)**	**B(2)**	**C(3)**	**D(4)**	**R1**	**R2**	**R3**	**Signal to Noise Ratio, S/N (dB)**
1	7	1	1	1	1	Y_{11}	Y_{12}	Y_{13}	S/N(1)
2	2	1	2	2	2	Y_{21}	Y_{22}	Y_{23}	S/N(2)
3	9	1	3	3	3	Y_{31}	Y_{32}	Y_{33}	S/N(3)
4	4	2	1	2	3	Y_{41}	Y_{42}	Y_{43}	S/N(4)
5	1	2	2	3	1	Y_{51}	Y_{52}	Y_{53}	S/N(5)
6	3	2	3	1	2	Y_{61}	Y_{62}	Y_{63}	S/N(6)
7	6	3	1	3	2	Y_{71}	Y_{72}	Y_{73}	S/N(7)
8	8	3	2	1	3	Y_{81}	Y_{82}	Y_{83}	S/N(8)
9	5	3	3	2	1	Y_{91}	Y_{92}	Y_{93}	S/N(9)

Table 3.5 : List of potential noise factors in porous Al fabrication

Number	**Parameters**
1	Particle size distribution
2	Dimension variation of the specimen (thickness, length and weight)
3	Quality of pore structure
4	Oxidation of the specimen

Table 3.6 : Actual experimental design based on Taguchi orthogonal array for porous Al fabrication focused on high energy mixing technique

Number	Sequence of Experiment Run	Factors			
		A	B	C	D
1	7	40 wt. %	200 MPa	450 °C	1.5 hr
2	2	45 wt. %	200 MPa	475 °C	2 hr
3	9	50 wt. %	300 MPa	475 °C	2.5 hr
4	4	50 wt. %	250 MPa	450 °C	2 hr
5	1	40 wt. %	300 MPa	500 °C	2 hr
6	3	45 wt. %	300 MPa	450 °C	2.5 hr
7	6	40 wt. %	250 MPa	475 °C	2.5 hr
8	8	50 wt. %	200 MPa	500 °C	2.5 hr
9	5	45 wt. %	250 MPa	500 °C	1.5 hr

Table 3.7 : Output parameters for porous Al fabrication

Number	Output parameters	Characteristic
1	Porosity	Larger the better characteristic
2	Overall density	Larger the better characteristic
3	Compressive strength	Larger the better characteristic

3.4 FABRICATION PROCESS OF POROUS ALUMINUM USING PHASE 2 ROUTE

Porous Al with porosity level between 10 wt. % to 30 wt. % has been fabricated in Phase 2. Details on the fabrication process that involved mixing, compaction and sintering are discussed in the following sections. For better understanding, a flowchart diagram showing the fabrication of porous Al in Phase 2 is presented in Figure 3.5.

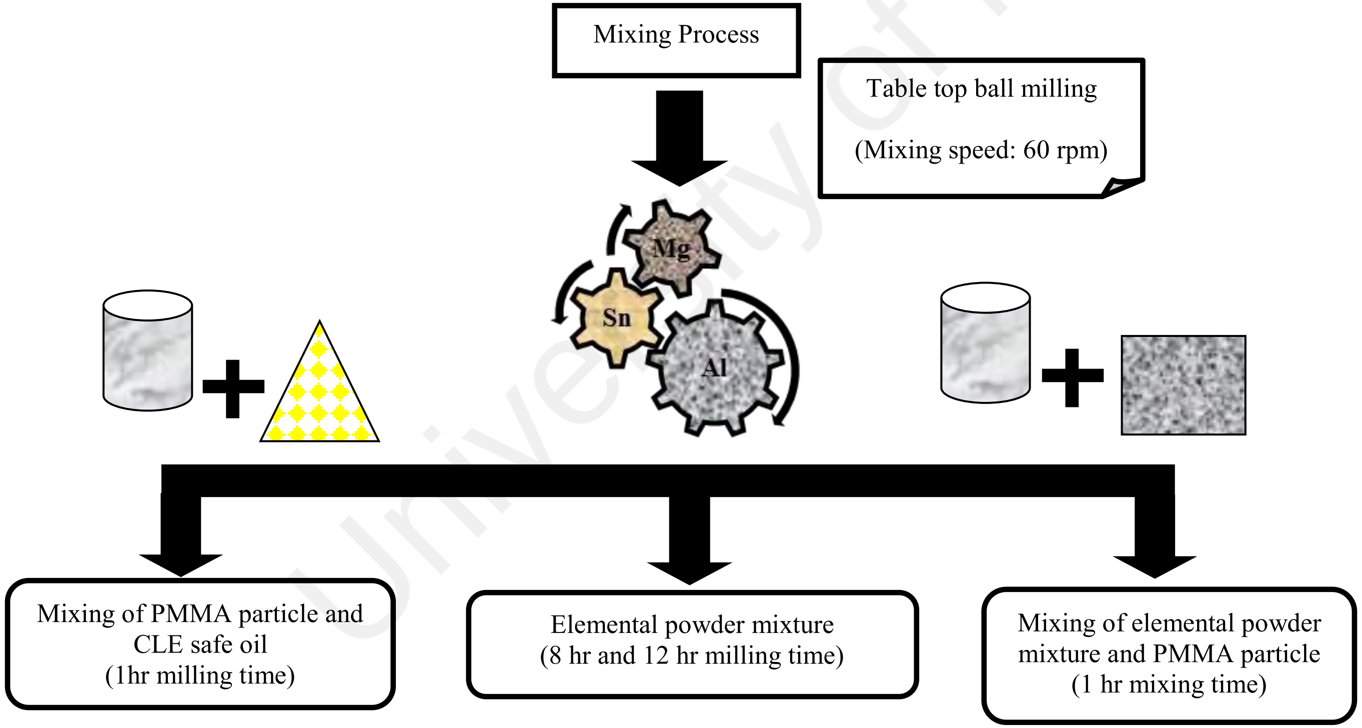

Figure 3.5 : A flowchart diagram of porous Al fabrication in Phase 2

‘Figure 3.5, Continued’

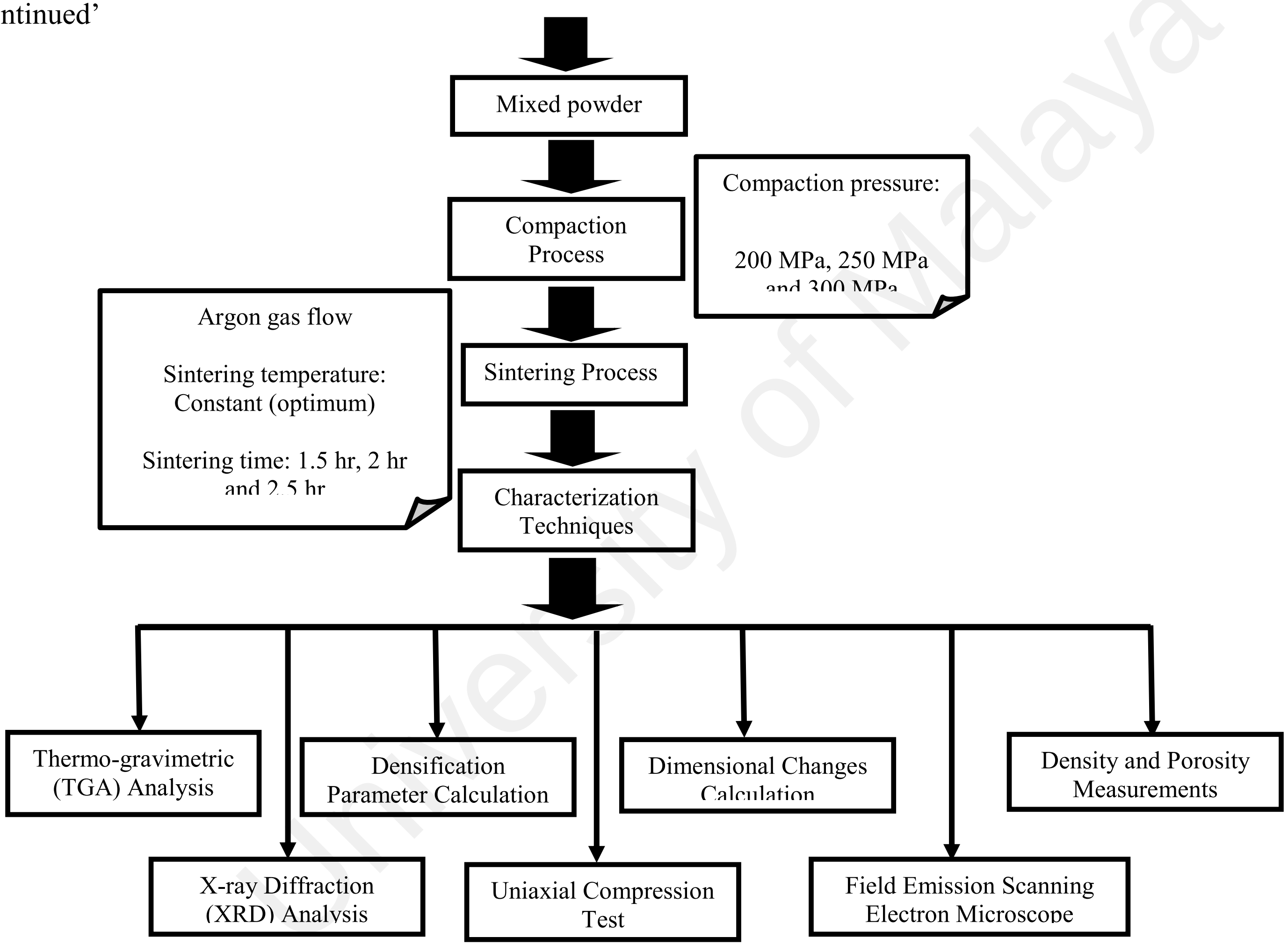

Figure 3.5 : A flowchart diagram of porous Al fabrication in Phase 2

3.4.1 PROCESSING PARAMETERS

In Phase 2, low energy mixing process using table-top ball mill equipment was employed during the mixing stage. Before mixing process proceeded, preliminary studies on the variation of Sn contents and sintering temperatures were performed prior to porous Al fabrication. Details on these preliminary studies that involved the variation of Sn contents and sintering temperatures were discussed in the following section. On the other hand, three mixing stages were adopted during mixing process prior to porous Al fabrication. The first mixing stage involved elemental powder mixture preparation, the second mixing stage involved mixing of PMMA particle and binder whereas the final mixing stage involved final powder preparation. The optimum time needed for elemental powder mixture preparation during the first mixing stage was selected based on the morphological examination using FESEM analysis equipped with energy dispersive x-ray diffraction (EDS). The selection of optimum mixing time was necessary to obtain uniform powder mixture. Details on the mixing process were discussed in the following section. In Phase 2, the variations of processing parameters rely on the space holder particle (PMMA) content, compaction pressure and sintering time. Table 3.8 presents the processing parameters applied in Phase 2.

Table 3.8 : Processing parameters for fabrication of porous Al in Phase 2

Processing Parameters **Number**	**PMMA Content (wt. %)**	**Compaction Pressure (MPa)**	**Sintering Time (hr)**
1	20	200	1.5
2	25	250	2
3	30	300	2.5

3.4.2 SUPPLEMENTARY STUDIES

Supplementary studies on the variation of Sn contents and sintering temperatures were done prior to porous Al fabrication. The contents of Sn powder were varied between 1.5 wt. %, 2 wt. % and 2.5 wt. % at fixed Mg content of 0.5 wt. %. Moreover, the sintering temperatures were varied between 580 °C, 590 °C and 600 °C. The effects of Sn contents on the physical characteristic, densities and morphology of sintered Al and porous Al at 30 wt. % of PMMA were investigated. The selection of optimum sintering temperature was made based on the physical characteristic (oxidation level, slumping, cracking, bloating and collapse of porous body), morphology and oxidation level of the resultant porous Al at 30 wt. % of PMMA.

3.4.3 MIXING PROCESS

Three stages mixing were applied in Phase 2. The first mixing process was performed by mixing different metallic material powders that consisted of Al, Sn and Mg powders prior to elemental powder mixture preparation using table-top ball milling equipment (Capco, United Kingdom). The image of table-top ball milling equipment is shown in Appendix A. At this stage, the mixing time was varied between 8 hr and 12 hr whereas the mixing speed was set constant at 60 rpm. The ball to powder ratio of 10 to 1, ball diameter of 20 mm, ball material of alumina and 500 ml capacity of polypropylene (PP) container were fixed during this process. The first mixing stage was done to select the optimum mixing time in order to obtain homogenous mixing prior to elemental powder mixture preparation. XRD analysis was performed to monitor phase and particle size changes associated with different mixing time. The second stage of mixing involved mixing of different content of PMMA spacer and 1 drop of CLE-safe oil using table-top ball mill to promote the adhesion of elemental powder mixture on PMMA particles and to create uniform agglomerates. The content of PMMA spacer was varied between 20 wt. %, 25 wt. % and 30 wt. %. Final mixing process that involved mixing of elemental powder mixture and PMMA spacer exploited the use of three dimensional (3D) turbular shaker mixer (Eskens, Netherlands) at constant mixing time of 1 hr (see Appendix A). The resultant mixture of elemental powder mixture and PMMA spacer was known as final powder mixture. Before these three stages of mixing proceeded, the amount of Al, Mg, Sn and PMMA spacer was weighed using electronic digital balance. The morphology of elemental powder mixture prepared in the first mixing stage and the final powder mixture prepared in the last mixing stage was analyzed using FESEM equipped with energy dispersive x-ray diffraction (EDS).

3.4.4 COMPACTION PROCESS

Similar compaction process as in Phase 1 was adopted in Phase 2. Details on this compaction technique can be found in section 3.3.3.

3.4.5 SINTERING PROCESS

In this process, similar sintering process was utilized as in Phase 1 as stated in section 3.3.4. The differences are on the sintering profile in which two steps sintering profile was used as well as sintering temperature. Due to poor sintering quality of the resultant porous Al obtained in Phase1, different sintering profile and sintering time was adopted in Phase 2. In addition, a supplementary study on sintering temperatures variation was made in which only one sintering temperature was selected based on the physical inspection of porous Al body as mentioned in section 3.4.2. Once the optimum sintering temperature was determined, this sintering temperature was set constant with respect to other processing parameters including PMMA content, compaction pressure and sintering time. The flowchart diagram for two steps sintering profile was plotted in

Figure 3.6 while the schematic diagram showing the fabrication of porous Al in Phase 2 is presented in Figure 3.7.

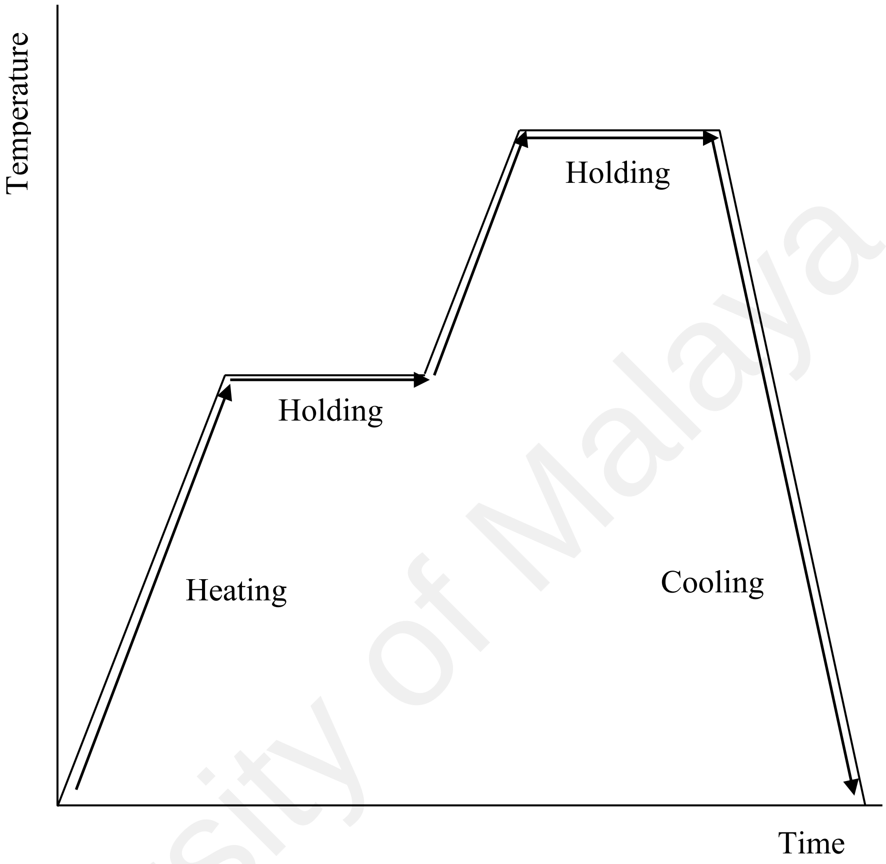

Figure 3.6 : Two steps sintering profile adopted in Phase 2 for porous Al fabrication

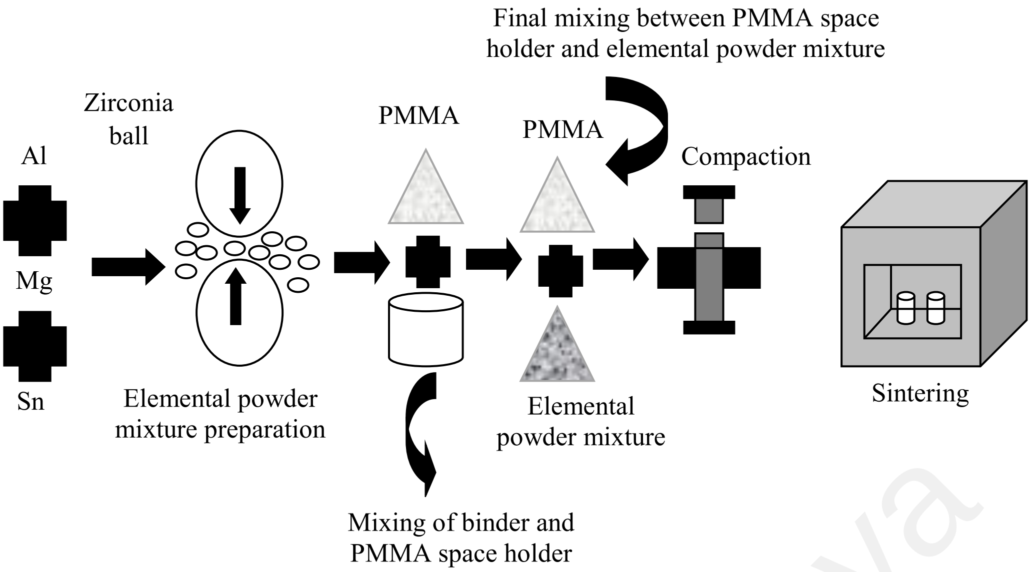

Figure 3.7 : Schematic representation of porous Al preparation in Phase 2

3.4.6 OPTIMIZATION OF PROCESSING PARAMETER

In Phase 2, full set of experiment was conducted for optimization of processing parameters. The actual design for the full set of experiment used in this study is demonstrated in Table 3.9.

Table 3.9 : Actual experimental design based on full set of experiment for porous Al fabrication in Phase 2

Number	**Sequence of Experiment Run**	**Factors**		
		A	B	D
1	1	20 wt. %	200 MPa	1.5 hr
2	2	25 wt. %	200 MPa	2 hr
3	3	30 wt. %	300 MPa	2.5 hr
4	4	20 wt. %	250 MPa	1.5 hr
5	5	25 wt. %	300 MPa	2. hr
6	6	30 wt. %	300 MPa	2.5 hr
7	7	20 wt. %	250 MPa	1.5 hr
8	8	25 wt. %	200 MPa	2. hr
9	9	30 wt. %	250 MPa	2.5 hr

3.5 CHARACTERIZATIONS OF POROUS ALUMINUM FABRICATED IN PHASE 1 AND PHASE 2

3.5.1 DIMENSIONAL CHANGES

Dimensional change measurements were based on the diameter of compacted specimen. The measurement of the diameter was done using a digital vernier caliper. The percentage of diameter change for green and sintered compacts was determined using the following equations:

$$\text{Percentage of diameter change (\%) for green compact} = \frac{d_d - d_g}{d_d} \times 100$$

(3.1) where;

d_g = diameter of green compact

d_d = diameter of die opening

$$\text{Percentage of diameter change (\%) for sintered compact} = \frac{d_s - d_g}{d_g} \times 100$$

(3.2)

where;

d_g = diameter of green compact

d_s = diameter of sintered compact

3.5.2 DENSITY AND POROSITY MEASUREMENTS

Density measurement was performed by utilizing the Archimedes principle as described in ASTM C830-93. According to this principle, any liquid exerts a buoyant force on a solid submerged in that liquid. The magnitude of this force is similar to the weight of the liquid displaced by the volume of the solid. The following procedure was done for density measurements of porous Al specimen:

(i) Porous Al specimen was dried by placing in an oven at 60 °C for at least 12 hours or until constant weight was obtained.

(ii) The dry weight of the specimen (W_d), was measured.

(iii) The specimen was then soaked in deionized water and vacuumed for 2 hours so that the water can fill the open pores of the specimen.

(iv) The specimen was removed from deionized water and wiped with a wet tissue followed by weighing of the specimen. The reading was then recorded as saturated mass, W_{ss}.

(v) The specimen was finally suspended in deionized water and the specimen mass was weighed. The reading was recorded as suspended mass, W_s.

The porosity of porous Al specimen were calculated using the following equations:

$$\text{Porosity, } P = \frac{W_{ss} - W_d}{W_{ss} - W_s} \times \rho_l$$

(3.3)

where;

W_d = unsaturated (dry) weight of sample

W_s = weight of saturated sample when submerged in liquid

W_{ss} = saturated weight (assumed that all pores were filled with liquid)

ρ_l = density of liquid (water) taken as 1 g/ml

3.5.3 UNIAXIAL COMPRESSION TEST

The compression test was done to evaluate the compressive behavior of porous Al and the compressive strength was determined from a stress-strain curve by applying load until the specimen was crushed. The compression test was done using standard circular Al sample having dimension of 10 mm diameter and 11.8 mm height according to ASTM E9-09. The minimum dimension for porous Al sample should be at least seven times the cell size to avoid size effects (Motz and Pippan, 2011). An Instron 5567 machine was used to perform compression test at room temperature with 10 kN load cell and crosshead speed of 0.5 mm/min. During loading, the applied force was recorded and the compressive strength σ_c was determined from the value of the load that caused the first failure of the resultant porous Al (Vilcekova et al., 2013). The compressive strength of the resultant porous Al was determined using the following equation:

$$\sigma_c = {}^{F}/_{A} \tag{3.4}$$

where F and A are the force and area of the resultant porous Al, respectively. On the other hand, the energy absorption capacity, W, of the resultant porous Al with the highest porosity level and considerable physical and compressive properties (in this case, the resultant porous Al fabricated in Phase 2) was determined by the area under the stress-strain curve using the following Equation (Baumeister et a., 1997).

$$W = \int_0^{\varepsilon} \sigma \, d\varepsilon \tag{3.5}$$

where σ and ε are the compression stress and strain, respectively. In this section, the relationship between relative density and energy absorption capability was emphasized and the following equation was implemented to calculate the relative density (Yu et al., 2007).

$$\text{Relative Density} = \rho^*/\rho_s \tag{3.6}$$

where ρ^* is the density of sintered porous Al and ρ_s is the theoretical density of Al which is equal to 2.7 g/cm^3.

3.5.4 THERMOGRAVIMETRIC/DIFFERENTIAL THERMAL (TG/DTA) ANALYSIS

This analytical method utilizes a sensitive balance to determine weight loss of a specimen through a range of temperatures. A specimen was loaded into a pan and then placed on the balance. A furnace then enclosed the sample and the temperature can be increased at a given rate and in a given environment. The constituents of the specimen will burn off at different rates making the weight percent of the constituents determinable. The decomposition behavior of PMMA was performed using thermogravimetric analysis (Perkin Elmer 7, United States of America) during heating up to 500 °C with 10 °C/min in argon atmosphere. The decomposition temperature for PMMA material was used as a reference temperature for sintering of final powder mixture compact.

3.5.5 X-RAY DIFFRACTION (XRD) ANALYSIS

X-ray diffraction (XRD) analysis (PANanalytical empyrean 1032, Netherlands) was performed using CuKα radiation to identify the phase transformation of elemental powder mixture, final powder mixture and sintered porous Al. The XRD patterns were documented in the 2θ range of 20–80°.

3.5.6 FIELD EMISSION SCANNING ELECTRON MICROSCOPY (FESEM)

The morphology of the as-received starting powders, PMMA particles, the elemental powder mixture and the final powder mixture was observed using field emission scanning electron microscopy (FESEM) (FEI, United States of America). For the microscopic examination of the sintered porous Al, the cross-section of the specimen was prepared. The microstructure and pore morphology of the specimen cross-section were then viewed by FESEM. In conjunction with FESEM, Energy dispersive spectroscopy (EDS) analysis was used to identify the remaining content of oxygen and carbon elements of the resultant porous Al in every stage.

CHAPTER 4: RESULTS AND DISCUSSION

4.1 INTRODUCTION

In this research, closed-cell porous Al with porosity less than 50% was developed via powder metallurgy technique that involved basic steps of mixing, compaction and sintering. Under this technique, similar compaction method but different processing conditions such as mixing equipment, binder types, sintering profiles and optimization techniques were utilized in the preparation of closed-cell porous Al. Details on the difference between Phase 1 and Phase 2 were mentioned in Chapter 1 and Chapter 3. Therefore, in this chapter, discussion on the properties of porous Al fabricated in Phase 1 and Phase 2 were divided into two sections for clearer and better understanding. Analyses on thermogravimetric/differential thermal (TG/DTA) of PMMA material and final powder mixture as well as morphology characterization of starting powders were initially performed prior to discussion on porous Al properties fabricated in Phase 1 and Phase 2.

4.1.1 THERMOGRAVIMETRIC/DIFFERENTIAL THERMAL (TG/DTA) ANALYSIS OF FINAL POWDER MIXTURE

TG/DTA analysis was performed to investigate the decomposition behavior of PMMA particle as space holder material as well as decomposition behavior of oil binder. Moreover, the melting behavior of final powder mixture (elemental powder mixture and PMMA space holder) was also studied in this analysis. TGA curve for the degradation behavior of PMMA and final powder mixture as a function of the temperature are shown in Figure 4.1 and Figure 4.2. As seen in Figure 4.1, thermo-gram for PMMA material shows single step decomposition process. Moreover, the analysis showed that the thermal decomposition of PMMA spacer started at 270 °C (T_s) and ended at 410 °C (T_f). Therefore, it is believed that PMMA in the compacted Al can be completely removed in the sintering process during first heating at 450 °C and then during second heating at 580 °C. On the other hand, TGA analysis for final powder mixture demonstrates weight loss in two stages in which corresponded to the decomposition of oil binder and PMMA material. It is important to note that double step degradation curve indicates that no chemical reaction has occurred between final powder mixture, space holder particle and oil binder during fabrication (Wang et al., 2012). This shows that oil is suitable as binder to promote the adhesion of elemental powder mixture on PMMA particles and to create uniform agglomerates.

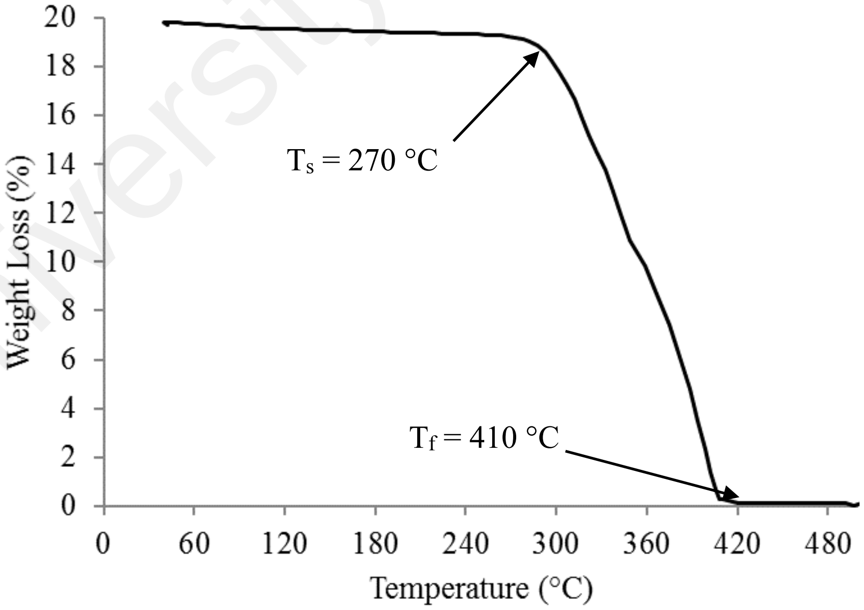

Figure 4.1 : TGA curve for PMMA material

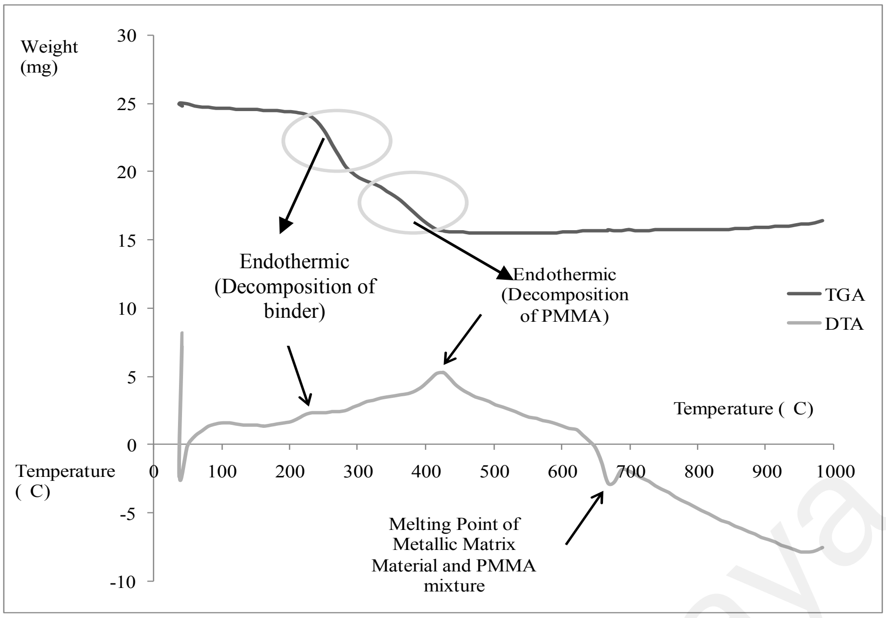

Figure 4.2: TGA curve of final powder mixture

Figure 4.2 shows the initial degradation of binder that started at 210 °C and ended approximately at 280 °C. The DTA curve also illustrates weak decomposition peak of binder and this is possibly due to the low content of binder added in the mixture (1 drop). On the other hand, the degradation temperature of PMMA added in the final powder mixture shows slightly reduced in temperature as compared to the decomposition temperature for single PMMA material. This is expected as addition of binder facilitates the thermal stability final powder mixture (Wang et al., 2003). In addition, DTA curve for final powder mixture exhibits strong decomposition peak for PMMA material. This is believed due to the large content of PMMA material that comprised 30 wt. % of total powder mixture. Although there are two decomposition peaks existed in the mixture as shown in Figure 4.2, the mixture composed of elemental powder mixture, PMMA and binder showed one maximum peak, indicating strong molecular interactions between different materials in the mixture (Wang et al., 2003). Finally, the melting peak for final powder mixture was found to be around 650 °C. This indicates that sintering should take place below the melting peak of final powder mixture to avoid partial melting or complete melting of porous body.

4.1.2 MORPHOLOGY CHARACTERIZATION OF STARTING POWDERS

Figure 4.3 (a-d) shows the FESEM images of each starting powders. Al and Mg powders were found to be mostly spherical in shape having average particle size of 32.5 μm and 6 μm, with some of Al particles were in irregular shape, as seen in Figure 4.3 (a-b), respectively. Similarly, Sn powder was found to be predominantly irregular in shape with average particle size of 30 μm whereas perfectly spherical shape with average particle size of 150 μm was observed for the PMMA particle, as shown in Figure 4.3 (c) and Figure 4.3 (d), respectively.

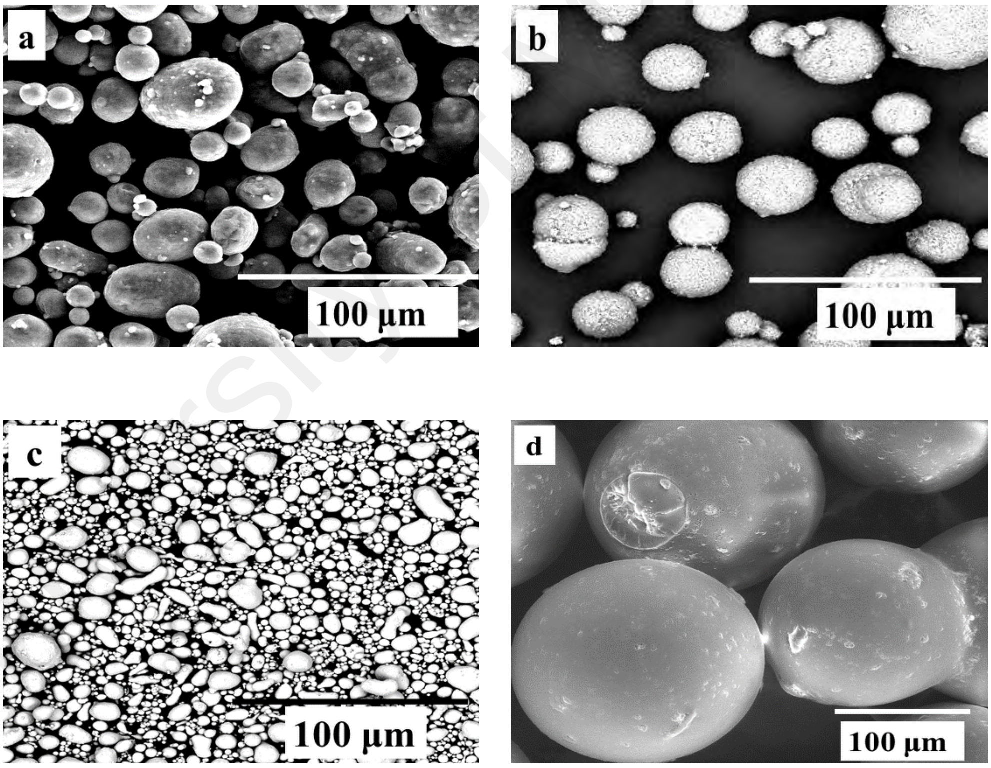

Figure 4.3 : FESEM micrographs of a) Al powder, b) Mg powder, c) Sn powder and d) PMMA particles

4.2 PHASE 1

Under powder metallurgy technique, fabrication of porous Al was carried out in three basic steps such as mixing, compacting and sintering. Specifically, high energy mixing by planetary ball milling equipment, ethanol binder, single step sintering profile and Taguchi robust design for optimization of processing parameters were exploited in this study to fabricate porous Al. Processing parameters such as space holder content (40 wt. %, 45 wt. % and 50 wt. %), compaction pressure (200 MPa, 250 MPa and 300 MPa), sintering time (1.5 hr, 2 hr and 2.5 hr) and sintering temperature (450 °C, 475 °C and 500 °C) were varied to evaluate the flexibility of this technique. The effects of processing parameters on the porosity level, densities, morphology and compressive behavior of closed-cell porous Al were also discussed in this chapter.

4.2.1 MIXING STAGE

Single mixing of Al, Mg and Sn powders along with PMMA space holder and polyethylene glycol (PEG) binder was performed using high energy planetary ball milling equipment to obtain metallic matrix powder and space holder particle (PMMA) mixture. Different batch of mixing was carried out to prepare metallic matrix powder and PMMA mixture with different PMMA content (40 wt. %, 45 wt. % and 50 wt. %). The effect of mixing time on the mixture of metallic matrix powder and PMMA was performed at maximum PMMA content of 50 wt. %. In this mixing process, PEG was applied as organic binder to minimize powders segregation as well as to ease the compaction process for the metallic matrix powder and PMMA particle mixture. The mixing time was varied at 1 hr, 3 hr, 6 hr and 9 hr while the mixing speed was set constant at 200 rpm. Morphology characterization of metallic matrix powder and PMMA mixture is then discussed in the following section.

4.2.2 FIELD EMISSION SCANNING ELECTRON MICROSCOPY (FESEM) ANALYSIS

Figure 4.4 (a-d) reveals the FESEM images of metallic matrix powder and PMMA mixture processed at different mixing time. As seen in Figure 4.4 (a), agglomeration of metallic matrix powder and PMMA particle mixture was obvious at short mixing time of 1 hr. Moreover, poor distribution between metallic matrix powder and PMMA particle was observed due to small amount of metallic matrix powder in the powder mixture. This indicates that mixing time of 1 hr was insufficient to promote homogenous distribution between metallic matrix powder and PMMA particle. Moreover, fracture of PMMA particle (dark color) was observed during 1 hr of mixing. The fracture of PMMA particle was noted due to the loss of starting spherical shape along with reduction in particle size (66.67 µm) of as supplied PMMA material.

On the other hand, the degree of PMMA dispersion was found to increase as the mixing time was increased to 3 hr. This could be attributed to the almost equal presence of PMMA particle and metallic matrix powder as shown in Figure 4.4 (b). This finding is in agreement with Tadayyon et al. (2011) who reported that longer milling time resulted in homogenous distribution of reinforcement particle in the matrix. Further fracture of PMMA particle but at small scale was evidenced after 3 hr mixing that resulted in the loss of original spherical shape along with reduction in particle size (63.72 µm) of as supplied PMMA. In addition, some of the PMMA particle had also distributed on the surface of metallic matrix powder. This is believed to be due to the dominance effect of fracturing on brittle PMMA particle during mixing (Torres and Schaeffer, 2010). Despite the fracturing of PMMA particles, the size of metallic matrix powder was still smaller compared to PMMA particle. This is necessary to ensure successful fabrication of porous structure in metallic matrix material. According to Ryan et al. (2006), the size of metal powder particle should be smaller than the average size of space holder particle during processing to ensure successful pores formation in the metallic structure.

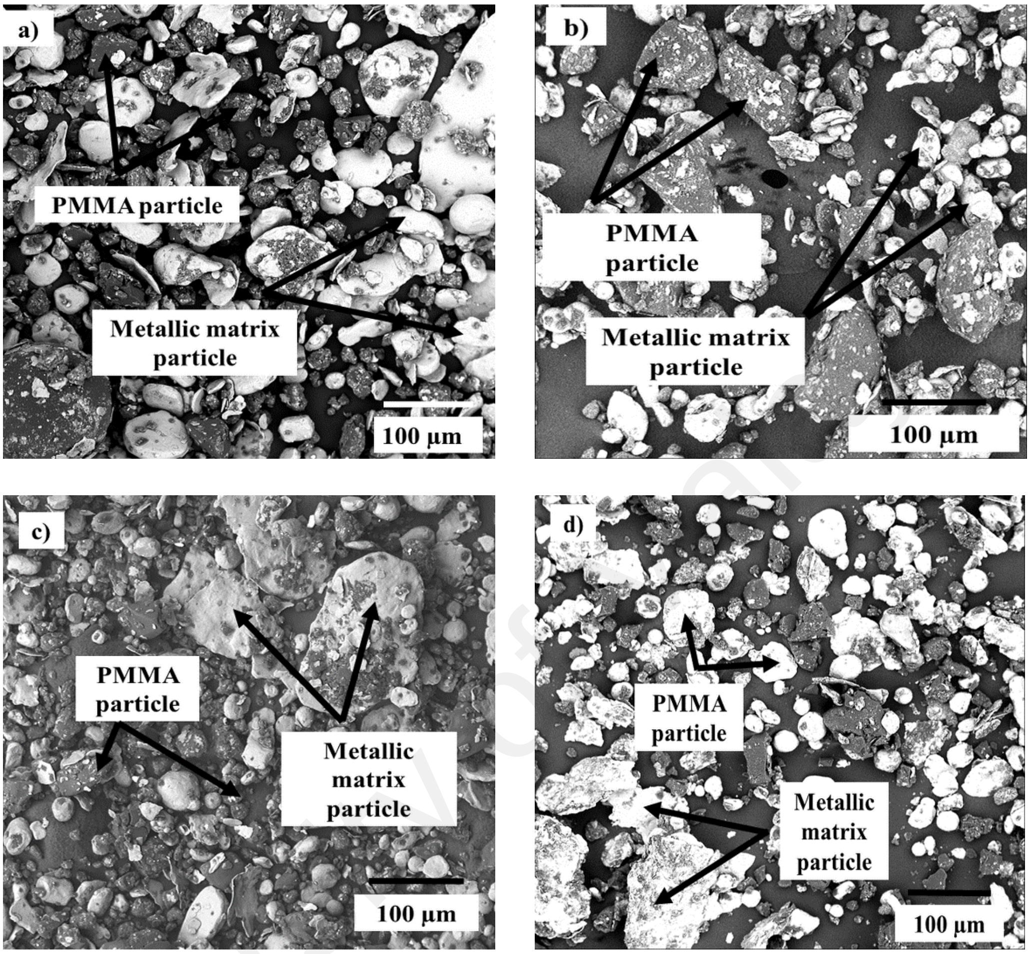

Figure 4.4 (a-d) : FESEM images of metallic matrix powder and PMMA particle mixture at different mixing time of a) 1 hr, b) 3 hr, c) 6 hr and d) 9 hr

At higher mixing time of 6 hr, the distribution between metallic matrix powder and PMMA particle in the mixture was enhanced as compared to mixing time of 1 hr and 3 hr as seen in Figure 4.4 (c). However, clear agglomeration of metallic matrix powder (bright color) was observed after 6 hr mixing that resulted in the formation of bigger particle size (146.15 µm). In addition, the morphology of metallic matrix particle was found to be flattened due to the impact forces exerted on the powder particle during mixing. This could be attributed to the dominance effect of cold welding that triggered agglomeration of metallic powder particle with flatten morphology (Ramezani and

Neitzert, 2012; Torres and Schaeffer, 2010). As evident in Figure 4.4 (c), the PMMA particle had undergone severe reduction in particle size (53.61 μm) caused by the impact energy induced by milling medium after mixing for 6 hr. Moreover, some of the PMMA particle (dark color) was also discovered to be in the form of powder instead of particle that resulted in PMMA agglomerates on the surface of metallic matrix powder (bright color) thus further reduction in PMMA particle size was expected. Therefore, unsuccessful pores formation in the structure of Al was predicted after mixing for longer duration due to the smaller size of PMMA particle compared to the metallic matrix powder. This can be attributed to the fact that when the size of the PMMA particles is smaller compared to the size of metallic matrix powder, PMMA particles are completely enclosed by the metallic matrix. These isolated PMMA particles are then unable to move into the liquid part (molten tin) during sintering and thus trapped in the metallic matrix, resulting in unsuccessful pores formation in the metallic structure. Similar findings were also reported in the literatures (Sadighikia et al., 2015; Joshi et al., 2015; Ryan et al., 2006). Therefore, it can concluded that prolong mixing using high energy ball milling equipment was undesirable due to the resultant mixture of smaller space holder particle and bigger metallic matrix particle. Similar observation was also observed with prolong mixing up to 9 hr due to the further reduction in the particle size of PMMA (48.77 μm) as well as persistent agglomeration of metallic matrix powder that resulted in bigger matrix particle as evidenced in Figure 4.4 (d).

4.2.3 X-RAY DIFFRACTION (XRD) ANALYSIS

Figure 4.5 (a-d) demonstrates the XRD analysis of metallic matrix powder and PMMA particle mixture at different mixing time. It is noted that Al rich phase was majorly found in the XRD pattern of all samples, characterized by the (111), (200), (220), (311), (222) and (400) diffraction peaks at 38.44°, 44.68°, 65.07°, 78.20°, 83.65° and 98.24° respectively. Moreover, small peaks that belong to Sn phase were identified, characterized by the (200) and (101) diffraction peaks at 30.66° and 32.02°, respectively. No additional peaks were seen in the XRD patterns of all the samples, suggesting absence of intermetallic compound formation during mixing. On the other hand, the intensity for metallic matrix powder and space holder particle mixture was found to decrease with increasing mixing time from 1 hr to 6 hr, indicating the decrease in powder mixture crystallinity and effective crystalline size when mixing time was prolonged (Lu et al., 1995). Further reduction in crystalline size as well as powder mixture crystallinity was observed with increasing mixing time to 9 hr due to the decreased in the intensity of the main XRD peak to 30 000. Ramezani and Neizert (2012) documented that repeated phenomenon of cold welding and fracturing was accountable for the decreasing in powder particle size and powder crystallinity during extended mixing.

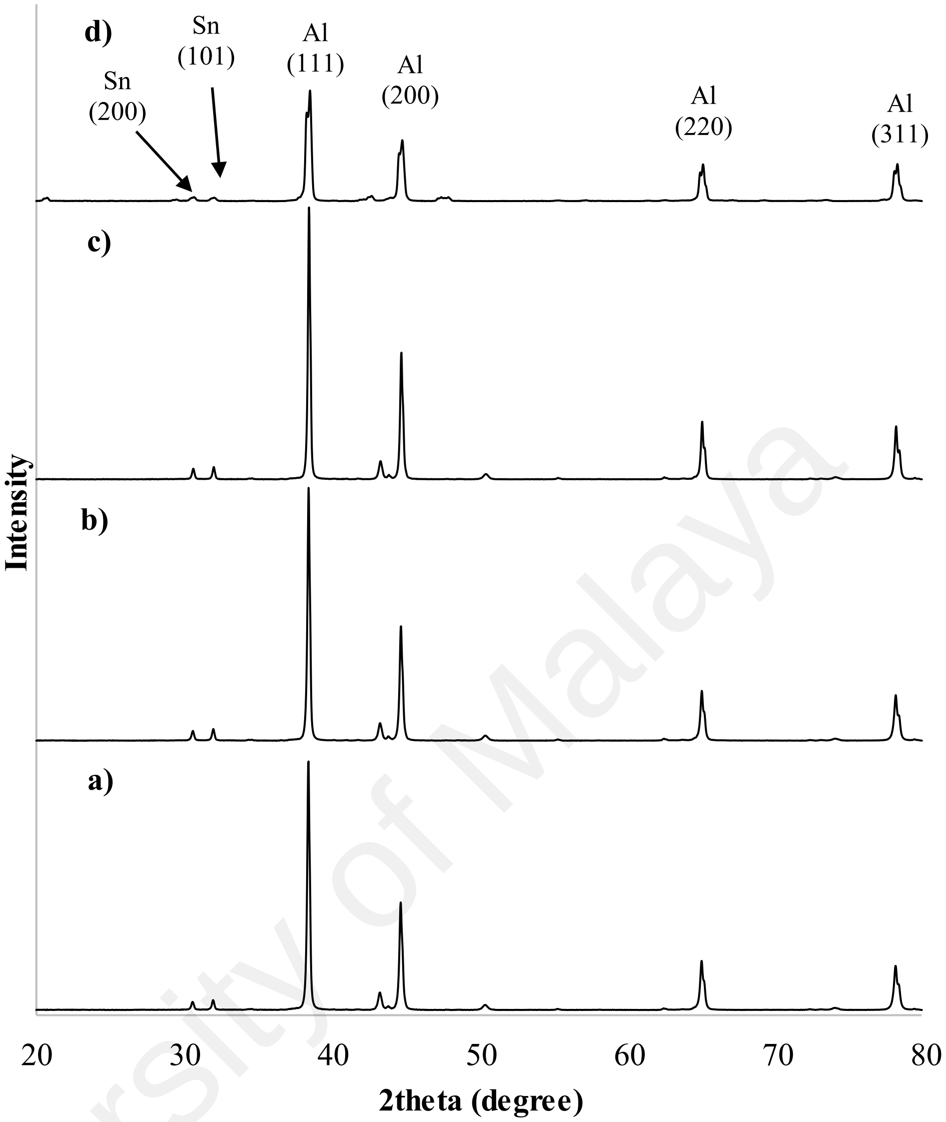

Figure 4.5 : XRD patterns of metallic matrix powder and PMMA mixture after mixing for a) 1 hr, b) 3 hr, c) 6 hr and d) 9 hr

On the other hand, the intensity Sn peaks, characterized by (200) and (101) were found to decrease with increasing mixing time particularly at mixing time of 6 hr and 9 hr. Moreover, diminishing of Sn peaks with prolong mixing time to 9 hr was observed, showing dissolution of Sn phase in Al phase and this is possibly due to the alloying of Al and Sn (Alaf et al., 2012). The presence of alloying element however was undetectable due to the minor content of Sn (1 wt. %) added in the powder mixture. In addition, the disappearance of Sn peak is undesirable as it tends to decrease the effectiveness of liquid phase sintering of compacted Al specimen. The addition of Sn as sintering aid at low content along with Mg powder is important in facilitating liquid phase sintering for compacted Al specimen (Schaffer et al., 2001). Therefore, it is reasonable to infer that prolong mixing in the current study is detrimental due to dissolution of Sn in Al phase as well as unsatisfactory morphology of powder mixture prior to porous Al fabrication (Al, Mg and Sn powders) as confirmed by FESEM image in Figure 4.4 (c-d).

4.3 PHYSICAL CHARACTERISTIC OF COMPACTED SPECIMEN

Compaction pressure is important not only to obtain sufficient bonding strength between Al particles but also to break the oxide films that cover the surface of Al particles. This is vital for fresh metallic contact formation between Al particles to ensure efficient sintering (Hao et al., 2009; Bafti and Habibolahzadeh, 2010). It is found that compaction pressure under 200 MPa and over 300 MPa formed unsatisfactory specimen due to severe cracking of compacted body (see Figures 4.6 (a) and Figure 4.6 (b)). A range of compaction pressure between 200 MPa to 300 MPa apparently found to be adequate to produce almost perfect porous specimens that retained its original shape with sharp edges as seen in Figure 4.6 (c). Based on these criteria, the selection of compaction pressure between 200 MPa to 300 MPa was selected for further evaluation.

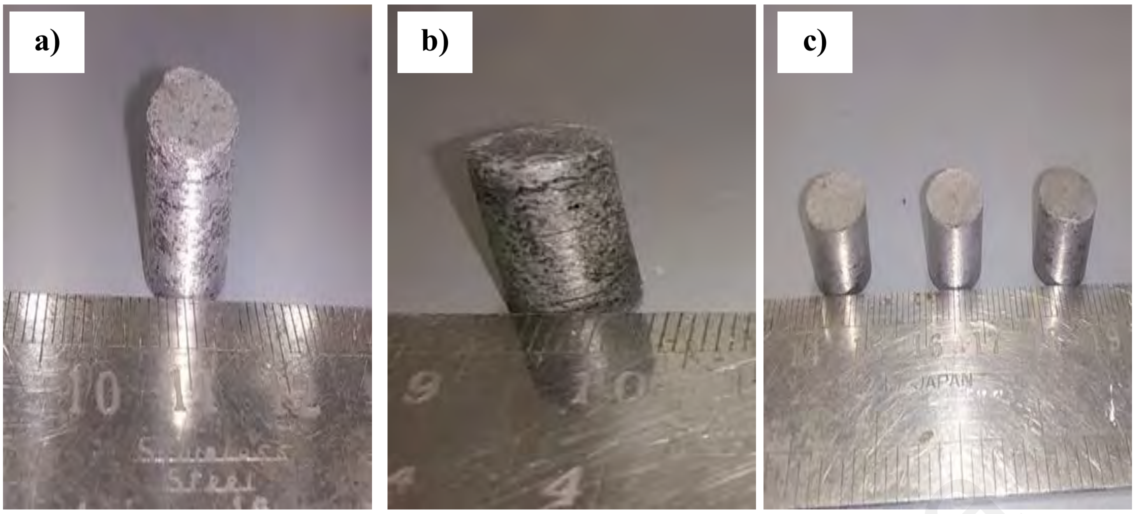

Figure 4.6 : Typical unsatisfactory samples, due to insufficient compacting pressure of a) less than 200 MPa, b) over 300 MPa and c) proper samples produced under sufficient pressure between 200 MPa and 300 MPa

4.4 SINTERED POROUS ALUMINUM

4.4.1 OUTPUT PARAMETERS AND SIGNAL TO NOISE RATIO

Taguchi robust design technique was utilized in this study particularly for optimization of processing parameters. The experimental results and signal to noise ratios (S/N) for each output parameters including sintered density, compressive strength, and percentage of porosity are shown in Table 4.1 until Table 4.4. The effects of different experimental conditions on the sintered density, compressive strength and porosity were plotted in the bar graphs as shown in Figure 4.8 (a), Figure 4.9 (a) and Figure 4.10 (a), respectively. Moreover, the average effects plot for each output parameters in term of S/N ratios were designed in Figure 4.8 (b), Figure 4.9 (b) and Figure 4.10 (b), respectively. The data for each output parameters was based on the mean value (refer Table 4.1 until Table 4.4). The (S/N) ratio was calculated based on the characteristics of each output parameter.

4.4.2 EXPERIMENTAL RESULTS

4.4.3 PHYSICAL OBSERVATION OF POROUS ALUMINUM SPECIMEN

Figure 4.7 (a-e) shows the physical characteristics of porous Al specimen at various processing conditions. After sintering, there was no clear observation in term of different porosity due to micron size pores formation. It can be seen that from Figure 4.7 (a) and Figure 4.7 (b), almost perfect porous Al specimens could be obtained at low sintering time and low compaction pressure of below 2.5 hr and 300 MPa. These porous specimens retained their original shapes, including sharp edges, and had satisfactory strength. As the sintering time and compaction pressure were increased to higher level of 2.5 hr and 300 MPa, crack formation was observed as seen in Figure 4.7 (c) and Figure 4.7 (d). This indicates that higher compaction pressure and longer sintering time are undesirable due to the formation of crack that affected the stability of porous body specimen. Finally, slumping and bloating of porous specimen was noted as depicted in Figure 4.9 (e) due to the excessive content of PMMA particle. Such condition was observed as PMMA content used in this study was more than 50 wt. %. Therefore, the PMMA content in the current study was varied up to maximum of 50 wt. %.

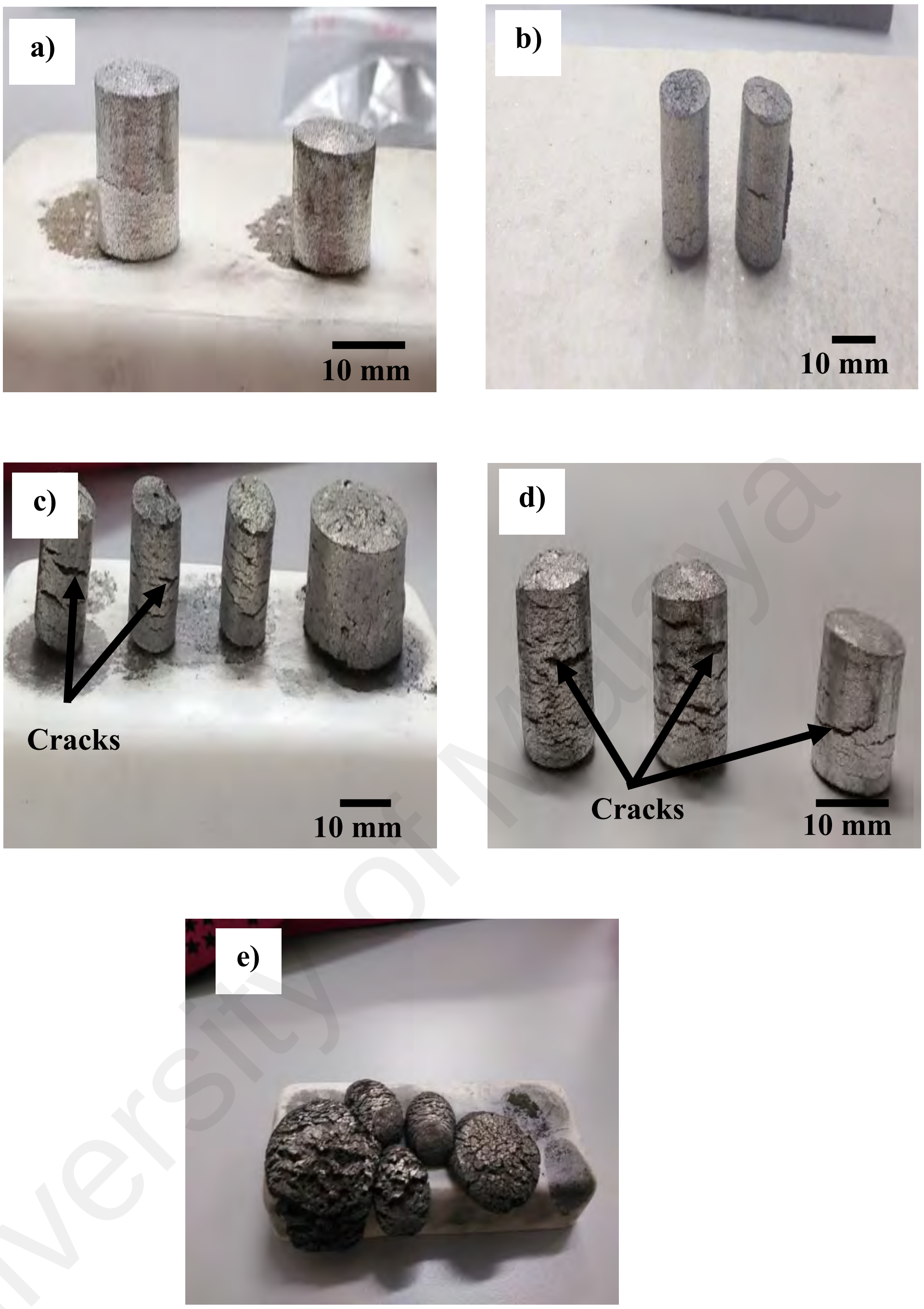

Figure 4.7 (a-e) : Physical characteristic of porous Al specimen at various processing conditions of : (a-b) sintering time and compaction pressure below 2.5 hr and 300 MPa, (c-d) sintering time and compaction pressure above 2.5 hr and 300 MPa and (e) PMMA content exceeds 50 wt. %

4.4.4 SINTERED DENSITY

Figure 4.8 (a) shows the average sintered density of porous Al specimen at various processing conditions. A low standard deviation of less than 0.002 was obtained for all specimens. Details on the average reading for percentage of diameter change can be found in Table 4.1. It can be seen that, the average sintered density of porous Al specimen slightly decreased with increasing PMMA content regardless of the sintering temperatures, suggesting decreased in densification. It has been reported that the presence of a high volume of pores due to many empty spaces after PMMA particle removal is accountable for the decreased in sintered density of the resultant porous specimen (Hussain and Suffin, 2011; Asavavisithchai and Nisaratanaporn, 2010). Moreover, Gokce and Findik (2008) also reported that greater amount of porosity decreased the sintered density due to a wide range of polymer burn off resulting in residual porosity.

It should be noted that the sintered densities of all the porous specimens in the current study were found to be lower compared to the reported sintered densities in the literatures (Jiang et al., 2005; Bafti and Habibolahzadeh, 2010; Jinnapat and Kennedy, 2011). This is possible due to the presence of larger number of micro-pores instead of macro-pores that usually resembles the initial morphology of space holder material in the metallic structure as shown in FESEM micrographs from Figure 4.11 (a-i). This shows that the presence of micro-pores is undesirable as it affected the densities of the resultant porous specimen. Studies have shown that it is important to ensure that the pores formation replicates the morphology of the initial space holder material in obtaining porous Al with better quality. Asavavisithchai and Nisaratanaporn (2010) revealed a declined in sintered density of silver foams due to irregular pores formation prior to asymmetrical shape of space holder material. In the present study, low sintered density can also be attributed to the poor metallurgical bonding between Al particles, implying incomplete sintering particularly at lower sintering temperature as depicted in FESEM micrographs from Figure 4.11 (a-i).

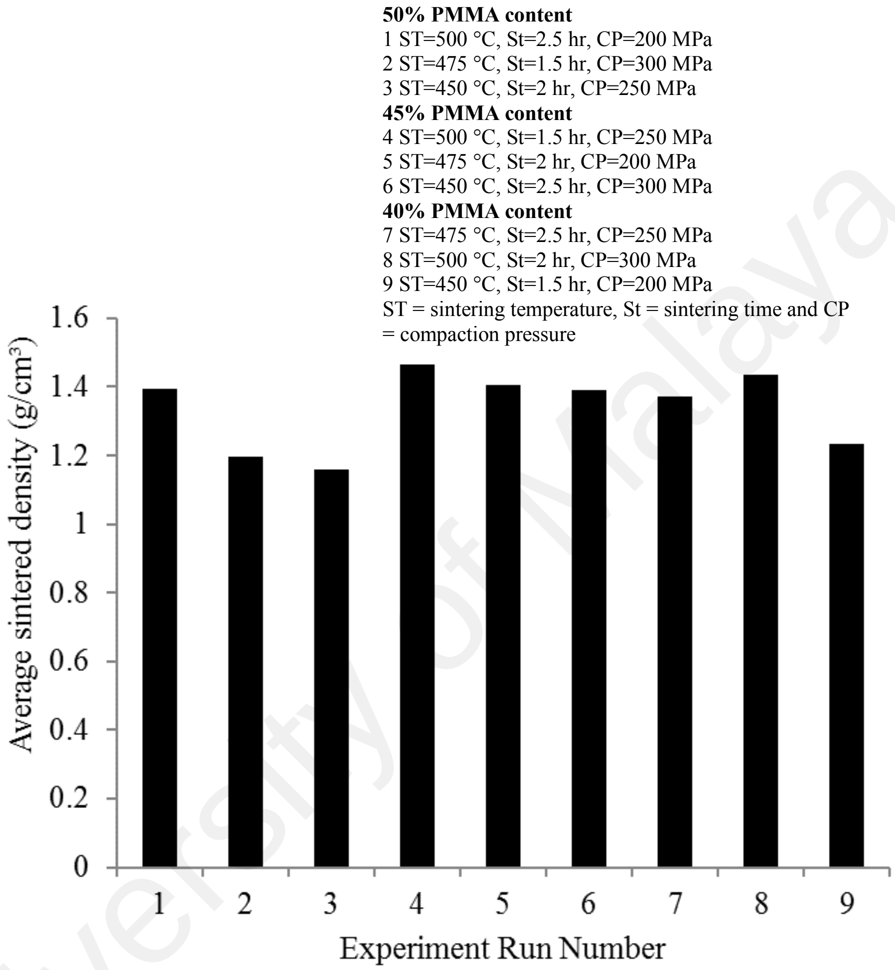

Figure 4.8 (a) : Average sintered density of porous Al at various processing parameters

Table 4.1 : Average sintered density porous Al at various processing parameters

Experiment number	**Experiment condition**				**Sintered density (g/cm^3)**					**Larger is better (S/N) ratio**
	A	B	C	D	y_0	y_1	y_2	ý	σ	$1/n\sum 1/y^2$
1	200	500	2.5	50	1.592	1.593	1.593	1.593	0.00042	4.864
2	300	475	1.5	50	1.195	1.196	1.196	1.196	0.00065	3.736
3	250	450	2	50	1.159	1.1591	1.1596	1.1592	0.00036	3.687
4	250	500	1.5	45	1.6657	1.6663	1.6666	1.662	0.00046	5.129
5	200	475	2	45	1.4047	1.4053	1.4057	1.4052	0.0005	4.235
6	300	450	2.5	45	1.3902	1.3909	1.3913	1.3908	0.00056	4.191
7	250	475	2.5	40	1.4717	1.4722	1.4724	1.4721	0.00036	4.446
8	300	500	2	40	1.7338	1.7343	1.7348	1.7343	0.0005	5.382
9	200	450	1.5	40	1.2322	1.2326	1.2328	1.233	0.00031	3.798

Nevertheless, the densification was found to increase with increasing sintering temperature to 500 °C at all the PMMA contents as seen in Figure 4.8 (a). This is probably due to the decreased in micro-pores formation and particles boundaries as shown in FESEM images (Figure 4.11 (g-i)). Jiang et al. (2005) and Ahmed et al. (2007) reported that higher sintering temperature increased the sintered densities due to the enhanced mechanical bonding between metallic matrix particles that resulting in decreasing voids and porosity. This result is in agreement with the micrograph images as depicted in FESEM micrographs from Figure 4.11 (a-f), in which weak bonding between Al particles was observed due to the presence of individual Al particle (particle boundary) along with the presence of large number of micro pores during sintering at lower temperature. As the sintering temperature was increased to 500 °C, the mechanical bonding between Al particles was slightly improved but the appearance of the individual Al particles was still clearly observe as illustrated in FESEM micrographs from Figure 4.11 (g-i). This indicates that the sintering temperature in the current study was insufficient to promote metallurgical bonding between Al particles thus resulting in decreased densification. In contrast, no clear finding on the effect of compaction pressure and sintering time on the densities of porous specimen, showing greater effect of PMMA content and sintering temperature during fabrication.

The S/N ratio for average sintered density of porous Al specimen sizes is given in Table 4.1. Furthermore, the average reading for S/N ratio (larger is better) is illustrated in Figure 4.8 (b). In the main effects plot as illustrated in Figure 4.8 (b), the parameter has no significant effect if the line for a particular parameter is close to horizontal. In contrast, the highest inclination for particular parameters indicates the most significant effect. In term of interaction plot, an interaction means non-parallelism of parameter effects. Therefore, if the lines on the interaction plots are nonparallel, interaction happens and if the lines intercept, strong interaction occurs between parameters.

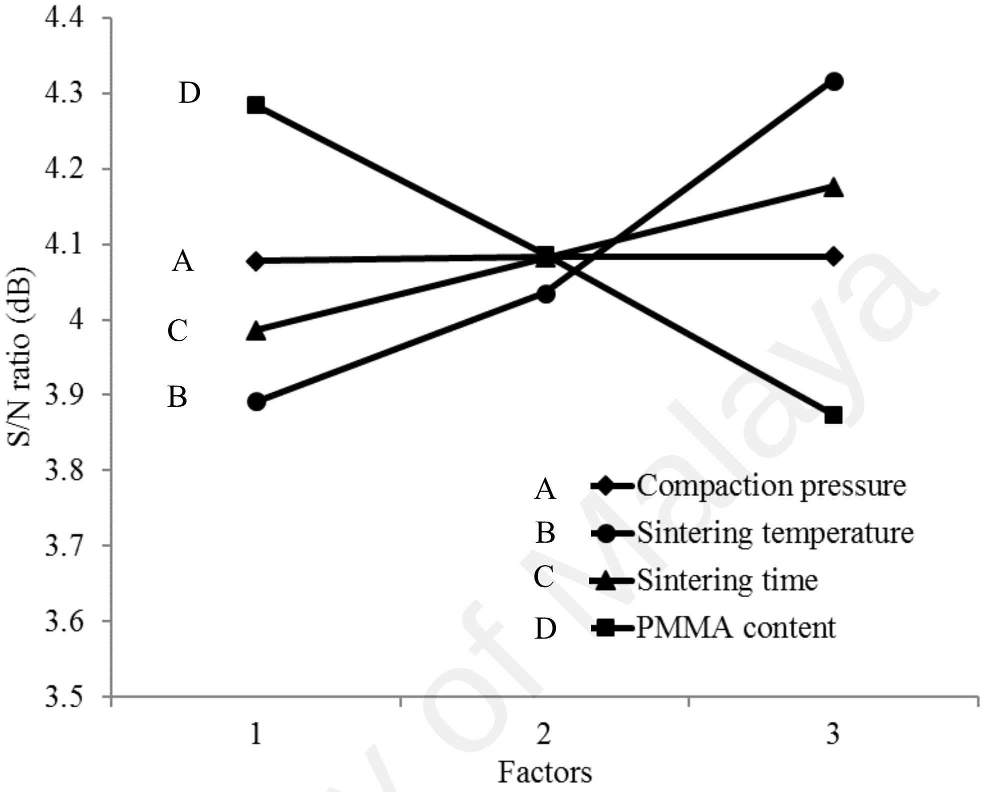

Figure 4.8 (b) : Average effects plot for sintered density of porous Al in term of S/N ratios at various processing parameters

From Figure 4.8 (b), it can be observed that strong interaction occurs between parameters A and C as well as between parameters B and D. Moreover, moderate interaction occurs between parameters A and B as well as between parameters A and D. Thus, the most significant factors that affect the average sintered density are identified as PMMA content and sintering temperature followed by sintering time. The least significant factor that affects the average sintered density is compaction pressure. The significant effect for larger is better for average sintered density occurred at A_2, B_2, C_2 and D_0. It means that the combination of 300 MPa compaction pressure, 500 °C sintering temperature, 2.5 hr sintering time and 40 wt. % PMMA content gives the optimum result in terms of average value of S/N ratio (larger-is-better-characteristic) for average sintered density of porous Al. This indicates that highest compaction pressure, highest sintering temperature, highest sintering time and lowest PMMA content resulted in highest average sintered density.

4.4.5 COMPRESSIVE STRENGTH

Figure 4.9 (a) shows the compressive strength of porous Al at various processing conditions. The bar graph indicated that the compressive strength was found to decrease with increasing PMMA content. This could be attributed to the increased in porosity with increasing PMMA content. According to Hussain and Suffin (2011), low compressive strength is associated with increasing porosity in the compact due to the empty spaces left by the space holder particle. Jamaludin et al. (2013) and Mustapha et al. (2010) also reported similar observation. Other than porosity, it is observed that the sintered densities strongly influenced the compressive strength of porous Al. The compressive strength of porous Al in this study was found to decrease with decreasing sintered density particularly at the highest PMMA content. Similar finding was also reported by Asavavisithchai and Nisaratanaporn (2010) and Jha et al. (2013). A decreased in compressive strength with increasing space holder content can be attributed to the decreased in the plasticity and ductility of the porous material (Ahmad Suffin et al., 2013).

It is important to note that the values of compressive strength of all the sintered porous specimen were considered lower compared to the reported compressive strength of porous Al. Jiang et al. (2005) successfully fabricated porous Al with compressive strength about 5 MPa compared to the compressive strength of porous specimen obtained in the current study processed under similar compaction pressure (300 MPa) and space holder content (40 wt. %) which is about 1.3 MPa. This can be attributed to the greater number of micro-porosity instead of macro-pores that usually replicates the starting morphology of PMMA spacer as well as individual Al particles found in all specimens as confirmed by FESEM analysis (Figure 4.11 (a-i)). As previously mentioned in section 4.3.8, it is important to ensure that the porous structure resembles the morphology of starting space holder material so that porous Al with better quality can be developed. In addition, lower compressive strength values obtained in the current study can also be associated with lower sintering temperature setting in the current study that resulted in incomplete sintering as revealed by FESEM analysis (Figure 4.11 (a-i)). According to Jiang et al. (2005), better metallurgical bonding between the metallic powder particles can be obtained at higher sintering temperature (Jiang et al., 2005). This is in agreement with FESEM micrographs in which considerable degree of mechanical bonding was observed at higher sintering temperature of 500 °C as compared to lower sintering temperature of 450 °C and 475 °C as illustrated in FESEM micrographs from Figure 4.11 (g-i). In contrast, no clear trend was observed for the effect of compaction pressure and sintering time on the compressive strength of porous Al showing pronounced effect of these processing parameters compared to the effect of sintering time and compaction pressure.

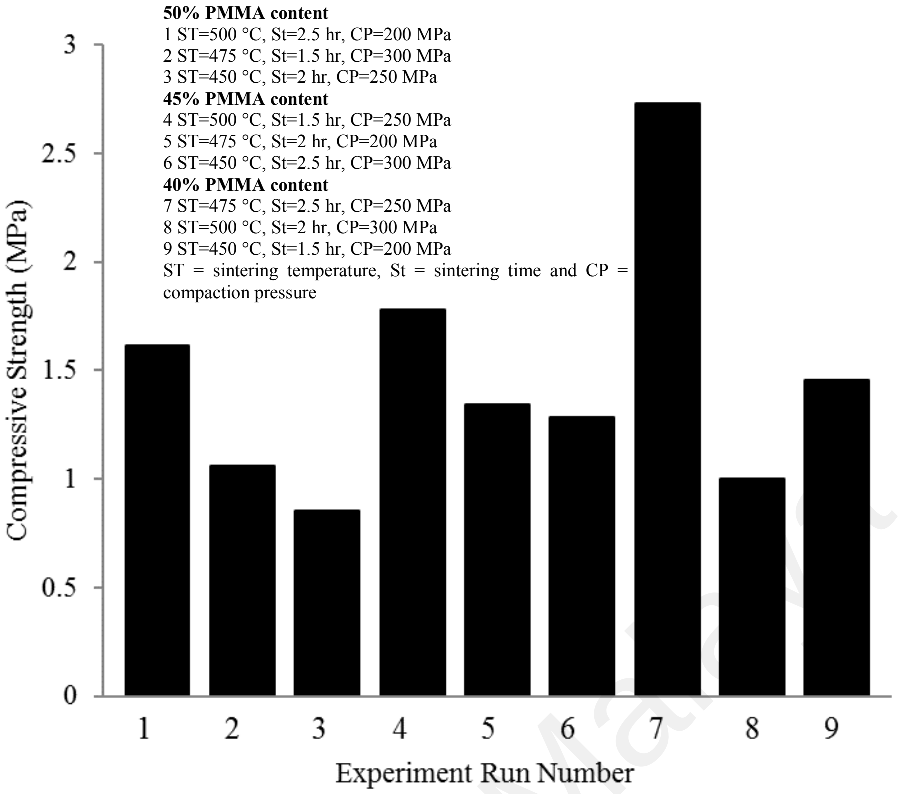

Figure 4.9 (a) : Average compressive strength of porous Al at various processing parameter

The S/N ratio for average compressive strength for porous Al specimen is given in Table 4.2. Furthermore, the average reading for S/N ratio (larger is better) is illustrated in Figure 4.9 (b). From Figure 4.9 (b), it can be viewed that strong interaction occurs between all parameters. Thus, the most significant factors that affect the average compressive strength are identified as PMMA content and sintering temperature followed by sintering time. The least significant factor that affects the average compressive strength is compacting pressure. The significant effect for larger is better for average compressive strength of porous Al specimen occurred at A_2, B_2, C_2 and D_0. It means that the combination of 300 MPa compaction pressure, 500 °C sintering temperature, 2.5 hr sintering time and 40 wt. % foaming agent content gives the optimum result in terms of average value of S/N ratio (larger-is-better-characteristic) for average compressive strength of porous Al. This indicates that highest compaction pressure, highest sintering temperature, highest sintering time and lowest PMMA content resulted in highest compressive strength.

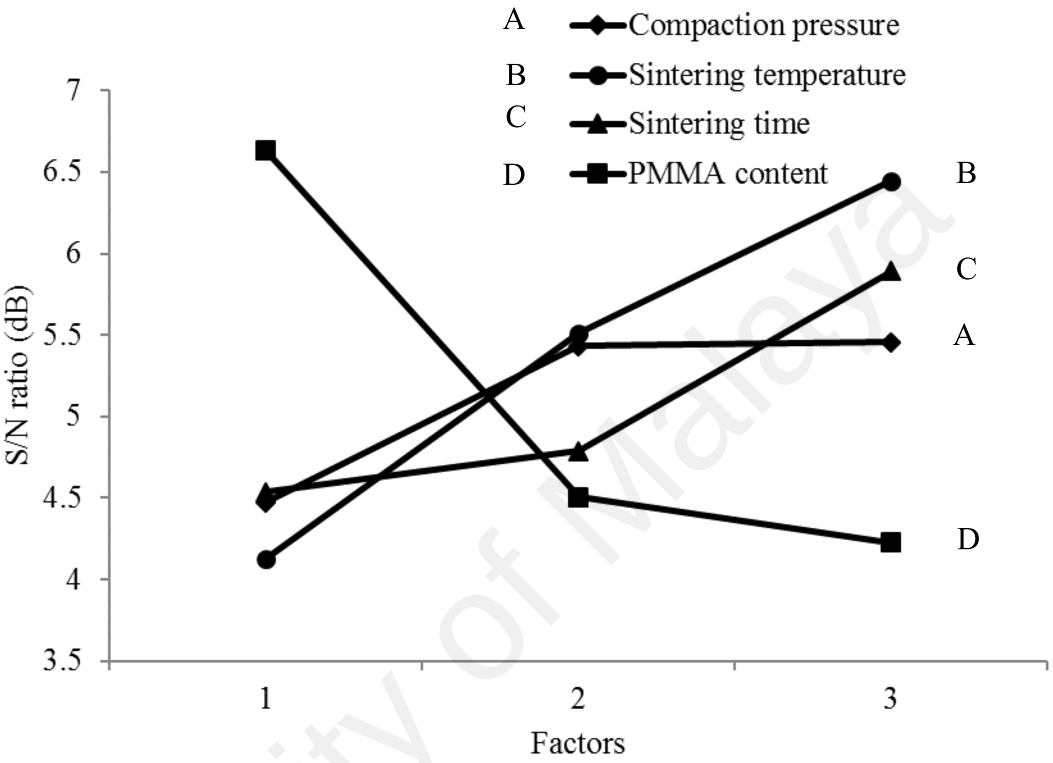

Figure 4.9 (b) : Average effects plot for compressive strength of porous Al in term of S/N ratios under various processing parameters

Table 4.2 : Average compressive strength of porous Al under various processing parameters

Experiment number	**Experiment condition**				**Compressive strength (MPa)**					**Larger is better (S/N) ratio**
	A	B	C	D	y_0	y_1	y_2	ý	σ	$1/n\sum 1/y^2$
1	200	500	2.5	50	1.614	1.616	1.618	1.616	0.002	4.9538
2	300	475	1.5	50	1.059	1.061	1.063	1.061	0.002	3.6465
3	250	450	2	50	0.849	0.854	0.85	0.851	0.00265	3.687
4	250	500	1.5	45	1.777	1.78	1.782	1.780	0.00252	4.076
5	200	475	2	45	1.34	1.342	1.344	1.342	0.002	4.061
6	300	450	2.5	45	1.28	1.283	1.282	1.282	0.002	3.900
7	250	475	2.5	40	2.078	2.083	2.08	2.08	0.00252	6.6596
8	300	500	2	40	2.727	2.731	2.73	2.73	0.00208	8.8263
9	200	450	1.5	40	1.46	1.451	1.458	1.456	0.00473	4.4096

4.4.6 PERCENTAGE OF POROSITY

The effect of various processing parameters on the average percentage of porosity of sintered specimen is demonstrated in Figure 4.10 (a). As seen in Figure 4.10 (a), the percentage of porosity of porous Al specimen was found to increase with increasing PMMA content. However, the average percentage porosity of porous specimen was found to deviate from the initial PMMA content added in the mixture during sintering at low temperatures of 450 °C and 475 °C, postulating entrapment of PMMA particle in the resultant porous specimen. Similar finding was also reported before (Dizlek et al., 2009; Arifvianto and Zhou, 2014). The average percentage of porosity of porous specimen after sintering at 450 °C was recorded as 32.96%, 38.5% and 42.73% as the content of PMMA was added between 40 wt. %, 45 wt. % and 50 wt. %. After sintering at 475 °C, the average percentage of porosity of porous specimen was slightly increased to 33.31%, 40.59% and 43.68% as the content of PMMA was added between 40 wt. %, 45 wt. % and 50 wt. %.

As shown in Table 4.3, EDS analysis confirmed entrapment of PMMA particle due to the greater content of carbon in the porous structure after sintering at low temperatures of 450 °C and 475 °C. Initially, the carbon content of the metallic matrix powder increased from 0.24 wt. % to 14.77 wt. %, 15.68% and 16.72% due to the addition of PMMA into the metallic matrix powder. After sintering at 450 °C, the carbon content of the resultant porous Al was greatly increased to 2.68%, 2.91% and 3.07% at 40 wt. %, 45 wt. % and 50 wt. % of PMMA. On the other hand, the carbon content of the resultant porous Al was slightly decreased to 2.08%, 2.31% and 2.68% at 40 wt. %, 45 wt. % and 50 wt. % of PMMA after sintering at 475 °C. This can be explained by the fact that when the sintering temperatures were lower (450 °C and 500 °C in this case), complete PMMA spacer removal could not be obtained, resulting in higher amount of carbon residue in the resultant porous Al that decreased the total porosity of porous specimen. In conjunction with this, an increased in sintered density and compressive strength of the sintered porous Al could not be obtained due to poor inter-particle bonding between Al particles and greater formation of micro porosity during sintering at low temperature of 450 °C and 475 °C.

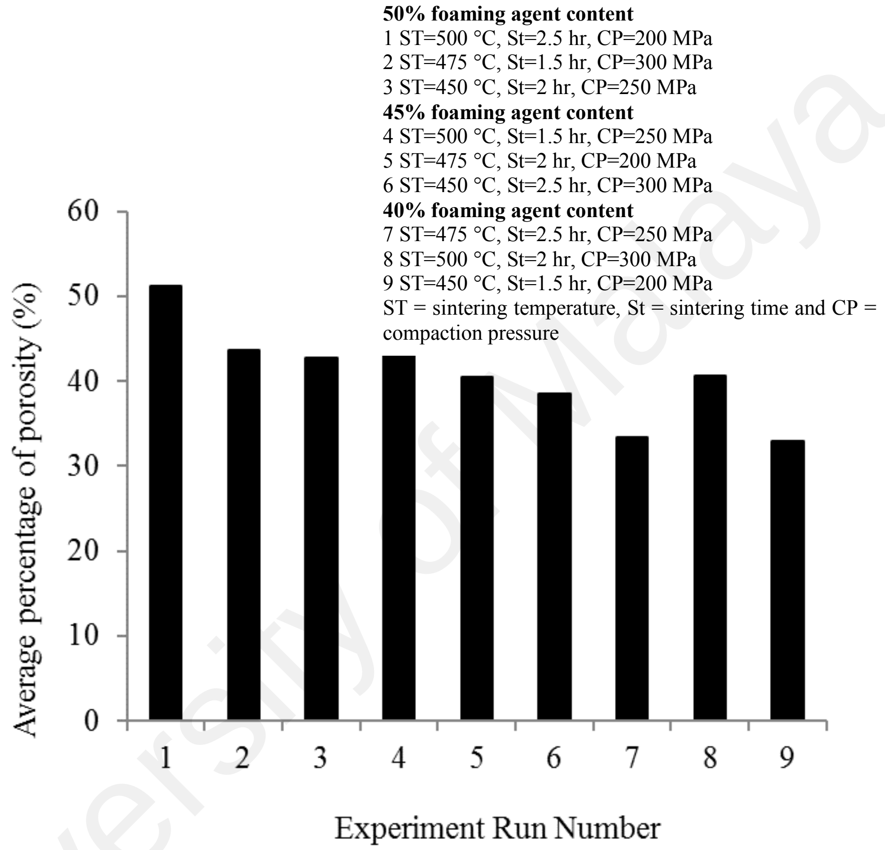

Figure 4.10 (a) : Average percentage of porosity of porous Al under various processing parameters

Table 4.3 : Carbon content reading from EDS analysis of metallic matrix powder, metallic matrix powder and PMMA mixture and porous Al specimen with different PMMA content and sintering temperature. Data are presented in mean ± standard deviation

Specimens	Sintering temperature (°C)	Carbon Content (wt. %)
Metallic matrix powder	-	0.24±0.10
Metallic matrix powder+40% PMMA content	-	14.77±0.09
Metallic matrix powder+45% PMMA content	-	15.68±0.14
Metallic matrix powder+50% PMMA content	-	16.72±0.12
Sintered porous Al at 40% PMMA content	450	2.68±0.13
Sintered porous Al at 45% PMMA content	450	2.91±0.11
Sintered porous Al at 50% PMMA content	450	3.07±0.18
Sintered porous Al at 40% PMMA content	475	2.08±0.16
Sintered porous Al at 45% PMMA content	475	2.31±0.16
Sintered porous Al at 50% PMMA content	475	2.68±0.10
Sintered porous Al at 40% PMMA content	500	0.76±0.06
Sintered porous Al at 45% PMMA content	500	0.92±0.04
Sintered porous Al at 50% PMMA content	500	1.08±0.10

On the other hand, the average percentage of porous specimen at all PMMA content corresponds nearly to the starting weight percentages of the space holder. In this case, the average percentage of porosity of porous specimen after sintering at 500 °C was recorded as 40.69%, 45.7% and 51.17% as the content of PMMA was added between 40 wt. %, 45 wt. % and 50 wt. %. This shows that complete removal of PMMA particle was obtained after sintering at 500 °C, suggesting proper sintering. Complete removal of PMMA particle is evidenced from Table 4.3 due to lower carbon content of 0.76 wt. %. 0.92 wt. % and 1.08 wt. % with the addition of 40 wt. %, 45 wt. % and 50 wt. % of PMMA. As a result, the sintered densities and compressive strength of porous specimen were found to be higher compared to the porous specimens with lower porosities level(in this case sintering at 450 °C and 475 °C) despite their higher porosity level owing to the enhanced in the degree of sintering as evidenced from FESEM micrographs as in Figure 4.11 (g-i).

In contrast, no clear trend was observed for the effect of compaction pressure and sintering time on the compressive strength of porous Al due to the pronounced effect of PMMA content and sintering temperature. The average reading for S/N ratio (larger-is-better-characteristic) as illustrated in Figure 4.10 (b) reveals a decreasing trend in the average percentage of porosity with increasing sintering temperature, sintering time, compaction pressure and PMMA contents. Detail on S/N ratio for average percentage of porosity for porous Al specimen is depicted in Table 4.4. From Figure 4.10 (b), it can be analyzed that strong interaction occurs between all parameters. Thus, the most significant factors that affect the average porosity are identified as PMMA content and sintering temperature followed by compaction pressure. The least significant factor that affects the average porosity is sintering time. The significant effect for larger is better for average percentage of porosity of porous Al occurred at A_0, B_2, C_2 and D_2. It means that the combination of 200 MPa compaction pressure, 500 °C sintering temperature, 2.5 hr sintering time and 50 wt. % PMMA content gives the optimum result in terms of average value of S/N ratio (larger-is-better-characteristic) for average percentage of porosity of porous Al. This indicates that lowest compaction pressure, lowest sintering temperature, lowest sintering time and highest PMMA content resulted in highest average percentage of porosity.

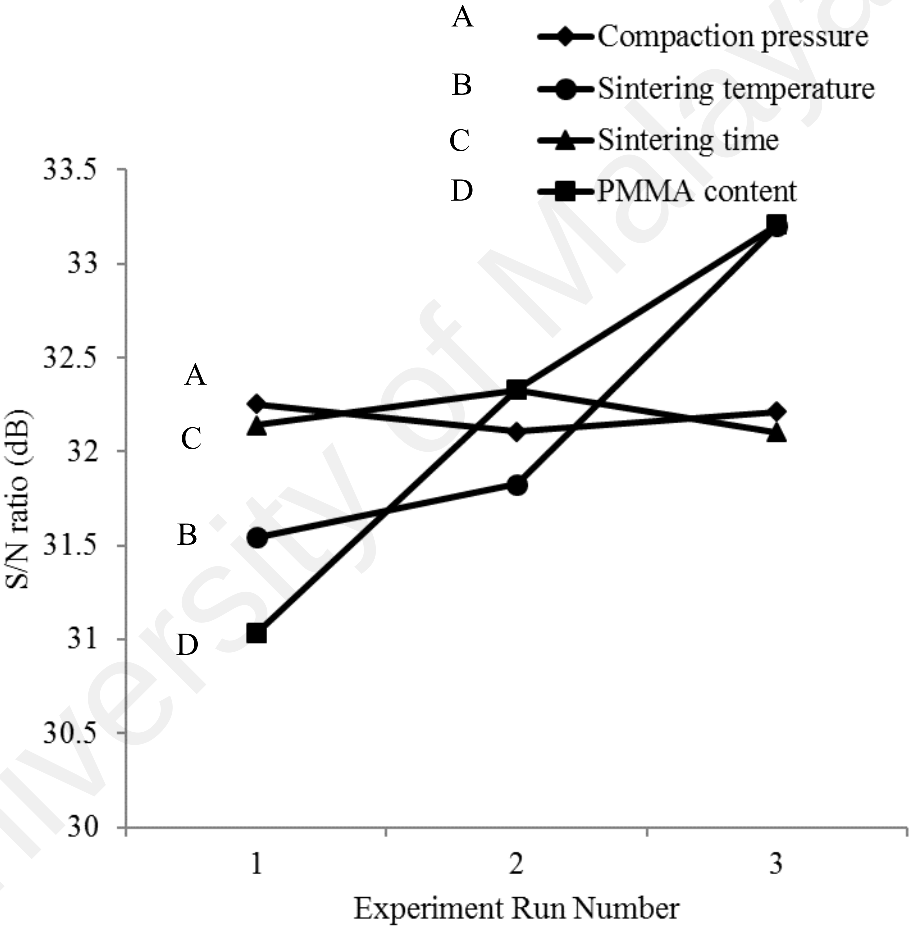

Figure 4.10 (b) : Average effects plot for percentage of porosity of porous Al in term of S/N ratios under various processing parameters

Table 4.4 : Average percentage of porosity of porous Al under various processing parameters

Experiment number	**Experiment condition**				**Average percentage of porosity (%)**					**Larger is better (S/N) ratio**
	A	B	C	D	y_0	y_1	y_2	ý	σ	$1/n\sum 1/y^2$
1	200	500	2.5	50	51.12	51.17	51.23	51.17333	0.05508	51.12
2	300	475	1.5	50	43.61	43.69	43.74	43.68	0.06756	43.61
3	250	450	2	50	42.6	42.67	42.73	42.66667	0.06506	42.6
4	250	500	1.5	45	45.63	45.71	45.76	45.7	0.06557	45.63
5	200	475	2	45	40.44	40.51	40.59	40.51333	0.07506	40.44
6	300	450	2.5	45	38.6	38.8	38.1	38.5	0.3606	38.6
7	250	475	2.5	40	33.31	33.41	33.49	33.40333	0.09018	33.31
8	300	500	2	40	40.64	40.68	40.74	40.68667	0.05033	40.64
9	200	450	1.5	40	32.7	33.08	33.11	32.96333	0.22855	32.7

4.4.7 PARETO ANOVA

Technique of Pareto analysis of variance (ANOVA) has been implemented to obtain the optimum combination of processing parameters based on the analyzation of S/N ratios. This techniques allows the evaluation of significant factors and interactions with different response parameters. In addition, the optimal levels of factors can be obtained separately within the tested range of processing parameters for different output (finding). The ANOVA results for porous Al specimen for sintered density, porosity and compressive strength of the resultant porous Al can be found in APPENDIX B.

4.4.8 FIELD EMISSION SCANNING ELECTRON MICROSCOPY (FESEM)

Figure 4.11 (a-i) reveals the FESEM micrographs of the resultant porous Al at different processing conditions. It can be obviously seen that the pores of all the resultant porous Al were mainly composed of open-celled micro-pores with irregular pores shape and different pores size (>100 μm). As evident in Figure 4.11 (a-i), these open-celled micro-pores were found to be homogeneously distributed in the resultant porous Al and were isolated from each other by a distinct particle boundaries (Al particle). It should be noted that, the morphology of these open-celled micro-pores did not replicate the initial morphology of the spherical PMMA particle, and this is possibly due to the fracture of PMMA space holder during fabrication as confirmed by FESEM images in section 4.2.2.

Poor metallurgical bonding between Al particles with visible appearance particle boundaries were also observed, signifying incomplete sintering that decreased the properties (densities and compressive strength) of porous specimen during sintering at lower temperatures of 450 °C and 500 °C. Nevertheless, the appearance of particle boundaries was slightly decreased with little neck formation between Al particles after sintering at 500 °C as evidenced in Figure 4.11 (g-i). This shows that sintering at 500 °C slightly enhanced the sintering quality of porous specimen. On the hand, no clear finding was observed for the effect of compaction pressure and sintering time on the morphology of the resultant porous specimens. Therefore, it is reasonable to infer that the morphology of porous specimen is greatly affected by the PMMA content and sintering temperature compared to the compaction pressure and sintering time. Furthermore, the range of sintering temperature in this study was found to be insufficient due to incomplete sintering characterized by the formation of visible particle boundaries with poor bonding between Al particles.

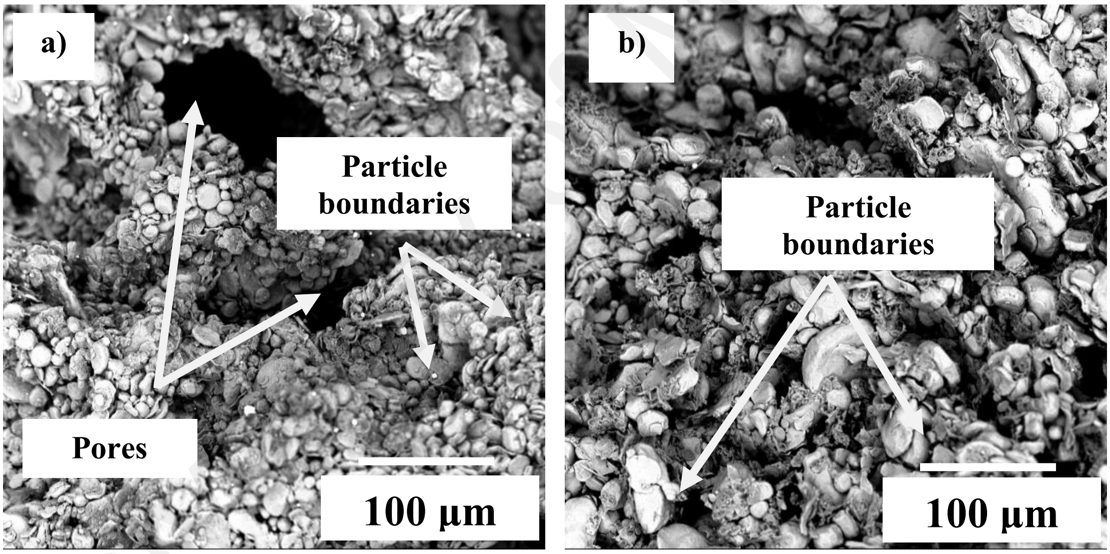

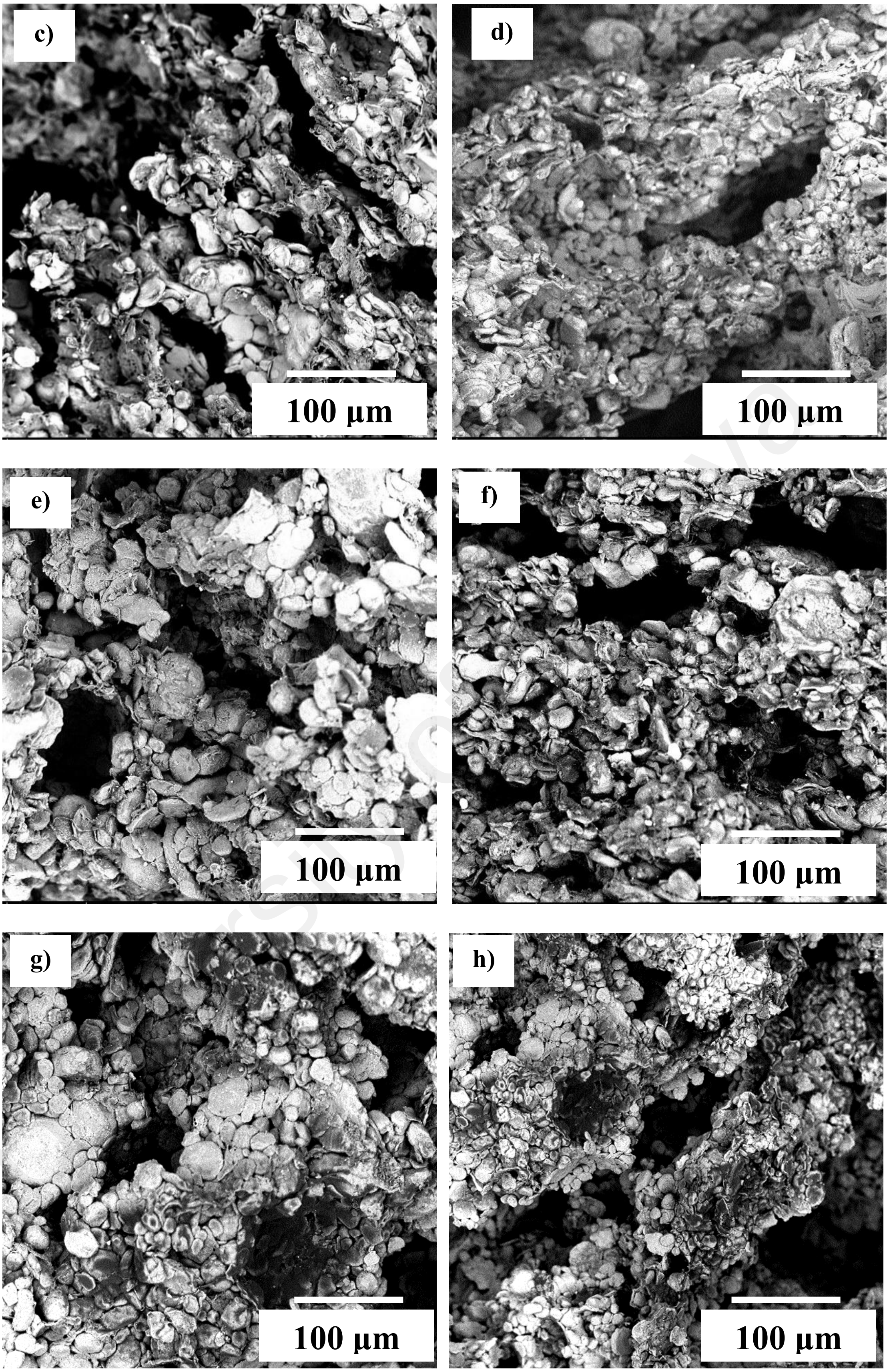
c)
100 µm
d)
100 µm
e)
100 µm
f)
100 µm
g)
100 µm
h)
100 µm

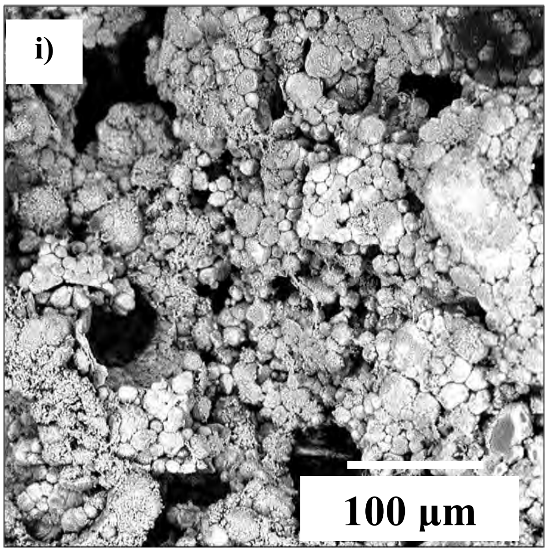

Figure 4.11 : FESEM micrograph of porous Al during sintering at a) 40 wt. % of PMMA and 450 °C sintering temperature, b) 45 wt. % of PMMA and 450 °C sintering temperature, c) 50 wt. % of PMMA and 450 °C sintering temperature, d) 40 wt. % of PMMA and 475 °C sintering temperature, e) 45 wt. % of PMMA and 475 °C sintering temperature, e) 50 wt. % of PMMA and 475 °C sintering temperature, f) 40 wt. % of PMMA and 500 °C sintering temperature, g) 45 wt. % of PMMA and 500 °C sintering temperature and e) 50 wt. % of PMMA and 500 °C sintering temperature

SUMMARY

Table 4.5 presents the summary of the important findings obtained on porous Al processing in Phase 1. Based on these findings, it can be summarized that fabrication of porous Al in Phase 1 based on the aforementioned processing parameters has resulted in unsatisfactory sintered densities, compressive strength and morphology of the resultant porous specimens. On the other hand, fracture of some PMMA particle as a space holder material was observed during mixing due to the impact of high energy planetary ball equipment that resulted in irregular pores shape and smaller pores size (micro-pores) in the metallic structure instead of macro-pores that replicates the initial morphology of PMMA space holder. This resulted in porous specimen with low densities and compressive strength. On the other hand, incomplete sintering was observed for all the sintered porous specimens at low sintering temperatures of 450 °C and 475 °C. A slight increase in sintering quality of porous specimen was obtained with the highest sintering temperature of 500 °C due to the minor reduction in particle boundaries and little neck formation between Al particles. Therefore, it is reasonable to summarize that the processing parameters along with mixing equipment introduced during fabrication were inappropriate to process porous Al with desirable properties and morphology. Based on these unsatisfactory findings, porous Al with different processing conditions (mixing equipment, sintering profile, PMMA content and sintering temperature) has been developed in Phase 2.

Table 4.5 : Summary of important findings on porous Al processing in Phase 1

Output	**Minimum sintering temperature of 450 °C**	**Maximum sintering temperature of 500 °C**	**PMMA content (wt. %)**
Density (g/cm^3)	1.233	1.7343	40
	1.3908	1.662	45
	1.1592	1.593	50
Porosity (%)	32.96	40.69	40
	38.5	45.7	45
	42.67	51.17	50
Compressive strength (MPa)	1.456	2.73	40
	1.282	1.780	45
	0.851	1.616	50

4.4 PHASE 2

4.4.1 SUPPLEMENTARY STUDIES

Supplementary studies based on the variation of Sn content and sintering temperature were performed to evaluate the sintering response of Al material prior to fabrication of porous Al. In the case of sintering temperature variation, the investigation was made based on the evaluation of physical characteristic and morphology of porous Al at 30 wt. % of PMMA. In contrast, the effect of Sn content on the physical characteristic, densities and morphology of sintered dense Al and porous Al at 30 wt. % of PMMA was studied prior to its optimization. Details on these supplementary studies are listed in the following section.

4.4.2 SINTERING TEMPERATURE VARIATION

In this section, the tested ranges of sintering temperature include 580 °C, 590 °C and 600 °C. The selection of optimum sintering temperature was made based on the physical characteristic inspection and morphology of porous Al at 30 wt. % of PMMA. An additional characterization by XRD analysis was done to monitor possible phase changes associated with sintering temperature variation.

4.4.3 PHYSICAL CHARACTERISTIC OF POROUS ALUMINUM SPECIMEN

Figure 4.12 (a-c) illustrates the images of physical characteristic of porous Al at 30 wt. % of PMMA sintered at various temperature. It can be seen that, perfect porous specimen that preserved its original shape with sharp edges was obtained during sintering at 580 °C. As the sintering temperature was increased to 590 °C, the porous specimen still maintained its original shape but severe cracking with rough surface and insufficient strength for further handling and testing were noticed. Further increased the sintering temperature to 600 °C resulted in imperfect porous specimens with long induced cracking, spalling and even collapsing of porous body.

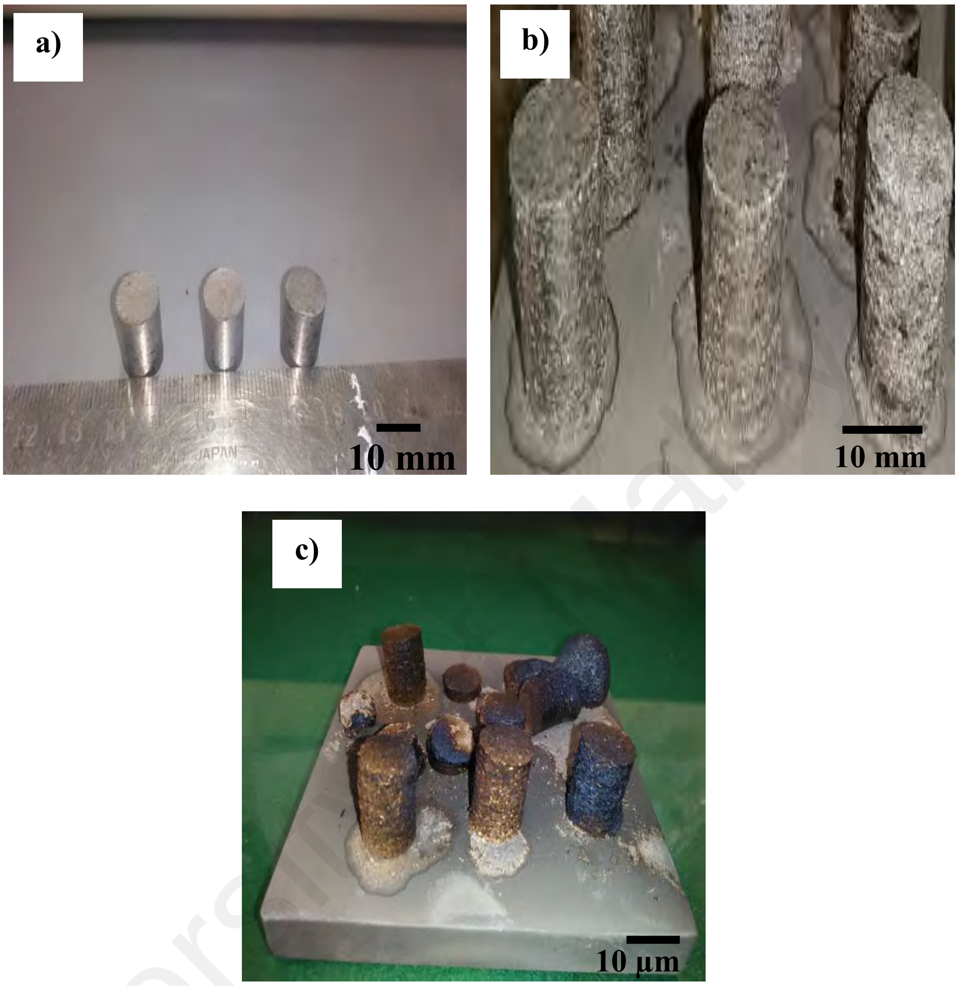

Figure 4.12 : Physical characteristic of porous Al at 30 wt. % PMMA content during sintering at a) 580 °C, b) 590 °C and c) 600 °C

It is assumed that severe oxidation level occurred at 600 °C, as the color of porous Al specimen turned into blue-black with some part was covered with gold-like color. Further test based on EDS analysis confirmed greater affinity of Al towards oxygen during sintering at higher temperatures as presented in Table 4.6. An increased in oxygen content from 0.45 wt. % to 0.98 wt. % was recorded during sintering at 580 °C whereas further increased of the oxygen content to 2.14% was observed with increasing sintering temperature to 600 °C. Therefore, it can be concluded that sintering above

580 °C is undesirable due to the resultant imperfect porous specimen with severe oxidation level that subsequently produce porous Al specimens with insufficient strength for further handling and testing.

4.4.4 X-RAY DIFFRACTION (XRD) ANALYSIS

The XRD patterns of sintered porous Al at 30 wt. % of PMMA at different sintering temperature are revealed in Figure 4.13 (a-c). It is noted that Al rich phase was majorly found in the XRD pattern of all samples, characterized by the (111), (200), (220) and (311) diffraction peaks at 38.58°, 44.83°, 65.21° and 78.32°, respectively. No additional peaks were seen in the XRD patterns of all the sintered porous Al, suggesting that Al did not react with PMMA space holder material during sintering. On the other hand, the intensity of all Al peaks were found to decrease with increasing sintering temperature from 580 °C to 590 °C and 600 °C, demonstrating inferior crystalline Al formation during sintering. It is postulated that sintering above 590 °C reduced the sintering effectiveness due to the increase in oxygen level as tabulated in Table 4.6 and thus it is recommended that sintering temperature should be maintained below this temperature.

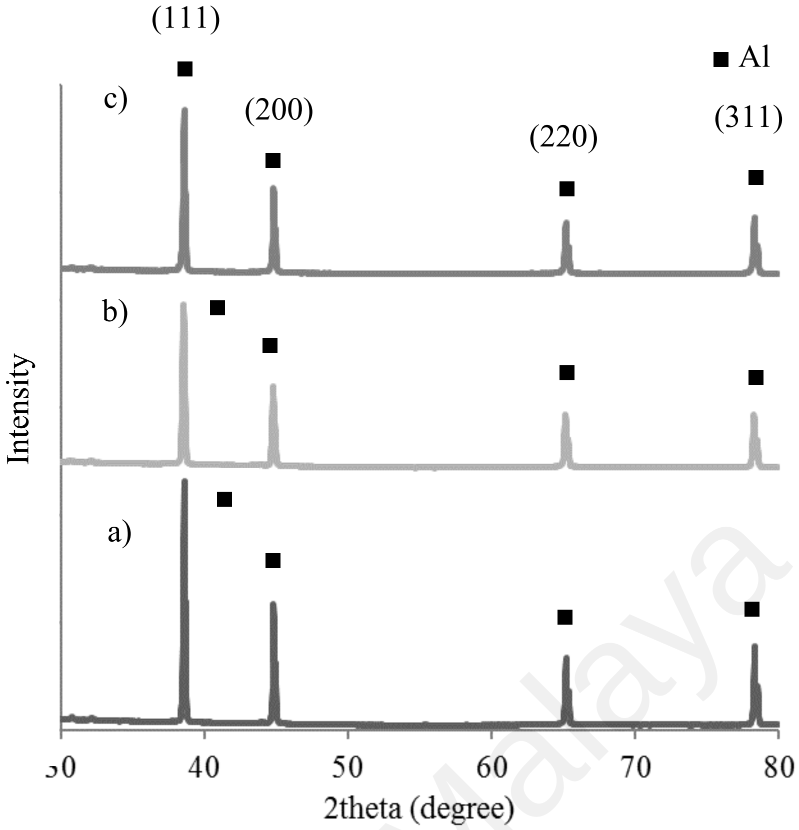

Figure 4.13 : XRD patterns of porous Al at 30 wt. % of PMMA during sintering at temperatures of a) 580 °C, b) 590 °C and c) 600 °C

4.4.5 FIELD EMISSION SCANNING ELECTRON MICROSCOPY (FESEM) ANALYSIS

Figure 4.14 (a-c) reveals the FESEM micrographs of the resultant cross section of porous Al with 30 wt. % of PMMA at different sintering temperature. It can be obviously seen that the pores in the resultant porous Al were mainly composed of closed macro-pores structure that homogenously distributed and isolated from each other by a distinct Al wall (average thickness of 45. 87 µm) regardless of the sintering temperature. However, in comparison to Figure 4.14 (a), the appearance of particle boundaries was obvious at the Al wall during sintering at 590 °C and 600 °C (Figure 4.14 (c)), conforming ineffective sintering due to the increased in oxygen level as demonstrated in Table 4.6. The oxygen content during sintering at 590 °C and 600 °C was increased from 0.45 wt. % to 1.08 wt. % and 2.14 wt. %. This shows that contamination had been inhibited sintering process that consequently prevented desirable metallurgical bonding between the cell walls of Al during sintering at higher temperatures of 590 °C and 600 °C. It is known that Al has strong attraction towards oxygen, thus excessive sintering temperature tends to elevate the oxidation level as realized in the current research. Studies have shown that it is important to guarantee effective metallurgical bonding between the Al walls in obtaining porous Al with better quality. Kim et al. (2013) reported on the brittle behavior of titanium scaffolds after sintering due to an increased in oxygen content from 0.297 to 1.118 wt. %. Similar findings were also found in the study of Hsu et al. (2013), in which further contamination of oxygen in titanium was documented with an increased in sintering temperature that deteriorated the compressive strength of porous titanium alloy. On the other hand, smooth porous structure with minimal appearance of particle boundaries was obtained during sintering at low temperature of 580 °C, showing desirable metallurgical bonding between the cell walls as evident in Figure 4.14 (a). In addition, a clear reduction in pores formation with increasing sintering temperature was also observed mainly at maximum temperature of 600 °C. This could be attributed to the accumulation of Al agglomerates on some areas of pores structure as evident in Figure 4.14 (c). From these findings, it is reasonable to infer that the sintering of closed-cell porous Al should take place below 590 °C to minimize contamination and as well as to preserve closed pores formation so that porous Al with better quality traits can be accomplished.

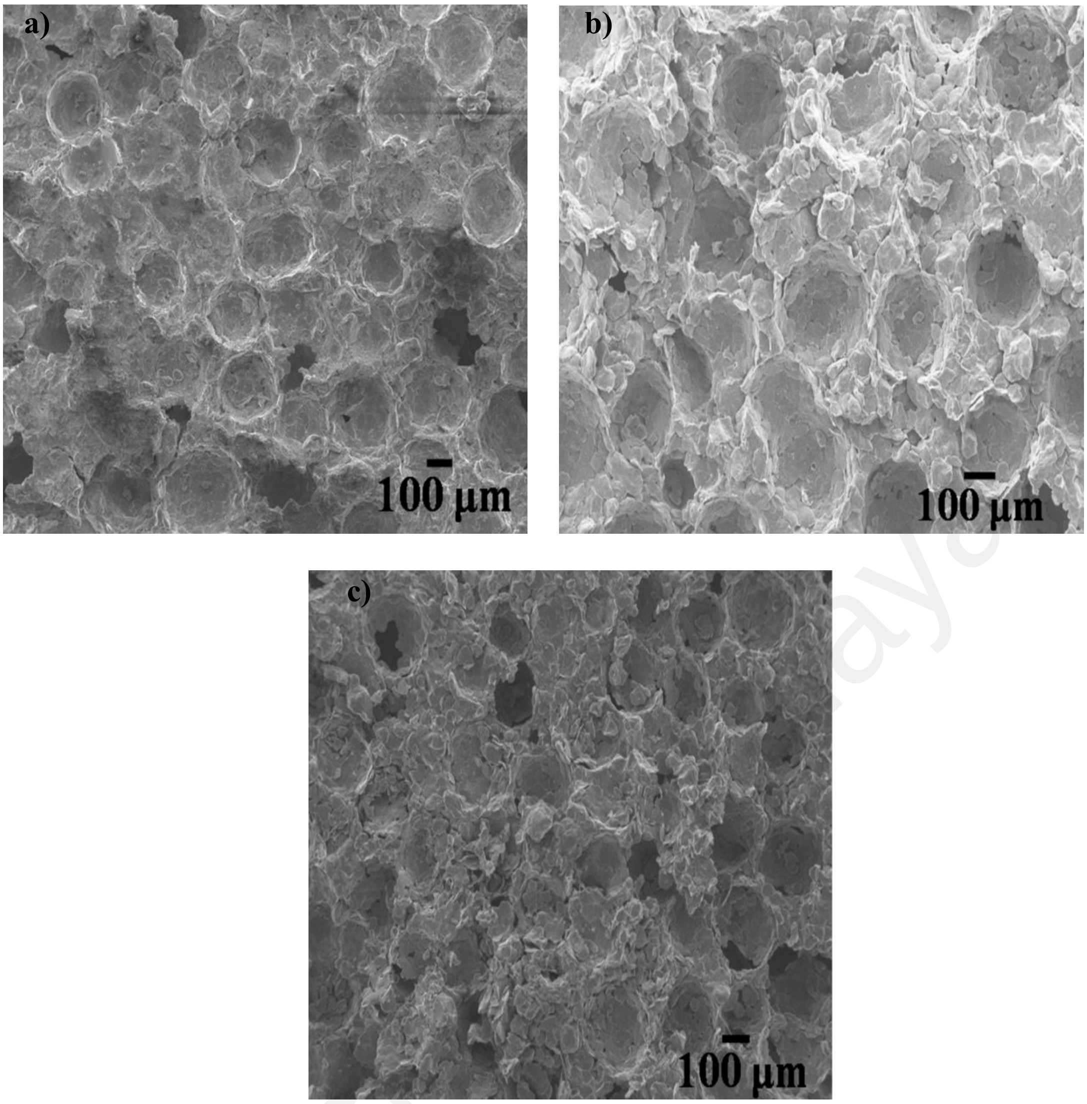

Figure 4.14 : FESEM micrographs of porous Al structure with 30 wt. % PMMA at sintering temperatures of a) 580 °C, b) 590 °C and c) 600 °C

Table 4.6 : Oxygen content of final powder mixture and sintered porous Al at 30 wt. % of PMMA at different sintering temperature from EDS analysis. Data are presented in mean ± standard deviation

Sintering Temperature (°C)	Oxygen Content (wt. %)
Final powder mixture (elemental powder mixture + PMMA)	0.45±0.08
580	0.63±0.13
590	1.08±0.14
600	2.14±0.11

4.4.6 TIN CONTENT VARIATION

Sintering of compacted Al is challenging considering Al is a passive material. This could be attributed to the presence of aluminum oxide (Al_2O_3) layer of 1 to 2 nm thickness that always cover the surface of Al particle (Katsuyoshi et al., 2007, Schaffer et al., 2001). Due to this fact, solid state sintering is usually challenging thus liquid state sintering was considered in this study with the use of Sn powder as sintering additive to assist liquid phase sintering of Al. Theoretically, Sn melts during sintering and fills the gaps between Al particles and wetting their surfaces (Katsuyoshi et al., 2007; MacAskill et al., 2010). In order to realize this theory, the addition of Mg is necessary to break up the Al_2O_3 layer and promote metal to metal contact between Al particles (Katsuyoshi et al., 2007; MacAskill et al., 2010).

Considering these facts, although a preliminary study to investigate the sintering response of Al via sintering temperature variation was performed; additional preliminary study on the effect of Sn content on the sintering response of Al was also considered. Therefore, in the current research, the contents of Sn were varied between 1.5 wt. %, 2 wt. % and 2.5 wt. % at fixed Mg content of 0.5 wt. % to investigate their effect on the sintering response of sintered Al and porous Al at 30 wt. % of PMMA (physical characteristic, green density, sintered density, and morphology). Based on the previous findings, similar sintering temperature was applied (580 °C) in the current study for sintering of compacted Al and compacted mixture of Al and PMMA spacer (30 wt. %) prior to optimization of Sn content.

4.4.7 ELEMENTAL POWDER MIXTURE WITH DIFFERENT TIN CONTENT

In this section, different batch of mixing was carried out to prepare elemental powder mixture with different Sn content of 1.5 wt. %, 2 wt. % and 2.5 wt. %. Mixing was carried out using low energy ball milling equipment with the presence of zirconia ball with the powder to ball ratio of 1:10 for 12 hr at speed of 60 rpm. Compaction of elemental powder mixture was performed at the pressure of 250 MPa followed by sintering at 580 °C for 2 hr. Morphology characterization of elemental powder mixture with different Sn content was initially discussed in the following section.

4.4.8 FIELD EMISSION SCANNING ELECTRON MICROSCOPY (FESEM) ANALYSIS

Figure 4.15 (a-c) shows the FESEM images of elemental powder mixture at different Sn content after mixing for 12 hr. The structures of elemental powder mixture were identified to be predominantly flattened and elongated with particle size less than 50 μm. The elongated structure of elemental powder mixture replicated the starting structure of Sn powder as illustrated from FESEM micrographs in Figure 4.3 (c). As the Sn content was increased to 2 wt. % and 2.5 wt. %, the elongated structure became noticeable thus confirmed an increased Sn content in the elemental powder mixture. In addition, the overlapping and intimate contact between the flattened particles was also became visible with increasing Sn content particularly at 2.5 wt. % that resulted in the formation of layered structure as seen in Figure 4.15 (b-c).

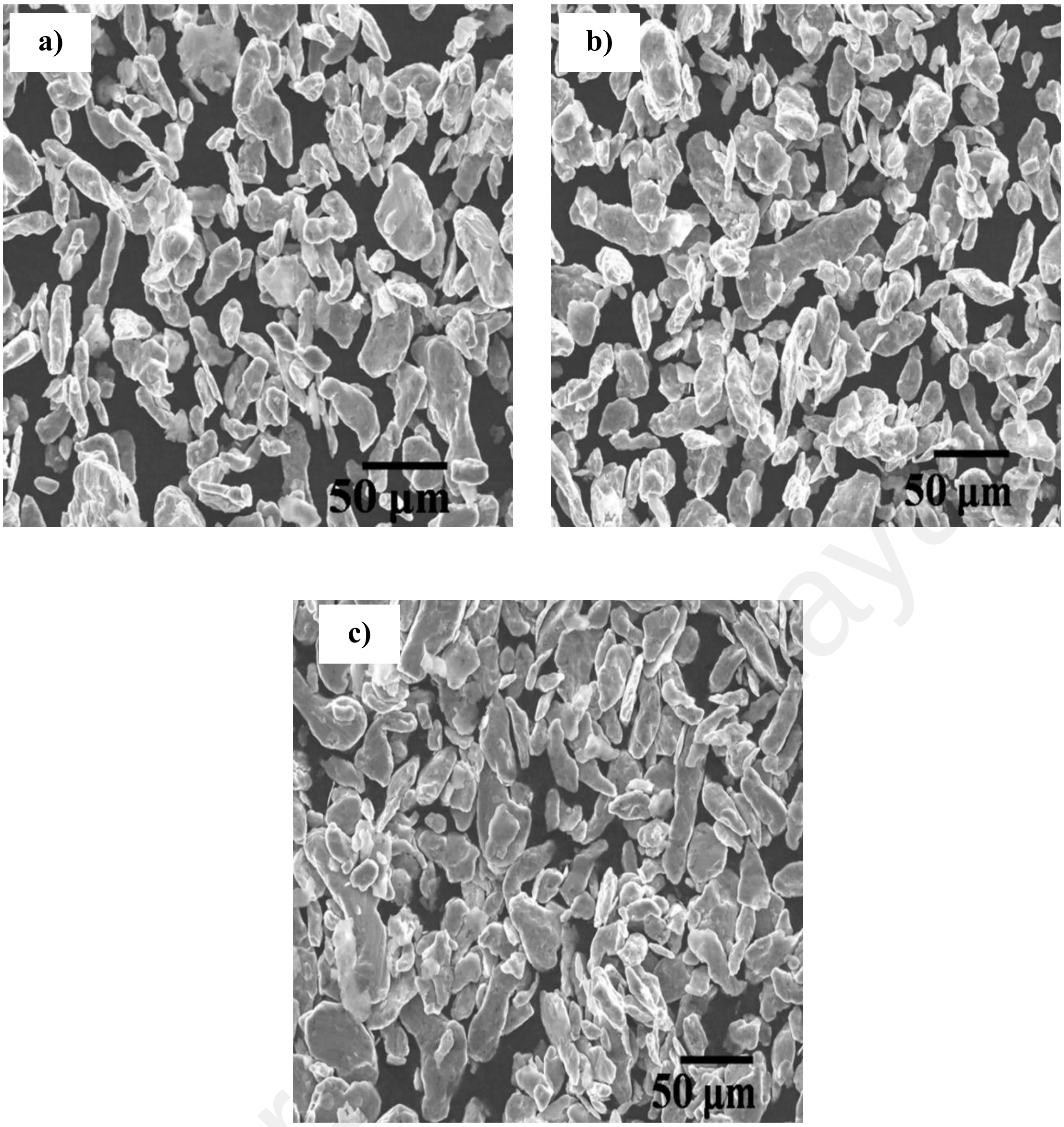

Figure 4.15 : FESEM micrographs of a) elemental powder mixture at 1.5 wt. % Sn content, b) elemental powder mixture at 2 wt. % Sn content and c) elemental powder mixture at 2.5 wt. % Sn content after 12 hr mixing

4.4.9 GREEN DENSITY OF COMPACTED ALUMINUM

Figure 4.16 illustrates the green density of compacted Al as a function of Sn contents. The green density of compacted Al increased with increasing Sn content and became stable at the utmost Sn content of 2.5 wt. %. The green densities of compacted Al increased from 2.524 g/cm^3 to 2.543g/cm^3 when the Sn content was increased from 1.5 wt. % to 2.5 wt. %. This could be attributed to the superior density of Sn element

(7.3 g/cm^3) compared to Al density (2.7 g/cm^3) (Dewidar, 2012). Consequently, higher green density was obtained when more content of Sn was added into the compacted powder. This designates that Sn powder aided compressibility of compacted Al. Similar finding was also reported before (Dhokey et al., 2013; Sercombe, 1998; Sercombe and Schaffer, 1999). According to Sercombe (1998), an increased in green density with increasing Sn content can be attributed to the deformation of soft Sn particle into pore spaces during compaction.

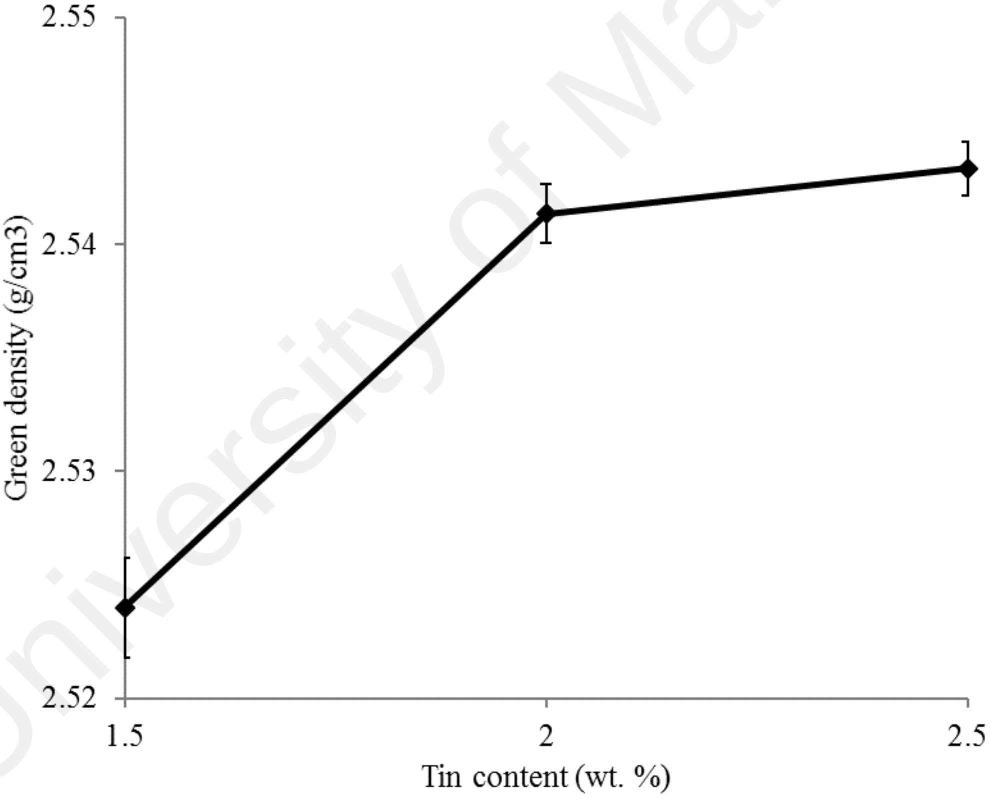

Figure 4.16 : Green density of compacted Al as a function of Sn content

4.4.10 SINTERED ALUMINUM SPECIMEN

4.4.11 PHYSICAL CHARACTERISTIC OF SINTERED ALUMINUM SPECIMEN

Figure 4.17 (a-c) illustrates the images of physical characteristic of sintered Al specimen at different content of Sn. It can be viewed that in term of color changes observation, the black color of sintered Al body that usually attributed to oxidation (higher coating of Al_2O_3 film on the surface of sintered Al body) reduced with increasing Sn content. The highest addition of Sn content (2.5 wt. %) resulted in silver-like color that replicated the color of starting Al powder. This shows that the film coating of Al_2O_3 was greatly disrupted with the addition of maximum Sn content of 2.5 wt. %. EDS analysis (Table 4.7) confirmed greater reduction of oxygen content to 0.44 wt. % for the resultant sintered Al with 2.5 wt. % of Sn compared to the oxygen content of 1.5 wt. % and 2 wt. % of Sn that shows the oxygen content of 0.58 wt. % and 0.51 wt. %.

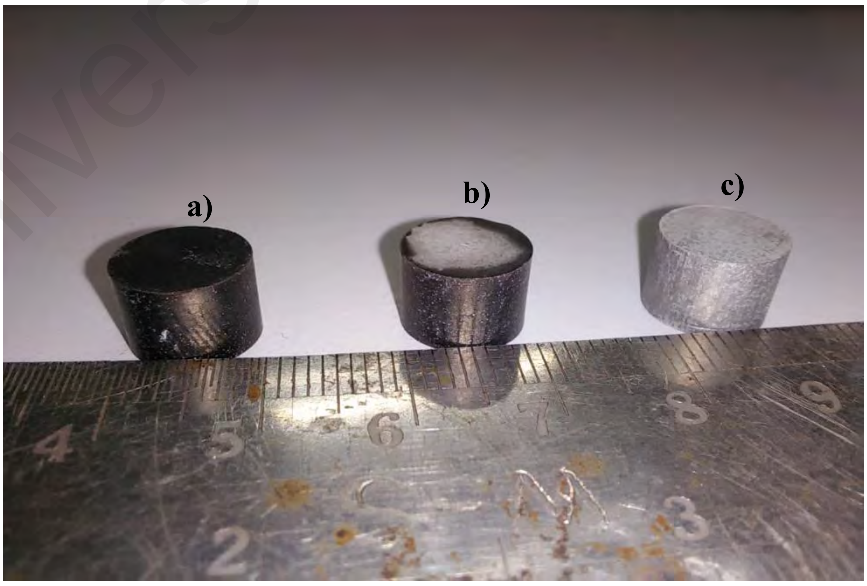

Figure 4.17 : Physical characteristic of sintered Al specimen at different Sn content of a) 1.5 wt. %, b) 2 wt. % and c) 2.5 wt%

Table 4.7 : Oxygen content reading of elemental powder mixture and sintered dense Al at various tin contents from EDS analysis. Data are presented in mean ± standard deviation

Tin content (wt. %)	Oxygen Content (wt. %)
Elemental powder mixture	0.22±0.10
1.5 (sintered at 580 °C)	0.58±0.12
2 (sintered at 580 °C)	0.51±0.13
2.5 (sintered at 580 °C)	0.44±0.11

4.4.12 FIELD EMISSION SCANNING ELECTRON MICROSCOPY (FESEM) ANALYSIS

Figure 4.18 (a-c) demonstrates the FESEM micrographs of unpolished cross section of sintered Al with 1.5 wt. %, 2 wt. % and 2.5 wt. % of Sn content. At low Sn content of 1.5 wt. %, poor sintering quality was observed due to minimal interparticle necking, profusion of particle boundaries and lack of pores rounding (isolated pores) as shown in Figure 4.18 (a). This indicates that lowest liquid level was found to be inadequate to fill all pores thus prevented efficient metallurgical bonding between Al particles. On the other hand, the sintering quality was improved with the addition of 2 wt. % and 2.5 wt. % of Sn content as evident in Figure 4.18 (b-c). Furthermore, the presence of particle boundaries also became less noticeable with enhanced interparticle necking and great pores reduction. It is postulated that higher liquid level was sufficient to fill the pores due to the effect of Sn wetting on the surface of Al particles that improved the metallic contact between Al particles (Katsuyoshi et al., 2007; MacAskill et al., 2010). In addition, Sn particles (bright colour) were identified to be distributed within the microstructure as confirmed by EDS analysis (Figure 4.19 (a-c)). Moreover, the segregation of these Sn particles could be attributed to the wetting effect of Sn particles on the Al phases that consequently enhanced the densification of compacted Al (MacAskill et al., 2010).

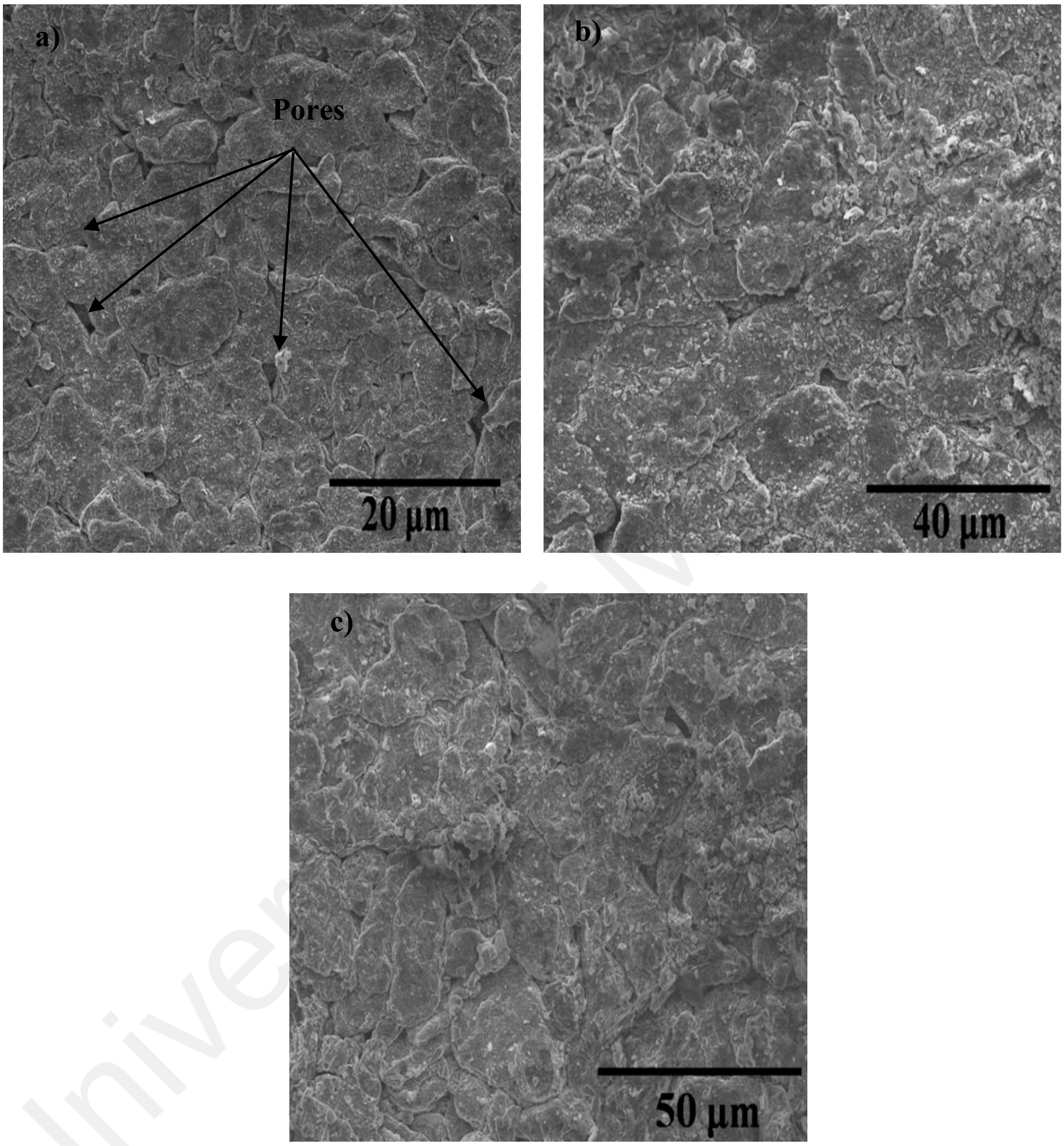

Figure 4.18 (a-c) : FESEM micrographs of sintered Al structure with Sn content of a) 1.5 wt. %, b) 2 wt. % and c) 2.5 wt. %

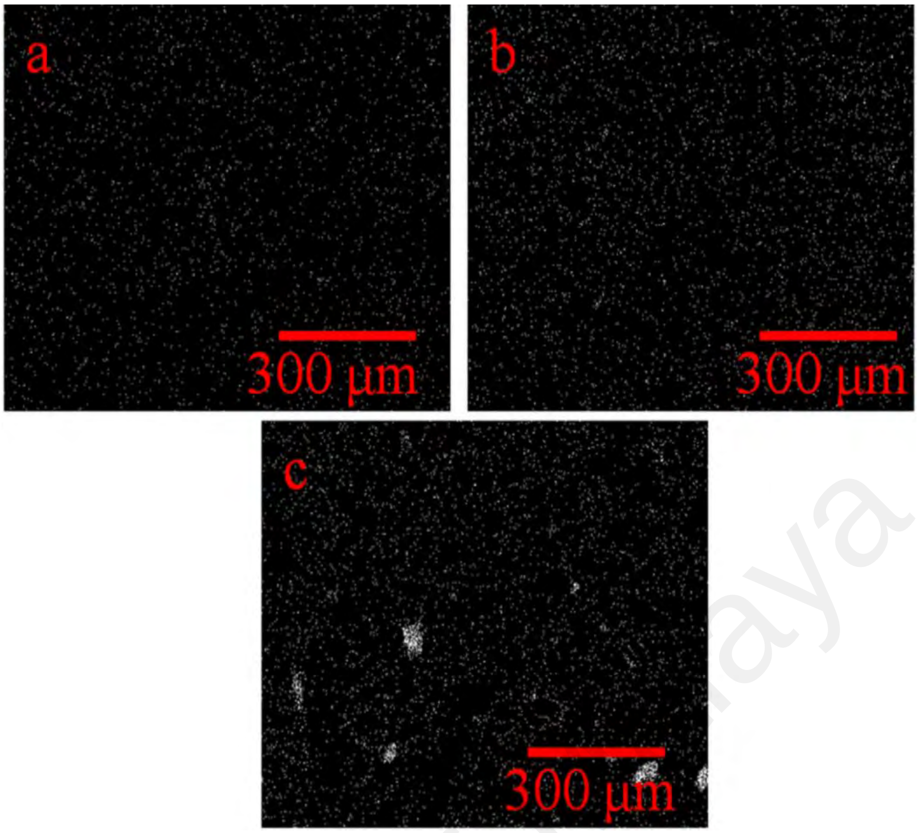

Figure 4.19 : EDS analysis of sintered Al with Sn content of a) 1.5 wt. %, b) 2 wt. % and
c) 2.5 wt. %

4.4.13 X-RAY DIFFRACTION (XRD) ANALYSIS

The XRD patterns of sintered Al with different Sn contents are revealed in Figure 4.20 (a-c). It is noted that Al rich phase was majorly found in the XRD pattern of all the samples, characterized by the (111), (200), (220) and (311) diffraction peaks at 38.87°, 45.42°, 67.16° and 78.54°, respectively. No additional peaks were seen in the XRD patterns of all the sintered Al suggesting absence of intermetallic phases formation during sintering. On the other hand, the intensity of Sn peak increased with Sn contents confirming higher Sn content in the sintered Al. As can be seen in Figure 4.20 (a-c), the peaks intensities for the sintered Al at Sn content of 2 wt. % and 2.5 wt. % were found to be higher compared to the Sn content of 1.5 wt. %, demonstrating the formation of higher crystalline Al during sintering. On the other hand, the presence of Mg peak could hardly be detected possibly due to the minor content of Mg powder employed (0.5 wt.%) during the fabrication process (Jha et al., 2013).

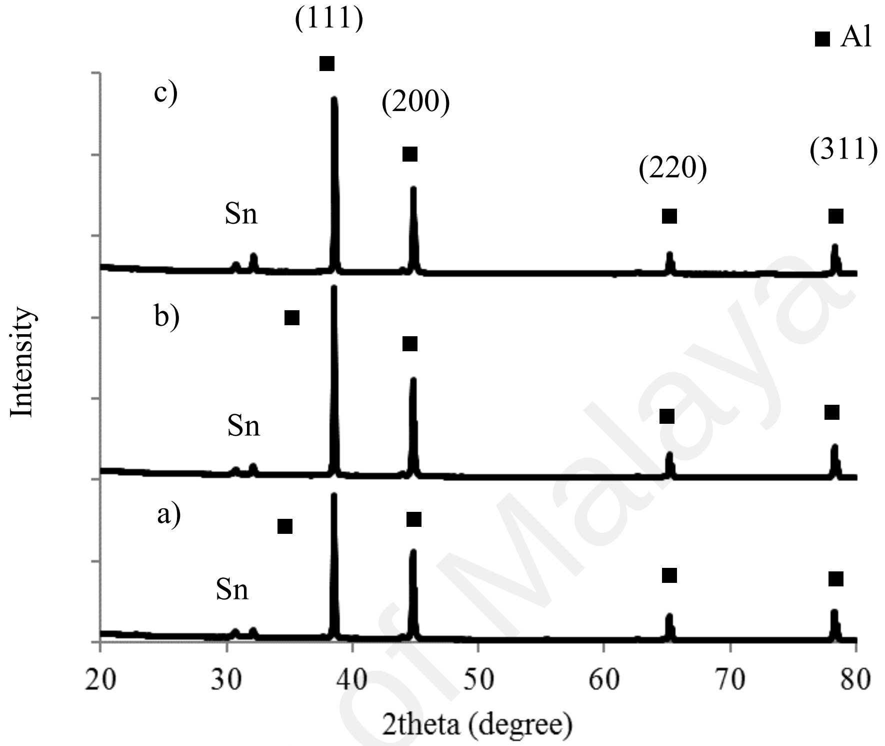

Figure 4.20 : XRD patterns of sintered Al with Sn contents of a) 1.5 wt. %, b) 2 wt. % and c) 2.5 wt. %

4.4.14 SINTERED DENSITY OF COMPACTED ALUMINUM

Figure 4.21 shows the sintered density of compacted Al with different Sn content. It can be observed that the sintered density of compacted Al increased with increasing Sn content. The sintered densities of compacted Al increased from 2.5397 g/cm^3 to 2.575 g/cm^3 when the Sn content was increased from 1.5 wt. % to 2.5 wt. %. It is clear that Sn promotes densification of sintered Al. This can be attributed to the pores reduction and particle boundaries disappearance when the Sn content is higher as confirmed by FESEM images in Figure 4.18 (b-c). Similar finding was also documented in the previous studies (Sercombe, 1998; Sercombe and Schaffer, 1999).

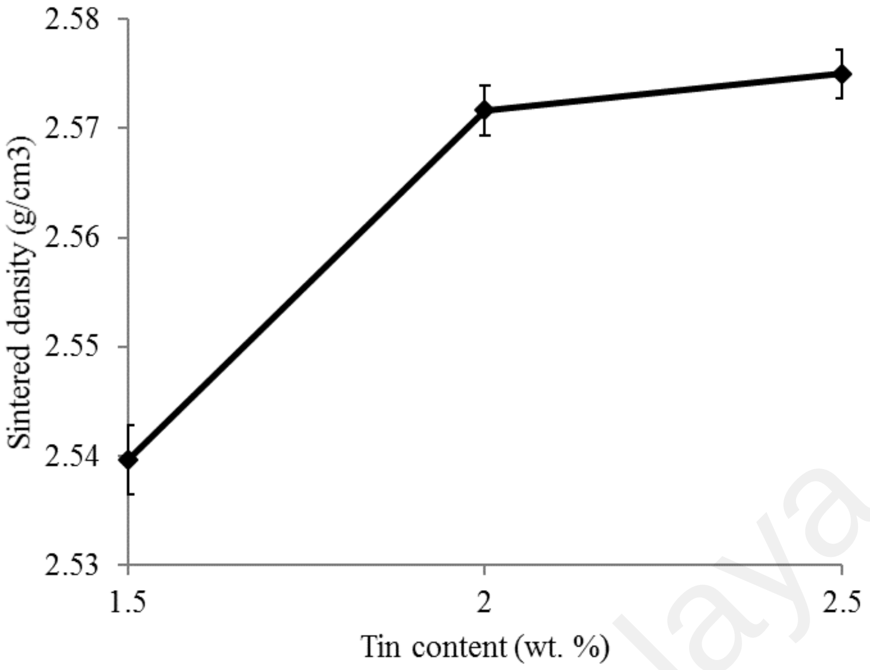

Figure 4.21 : Sintered density of compacted Al as a function of different Sn content

4.4.15 SINTERED POROUS ALUMINUM SPECIMEN

4.4.16 FIELD EMISSION SCANNING ELECTRON MICROSCOPY (FESEM) ANALYSIS

Figure 4.22 (a-c) demonstrates the FESEM micrographs of cross section of porous Al at 30 wt. % of PMMA with 1.5 wt. %, 2 wt. % and 2.5 wt. % of Sn content. It is noticed that the sintering quality of porous Al at 30 wt. % of PMMA was identical regardless of the Sn content. The formation of particle boundaries was hardly seen on the cell walls of porous Al at all content of Sn, suggesting desirable sintering quality of porous Al. On the other hand, the pores in the resultant porous Al were mainly composed of closed macro-pores structure that homogenously distributed and isolated from each other by a distinct Al wall at all Sn content. However, in comparison to Figure 4.22 (a-b), the number of pores formation was lessened for the porous Al with 2.5 wt. % of Sn (Figure 4.22 (c)) due to the development of dense cell wall, showing that 2.5 wt. % of Sn content promoted densification of porous Al as confirmed from sintered density result as in Figure 4.23.

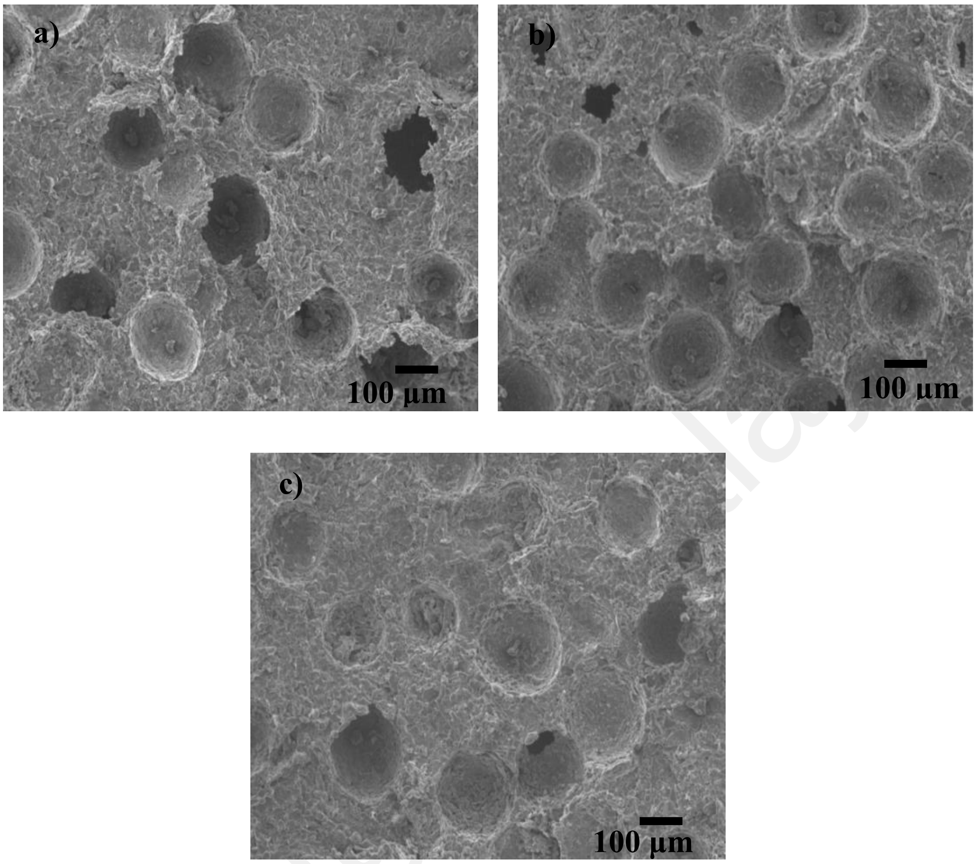

Figure 4.22 : FESEM micrographs of porous Al structure at 30 wt. % of PMMA with a) 1.5 wt. % Sn, b) 2 wt. % Sn and c) 2.5 wt. % Sn

Considering trivial solubility of Sn in Al, persistent liquid formation throughout the entire sintering was expected thus it is assumed that higher Sn content of 2.5 wt. % was able to seal some micro pores hence decreased the pores formation (Sercombe and Schaffer, 1999). Remarkable elimination of porosity or macro pores as noticed in the current study with the addition of Sn greater than 2 wt. % was also reported in the study of Sercombe and Schaffer (1999). Therefore, it is suggested that the Sn content should not exceed 2 wt. % in order to preserve the macro pores formation.

4.4.17 SINTERED DENSITY OF POROUS ALUMINUM

Figure 4.23 shows the sintered density of porous Al at 30 wt. % of PMMA as a function of Sn content. A considerable increased in the sintered density of porous Al with increasing Sn content was observed, verifying densification of porous specimen. The sintered density of porous Al increased from 1.207 g/cm^3 to 1.482 g/cm^3 when the Sn content was increased from 1.5 wt. % to 2.5 wt. %.

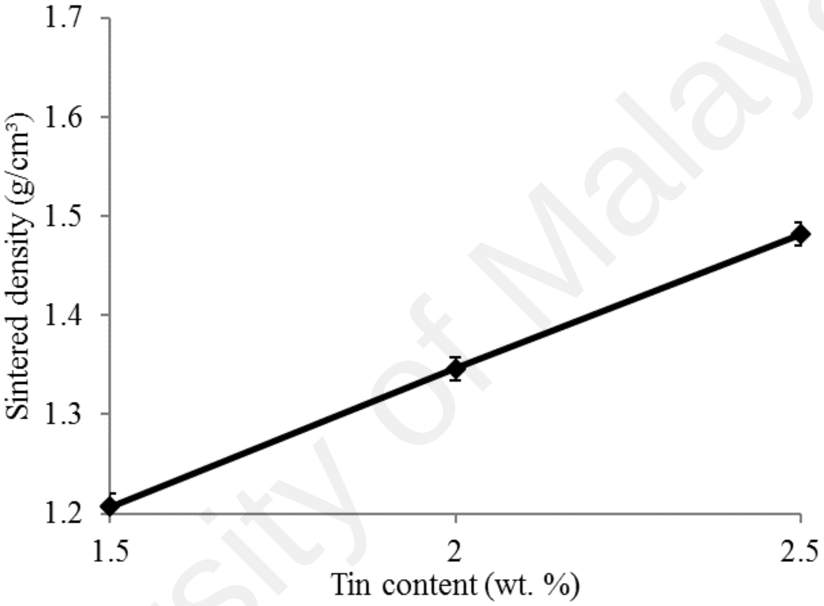

Figure 4.23 : Sintered density of porous Al at 30 wt. % of PMMA as a function of Sn content (wt. %)

Clearly, the addition of Sn content as sintering additive during fabrication enhanced the sintered density of the porous Al. This can be attributed to the fact that lower volume of closed pores was created owing to the densification of Al cell walls when the Sn content is higher as evidenced in Figure 4.22 (c). In contrast, low sintered density of porous Al with the addition of 1.5 wt. % and 2 wt. % Sn was associated with higher number of closed pores with thinner cell walls as evidenced in Figure 4.22 (a-b). Similar finding was also reported by Sercombe and Schaffer (1999).

4.4.18 X-RAY DIFFRACTION (XRD) ANALYSIS

The XRD patterns of sintered porous Al at different Sn contents are revealed in Figure 4.24 (a-c). It is noted that Al rich phase was majorly found in the XRD pattern of all the samples, characterized by the (111), (200), (220) and (311) diffraction peaks at 38.59°, 44.83°, 65.21° and 78.32°, respectively. Moreover, no additional peaks were seen in the XRD patterns of all the sintered porous Al, suggesting that Al did not react with PMMA spacer during sintering.

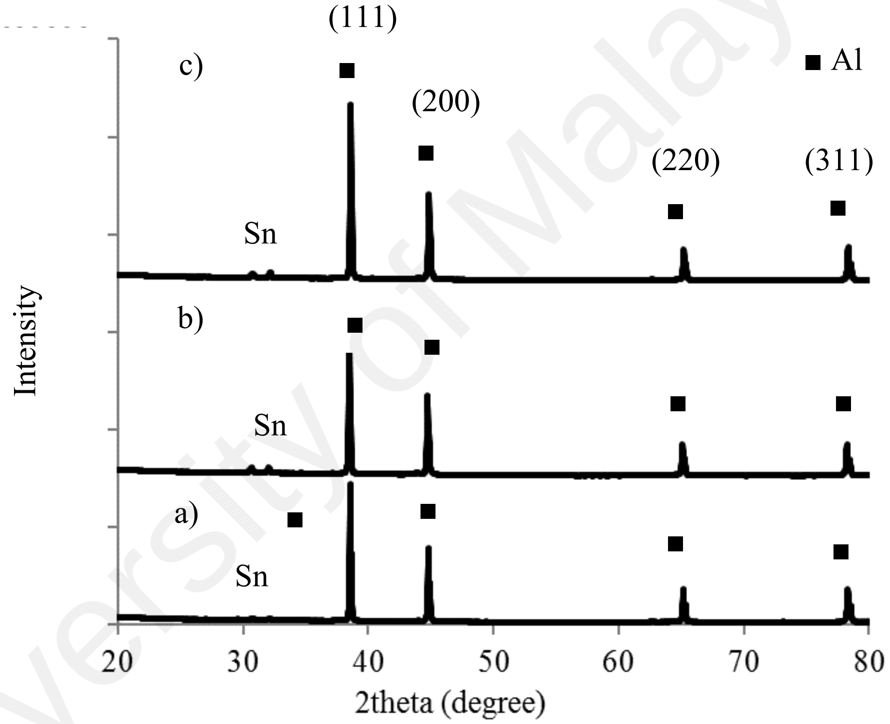

Figure 4.24 : XRD patterns of sintered porous Al at 30 wt. % of PMMA with Sn contents of a) 1.5 wt. %, b) 2 wt. % and c) 2.5 wt. %

As can be seen in Figure 4.24 (b-c), the peaks intensities for the sintered porous Al at higher Sn content of 2 wt. % and 2.5 wt. % were found to be slightly higher compared to the porous Al at Sn content of 1.5 wt. %, demonstrating the formation of higher crystalline Al during complete sintering. On the other hand, the intensity of Sn peak increased with Sn contents validating higher Sn content in the resultant porous Al. Moreover, the presence of Mg peak could hardly be detected possibly due to the minor content of Mg powder employed (0.5 wt.%) during the fabrication process (Jha et al., 2013).

SUMMARY

Based on the findings on the sintering temperature variation, it is reasonable to infer that low sintering temperature of 580 °C (88% of the melting point of Al) is desirable for sintering purpose of porous Al due to the contamination free with satisfactory degree of bonding between cell walls of aluminum that sustained the formation of closed macro-pores structure. On the other hand, the variation in tin content revealed least oxygen contamination with desirable metallic bonding and densification with increasing tin content particularly at 2.5 wt. % were documented in the case of sintered dense Al. Similar observation was also recorded for porous Al at 30 wt. % of PMMA. However, a clear reduction in the formation of macro closed-pores structure was evidenced with the addition of higher tin content mainly at 2.5 wt. %, thus intermediate range of 2 wt. % of Sn addition as sintering additive is selected for further study. Therefore, the values of sintering temperature and tin content were optimized at 580 °C and 2 wt. %.

4.5 PHASE 2 CONTINUATION

Based on the findings in terms of variation in sintering temperature and Sn content, the sintering temperature and Sn content were fixed at 580 °C and 2 wt. % throughout the development of porous Al. Details on the findings of porous Al at various processing parameters are discussed in the following sections.

4.5.1 STAGES IN MIXING PROCESS

4.5.1.1 MORPHOLOGY CHARACTERIZATION OF ELEMENTAL POWDER MIXTURE

In this study, three stages mixing process were employed prior to porous Al fabrication. FESEM analysis was done to study the homogeneity level of elemental powder mixture to determine the optimum mixing time during the first stage of mixing process. Figure 4.25 (a-b) shows the FESEM images of elemental powder mixture at different mixing time. At this initial mixing stage, the mixing time was varied between 8 hr and 12 hr while the mixing speed was set constant at 60 rpm. The term 'low energy' was adopted in this section due to the low energy (low speed) applied during the mixing process. From inspection of Figure 4.25 (a), the particle size of elemental powder mixture was noticed to be irregular after 8 hr of mixing process. Moreover, agglomeration of elemental powder mixture was discovered due to the bulky geometrical shape of powder mixture particle whereas the rest was found to be flattened. It is known that Al, Mg and Sn powders are characterized as soft materials due to their ductile nature thus excessive welding is dominant at this stage in which increasing in powder particle size was observed (Ramezani and Neitzert, 2012). This suggests that 8 hr of mixing is inadequate to induce uniform particle size and distribution of elemental powder mixture.

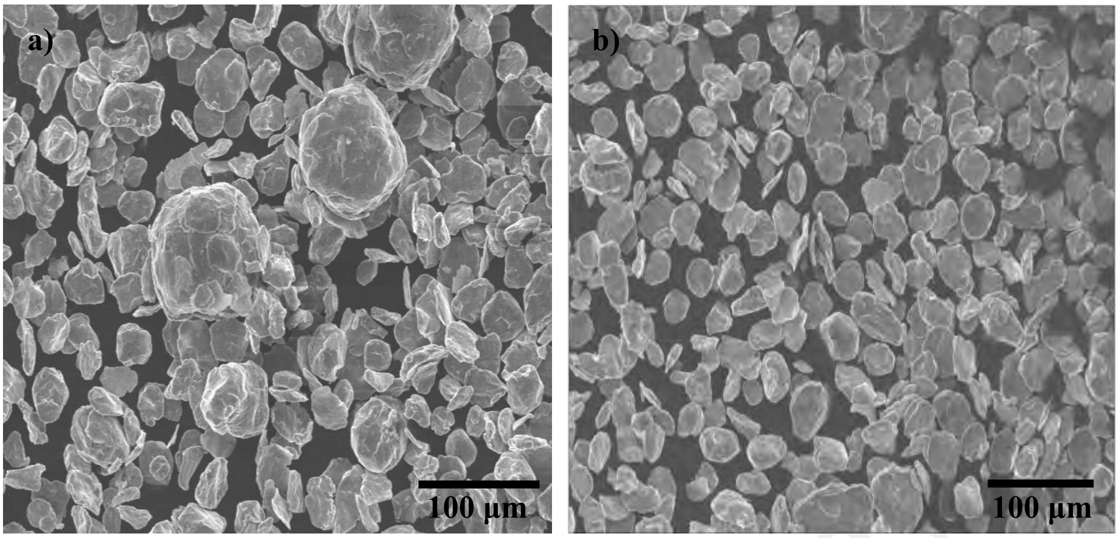

Figure 4.25 : FESEM micrograph of elemental powder mixture after mixing for a) 8 hr and b) 12 hr

As the mixing duration was increased to 12 hr, most of the elemental powder mixture particle was plastically deformed by having lamellar structure as shown in Figure 4.25 (b). These elemental powder mixture particles size were also detected to be smaller with enhanced distribution. The disappearance in agglomeration of elemental powder mixture was also noted as the mixing duration increased which is believed due to the leading process of fracturing over welding (Ramezani and Neitzert, 2012). In addition, EDS analysis confirmed that greater enhancement in the distribution of Sn and Mg powders was achieved at 12 hr of mixing as compared to 8 hr of mixing as seen in Figure 4.26 (a-d). This suggests that 12 hr of mixing was sufficient to obtain uniform particle size and distribution of elemental powder mixture. It can be concluded that repeated processes of welding, deformation and fracturing were accountable for such phenomena as discussed above.

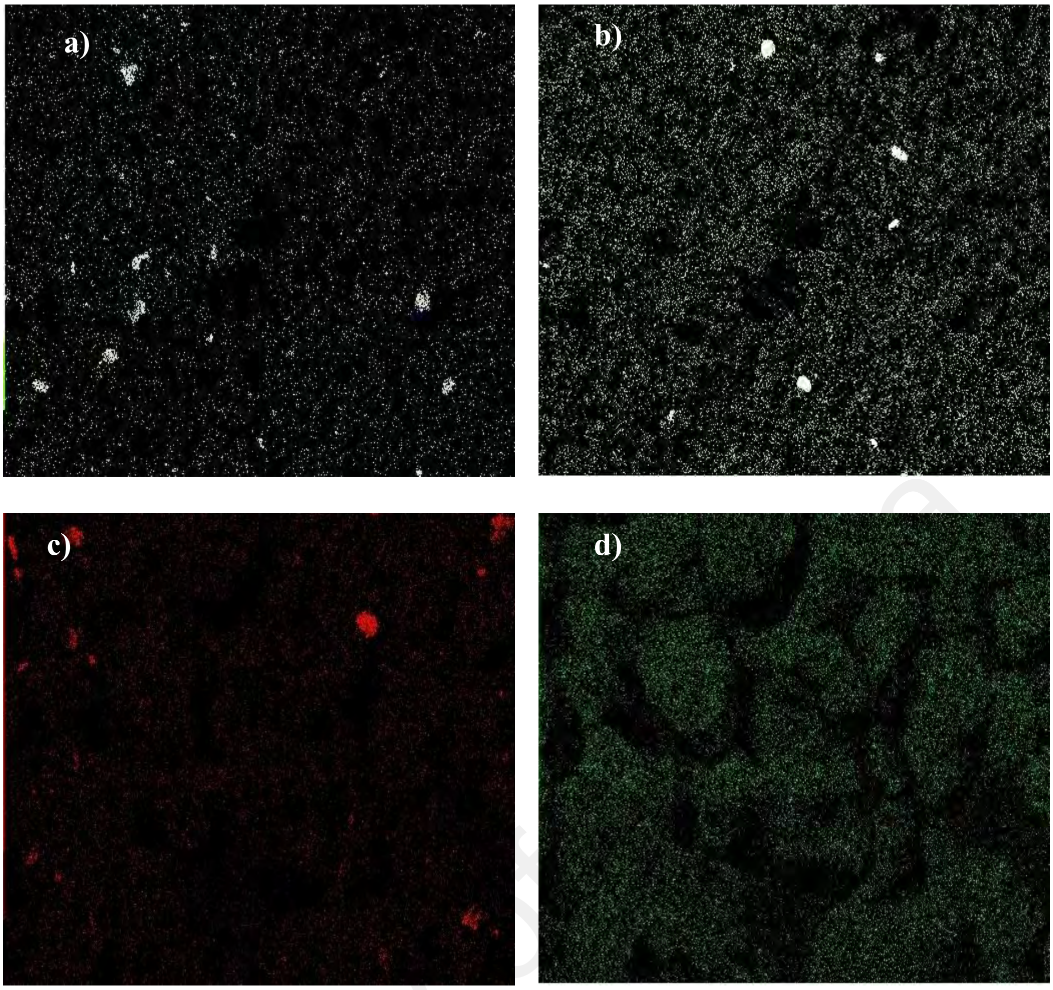

Figure 4.26 : EDS micrographs of (a) Sn powder particle and (b) Mg powder particle after 8 hr of mixing and (c) Sn powder particle and (d) Mg powder particle after12 hr of mixing

On the other hand, Figure 4.27 displays the successful adhesion of elemental powder mixture on the surface of PMMA particle during the final stage of mixing process. This shows that the use of CLE-safe oil encourages the adhesion of elemental powder mixture on the surface of PMMA thus promoting homogenous powder distribution (Kim et al., 2013). It can be seen that the initial morphology (particle size and shape) of PMMA particle was also preserved. This is important in order to ensure that the pores formation resembles the morphology of PMMA spacer thus better quality of porous Al traits can be accomplished. A study done by Zhang et al. (2005) revealed a decline in compressive strength and elastic modulus of polymeric foams was observed due to irregular pores formation prior to asymmetrical shape of spacer material. Bekoz and

Oktay (2012) also reported on decreased apparent densities and compressive behaviors of stainless steel foam with respect to irregular shape of space holder material. Jiang et al. (2005) also shared similar view in which higher compressive strength of Al foam was obtained with the use of spherical spacer holder material as compared with irregular one.

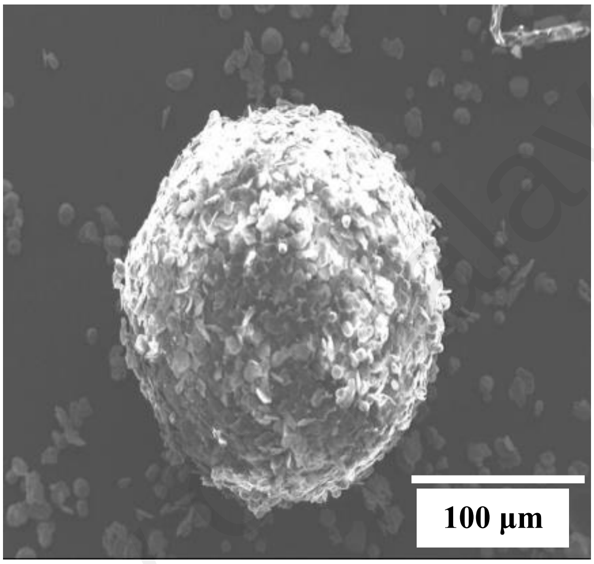

Figure 4.27 : FESEM micrograph of elemental powder mixture adhesion on the surface of space holder particle (PMMA)

4.5.1.2 X-RAY DIFFRACTION (XRD) ANALYSIS

The XRD patterns of elemental powder mixture after mixing for 8 hr and 12 hr are revealed in Figure 4.28 (a-b). It is clear that Al rich phase exists in both XRD patterns along with small peak of Sn powder. Absence of additional phases was seen for both XRD patterns, implying absence of intermetallic compound formation. Moreover, the peak intensity of elemental powder mixture was reduced with increasing mixing time indicates reduction in the particle size of elemental powder mixture as confirmed in Figure 4.28 (b).

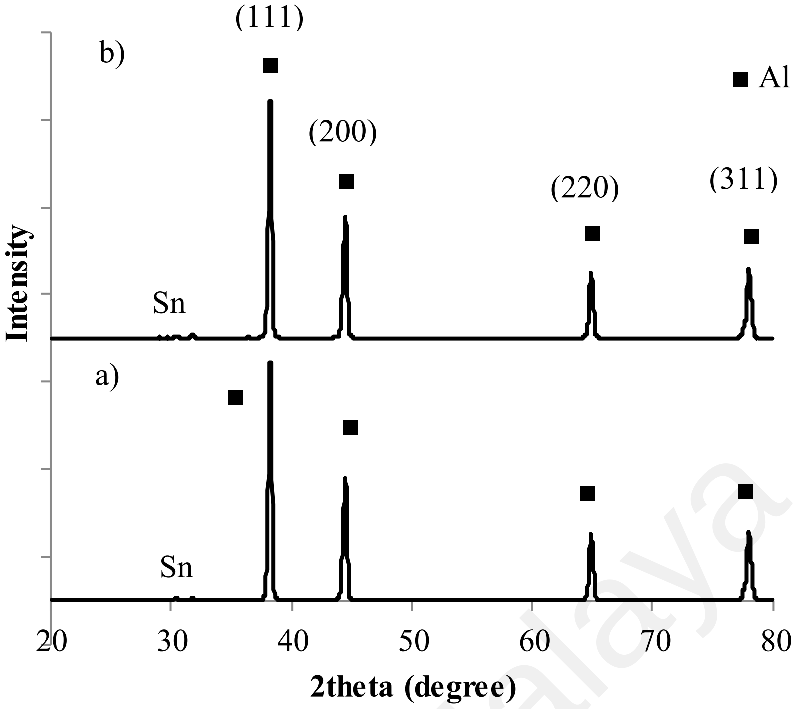

Figure 4.28 : XRD patterns of elemental powder mixture a) after 8 hr of mixing and b) after 12 hr of mixing

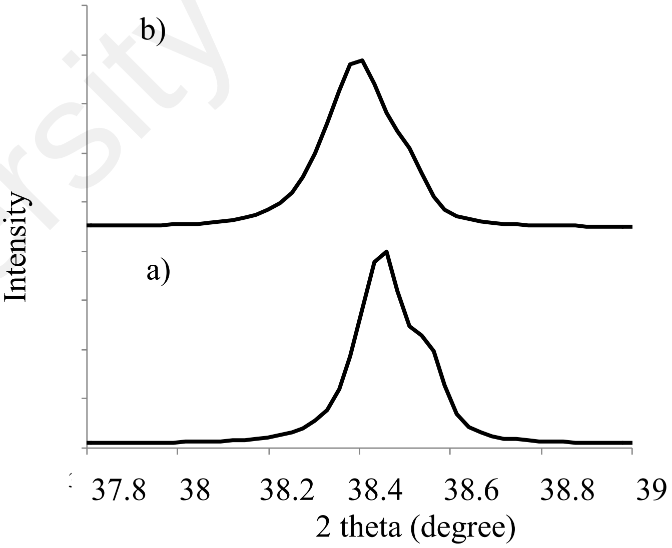

Figure 4.29 : Difference between Al peak positions after a) 8 hr of mixing and b) 12 hr of mixing

On the other hand, the presence of Sn peak disappeared with increasing mixing time to 12 hr indicates grain size reduction and accumulation of mechanical strains (Nouri et al., 2011). The disappearance of Sn peak can also be related to the diffusion of Sn atoms into Al lattice that resulted in the formation of the face centered cubic (FCC) supersaturated solid solution of Al–Sn (Wagih, 2014). This is confirmed by the clear shift of the Al peak towards lower angle as seen in Figure 4.29 (a-b). In this analysis, the presence of Mg peak could hardly be detected possibly due to the minor content (0.5 wt. %) of Mg powder added in the elemental powder mixture during the fabrication process (Jha et al., 2013).

4.5.2 COMPACTED GREEN SPECIMEN

4.5.2.1 PHYSICAL CHARACTERISTIC OF COMPACTED SPECIMEN

Similar explanation for physical characteristic of compacted specimen with different compaction pressure was obtained in this Phase 2 as in section 4.3 (Phase 1) considering similar values of pressure applied during compaction of final powder mixture (mixture of elemental powder mixture and PMMA).

4.5.2.2 PERCENTAGE OF DIAMETER CHANGE

Figure 4.30 (a-c) shows the percentage of diameter change of compacted specimen with different PMMA content as a function of compaction pressure. It can be seen that the percentage of diameter change of compacted specimen was found to increase with increasing compaction pressure and decreased with increasing PMMA content. The percentage of diameter change of compacted specimen with 20 wt. % of PMMA increased from 0.004% to 0.006% when the compaction pressure was increased from 200 MPa to 300 MPa. On the other hand, the percentage of compacted specimen was enhanced from 0.004% to 0.005% as the compaction pressure increased from 200 MPa to 300 MPa for compacted specimen with 25 wt. % of PMMA. In addition, the percentage of diameter change was increased from 0.003% to 0.004% with increasing compaction pressure at PMMA content of 30 wt. %.

Higher percentage of diameter change is usually attributed to greater spring-back or green expansion of compacted specimen (Gosh and Chatterje, 2014; Luk et al., 1997). In this context, spring-back can be defined as the expansion of a compact in three dimensions after die cavity ejection (Luk et al., 1997). Theoretically, higher green density leads to greater green expansion (Gosh and Chatterje, 2014; Luk et al., 1997). Clearly, an increased in compaction pressure increased the average percentage of diameter change whereas increasing PMMA content reduced the average percentage of diameter change of compacted specimen. Similar finding in term of compaction pressure effect on the average percentage of diameter of compacted specimen was also reported in the literature (Gosh and Chatterje, 2014; Luk et al., 1997).

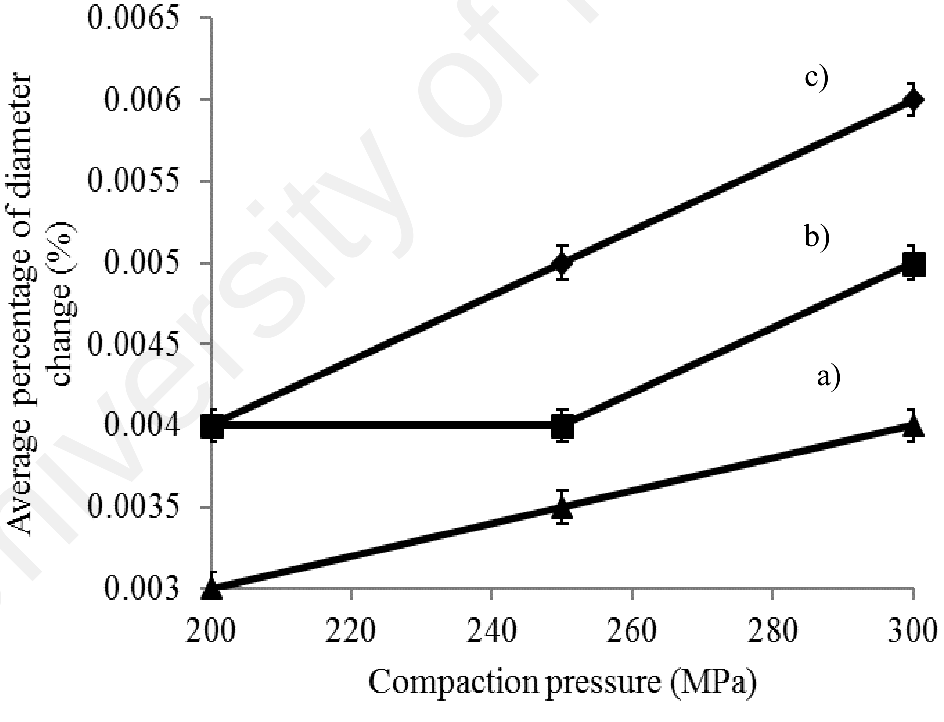

Figure 4.30 : Average percentage of diameter change of compacted specimen as a function of compaction pressure at PMMA content of a) 20 wt. %, b) 25 wt. % and c) 30 wt. %

In contrast, the result obtained in term of PMMA content effect on the average percentage of diameter change is not in agreement with the result obtained by Gosh and Chatterjee (2014) and Sai (2014) who reported that average percentage of diameter change increased with increasing reinforcement or space holder content. This can be explained by the fact that the authors introduced nano size reinforcement during fabrication that occupied the voids created by larger Al particles thus resulted in higher average percentage of diameter change with increasing reinforcement content. Therefore, the average percentage of diameter change in the current study was found to decrease with increasing PMMA content due to the use of larger PMMA particle compared to smaller Al particle.

4.5.2.3 GREEN DENSITY

Figure 4.31 (a-c) reveals the average green density of compacted specimen with various PMMA content as a function of compaction pressure. The average green density of compacted specimen was found to be sensitive with the compaction pressure. It is observed that the green density increased with compaction pressure and decreased with increasing PMMA content. This indicates that densification of compacted powder enhanced with increasing compaction pressures and decreasing PMMA contents. Similar finding was also reported in the literatures (Bakan, 2006; Bafti and Habibolahzadeh, 2010). Bakan (2006) found that the green density of stainless steel powder and carbamide mixture slightly improved with increasing compaction pressure. An increased in the green density of Al powder and carbamide mixture with respect to compaction pressure was also reported in the study of Bafti and Habibolahzadeh (2010). In the current research, the green density of compacted specimen with 20 wt. %, 25 wt. % and 30 wt. % of PMMA increased from 1.8479 g/cm^3 to 1.936 g/cm^3, 1.7878 g/cm^3 to 1.8575 g/cm^3 and 1.7182 g/cm3 to 1.7782 g/cm3 as the compaction pressure increased from 200 MPa to 300 MPa. Such phenomenon could be related to the improvement in metal-to-metal contact as well as rearrangement of metal and spacer holder particles that promote the disruption of oxide films at the surface of passive material like Al (Hao et al., 2009; Bafti and Habibolahzadeh, 2010).

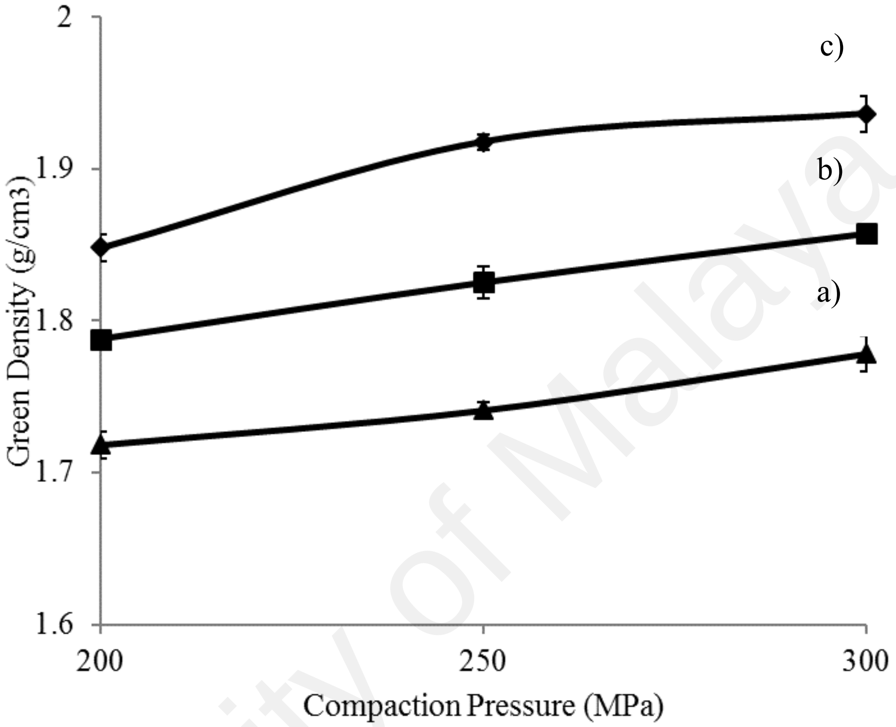

Figure 4.31 : Average green density of compacted specimen as a function of compaction pressure with PMMA content of a) 20 wt. %, b) 25 wt. % and c) 30 wt. %

According to Hao et al. (2009), two mechanisms are accountable for the disruption of these oxide films including yielding of large shear strain and shear stress in the areas of Al particles that are in direct contact with the neighboring particles resulting in the development of fresh metallic contact. The second mechanism is scratching or jabbing between Al particle and PMMA particle are possible during rearrangement of these particles under increasing pressure that eventually break up the oxide films thus encouraging fresh metallic contact (Hao et al., 2009). This is essential in order to achieve effective metallurgical bonding during subsequent sintering process. On the contrary, the average green density of compacted specimen reduced with increasing

PMMA content regardless of the compaction value. This is believed due to the lower density of PMMA (1.18 g/cm^3) as compared to Al (2.7 g/cm^3) in which as the content of PMMA increased, the average green density decreased (Dewidar et al., 2008; Barletta et al., 2009; Arifvianto and Zhou, 2014).

4.5.3 SINTERED POROUS ALUMINUM SPECIMEN

4.5.3.1 MICROSTRUCTURE CHARACTERIZATION OF POROUS ALUMINUM

Figure 4.32 (a-c) until Figure 4.40 (a-c) reveal the FESEM micrographs of the resultant porous Al with different PMMA content, compaction pressure and sintering time. It can be obviously seen that the pores in the resultant porous Al were mainly composed of closed macro-pores structure regardless of compaction pressure and sintering time, especially in the case of 25 wt. % and 30 wt. % of PMMA. However, in comparison to Figure 4.32 (a-c) until Figure 4.37 (a-c), the appearance of pores formation was hardly seen on the porous Al with 20 wt. % of PMMA (Figure 4.38 (a-c) until Figure 4.39 (a-c)) due to the development of dense cell wall, showing that 20 wt. % of PMMA content was insufficient to create the desired closed pore structure in the porous Al. It is demonstrated that the macro-pores of the porous Al are obtained by the removal of the space holder particle and are largely depend on the size and shape of the space holder particle (Dewidar et al., 2012). As evident in Figure 4.32 (a-c) until Figure 4.37 (a-c), these macro-pores were found to be homogeneously distributed in the resultant porous Al and were isolated from each other by a distinct cell wall (average thickness of 52.94 µm in the case of 25 wt. % PMMA and 45. 87 µm in the case of 30 wt. % PMMA), further corroborating the formation of closed-cell structure in the resultant porous Al (Arifvianto and Zhou, 2014). The morphology of these closed macro-pores was also observed to replicate the initial morphology of the spherical PMMA particle. The average pore size was around 159 µm (in the case of 25 wt. % and 30 wt. % of PMMA), which is almost equal to the size of PMMA particle. Studies have shown that it is important to ensure that the pores formation resembles the morphology of space holder material in obtaining porous Al with better quality. Zhang et al. (2005) revealed a decline in compressive strength and elastic modulus of porous polymeric due to irregular pores formation prior to asymmetrical shape of space holder material. Similar findings were also found in the study of Bekoz and Oktay (2012), in which higher compressive properties of porous Al was obtained with the use of spherical spacer holder material as compared to the irregular one. On the other hand, only a few micro pores were observed in the cell wall of porous Al as shown in Figure 4.32 (a-c) until Figure 4.37 (a-c) and this is probably due to incomplete sintering of Al particle. In the present study, the formation of the highest quantities of pores was obtained on the porous Al with the highest content of PMMA (30 wt. %), followed by 25 wt. % and 20 wt. % of PMMA contents at any given compaction pressure and sintering time as seen in Figure 4.32 (a-c) until Figure 4.40 (a-c), respectively.

In term of compaction pressure effect on the morphology of all the porous specimen, the appearance of pores formation was found to decrease with the maximum compaction pressure of 300 MPa due to the development of dense cell wall, suggesting that compaction pressure of 300 MPa was unfavorable to create the desired closed macro-pores structure in the porous Al, as evidenced in Figure 4.32 (c), Figure 4.33 (c), Figure 4.34 (c), Figure 4.35 (c), Figure 4.36 (c) and Figure 4.37 (c), respectively. In addition, EDS analysis (Table 4.8) confirmed the entrapment of some PMMA particle in the metallic structure due to the clear increased in the content of carbon residue, implying that the use of 300 MPa pressure during compaction resulted in difficulty of PMMA removal as the space holder particle was completely enclosed by the Al matrix (Kennedy, 2012; Arifvianto and Zhou, 2014). Owing to low and medium content of PMMA employed during fabrication, the degree of entrapment was found to increase due the increased of isolated PMMA particles mainly at the lowest content of PMMA (20 wt. %) employed (Kennedy (2012); Arifvianto and Zhou, 2014). According to Kennedy (2012), the residual space holder were likely to be enclosed within the structure when the space holder added was below 50 wt. %. Therefore, it is worthwhile to maintain the compaction pressure below 300 MPa to avoid severe PMMA entrapment during processing considering low to medium content of PMMA employed in the current study. Moreover, deformation of closed macro-pores structure was also observed due to PMMA particle disintegration during compaction with the maximum pressure of 300 MPa, particularly after prolonged sintering up to 2.5 hr (in the case of 25 wt. % and 30 wt. % of PMMA). In one study performed by Zhao et al. (2004), fragmentation of NaCl space holder was observed due to the excessive pressure (>300 MPa) applied during compaction. Deterioration of porous metals properties due to the deformation of closed macro-pores structure as aforementioned has also been reported in the literatures (Zhang et al., 2005; Bekoz and Oktay, 2012). In the case of low to medium range of compaction pressure (200 MPa and 250 MPa), almost comparable degree of Al particle bonding was observed with increasing compaction pressure as seen in Figure 4.32 (a-c) until Figure 4.37 (a-c), respectively. However, coalescence between closed macro-pores of all the porous specimen (in the case of 25 wt. % and 30 wt. % of PMMA) were noticed with increased in compaction pressure from 200 MPa to 250 MPa as evidenced in Figure 4.32 (b), Figure 4.33 (b), Figure 4.34 (b), Figure 4.35 (b) , Figure 4.36 (b) and Figure 4.37 (b), respectively. Similar finding was also documented in the previous studies (Torres et al., 2012a, 2012b) in which they reported that the coalescence between pores with increasing compaction pressure from

200 MPa to 800 MPa can be attributed to the plastic deformation of space holder particle that resulted in higher interconnected porosity and thus easier elimination during subsequent sintering of titanium compact. Nevertheless, interconnected porosity of all porous specimens was not observed in the current study owing to the low and medium PMMA content employed during fabrication. On the contrary, such phenomenon was not observed with further increased in compaction pressure to 300 MPa due to the abovementioned entrapment of PMMA space holder in the Al matrix.

Based on the FESEM micrographs from Figure 4.33 (a-c), Figure 4.37 (a-c) and Figure 4.40 (a-c), different sintering time did not significantly affect the morphology of porous specimen. The formation of closed macro-pores structure that resembled the starting morphology of PMMA particle was still preserved with increasing sintering time from 1.5 hr to 2.5 hr especially in the case of 25 wt. % and 30 wt. % of PMMA. However, a slight increased in the formation of closed macro-pores structure was observed with increasing sintering time from 1.5 hr to 2 hr as revealed in Figure 4.32 (a-c) and Figure 4.33 (a-c) (in the case 25 wt. % and 30 wt. % of PMMA due to the desirable closed macro-pores structure), suggesting that higher processing time enhanced the degree of PMMA removal. EDS analysis (Table 4.8) further validated this finding by presenting a slight decreased in the amount of carbon residue during sintering from 1.5 hr to to 2 hr. Although the morphology of the resultant porous specimen is almost comparable at any given sintering time, prolonged sintering to 2.5 hr was found to increase the contamination level of all the resultant porous Al as evidenced from oxygen content analysis (Table 4.9). Considering liquid phase sintering introduced in the current study, shorter time was usually sufficient to achieve complete sintering of porous Al compared to conventional practiced of solid state sintering, thus prolonged sintering might triggered the oxidation level (Bafti and Habibolahzadeh, 2010; Surace and Filippis, 2010). Surace and Filippis (2010) also reported on severe oxidation of Al foam associated with prolonged solid state sintering from 2 hr to 20 hr. It has been documented that higher oxidation level can reduce the quality of the resultant porous Al as well as dense Al (Surace and Filippis, 2010; Siemiaszko et al., 2013; Grabke, 1999). A slight increased in the sintered density of Fe40Al alloy compact with decreasing in the oxides content was documented in the study of Siemiaszko et al. (2015). Taking into account higher affinity of Al towards oxygen, prolong sintering time in the current study is found to be detrimental in order to fabricate porous Al with good quality. In contrast, the preferred shrinkage of micro-pores within the Al framework as mostly reported in the literatures with increasing sintering response was not obviously noticed due to the nature of liquid phase sintering introduced in the current study (Dewidar et al., 2012; Laptev et al., 2004). Therefore, densification of porous Al was expected at any given sintering time and compaction pressure during processing. From these findings, it is reasonable to infer that the fabrication of closed-cell porous Al using PMMA as the space holder is practically feasible, and porous Al with higher porosity can be obtained by increasing the weight percentage of PMMA particles. Moreover, highest compaction pressure (300 MPa) and sintering time (2.5 hr) are found to be disadvantageous due to the development of dense cell wall that affected the formation of desired closed macro-pores structure as well as an increased in the contamination level (oxygen) that can affect the quality of the resultant porous Al.

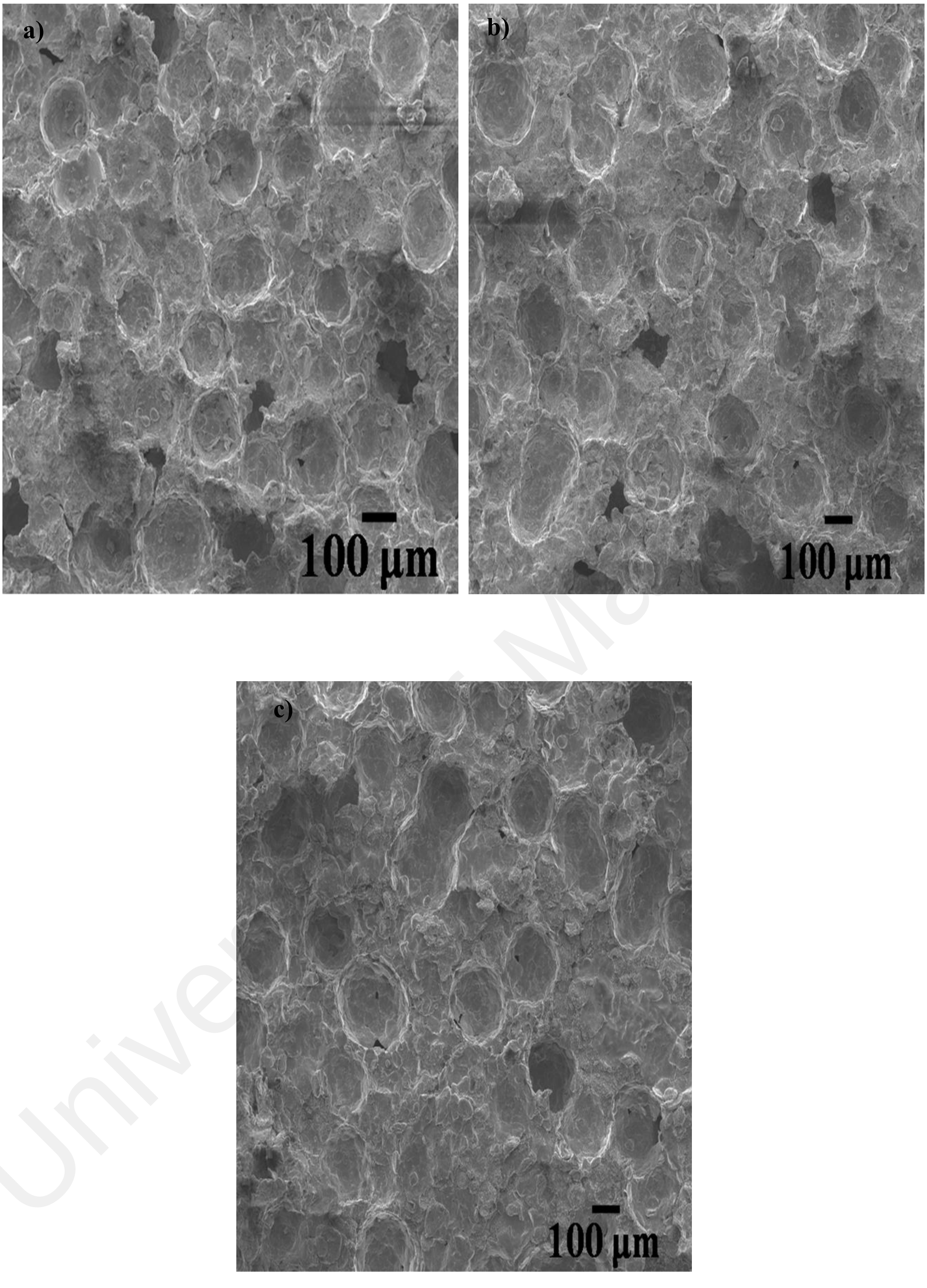

Figure 4.32 (a-c) : FESEM micrographs of porous Al structure with 30 wt. % PMMA and sintered at 1.5 hr under compaction pressure of a) 200 MPa, b) 250 MPa and c) 300 MPa

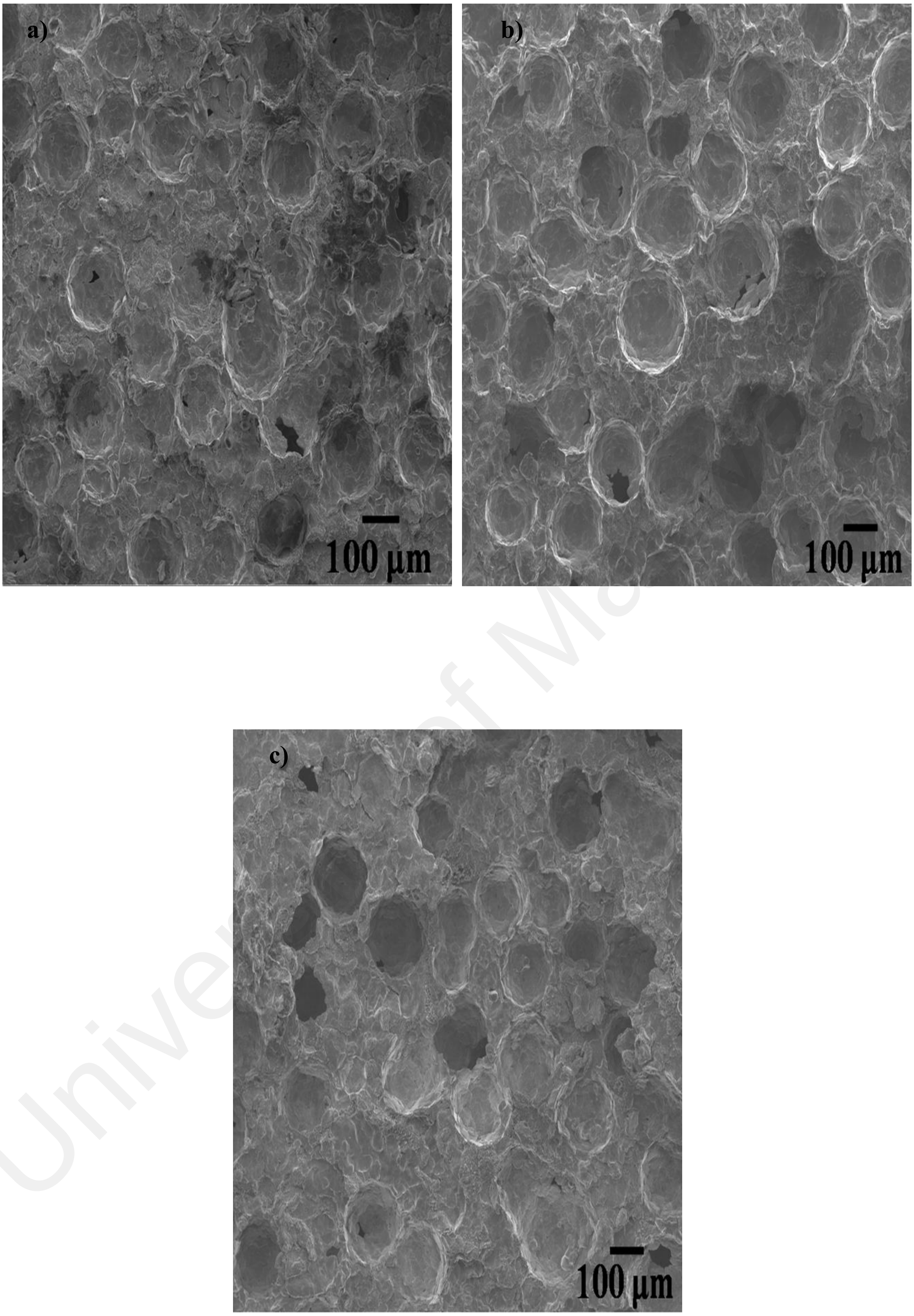

Figure 4.33 (a-c) : FESEM micrographs of porous Al structure with 30 wt. % PMMA and sintered at 2 hr under compaction pressure of a) 200 MPa, b) 250 MPa and c) 300 MPa

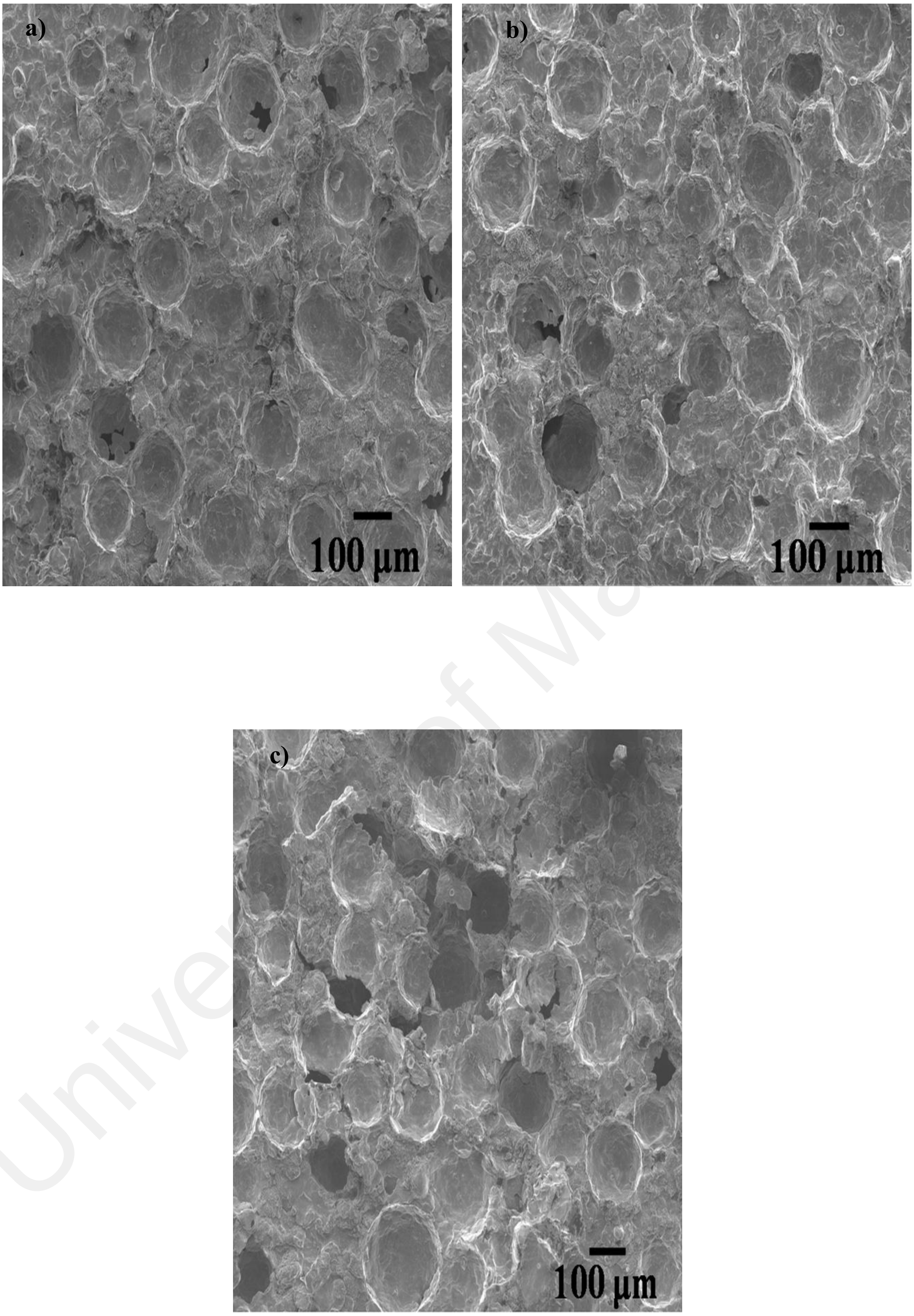

Figure 4.34 (a-c) : FESEM micrographs of porous Al structure with 30 wt. % PMMA and sintered at 2.5 hr under compaction pressure of a) 200 MPa, b) 250 MPa and c) 300 MPa

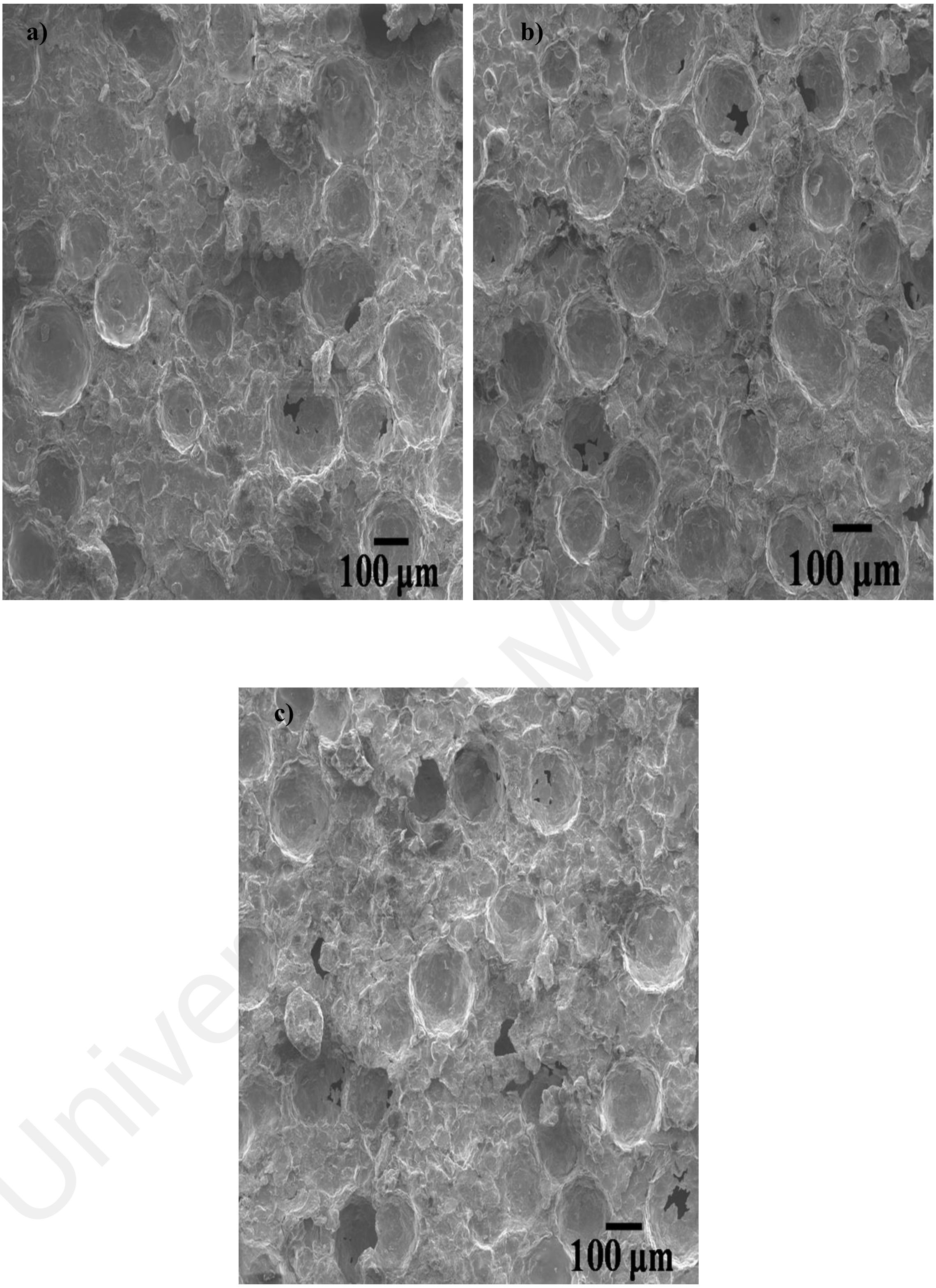

Figure 4.35 (a-c) : FESEM micrographs of porous Al structure with 25 wt. % PMMA and sintered at 1.5 hr under compaction pressure of a) 200 MPa, b) 250 MPa and c) 300 MPa

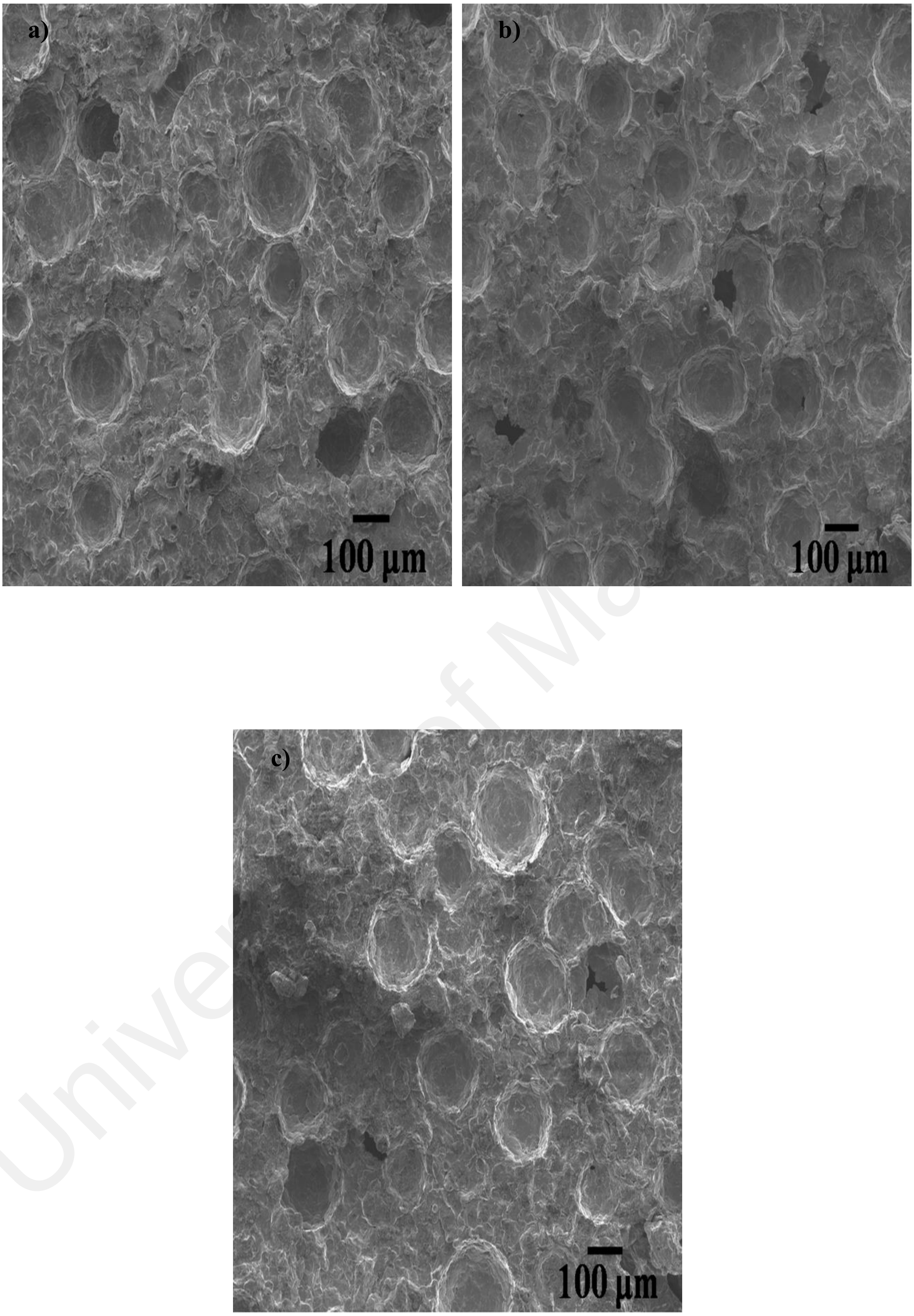

Figure 4.36 (a-c) : FESEM micrographs of porous Al structure with 25 wt. % PMMA and sintered at 2 hr under compaction pressure of a) 200 MPa, b) 250 MPa and c) 300 MPa

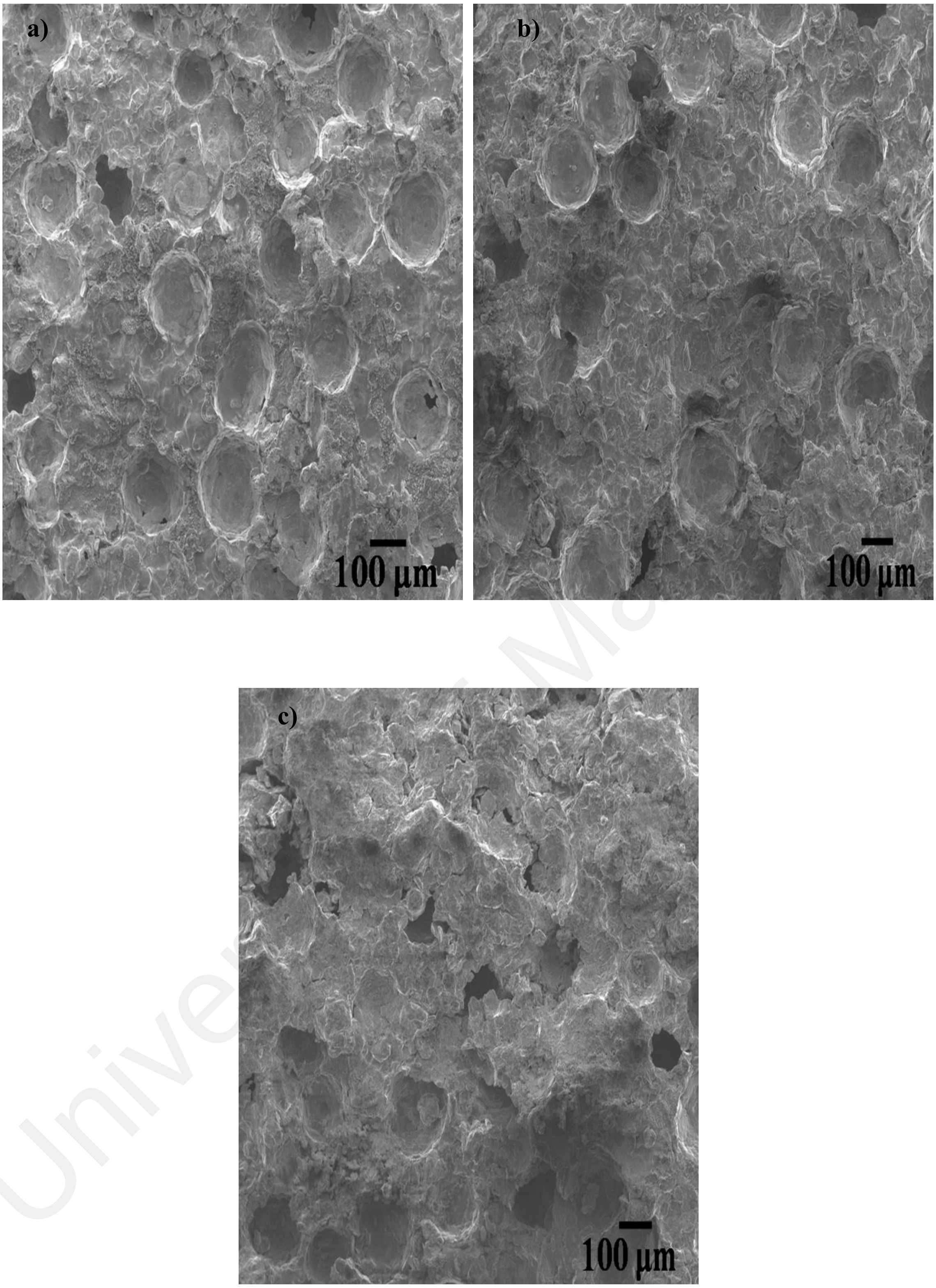

Figure 4.37 (a-c) : FESEM micrographs of porous Al structure with 25 wt. % PMMA and sintered at 2.5 hr under compaction pressure of a) 200 MPa, b) 250 MPa and c) 300 MPa

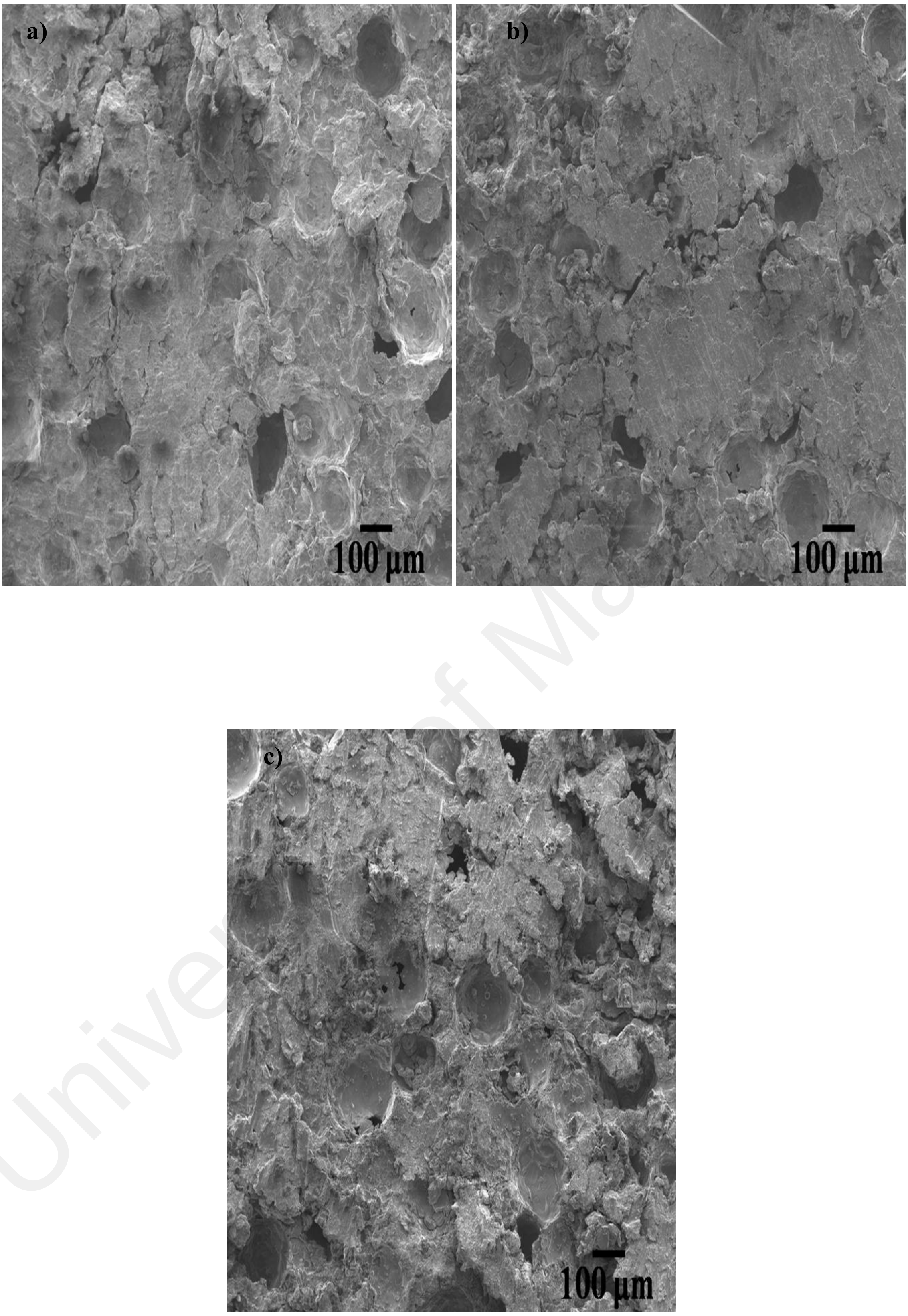

Figure 4.38 (a-c) : FESEM micrographs of porous Al structure with 20 wt. % PMMA and sintered at 1.5 hr under compaction pressure of a) 200 MPa, b) 250 MPa and c) 300 MPa

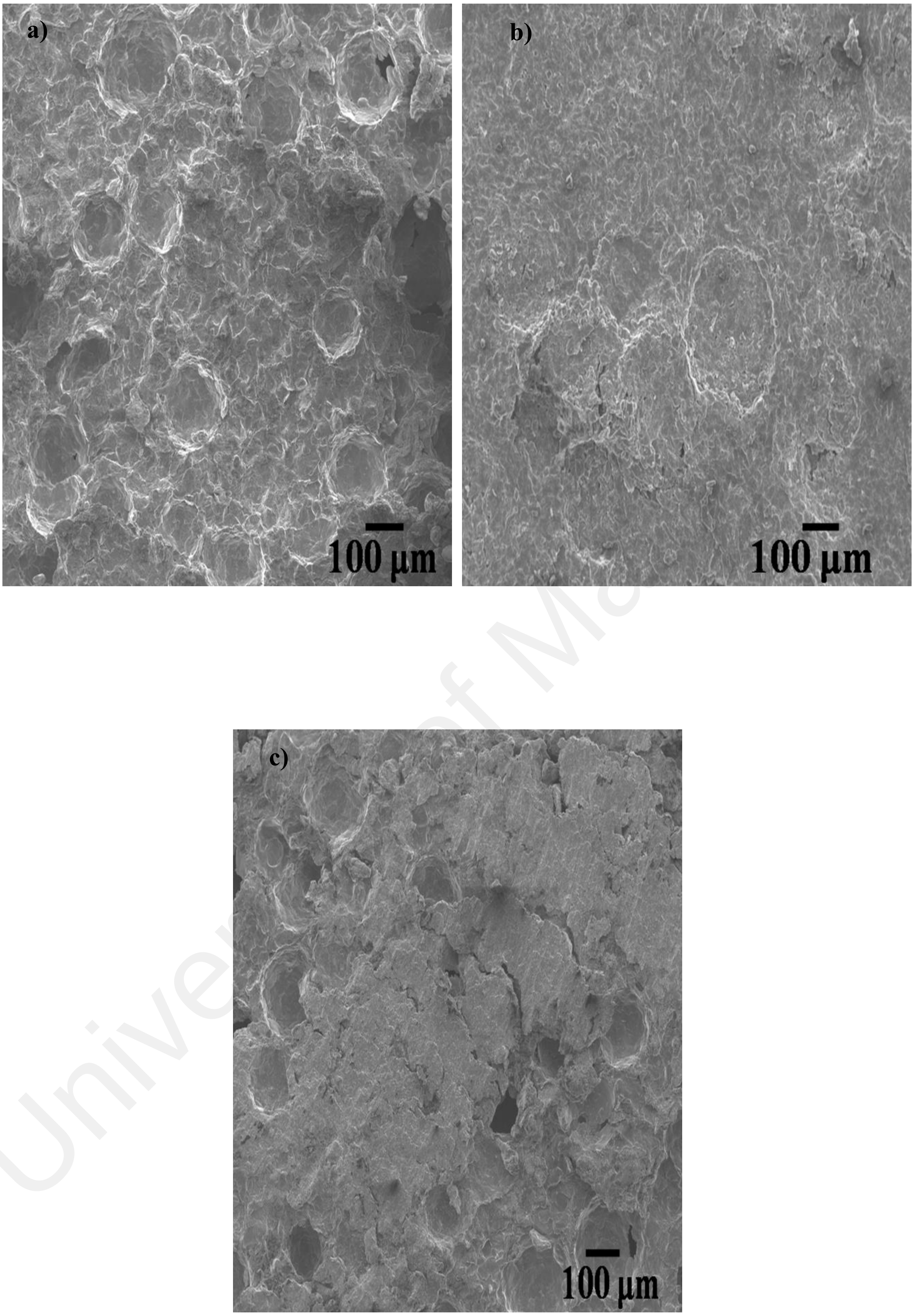

Figure 4.39 (a-c) : FESEM micrographs of porous Al structure with 20 wt. % PMMA and sintered at 2 hr under compaction pressure of a) 200 MPa, b) 250 MPa and c) 300 MPa

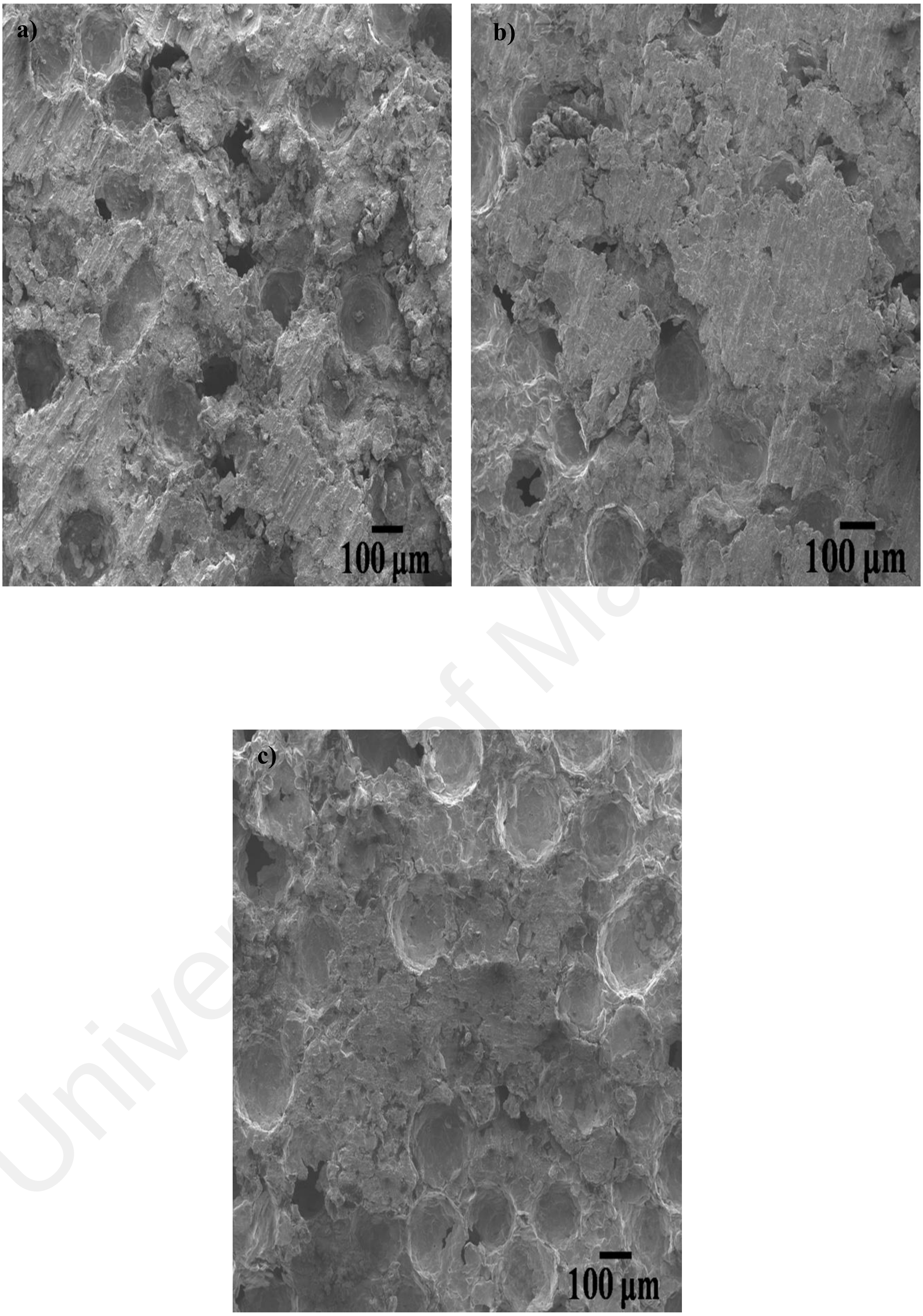

Figure 4.40 (a-c) : FESEM micrographs of porous Al structure with 20 wt. % PMMA and sintered at 2.5 hr under compaction pressure of a) 200 MPa, b) 250 MPa and c) 300 MPa

4.5.3.2 PERCENTAGE OF DIAMETER CHANGE OF POROUS ALUMINUM

Figure 4.41 (a-b) demonstrates the percentage of diameter change or linear shrinkage of the resultant porous Al with different PMMA content, compaction pressure and sintering time. It is evident that the percentage of diameter change or linear shrinkage of all the porous specimen was found to slightly increased with increasing compaction pressure from 200 MPa to 250 MPa and slightly decreased with further increased in compaction pressure to 300 MPa at any given PMMA content and sintering time. The linear shrinkage of the resultant porous specimen with PMMA content of 20 wt. %, 25 wt. % and 30 wt. % increased from -0.00738% to -0.00775%, -0.00601% to -0.00634% and -0.00504% to -0.00562% when the compaction pressure was increased from 200 MPa to 250 MPa after sintering for 1.5 hr as shown in Figure 4.41 (a). Similarly, the linear shrinkage of the resultant porous Al with PMMA content of 20 wt. %, 25 wt. % and 30 wt. % after 2 hr processing time improved from -0.00786% to -0.00837%, -0.00601% to -0.00635% and -0.0051% to -0.00566% as the compaction pressure was increased from 200 MPa to 250 MPa as seen in Figure 4.41 (b). In the same way, the linear shrinkage of the resultant porous specimen with PMMA content of 20 wt. %, 25 wt. % and 30 wt. % inclined from -0.00511% to -0.00525%, -0.00431% to -0.00474% and -0.00367% to -0.00425% when the compaction pressure was enhanced from 200 MPa to 250 MPa after sintering for 2.5 hr as depicted in Figure 4.41 (c). As evidenced from FESEM micrographs (Figure 4.32 (b), Figure 4.33 (b), Figure 4.34 (b), Figure 4.35(b), Figure 4.36 (b) and Figure 4.37 (b)), higher compaction pressure of 250 MPa permitted coalescence between closed macro-pores and consequently increased the porosity of the resultant porous specimen. Similar finding was reported in the study of Torres et al. (2012(a)), in which a slight increased in the porosity level of porous titanium was observed with increasing compaction pressure from 200 MPa to 800 MPa due to the coalescence effect between macro-pores that resulted in easier elimination of space holder particle during subsequent sintering. Owing to an increased in the level of porosity, the resultant porous Al then became lighter (low density) and thus hindered their resistance towards linear shrinkage (higher linear shrinkage). On the contrary, the linear shrinkage of all the porous specimen was found to lessen with further increased in compaction pressure to 300 MPa. This can be attributed to the decrease in the porosity level of the resultant porous Al, suggesting the entrapment of some PMMA particles in the Al matrix. EDS analysis as presented in Table 4.8 confirmed the entrapment of some PMMA particles with the maximum application of compaction pressure due to the increased in the amount of carbon residue in the resultant porous specimen. This finding also implies that some of PMMA particles have been fractured during fabrication that resulted in difficulty of PMMA removal. The resultant porous specimen was then become stronger and able to resist further linear shrinkage due to incomplete removal of these PMMA residuals (Amaranan and Manonukul, 2010). Similar observation was mentioned in the study of Zhao et al. (2004). In their study, the linear shrinkage of Al foam was found to decrease from 10% to 6% with increasing compaction pressure from 200 MPa to 250 MPa. This observation is also in good agreement with the results obtained from the microstructural characterization as revealed in Figure 4.32 (c), Figure 4.33 (c), Figure 4.34 (c), Figure 4.35 (c), Figure 4.36 (c) and Figure 4.37 (c), in which a lower number of closed macro-pores with dense cell walls were observed with further increased in compaction pressure to 300 MPa. In the current study, the linear shrinkage of the resultant porous Al with PMMA content of 20 wt. %, 25 wt. % and 30 wt. % after 1.5 hr processing time declined from -0.00775% to -0.00717%, -0.00634% to -0.00546% and -0.00562% to -0.00468% as the compaction pressure was increased from 250 MPa to 300 MPa as shown in Figure 4.41 (a). Similarly, as the sintering time was increased to 2 hr, the linear shrinkage of the resultant porous specimen with PMMA content of 20 wt. %, 25 wt. % and 30 wt. % fell from -0.00837% to -0.00771%,

-0.00635% to -0.00587% and -0.00566% to -0.00489% as the compaction pressure was enhanced from 250 MPa to 300 MPa as illustrated in Figure 4.41 (b). In the same way, the linear shrinkage of the resultant porous Al decreased from -0.00525% to -0.00499%, -0.00474% to -0.00426% and -0.00425% to -0.00382% after 2.5 hr of sintering as illustrated in Figure 4.41 (c).

Although similar increasing and decreasing pattern in the linear shrinkage effect was obtained with different compaction pressure at any given PMMA content and sintering time, the degree of the linear shrinkage of all porous Al was found to reduce with decreasing PMMA content. The reason for this observation can be related to the increased in the corresponding Al weight percentage (Zhao et al., 2004; Michailidis and Stergioudi, 2011). Moreover, the entrapment of some PMMA particles was observed to be severed with the lowest content of PMMA employed (20 wt. %). EDS analysis (Table 4.8) revealed an increased in the content of carbon residue with the addition of lowest PMMA content (20 wt. %) that substantiated incomplete PMMA removal during sintering. It is assumed that most of the PMMA particles are well dispersed in the Al matrix and can be burnt off easily when there is sufficient amount of PMMA (25–30 wt % in this case) in the Al matrix, and hence only a small amount of carbon residue is left in the resultant porous Al after sintering. On the contrary, when the amount of the PMMA particles is insufficient (20 wt % in this case), some PMMA particles are completely enclosed by the Al matrix. These isolated PMMA particles are then unable to move into the liquid part (molten tin) during sintering and thus become trapped in the Al matrix, resulting in higher amount of carbon residue in the resultant porous Al. Similar finding was also documented in the studies of Zhao et al. (2004) and Michailidis and Stergioudi (2011). They mentioned that some of the space holder particles are completely enclosed by the Al matrix with the addition of space holder content below

50 wt. % due to the increased in the degree of isolated pores, resulting in higher linear shrinkage (Michailidis and Stergioudi, 2011). However, incomplete removal of PMMA particle in the current study was observed with the addition of PMMA content below 25 wt. %. Therefore, densification and resistance of the resultant porous Al towards linear shrinkage (lower linear shrinkage) were found to be slightly improved due to the presence of some residual PMMA particles in the Al matrix. Given the fact that Al compact was undergone liquid phase during sintering, the resultant porous Al was expected to experience linear shrinkage but the degree of linear shrinkage was found to increase with increasing PMMA content due to the aforementioned reasons.

On the other hand, a minor increased in the linear shrinkage level of all porous specimens was observed with increasing processing time from 1.5 hr to 2 hr as shown in Figure 4.41 (a-b) at any given compaction pressure and PMMA content. As verified from FESEM micrographs as in Figure 4.32 (a-c) and Figure 4.36 (a-c) (in the case of 25 wt. % and 30 wt. % of PMMA due to desirable closed macro-pores formation), an increased in the formation of closed macro-pores was accountable for such increased, suggesting that higher processing time enhanced the degree of PMMA removal. A slightly higher content of carbon residue during sintering at 1.5 hr compared to 2 hr was validated by EDS analysis (Table 4.8), showing that a small amount of carbon residue was still left in the resultant porous Al after sintering for 1.5 hr. Further increased in the linear shrinkage of all the sintered porous Al was observed with prolonged sintering time to 2.5 hr. However, in this case, a slight increased in the content of oxygen was responsible for further increased in the linear shrinkage level of all the porous specimens as confirmed by EDS analysis from Table 4.9. According to Dewidar (2012), linear shrinkage of the sintered materials depends on a few factors such as powder composition, green compact geometry, green density, sintering atmosphere and sintering temperature. In this case, sintering atmosphere played significant role in which contamination by oxygen was observed with prolonged sintering to 2.5 hr considering the fact that Al particles are always covered by Al_2O_3 passive layer (Katsuyoshi et al., 2007, Schaffer et al., 2001). Therefore, it is reasonable to deduce that processing time less than 2.5 hr is sufficient to achieve complete sintering of compact Al due to the application of liquid phase sintering in the current study in order to minimize undesirable contamination. Bafti and Habibolahzadeh (2010) also documented that shorter sintering time of 2 hr was found to be sufficient to achieve complete sintering of the resultant Al foam owing to the nature of liquid phase sintering introduced in their study. It is important to note that contamination by oxygen can further increase the thickness of oxide (Al_2O_3) layer that already existed on the surface of Al particle and deteriorate the mechanical properties of the resultant porous Al (Siemiaszko et al., 2015; Katsuyoshi et al., 2007, Schaffer et al., 2001; Grabke, 1999).

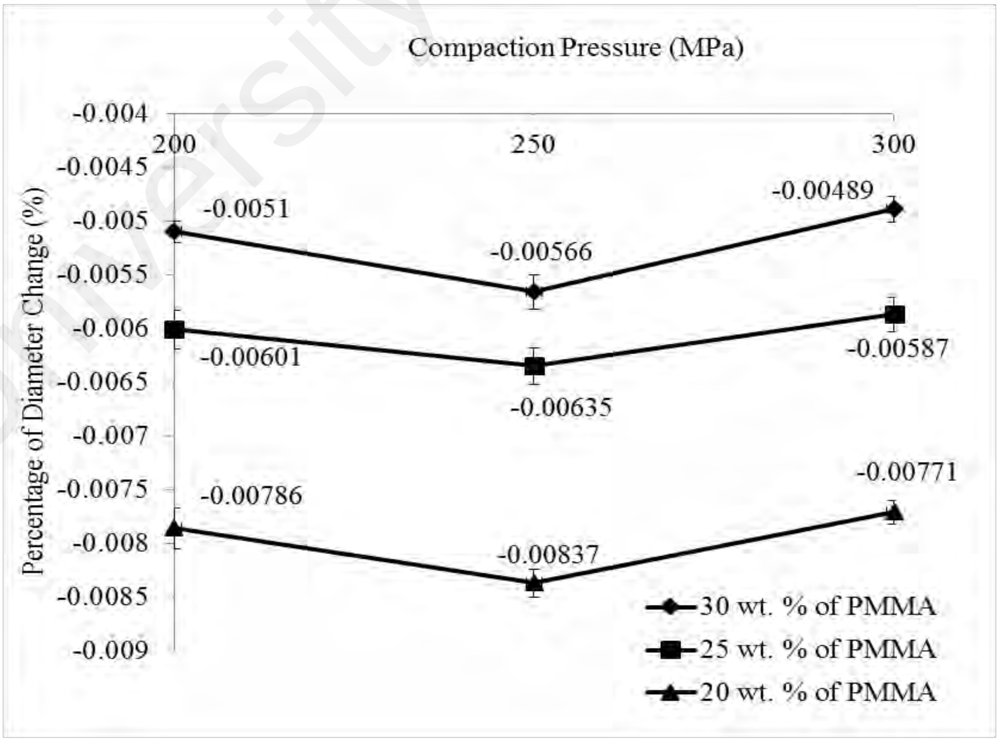

Figure 4.41 (a) : Percentage of diameter change of the resultant porous Al with different PMMA content and compaction pressure after sintering for 1.5 hr

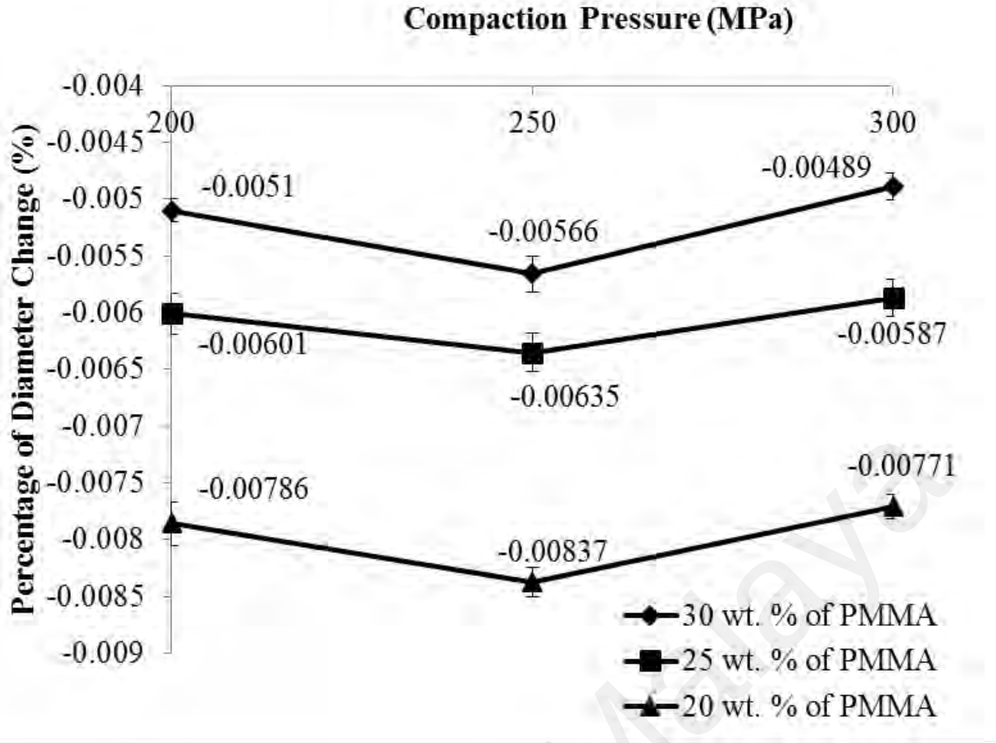

Figure 4.41 (b) : Percentage of diameter change of the resultant porous Al with different PMMA content and compaction pressure after sintering for 2 hr

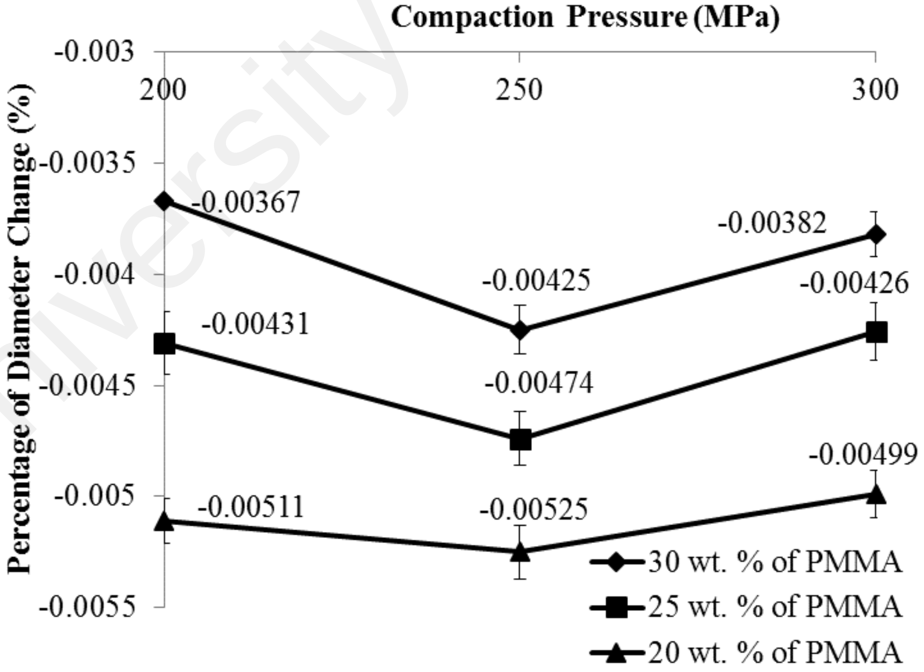

Figure 4.41 (c) : Percentage of diameter change of the resultant porous Al with different PMMA content and compaction pressure after sintering for 2.5 hr

4.5.3.3 SINTERED DENSITY AND POROSITY OF THE AS-PRODUCED POROUS ALUMINUM

Figure 4.42 (a-c) shows the sintered density and porosity of the as-produced closed-cell porous Al with different PMMA content, compaction pressure and sintering time. It can be observed that the sintered density of the porous Al decreased, and the porosity of the porous Al increased with increasing PMMA content at any given compaction pressure and sintering time. The sintered densities of the porous Al after 1.5 hr sintering decreased from 1.6546 g/cm^3 to 1.391 g/cm^3, 1.6044 g/cm^3 to 1.3549 g/cm^3 and 1.6788 g/cm^3 to 1.4933 g/cm^3 when the PMMA content was increased from 20 wt % to 30 wt % after compacted at 200 MPa, 250 MPa and 300 MPa as seen in Figure 4.42 (a). In contrast, the porosity level of the porous Al increased from 12.063% to 30.782%, 12.681% to 31.655%, and 9.654% to 29.102% as the content of PMMA was increased from 20 wt % to 30 wt % after compacted at 200 MPa, 250 MPa and 300 MPa. Similarly, the sintered densities of the porous Al after 2 hr sintering decreased from 1.6478 g/cm^3 to 1.3805 g/cm^3, 1.5991 g/cm^3 to 1.3492 g/cm^3 and 1.6711 g/cm^3 to 1.4885 g/cm^3 when the PMMA content was increased from 20 wt % to 30 wt % after compacted at 200 MPa, 250 MPa and 300 MPa as shown in Figure 4.42 (b). On the contrary, the porosity level of the porous Al increased from 12.199% to 30.846%, 12.7741% to 31.87% and 9.864% to 29.272% as the content of PMMA was increased from 20 wt % to 30 wt % after compacted at 200 MPa, 250 MPa and 300 MPa. In the same way, the sintered densities of the porous Al after 2.5 hr sintering decreased from 1.6235 g/cm^3 to 1.3776 g/cm^3, 1.5833 g/cm^3 to 1.3188 g/cm^3 and 1.6684 g/cm^3 to 1.4783 g/cm^3 when the PMMA content was increased from 20 wt % to 30 wt % after compacted at 200 MPa, 250 MPa and 300 MPa as revealed in Figure 4.42 (c). Conversely, the porosity level of the porous Al increased from 12.069% to 30.683%, 12.6349% to 31.69% and 9.647% to 29.084% as the content of PMMA was increased from 20 wt % to 30 wt % after compacted at 200 MPa, 250 MPa and 300 MPa. Clearly, the addition of PMMA particle as the space holder material during fabrication reduced the density of the porous Al and consequently increased the porosity of the porous specimen. This can be attributed to the fact that a higher volume of closed pores is created when the PMMA content is higher. In this technique, the closed pores in the porous Al were created through the thermal decomposition of PMMA particles during sintering. Therefore, more closed pores were created as more content of PMMA was added, making the porous specimen possess higher porosity and become lighter. Similar observation was documented in the study of Manonukul et al. (2010). This observation is also in good agreement with the results obtained from the microstructural characterization as revealed in Figure 4.32 (a–c) until Figure 4.40 (a-c), in which a higher number of closed pores with thinner cell walls were found with increasing content of PMMA particles. It is therefore clear that the sintered density and porosity of the porous Al can be tailored by varying the content of the space holder material.

On the other hand, an increased in compaction pressure from 200 MPa to 250 MPa decreased the density of the porous Al and thus increased the porosity of the porous specimen. This shows that densification lessened with increasing compaction pressure due to the coalescence effect between macro closed-pores as evidenced from FESEM images as in Figure 4.32 (b) until Figure 4.37 (b). Similar result was also presented in the study of Torres et al. (2012(a)). In contrast, further increased the compaction pressure to 300 MPa improved the density of the porous Al and consequently decreased the porosity of the resultant porous specimen. This can be attributed to the fact that some of the PMMA particles have been fractured with the application of 300 MPa compaction pressure, showing excessive pressure during compaction. These fractured space holder particles are then trapped inside the Al matrix and cannot be completely eliminated during sintering. As a result, the entrapped PMMA particles increased the density of the porous Al and hence decreased the porosity of the porous specimen. An increased in the amount of carbon residue associated with incomplete PMMA removal was obtained from EDS analysis as presented in Table 4.8. Similar discovery was also documented in the study of Zhao et al. (2004). This finding is also in good agreement with the results obtained from the microstructural characterization as discovered from FESEM images as in Figure 4.32 (c) until Figure 4.37 (c), in which a lower number of closed pores with dense cell walls were found with maximum compaction pressure of 300 MPa. It is therefore understandable that excessive compaction pressure enhanced the sintered density of the porous Al at the expense of their porosity level due to the entrapment of some PMMA residuals.

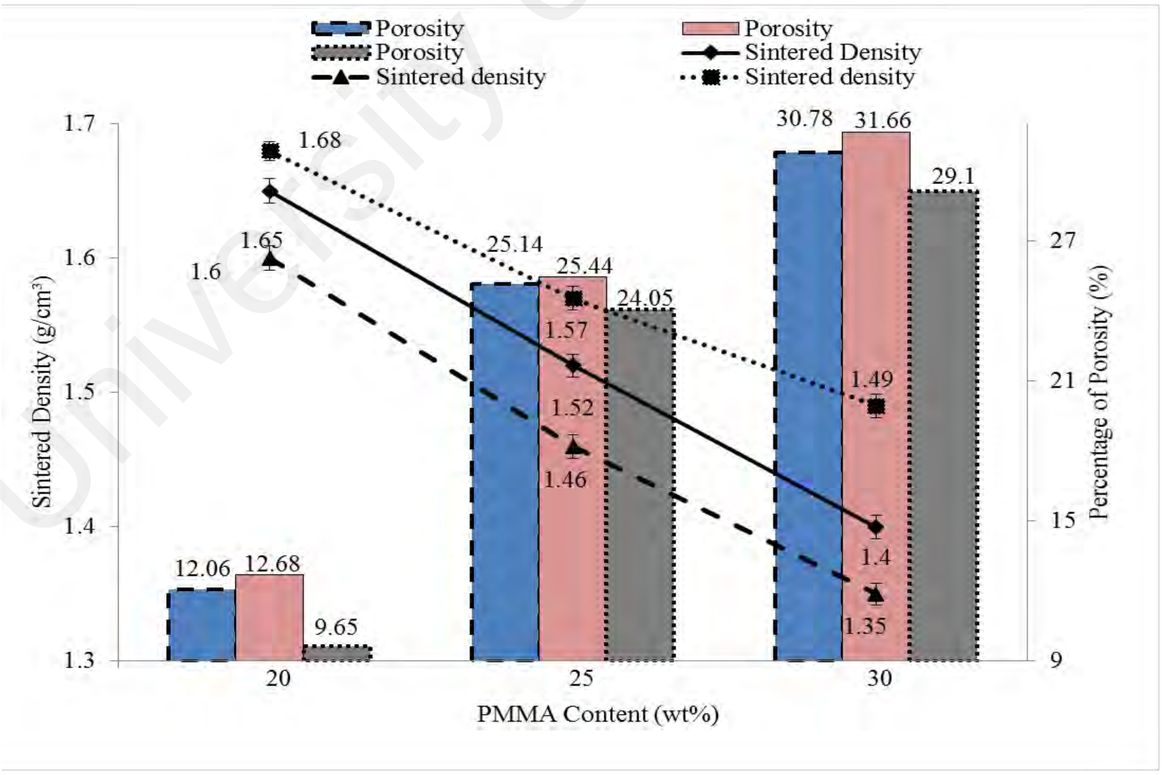

Figure 4.42 (a) : Sintered density and percentage of porosity with different PMMA content (wt %) and compaction pressure (MPa) after sintering at 1.5 hr

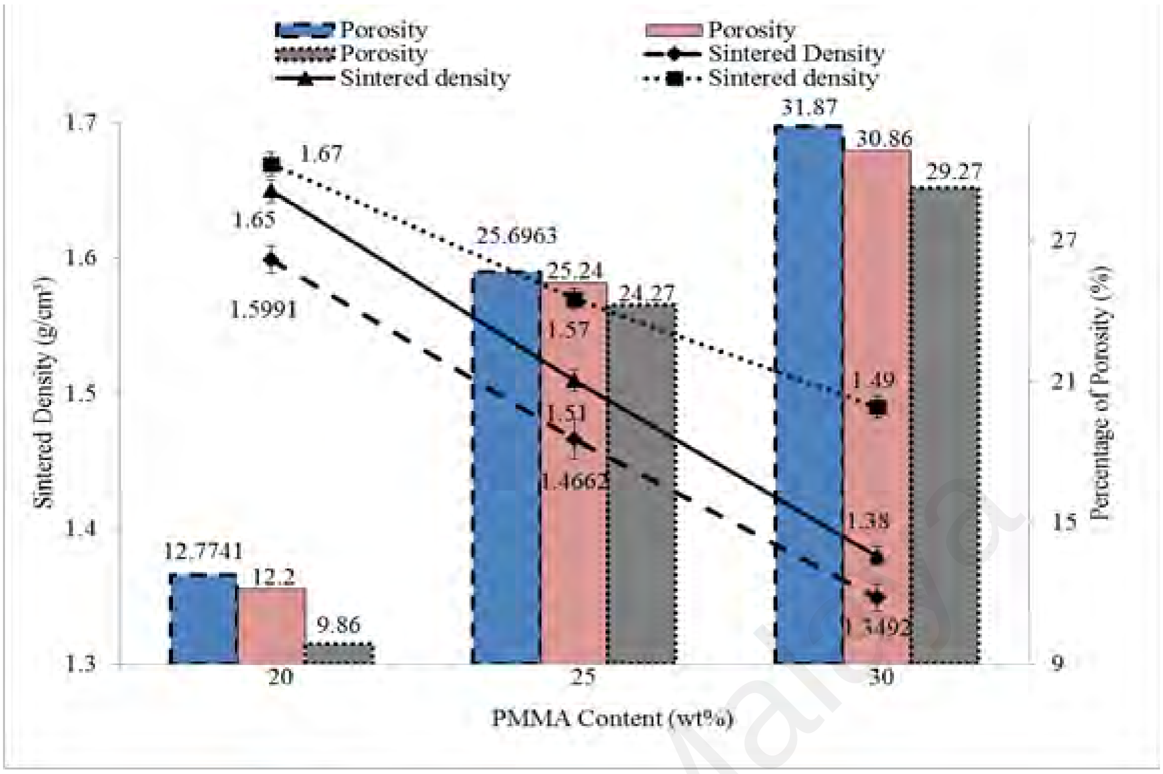

Figure 4.42 (b) : Sintered density and percentage of porosity with different PMMA content (wt %) and compaction pressure (MPa) after sintering at 2 hr

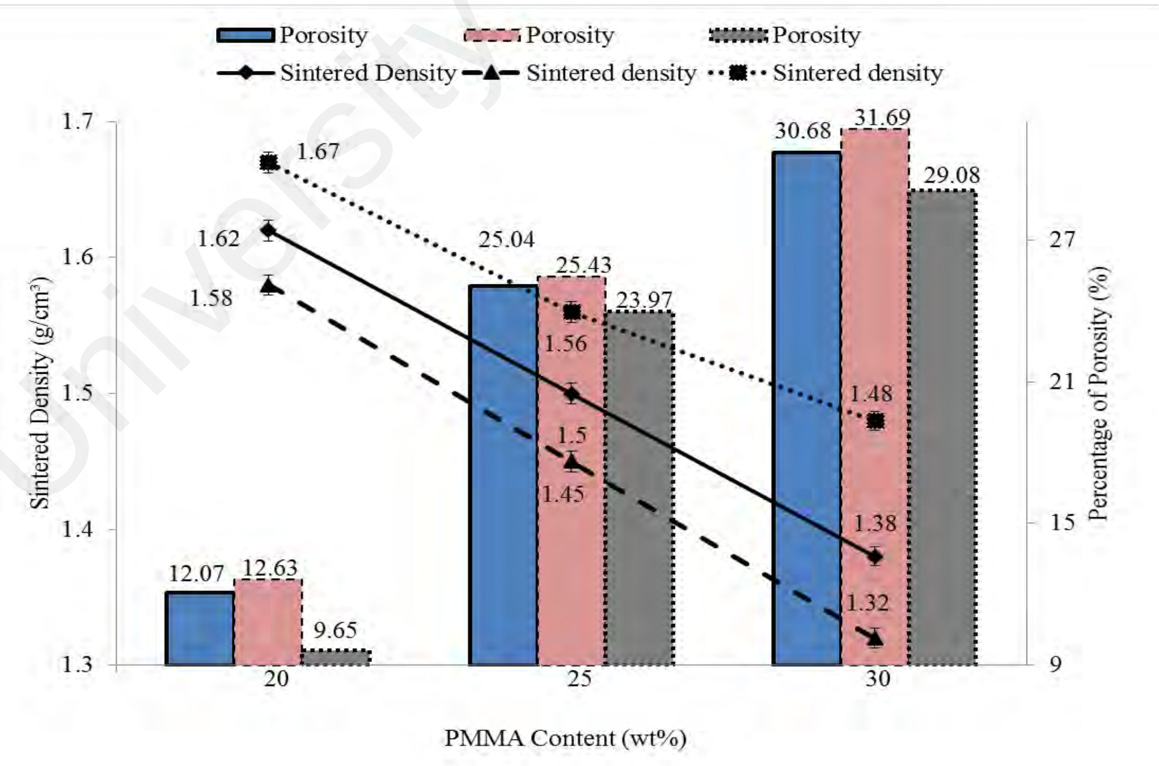

Figure 4.42 (c) : Sintered density and percentage of porosity with different PMMA content (wt %) and compaction pressure (MPa) after sintering at 2.5 hr

Furthermore, an increased in sintering time from 1.5 hr to 2 hr was found to reduce the density of the porous Al and consequently increased the porosity of the porous specimen. Similar observation has been reported in the study of Raza et al. (2015). This shows that densification decreased whereas porosity increased with increasing sintering time due to the increased in the formation of macro closed-pores as demonstrated from FESEM images as in Figure 4.32 (a-c) and Figure 4.33 (a-c) (in the case of 25 wt. % and 30 wt. % of PMMA due to desirable closed macro-pores formation), showing that higher processing time enhanced the degree of PMMA removal. EDS analysis as presented in Table 4.8 confirmed a slightly higher content of carbon residue during sintering at 1.5 hr compared to 2 hr, implying that a small amount of carbon residue was still presented in the resultant porous Al after sintering for 1.5 hr. In contrast, further increased the sintering time 2.5 hr reduced the density of the resultant porous Al with no significant change in its porosity level and this is probably due to the increased in the contamination level of oxygen in the resultant porous specimen as further corroborated by EDS analysis (Table 4.9). Similar finding has been documented in the study of Sun and Zhao (2003). It has been reported that atmosphere contamination during sintering reduced the relative sintered densities of Al foam from 0.65 to 0.17 as the processing time increased from 2.5 hr to 30 hr (Sun and Zhao, 2003). Considering strong affection of Al towards oxygen as aforementioned in previous sections, prolonged sintering is found to be detrimental due to the increase in the level of oxygen content that can lower the properties of the resultant porous Al. Therefore, sintering of Al compact in the current study should take place below 2.5 hr.

4.5.4 X-RAY DIFFRACTION (XRD) ANALYSIS

The XRD patterns of elemental powder mixture, final powder mixture and sintered porous Al with different sintering time are revealed in Figure 4.43 (a-e). Considering the XRD diffraction patterns for sintered porous Al with various PMMA contents and compaction pressures are comparable, only one XRD diffraction pattern for each PMMA content (30 wt. % of PMMA) and compaction pressure (200 MPa), is chosen for discussion in this section. Taking into account the amorphous structure of PMMA particles, incomplete removal of some space holder particles (denoted with the presence of carbon residue) cannot be detected by XRD analysis. Similar observation is also accounted for compaction pressure effect. It is noted that Al rich phase was primarily found in the XRD pattern of all the samples, characterized by the (111), (200), (220) and (311) diffraction peaks at 38.47°, 44.71°, 65.07° and 78.22°, respectively. Moreover, no additional peaks were seen in the XRD patterns of the sintered porous Al, suggesting that Al did not react with PMMA spacer during sintering.

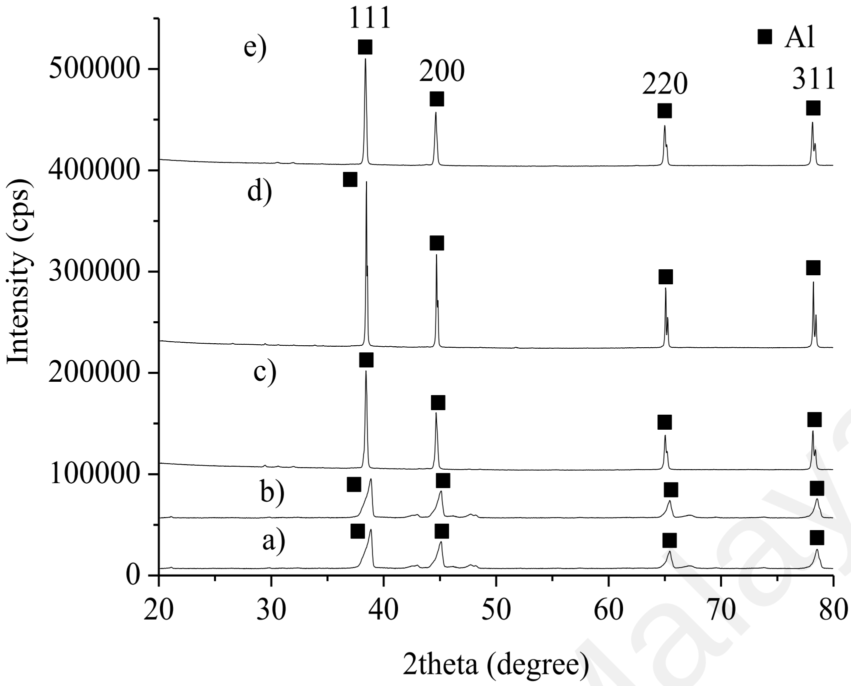

Figure 4.43 : XRD patterns of a) elemental powder mixture, b) final powder mixture, c) porous Al with 30 wt % PMMA content after sintering for 1.5 hr, d) porous Al with 30 wt % PMMA content after sintering for 2 hr and e) porous Al with 30 wt % PMMA content after sintering for 2.5 hr

As can be seen in Figure 4.43 (c-e), the peak intensities for all the sintered porous Al were found to be higher and sharper compared to the green compact specimen (final powder mixture), demonstrating the formation of crystalline Al during complete sintering. However, the peak intensity of the sintered porous Al after 2 hr processing was found to be higher compared to the sintered porous Al processed at 1.5 hr and 2.5 hr, signifying higher crystalline Al formation during complete sintering. A clear reduction in the peak intensity of the sintered porous specimen with prolonged sintering to 2.5 hr was observed, demonstrating inferior crystalline Al formation during sintering. This can be attributed to the fact that contamination level (higher oxygen content) as presented in Table 4.9 increases with prolong sintering time considering typical Al particle that always covered by oxide layer of Al_2O_3. Therefore, it is sensible to deduce that maximum processing time of 2.5 hr enhanced the contamination level and consequently reduced the sintering response of the sintered porous Al. On the other hand, the presence of Mg peak could hardly be detected, possibly due to the minor content of Mg powder employed (0.5 wt %) during the fabrication process (Jha et al., 2013).

4.5.5 CARBON CONTENT ANALYSIS FOR ELEMENTAL POWDER MIXTURE, FINAL POWDER MIXTURE AND POROUS ALUMINUM SPECIMEN

It is known that methyl methacrylate (MMA, monomer) is the dominant volatile product of the decomposition of PMMA, and the decomposition of MMA was accompanied by formation of a number of low molecular weight stable species such as H_2, CO, CO_2, CH_4, C_2H_4, CH_3COOH in trace amounts (Bi et al., 2015). To ensure that there is a complete removal of PMMA during the sintering process in producing pure porous Al, the chemical analysis of carbon (C) element before and after the sintering process was performed and the results are presented in Table 4.8. Initially, the carbon content of the final powder mixtures increased from 0.22 wt % to the range of 11.29 wt % to 13.03 wt % due to the addition of the PMMA into the elemental powder mixture. After sintering for 1.5 hr, the carbon content of the resultant porous Al compacted at pressures of 200 MPa, 250 MPa and 300 MPa was greatly reduced to the range of 4.01 wt. % to 0.53 wt. %, 3.96 wt. % to 0.51% and 4.22% to 1.19%. Similarly, after processing for 2 hr, the carbon content of the resultant porous specimen compacted at pressures of 200 MPa, 250 MPa and 300 MPa was clearly decreased to the range of 3.91% to 0.47%, 3.87% to 0.43%, and 4.16% to 1.08%. In the same way, the carbon content of the resultant porous Al after 2.5 hr sintering compacted at pressures of 200 MPa, 250 MPa and 300 MPa was visibly lessened to the range of 3.96 wt. % to 0.51 wt. %, 3.90 wt. % to 0.47 wt. % and 4.19 wt. % to 1.11 wt. %.

These results indicate that almost all the PMMA particles were completely decomposed during the sintering process, except for the resultant porous Al with 20 wt % PMMA as well as for all sintered porous Al compacted under 300 MPa pressure (Dewidar, 2012). The reason for this observation can be related to the entrapment of the PMMA particle in the Al matrix. In the case of PMMA content effect, it is postulated that most of the PMMA particles are well dispersed in the Al matrix and can be burnt off easily when there is sufficient amount of PMMA (25–30 wt % in this case) in the Al matrix, and hence only a small amount of carbon residue is left in the resultant porous Al after sintering. On the contrary, when the amount of the PMMA particles is insufficient (20 wt % in this case), some PMMA particles are completely enclosed by the Al matrix. These isolated PMMA particles are then unable to move into the liquid part (molten tin) during sintering and thus become trapped in the Al matrix, resulting in higher amount of carbon residue in the resultant porous Al. Similar findings were also reported in the study of Zhao et al. (2004) and Michailidis and Stergioudi (2011). Therefore, it can be further concluded that the addition of 20 wt % of PMMA content was inadequate to produce closed pore structure in the fabrication of porous Al specimen via the space holder method.

Table 4.8 : Carbon content of elemental powder mixture, final powder mixture and sintered porous Al with various PMMA contents, compaction pressure and sintering time. Data are presented in mean ± standard deviation

Specimen	**Carbon Content (wt. %)**
Green specimen	
Elemental powder mixture (Al-Mg-Sn)	0.22 ± 0.52
Final powder mixture with 20 wt. % PMMA	11.29 ± 0.52
Final powder mixture with 25 wt. % PMMA	12.17 ± 0.43
Final powder mixture with 30 wt. % PMMA	13.03 ± 0.61
Sintered specimen	
1.5 hr sintering	
200 MPa compaction pressure	
Sintered porous Al with 20 wt. % PMMA	4.01 ± 0.41
Sintered porous Al with 25 wt. % PMMA	0.50 ± 0.15
Sintered porous Al with 30 wt. % PMMA	0.53 ± 0.16
250 MPa compaction pressure	
Sintered porous Al with 20 wt. % PMMA	3.96 ± 0.52
Sintered porous Al with 25 wt. % PMMA	0.49 ± 0.14
Sintered porous Al with 30 wt. % PMMA	0.51 ± 0.13
300 MPa compaction pressure	
Sintered porous Al with 20 wt. % PMMA	4.22 ± 0.40
Sintered porous Al with 25 wt. % PMMA	1.12 ± 0.17
Sintered porous Al with 30 wt. % PMMA	1.19 ± 0.15
2 hr sintering	
200 MPa compaction pressure	
Sintered porous Al with 20 wt. % PMMA	3.91 ± 0.43
Sintered porous Al with 25 wt. % PMMA	0.45 ± 0.17
Sintered porous Al with 30 wt. % PMMA	0.47 ± 0.14
250 MPa compaction pressure	
Sintered porous Al with 20 wt. % PMMA	3.87 ± 0.54
Sintered porous Al with 25 wt. % PMMA	0.41 ± 0.15
Sintered porous Al with 30 wt. % PMMA	

‘Table 4.8, continued’

Specimen	**Carbon content (wt. %)**
300 MPa compaction pressure	
Sintered porous Al with 20 wt. % PMMA	4.16 ± 0.39
Sintered porous Al with 25 wt. % PMMA	1.03 ± 0.14
Sintered porous Al with 30 wt. % PMMA	1.08 ± 0.15
2.5 hr sintering	
200 MPa compaction pressure	
Sintered porous Al with 20 wt. % PMMA	3.96± 0.44
Sintered porous Al with 25 wt. % PMMA	0.49 ± 0.15
Sintered porous Al with 30 wt. % PMMA	0.51 ± 0.17
250 MPa compaction pressure	
Sintered porous Al with 20 wt. % PMMA	3.90 ± 0.55
Sintered porous Al with 25 wt. % PMMA	0.45 ± 0.19
Sintered porous Al with 30 wt. % PMMA	0.47 ± 0.14
300 MPa compaction pressure	
Sintered porous Al with 20 wt. % PMMA	4.19 ± 0.42
Sintered porous Al with 25 wt. % PMMA	1.06 ± 0.13
Sintered porous Al with 30 wt. % PMMA	1.11 ± 0.14

On the other hand, similar observation was also obtained in the case of compaction pressure effect on the carbon content of the resultant porous Al. The entrapment of some PMMA particles in the Al matrix after compacted at maximum pressure of 300 MPa was found to increase the content of carbon residue at any given PMMA content and sintering time, suggesting fracture of some PMMA particle during processing (Zhao et al., 2004). These fractured PMMA particles are then trapped in the Al matrix and thus arising the carbon content in the sintered porous specimen. On the other hand, no noticeable effect was observed on the carbon content of the resultant porous Al with increasing sintering time to 2.5 hr, suggesting that sintering time less than 2.5 hr is sufficient to completely remove PMMA particles in the Al matrix (in the case of 25 wt. % and 30 wt. % PMMA).

4.5.6 OXYGEN CONTENT ANALYSIS FOR ELEMENTAL POWDER MIXTURE, FINAL POWDER MIXTURE AND POROUS ALUMINUM SPECIMEN

It has been documented that contamination by oxygen during sintering can reduce the mechanical properties of the resultant porous specimen. Therefore, the effect of PMMA content, compaction pressure and sintering time on the oxygen content of the sintered porous Al was investigated and the finding is presented in Table 4.9. In the study of Zhao and Monaghan (2008), they reported that greater oxide growth was observed with increasing sintering time from 4 hr to 6 hr. In addition, Siemiaszko et al. (2013) and Grabke (1999) also documented on the deterioration of the resultant specimen mechanical properties due to the increase in the oxidation level. As in this study, it can be seen that the oxygent content of all the porous specimen after sintering for 1.5 hr and 2 hr remains nearly unchanged at any given PMMA content and compaction pressure.

Table 4.9 : Oxygen content of elemental powder mixture, final powder mixture and sintered porous Al with various PMMA contents, compaction pressure and sintering time. Data are presented in mean ± standard deviation

Specimen	Oxygen Content (wt. %)
Green specimen	
Elemental powder mixture (Al-Mg-Sn)	0.40 ± 0.10
Final powder mixture with 20 wt. % PMMA	0.42 ± 0.09
Final powder mixture with 25 wt. % PMMA	0.43 ± 0.12
Final powder mixture with 30 wt. % PMMA	0.45 ± 0.08
Sintered specimen	
1.5 hr sintering	
200 MPa compaction pressure	
Sintered porous Al with 20 wt. % PMMA	0.44 ± 0.11
Sintered porous Al with 25 wt. % PMMA	0.46 ± 0.13
Sintered porous Al with 30 wt. % PMMA	0.48 ± 0.10
250 MPa compaction pressure	
Sintered porous Al with 20 wt. % PMMA	0.43 ± 0.12
Sintered porous Al with 25 wt. % PMMA	0.47 ± 0.11
Sintered porous Al with 30 wt. % PMMA	0.49 ± 0.14
300 MPa compaction pressure	
Sintered porous Al with 20 wt. % PMMA	0.45 ± 0.13
Sintered porous Al with 25 wt. % PMMA	0.44 ± 0.11
Sintered porous Al with 30 wt. % PMMA	0.47 ± 0.10
2 hr sintering	
200 MPa compaction pressure	
Sintered porous Al with 20 wt. % PMMA	0.46 ± 0.12
Sintered porous Al with 25 wt. % PMMA	0.48 ± 0.11
Sintered porous Al with 30 wt. % PMMA	0.49 ± 0.12
250 MPa compaction pressure	
Sintered porous Al with 20 wt. % PMMA	0.45 ± 0.11
Sintered porous Al with 25 wt. % PMMA	0.47 ± 0.12
Sintered porous Al with 30 wt. % PMMA	0.48 ± 0.13

‘Table 4.9, continued’

Specimen	**Oxygen content (wt. %)**
300 MPa compaction pressure	
Sintered porous Al with 20 wt. % PMMA	0.44 ± 0.13
Sintered porous Al with 25 wt. % PMMA	0.48 ± 0.13
Sintered porous Al with 30 wt. % PMMA	0.49 ± 0.10
2.5 hr sintering	
200 MPa compaction pressure	
Sintered porous Al with 20 wt. % PMMA	2.65 ± 0.11
Sintered porous Al with 25 wt. % PMMA	2.71 ± 0.13
Sintered porous Al with 30 wt. % PMMA	2.73 ± 0.10
250 MPa compaction pressure	
Sintered porous Al with 20 wt. % PMMA	2.71 ± 0.12
Sintered porous Al with 25 wt. % PMMA	2.69 ± 0.11
Sintered porous Al with 30 wt. % PMMA	2.67 ± 0.12
300 MPa compaction pressure	
Sintered porous Al with 20 wt. % PMMA	2.68 ± 0.13
Sintered porous Al with 25 wt. % PMMA	2.72 ± 0.11
Sintered porous Al with 30 wt. % PMMA	2.70 ± 0.11

However, the oxygen content of all the resultant porous Al was observed to increase with increasing sintering time to the maximum level of 2.5 hr. The oxygen content was clearly increased from 0.4 wt. % (final powder mixture) to the range of 2.65 wt. % and 2.73 wt. % at any given PMMA content and compaction pressure. Based on the fact that oxygen is insoluble in the liquid state of Al, oxygen contamination is found to be severed with prolong sintering to 2.5 hr, resulting in increase in the oxide layer of Al particle that already existed in its as-received form (Friedrich et al., 2005). Therefore, it is reasonable to summarize that prolong sintering to 2.5 hr is unnessary due to the clear increase in the level of oxygen contamination as tabulated in Figure 4.9 that can affect the properties of the resultant porous Al.

4.5.7 COMPRESSIVE BEHAVIOUR OF AS PRODUCED POROUS ALUMINUM

4.5.7.1 COMPRESSIVE STRENGTH OF AS PRODUCED POROUS ALUMINUM

The resultant porous Al with different PMMA content in the current study displayed the typical deformation pattern for closed-cell porous metals as shown in Figure 4.44, which can be divided into three distinct stages: (1) a linear elastic region at the beginning of the deformation where cell wall bending and face stretching occur; (2) a plateau region that is characterized by a plastic deformation at a nearly constant flow stress and (3) a final densification region where the flow stress abruptly increased (Yu et al., 2007; Liu et al., 2008; Li et al., 2013; Nesic et al., 2014). In this study, the value of the load that caused the first failure of the specimen was utilized to determine the compressive strength of the resultant porous Al (Vilcekova et al., 2013). For clearer view, the compressive strength of all the sintered porous Al along with its sintered density and porosity are listed in Table 4.10.

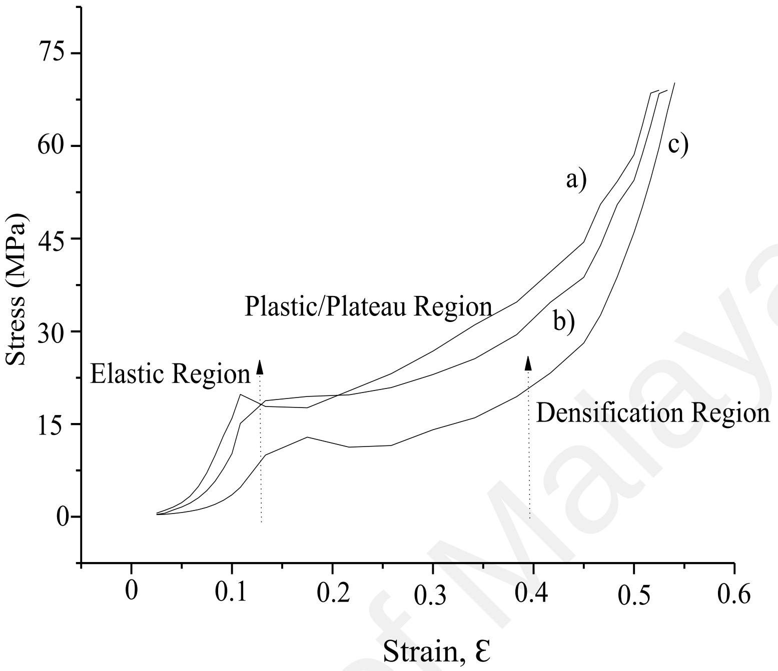

Figure 4.44 : Stress-strain curves for different PMMA content of a) 20 wt. %, 25 wt. % and c) 30 wt. %

It is clear that the compressive strength of all the sintered porous Al decreased with increasing PMMA content at any given sintering time and compaction pressure. The compressive strength of porous specimen compacted at 200 MPa, 250 MPa and 300 MPa decreased from 20.57 MPa to 18.33 MPa, 17.19 MPa to 15.08 MPa and 22.43 MPa to 19.86 MPa with increasing PMMA content from 20 wt. % to 30 wt. % after sintering for 1.5 hr. Similarly, the compressive strength of the resultant porous Al compacted at 200 MPa, 250 MPa and 300 MPa reduced from 19.62 MPa to 17.81 MPa, 6.43 MPa to 14.66 MPa and 21.77 MPa to 18.68 MPa as the PMMA content increased from 20 wt. % to 30 wt.% after sintering for 2 hr. In the same way, the compressive strength of the resultant porous specimen compacted at 200 MPa, 250 MPa and 300 MPa declined from 18.70 MPa to 15.99 MPa, 15.08 MPa to 13.12 MPa and 19.59 MPa to 17.44 MPa, with increasing PMMA content from 20 wt. % to 30 wt. % after sintering for 2.5 hr. This can be attributed to the fact that a higher volume of closed pores is created after PMMA removal and this phenomenon becomes intense with increasing PMMA content that consequently increased the porosity level and reduced the sintered density and compressive strength of the resultant porous Al. Similar finding was also mentioned in the studies of Dewidar (2006), Yu et al., (2007), Li et al., (2013) and Vilcekova et al., (2013).

On the other hand, an increased in the compaction pressure from 200 MPa to 250 MPa was found to reduce the compressive strength of all the sintered porous Al. This can be attributed to the coalescence effect between closed macro-pores (as evidenced from FESEM images as in Figure 4.32 (b) until Figure 4.37 (b)) as aforestated in the previous sections that resulted in higher porosity and lower sintered density. On the contrary, maximum compaction pressure of 300 MPa enhanced the compressive strength of all the sintered porous Al and this is possibly due to the entrapment of some PMMA particles in the Al matrix that cannot be completely eliminated during sintering that also resulted in higher sintered density and lower porosity level. Owing to severe oxygen contamination during prolonged sintering of 2.5 hr, lowest compressive strength values of all the sintered porous Al were obtained compared to the compressive strength values of all the porous specimen sintered for 1.5 hr and 2 hr regardless of PMMA content and compaction pressure variation. Based on these findings, it can be summarized that compressive strength of the resultant porous Al in the current study is highly influenced by the porosity, sintered density as well as residuals from the carbon and oxygen elements in which higher porosity and oxygen residue reduce the compressive strength of the resultant porous Al whereas higher density and carbon residue enhance the compressive strength value of the resultant porous specimen.

Table 4.10 : Compressive strength of the resultant porous Al fabricated under various processing conditions. Data are presented in mean ± standard deviation

	Processing Conditions			**Compressive Strength (MPa)**
No	PMMA content (wt. %)	Compaction pressure (MPa)	Sintering time (hr)	
1	20	200	1.5	21.15 ± 0.06
2	20	250	1.5	19.86 ± 0.05
3	20	300	1.5	22.43 ± 0.06
4	25	200	1.5	19.64 ± 0.05
5	25	250	1.5	19.64 ± 0.05
6	25	300	1.5	20.57 ± 0.08
7	30	200	1.5	16.71 ± 0.09
8	30	250	1.5	15.08 ± 0.05
9	30	300	1.5	17.19 ± 0.09
10	20	200	2	20.19 ± 0.06
11	20	250	2	18.68 ± 0.08
12	20	300	2	21.77 ± 0.08
13	25	200	2	18.54 ± 0.09
14	25	250	2	17.81 ± 0.08
15	25	300	2	19.62 ± 0.10
16	30	200	2	15.27 ± 0.05
17	30	250	2	14.66 ± 0.07
18	30	300	2	16.43 ± 0.07
19	20	200	2.5	18.63 ± 0.07
20	20	250	2.5	17.44 ± 0.07
21	20	300	2.5	19.59 ± 0.06
22	25	200	2.5	16.82 ± 0.06
23	25	250	2.5	15.99 ± 0.07
24	25	300	2.5	18.70 ± 0.08
25	30	200	2.5	14.75 ± 0.08
26	30	250	2.5	13.12 ± 0.09
27	30	300	2.5	15.08 ± 0.06

4.5.7.2 ENERGY ABSORPTION CHARACTERISTIC OF AS PRODUCED POROUS ALUMINUM

In this study, the energy absorption characteristic of the resultant porous Al was evaluated to identify its potential as energy absorber. It has been reported that porosity plays important role along with its sintered density and compressive strength in obtaining porous specimen with good energy absorption characteristic (Yu et al., 2007;

Hamada et al., 2009; Mustapha et al., 2010). Based on the highest porosity level obtained along with considerable values of sintered density and compressive strength, as well as contamination free from carbon and oxygen compared to the other porous specimens, porous Al with different PMMA contents and processed under the compaction pressure of 250 MPa and sintering time of 2 hr is selected for further study in this section to evaluate its capability as energy absorber potential. With respect to sintered density and compressive strength, the relative density and plateau stress of the resultant porous Al were measured to study the energy absorption characteristic of porous specimen. It has been documented that the most important microstructural feature that affects the compressive properties of porous Al is the plateau stress as well as relative density (ρ^*/ρ_s), which is the ratio of the density of the porous Al to that of the solid (Yu et al., 2007; Astaraie et al., 2015). Therefore, the compressive stress-strain curves of the resultant porous Al having different relative densities are plotted in Figure 4.45, while the value of the relative density and the plateau stress are tabulated in Table 4.11. In this study, the plateau stress was taken as the average stress in the strain range from 0.05 to 0.5 (Rabiei et al., 2006). It is observed that all curves exhibited the typical deformation pattern for closed-cell porous metals as aforementioned in section 4.5.7.1. As illustrated in Figure 4.45, the plateau stress increased with increasing relative density. Due to the presence of the denser cell wall, higher buckling and bending deformation resistance of the cell walls are required during the elastic deformation, and thus porous Al with 20 wt % of PMMA content (relative density of 0.61) exhibited the highest plateau stress. In contrast, porous Al with 30 wt % of PMMA (relative density of 0.51) displayed the smallest plateau stress because elastic deformation may easily occur as a result of higher porosity of porous Al, resulting in reduction in the plateau stress. Similar findings were also reported previously (Yu et al., 2007; Hamada et al., 2009).

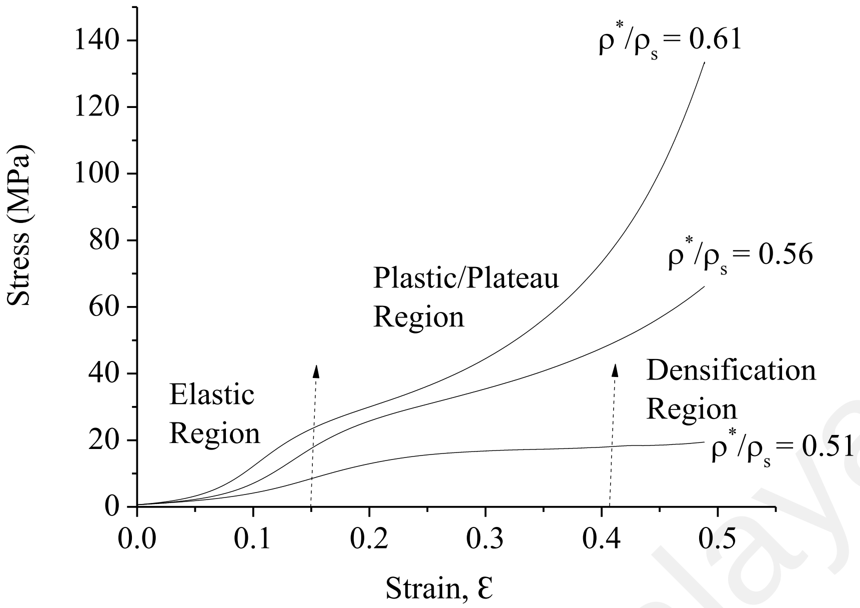

Figure 4.45 : Stress-strain curves for different relative densities

Table 4.11 : Compressive behavior of porous Al with different PMMA contents. Data are presented in mean ± standard deviation

PMMA Content (wt %)	**Plateau Stress (MPa)**	**Relative Density(ρ^*/ρ_s)**	**Energy Absorption Capability (MJ/m^3)**
20	29.41 ± 0.42	0.61 ± 0.32	1.61 ± 0.60
25	24.76 ± 0.55	0.56 ± 0.28	3.65 ± 0.57
30	17.17 ± 0.49	0.51 ± 0.41	1.41 ± 0.44

During compression, a large amount of energy is absorbed during the stages of bending and collapse of the cell walls in the porous specimen, which occur mainly in the plateau region. Therefore, the plateau region plays an important role in determining the energy absorption capacity of the resultant porous Al. In the present study, the energy absorption capacity of the resultant porous Al with different relative densities was calculated from the area under the stress-strain curve in the strain range from 0.05 to 0.6 according to Equation (3.5), and the results are presented in Table 4.11. It can be noticed that the energy absorption capacity of the porous Al increased with decreasing relative density, though this trend was not observed for the porous Al with lowest relative density (30 wt % of PMMA content). The highest value of energy absorption capacity of 3.65 MJ/m^3 was achieved in the porous Al with medium relative density, which is porous Al with 25 wt % of PMMA contents. This is probably because the porosity and cell walls of this porous Al formed a more homogeneous pore structure than the other porous Al, and thus exhibited better compressive and energy absorption behavior.

As can be seen in Figure 4.45, although the longest plateau length was observed for the porous Al with lowest relative density (30 wt % of PMMA contents), the energy absorption capacity was the lowest (as indicated by the small area under its stress-strain curve) as compared to the other counterparts, with its value comparable to that of the porous Al with highest relative density (20 wt % of PMMA contents). This phenomenon revealed that the cell structures in the resultant porous Al with 20 wt % and 30 wt % of PMMA particles could not support higher compressive loading before they fractured. The low value of energy absorption capacity in the porous Al with 20 wt % of PMMA contents is probably due to the inadequate pore formation as a result of insufficient amount of PMMA particles introduced. In the case of the porous Al with 30 wt % of PMMA contents, excessive space holder content caused the porous Al that possessed the highest porosity with thinner cell walls, and thus formed a weak porous Al structure that did not support further loading during the compression test. Taken together, it can be concluded that the optimum content of PMMA should be around 25 wt % since closed-cell porous Al with moderate plateau stress and highest energy absorption capacity could be produced.

SUMMARY

From these findings, it can be deduced that the use of PMMA as a space holder material is practically feasible in successful fabrication of closed-cell porous Al with controlled porosity ranging between 12% and 32% by varying the amount of PMMA content in the range of 20–30 wt %. It is demonstrated that the density of the porous Al decreased and the porosity of the porous Al increased with increasing PMMA content due to an increase in the density of closed-cell pores. On the other hand, it has been found that excessive compaction pressure of 300 MPa caused entrapment of some PMMA particles in the Al matrix that consequently increased the sintered density and compressive strength of the resultant porous Al at the expense of porosity level reduction at any given PMMA content and sintering time. On the contrary, prolonged sintering time of 2.5 hr deteriorated the sintered density and compressive strength of all the porous specimen due to the significant increased in the level of oxygen contamination regardless of compaction pressure and sintering time variation. EDS analysis further validated this finding by displaying a clear increased in the content of carbon and oxygen associated with PMMA particle entrapment and contamination during fabrication.

The resultant porous Al processed with different PMMA contents, compacted at 250 MPa and sintered for 2 hr showed optimum processing conditions due to the highest porosity level obtained which are 12.77%, 25.70% and 31.87% (in the case of 20 wt. %, 25 wt. % and 30 wt. % PMMA) with considerable values of sintered density of 1.5991 g/cm^3, 1.4662 g/cm^3 and 1.3492 g/cm^3 and compressive strength of 20.19 MPa, 18.54 MPa and 15.27 MPa. Based on the abovementioned optimum processing conditions, the energy absorption capability of the resultant porous specimens with different PMMA contents was evaluated and the compressive stress-strain curves showed that there was a decrease in the plateau stress and an increase in the energy absorption capacity with an increase in the amount of PMMA particles in general. However, the highest energy absorption capacity value was observed on the resultant porous Al with 25 wt % of PMMA content due to the porosity and cell walls of this porous Al forming a more homogeneous pore structure than the other counterparts, suggesting the optimum content of PMMA should be around 25 wt % under the present experimental conditions. In comparison to the results obtained in Phase 1, the sintered density and compressive of the resultant porous Al fabricated in Phase 2 were clearly higher at any given processing parameters with desirable formation of macro-pores structure that replicated the initial morphology of PMMA space holder. Therefore, it can be further summarized that fabrication of porous Al using Phase 2 route is more practical due to the desirable morphology of the resultant porous specimen with satisfied physical and mechanical properties.

CHAPTER 5: CONCLUSIONS AND RECOMMENDATION

5.1 CONCLUSIONS

The pertinent findings of this research can be concluded as follows:

1) Porous Al with porosities of 20% to 32% has been successfully fabricated via powder metallurgy technique by utilizing different processing parameters such as PMMA content (20 wt. %, 25 wt. % and 30 wt. %), compaction pressure (200 MPa, 250 MPa and 300 MPa) and sintering time (1.5 hr, 2 hr and 2.5 hr).

2) The density and compressive strength of the porous Al was found to decrease whereas the porosity of the porous Al increased with increasing PMMA content due to an increase in the density of closed-cell pores regardless of compaction pressure and sintering time.

   2.1) The highest sintered density and compressive strength of the resultant porous Al was obtained with the processing conditions of 1.5 hr sintering and 300 MPa compaction in which the sintered density and compressive strength reduced from 1.6788 g/cm^3 to 1.4933 g/cm^3 and 22.43 MPa to 17.19 MPa when the PMMA content was increased from 20 wt % to 30 wt %.

   2.2) The lowest sintered density and compressive strength of the resultant porous Al was obtained with the processing conditions of 2.5 hr sintering and 250 MPa compaction in which the sintered density and compressive strength decreased from 1.5833 g/cm^3 to 1.3188 g/cm^3 and 17.44 MPa to 13.12 MPa when the PMMA content was increased from 20 wt % to 30 wt %.

   2.3) The highest porosity of the resultant porous Al was obtained with the processing conditions of 2 hr sintering and 250 MPa compaction pressure in which the porosity of the sintered porous specimen increased from 12.77% to 31.87% as the PMMA content was increased from 20 wt. % and 30 wt. %. On the contrary, the lowest porosity of the resultant porous Al was achieved with the processing conditions of 1.5 hr sintering and 300 MPa compaction pressure in which the porosity was found to increase from 9.6% to 29.1% with increasing PMMA content from 20 wt. % to 30 wt. %.

3) Considering higher porosity is necessary in the application of energy absorption capacity, the optimum processing conditions were selected from the resultant porous Al at different PMMA content and fabricated under compaction pressure of 250 MPa and sintering time of 2 hr. Under this condition, the reported porosity were 12.77%, 25.70% and 31.87% (in the case of 20 wt. %, 25 wt. % and 30 wt. % PMMA), having sintered density of 1.5991 g/cm^3, 1.4662 g/cm^3 and 1.3492 g/cm^3 as well as compressive strength of 20.19 MPa, 18.54 MPa and 15.27 MPa.

3.1) The compressive stress-strain curves showed that there was a decrease in the plateau stress and an increase in the energy absorption capacity with an increase in the amount of PMMA particles in general. The highest energy absorption capacity value of 3.65 MJ/m^3 however was observed on the resultant porous Al with 25 wt % of PMMA content due to the porosity and cell walls of this porous Al forming a more homogeneous pore structure than the other counterparts, suggesting the optimum content of PMMA should be around 25 wt % in order to fabricate efficient energy absorption capacity of closed-cell porous Al.

It is important to note that Phase 1 has been initially implemented to fabricate porous Al with porosity range between 33% to 52%. In this Phase 1, instead of getting macro-pores that mimic the morphology (size and shape) of PMMA space holder particle, micro-pores structure was obtained due to the fracture of PMMA particles during high energy mixing, resulting in lower sintered densities and compressive strength of the resultant porous Al (stress-strain curves did not follow typical porous metals deformation pattern). Moreover, due to the introduction of lower sintering temperature (450 °C, 475 °C and 500 °C), poor sintering quality of all the sintered porous specimen was obtained that also further contributed to low sintered densities and compressive strength of all the sintered porous Al. Based on the observations in this phase of work, Phase 2 was initiated with different processing conditions in which higher sintered density and compressive strength (stress-strain curves followed typical porous metals deformation pattern) of the resultant porous Al were obtained at any given processing parameters with desirable formation of macro-pores structure that replicated the initial morphology (size and shape) of PMMA space holder material. In addition, porous Al fabricated in Phase 2 had greater potential as energy absorber with maximum energy absorption capacity value of 3.65 MJ/m^3 in the case of using 25 wt. % of PMMA. Therefore, it can be further concluded that fabrication of porous Al under this route was practical due to the desirable morphology (formation of closed macro-pores structure) of the resultant porous specimen with satisfied physical and mechanical properties and consequently greater potential as energy absorber.

5.2 RECOMMENDATION FOR FUTURE WORK

Based on the abovementioned findings of the study, following are some recommendation for further work:

1) Although satisfactory findings in terms of porosity, sintered density and compressive strength can be obtained with the introduction of sintering time less than 3

hr, the use of pure argon gas with 99.999% purity could be explored during sintering to study the effect of oxygen on the sintering behavior of porous Al.

2) Further testing of the resultant porous Al under a variety of loading conditions such as tensile test, flexural test and fracture toughness test with a tailored design material parameters would be valuable to explore other potential applications for porous Al specimen such as cores in sandwich panels, cores for casting and acoustic and thermal control.

3) Incorporation of other metal materials such as copper, titanium and silver as filler or reinforcement to enhance the physical and mechanical properties of porous Al considering the aforementioned properties of porous specimen which is usually not strong enough. However, better understanding on the sintering response of Al material with the abovementioned filler should be emphasized due to the complexity of sintering Al material either under solid state or liquid state condition.

REFERENCES

Ashby, M.F., Evans, A., Fleck, N., & Wadley, H. N. G. (2000). Metal Foams: A Design Guide. Oxford, United Kingdom: Butterwoth-heinemann.

Arifvianto, B., & Zhou, J. (2014). Fabrication of metallic biomedical scaffolds with the space holder method: A review. Materials, 7, 3588–3622.

Arenas, J. P., & Crocker, M. J. (2011). Recent trends in porous sound-absorbing materials for noise control. *Sound and Vibration*, 44(7), 12-17.

Aqida, S. N., Ghazali, M. I., & Hashim, J. (2004). Effects of porosity on mechanical properties of metal matrix composite: An Overview. *Journal of Technology*, 40(A), 17–32.

Asavavisithchai, S., Preuksarattanawut, T., & Nisaratanaporn, E. (2014). Microstructure and Compressive Properties of Open-Cell Silver Foams With Different Pore Architectures. *Procedia Materials Science*, 4, 51 – 55.

Al-Grafi, M. W. (2014). Characteristics of High-Density Al-Foam Manufactured Using Powder Metallurgy Technique. *Middle-East Journal of Scientific Research*, 21 (8), 1351-1356.

Adamiak, M. (2008). Mechanical alloying for fabrication of aluminium matrix composite powders with Ti-Al intermetallics reinforcement. *Journal of Achievements in Materials and Manufacturing Engineering*, 31, 191-196.

Ardakani, M. E., Milani, A. S., Yannacopoulos, S., Bichler, L., Troudel-Boucher, D., Shokouhi, G., & Borazghi, H. (2013). Microtomographic analysis of impact damage in FRP composite laminates: A comparative study. *Advances in Materials Science and Engineering*, 2013(2013), 1-10.

Amsterdam, E., Hosson, J. T. M. D., & Onck, P. R. (2006). Failure mechanisms of closed-cell aluminum foam under monotonic and cyclic loading. *Acta Materialia*, 54, 4465-4472.

Alizadeh, M., & Aliabadi, M. M. (2011). Compressive properties and energy absorption behavior of Al–Al2O3 composite foam synthesized by space-holder technique. *Materials and Design*, 35, 419-424.

Alaf, M., Gultekin, D., & Akbulut, H. (2012). Tin/Tin Oxide (Sn/SnO2) Nanocomposites Thin Films as Negative-Electrode Materials for Li-Ion Batteries. *Acta Physica Polonica A*, 123(2), 323-325.

Asavavisithchai, S., & Nisaratanaporn, E. (2010). Fabrication of Open-Cell Silver Foams Using Disaccharide as Space Holders. *Chiang Mai Journal of Science*, 37(2), 222-230.

Ahmed, Y. M. Z., Riad M. I., Sayed, A. S., Ahlam, M. K., & Shalabi, M. E. H. (2007). Correlation between factors controlling preparation of porous copper via sintering technique using experimental design. *La Metallurgia Italiana*, 10, 41-46.

Ahmad Suffin, N. S., Abu Seman, A., & Hussain, Z. (2013). Effect of Dissolution Times on Compressive Properties and Energy Absorption of Aluminum Foam. *Sains Malaysiana*, 42(12), 1755-1761.

Amaranan, S., & Mononukul, A. (2010). Study of Process Parameters in Conventional Powder Metallurgy of Silver. *Journal of Metals, Materials and Minerals*, 20(1), 51-55.

Bin, J., Zejuna, W., & Naiqin, Z. (2007). Effect of pore size and relative density on the mechanical properties of open cell aluminum foams. Scripta Materialia, 56, 169–172.

Banhart, J. (2001). Manufacturer, Characterization and Application of Cellular Metals and Metal Foams. Program in Materials Science, 46, 559–632.

Bafti, H., &Habibolahzadeh, A. (2010). Production of Aluminum Foam by Spherical Carbamide Space holder particle Technique-Processing Parameters. *Materials and Design*, 31(9), 4122-4129.

Bi, Y., Zheng, Y., & Li, Y. (2015). Microstructure and mechanical properties of sintered porous magnesium using polymethyl methacrylate as the space holder. *Materials Letters*, 161, 583–586.

Benjamin, J. S. (1976). Mechanical alloying. *Scientific American*, 234(5), 40-49.

Babscan, N., Leitmeier, D., Degischer, H. P. (2003). Foamability of particle reinforced aluminum melt. *Material Science and Engineering Technology*, 34(1), 22-29.

Banhart, J. (2001). Manufacture, characterisation and application of cellular metals and metal foams. *Progress in Materials Science*, 46, 559–632.

Bram, M., Stiller, C., Buchkremer, H. P., Stover, D., & Baur, H. (2000). High Porosity Titanium, Stainless Steel and Superalloy Parts. *Adv. Eng. Mater*, 2, 196-199.

Bekoz, N., & Oktay, E. (2012). Effects of Carbamide Shape and Content on Processing and Properties of Steel Foams. *J. Mater. Process. Technol.*, 212, 2109–2116.

Bakan, H. (2006). A Novel Water Leaching and Sintering Process For Manufacturing Highly Porous Stainless Steel. *Scr. Mater.*, 55, 203–206.

Blaskov, V., Radev, V. V., Klissurski, D., Yordanov, N. D. (1994). On the Magnetic properties of Nanosized $CoFe_2O_4$. Journal of Alloys and Compounds, 206(2), 67-70.

Bonaccorsi, L and Proverbio, E. (2006). Powder Compaction Effect on Foaming Behavior of Uni-Axial Pressed PM Precursors. *Advanced Engineering Materials*, 8(9).864-869.

Barletta, M., Gisario, A., Guarino, S., & Rubino, G. (2009). Production of open cell aluminum foams by using the dissolution and sintering process (DSP). *Journal of Manufacturing Science and Engineering*, 131(4), 1-38.

Byakova, A., Kartuvoz, I., Gnyloskurenko, S., & Nakamura, T. (2014). The Role of Foaming Agent and Processing Route in Mechanical Performance of Fabricated Aluminum Foams. *Advances in Materials Science and Engineering*, 2014, 1-9.

Baumeister, J., Banhart, J., & Weber, M. (1997). Aluminium foams for transport industry. *Materials and Design*, 18(4/6), 217-220.

Chen, S., Bourham, M., & Rabiei, A. Applications of open-cell and closed-cell metal foams for radiation shielding. (2014). *Procedia Materials Science*, 4, 293–298.

Capek, J., & Vojtech, D. (2013). Properties of porous magnesium prepared by powder metallurgy. *Materials Science and Engineering C*, 33 (2013), 564–569.

Chen, P., Kim, G. Y., & Ni, J. (2007). Investigations in the compaction and sintering of large ceramic parts. *Journal of Materials Processing Technology*, 190 (2007), 243–250.

Coble, R. L. (1961). Sintering Crystalline Solids 1: Intermediate and Final State Diffusion Models. *Journal of Applied Physics*, 32(5), 787-791.

Chhillar, P., Agrawal, D., & Adair, J. H. (2008). Sintering of Molybdenum Metal Powder Using Microwave Energy. *Powder Metallurgy*, 51(2), 182-187.

Cicek, A., Kivak, T., & Samtas, G. (2012). Application of Taguchi Method for Surface Roughness and Roundness Error in Drilling of AISI 316 Stainless Steel. *Journal of Mechanical Engineering*, 58(3), 165-174.

Calka, A., & Radlinski, A. P. (1991). Formation of amorphous Fe-B alloys by mechanical alloying. *Journal of Applied Physics Letters*, 58(2), 119-121.

Dewidar, M. (2012). Influence of processing parameters and sintering atmosphere on the mechanical properties and microstructure of porous 316L stainless steel for possible hard-tissue applications. International Journal of Mechanical and Mechatronics Engineering, 12, 10-24.

Dawood, A. K., & Nazirudeen, M. S. S. (2010). A development of technology for making porous metal foam castings. *Jordan Journal of Mechanical and Industrial Engineering*, 4(2), 292-299.

Dobrzanski, L. A., Kremzer, M., Adamiak, M., & Włodarczyk-Fligier, A. (2008). Manufacturing of Aluminium Matrix Composite Materials Reinforced By Al2O3 Particles. *Journal of Achievements in Material and Manufacturing Engineering*, 27(1), 99-102.

Dunnett, K., Mueller, R., & Bishop, D. (2008). Development of Al–Ni–Mg–(Cu) aluminum P/M alloys. *Journal of Materials Processing Technology*,198 (1-3), 31-40.

Dabrowski, B., Swieszkowski, W., Godlinski, D., & Kurzydlowski, K.J. (2010). Highly Porous Titanium Scaffolds for Orthopaedic Applications. *J. Biomed. Mater. Res. B Appl. Biomater.*, 95, 53–61.

Davis, R. M., & Koch, C. C. (1987). Mechanical Alloying of Brittle Components: Silicon and Germanium. *Scripta Metallurgica*, 21, 305-310.

Dehaqani, M. T., &Akbari, G. H. (2010). Behavior of Cu-Cr Powder Mixtures During Mechanical Alloying. *IJE Transactions B: Applications*, 23(1), 29-76.

Dizlek, M. E., Guden, M., Turkan, U., & Tasdemirci, A. (2009). Processing and compression testing of Ti6Al4V foams for biomedical applications. *Journal of Materials Science*, 44, 1512-1519.

Dhokey, N. B., Athavale, V. A., Narkhede, N., & Kamble, M. (2013). Effect of processing conditions on transient liquid phase sintering of premixed aluminium alloy powders. *Advanced Materials Letters*, 4(3), 235-240.

Dewidar, M., Mohamed, H. F., & Lim, J. K. (2008). A New Approach for Manufacturing a High Porosity Ti-6Al-4V Scaffolds for Biomedical Applications. *Journal of Materials Science and Technology*, 24(6), 931-935.

Dewidar, M. (2006). Mechanical and Microstructure Properties of High Porosity Sintered Ti-6Al-4V Powder for Biomedical Applications. *Journal of Engineering Sciences*, 34(6), 1929-1940.

Eksi, A. K., & Saritas, S. (2002). Effects of Powder Hardness and Particle Size on the Densication of Cold Isostatically Pressed Powders. *Turkish J. Eng. Env. Sci.*, 26 (2002), 377-384.

Esen, Z., & Bor, S. (2011). Characterization of Ti-6Al-4V Alloy Foams Synthesized by Space holder particle Technique. *Mater. Sci. Eng. A*, 528, 3200–3209.

Esen, Z., & Bor, S. (2007). Processing of Titanium Foams Using Magnesium Spacer Particles. *Scripta Materialia*, 56, 341–344.

Friedrich, B., & Krautlein, C. (2005). Melt Treatment of Copper and Aluminium-The Complex Step Before Casting. *Metalurgija- Journal of Metallurgy*, 44, 251-266.

Gokce, A., Findik, F., & Kurt, A. (2011). Microstructural Examination and Properties of Premixed Al–Cu–Mg Powder Metallurgy Alloy. Materials Characterization. 62(7), 730-735.

Gulsoy, H.O., & German, R.M. (2008). Production of micro-porous austenitic stainless steel by powder injection molding. *Scripta Materialia*, 58, 295–298.

Gibson, L.J. and Ashby, M.F. (1997). Cellular Solids: Structure and Properties, Second Edition, Cambridge University Press, Cambridge, U.K, 31-34.

Gokhale, A. A., Ravi Kumar, N. V., Sudhakar, B., Sahu, S. N., Basumatary, H., & Dhara, S. (2011). Cellular metals and ceramics for defence applications. *Defence Science Journal*, 61(6), 567-575.

German, R. M. (2005). Powder metallurgy and particulate materials processing: The processes, materials, products, properties and applications. New Jersey, Princeton: Metal Powder Industries Federation.

Gokce, A., & Fındık, F. (2008). Mechanical and physical properties of sintered aluminum powders. *Journal of Achievements in Materials and Manufacturing Engineering*, 30(2), 157-164.

Guden, M., Celik, E., Hizal, A., Altindis, M., & Cetiner, S. (2008). Effects of Compaction Pressure and Particle Shape on the Porosity and Compression Mechanical Properties of Sintered Ti6Al4V Powder Compacts For Hard Tissue Implantation. *J. Biomed. Mater. Res. B Appl. Biomater*, 85, 547-555.

Golabgir, M.H., Ebrahimi-Kahrizsangi, R., Torabi, O., & Saatchi, A. (2014). Fabrication of Open Cell Fe-10%Al Foam by Space holder particle Technique. *Archives of Metallurgy and Materials*, 59(1), 41-46.

Gilani, H., Jafari, S., Gholami, R., Habibolahzadeh, A., & Mirshahi, M. (2012). Effect of Processing Parameters and Glycerin Addition on the Properties of Al Foams. *Met. Mater*. Int., 18(2), 327-333.

German, R. M., Suri, P., & Park, S. J. (2009). Review: Liquid Phase Sintering. *Journal of Materials Science*, 44, 1-39.

Goel, M. D., Matsagar, V. A., & Gupta, A. K. (2014). Blast Resistance of Stiffened Sandwich Panels with Closed-Cell Aluminum Foam. *Latin American Journal of Solids and Structures*, 11, 2497-2515.

Grilec, K., Maric, G., & Milos, K. (2012). Aluminium Foams in the Design of Transport Means. *Promet – Traffic and Transportation*, 24(4), 295-304.

Gosh, A., & Chatterje, S. (2014). Effect of Al_2O_3 Content and Process Variables on Structure and Properties of Al-Al_2O_3 Compacts. *Journal of Minerals and Materials Characterization and Engineering*, 2, 121-128.

Grabke, H. J. (1999). Oxidation of NiAl and FeAl. *Intermetallics*, 7, 1153-1158.

Heydari Astaraie, A., Shahverdi, H. R., & Elahi, S. H. (2015). Compressive behavior of Zn–22Al closed-cell foams under uniaxial quasi-static loading. Transactions of Nonferrous Metals Society of China, 25, 162-169.

Hardt, C.R., Grondahl, K., Lekholm, U., Wennstrom, J. L. (2002). Outcome of implant therapy in relation to experienced loss of periodontal bone support: A retrospective 5- year study. *Clinical Oral Implants Res*, 13, 488-494

Hassani, A., Habibolahzadeh, A., & Bafti, H. (2012). Production of Graded Aluminum Foams via Powder Space holder particle Technique. *Materials and Design*, 40, 510-515.

Hao, G. L., Han, F. S., & Li, W. D. (2008). Processing and Mechanical Properties of Magnesium Foams. *Journal of Porous Materials,* 16, 251–256

Hussain, Z., & Suffin, N. S. A. (2011). Microstructure and mechanical behaviour of aluminium foam produced by sintering dissolution process using NaCl space holder particle. *Journal of Engineering Science*, 7, 37–49.

Hao, G. L., Han, F. S., & Li, W. D. (2009). Processing and mechanical properties of magnesium foams. *Journal of Porous Materials*, 16, 251-256.

Hsu, H. C., Hsu, S. K., Wu, S. C., Wang, P. H., & Ho, W. F. (2013). Design and characterization of highly porous titanium foams with bioactive surface sintering in air. *Journal of Alloys and Compounds*, 575, 326-332.

Hamada, T., Kanahashi, H., Miyoshi, T., & Kanetake, N. (2009). Effects of the strain rate and alloying on the compression characteristics of closed cell aluminum foams. *Materials Transactions*, 50, 1418-1425.

Inoguchi, N., Kobashi, M., & Kanetake, N. (2009). Synthesis of porous Al3Ti/Al composite and effect of precursor processing condition on cell morphology. *Materials Transactions*, 50(11), 2609-2614.

Jain, N., Ottino, J. M., & Lueptow, R. M. Regimes of Segregation and Mixing In Combined Size and Density Granular Systems: An Experimental Study. *Granul. Matter*, 7, 69–81.

Jiang, B., Zhao, N. Q., Shi, C. S., & Li, J. J. (2005). Processing Of Open Cell Aluminum Foams with Tailored Porous Morphology. Scripta Materialia, 53, 781–785.

Jha, N., Mondal, D. P., Dutta Majumdar, J., Badkul, A., Jha, A. K., & Khare, A. K. (2013). Highly porous open cell Ti-foam using NaCl as temporary space holder through powder metallurgy route. *Materials and Design*, 47, 810–819.

Jeon, K. C., Kim, Y. D., Suk, M. J., & Oh, S. T. (2015). Fabrication of porous Ti by thermal decomposition and sintering of PMMA/TiH2powder compact. *Archives of Metallurgy and Materials*, 60, 26–28.

Jamaludin, S. B., Yi, C. X., Abdullah, A., & Hussin, K. (2013). Effect of Space holder particle and Compaction Pressure on the Porosity of Sintered Copper. *Advanced Materials Research*, 795, 2013, 82-86.

Joshi, S., Gupta, G. K., Sharma, M., Telang, A., & Mahra, T. (2015). Synthesis & Characterization of Stainless Steel foam via Powder Metallurgy Taking Acicular Urea as Space Holder. *Material Science Research India*, 12(1), 43-49.

Jinnapat, A., & Kennedy, A. (2011). The Manufacture and Characterisation of Aluminium Foams Made by Investment Casting Using Dissolvable Spherical Sodium Chloride Bead Preforms. *Metals*, 1, 49-64.

Jha, N., Mondal, D. P., Dutta Majumdar, J., Badkul, A., Jha, A. K., & Khare, A. K. (2013). Highly porous open cell Ti-foam using NaCl as temporary space holder through powder metallurgy route. *Materials and Design*, 47, 810–819.

Jabur, A. S. (2013). Effect of powder metallurgy conditions on the properties of porous bronze. *Powder Technology*, 237(2013), 477–483.

Kato, O. (2012). Fabrication of Porous Fe/TiB2 Composites by Reactive Precursor Method. Journal of Materials Science Research, 1(2), 110-118.

Kevorkijan, V., Kapin, S. D., Paulin, I., Sustarsic, B., & Jenko, M. (2010). Synthesis and Characterisation of Closed Cells Aluminium Foams Containing Dolomite Powder as Foaming Agent. Materials and Technology, 44, 6, 363-371.

Koizumi, T., Kido, K.; Kita, K., Mikado, K., Gnyloskurenko, S., & Nakamura, T. (2011). Method of Preventing Shrinkage of Aluminum Foam Using Carbonates. Metals, 2, 1-9.

Katsuyoshi, K., Tachai, L., Thotsaphon, T., & Atsushi, K. (2007). Local Appearance of Sn Liquid Phase at Surface of Aluminum Alloy Powder during Heating. Transactions of JWRI, 36(2), 29-33.

Kavei, G. (2015). Mechanical Properties of Aluminum Foam Fabricated by Aluminum Powders with Na or Carbamide Replica, 1(2), 22–30.

Kamaruddin, S., Khan, Z. A., & Wan, K. S. (2004). The Use of the Taguchi Method in Determining the Optimum Plastic Injection Moulding Parameters for the Production of a Consumer Product. *Journal of Mechanical*, 18, 98-110.

Kheder, A. R. I., Marahleh, G. S., & Al-Jamea, D. M. K. (2011). Strengthening Of Aluminum By SiC, Al2O3 and MgO. *Jordan Journal of Mechanical and Industrial Engineering*, 5(6), 533-541.

Koch, C. C. (1991). Processing of Metals and Alloys, Materials Science and Technology-A Comprehensive Treatment. Weinheim, Germany: VCH.

Khakbiz, M. (2008). Effect of mechanical alloying process parameters on characteristics of Al-B4C nanocomposite-nanocrystlline powder particles. *International Journal of Modern Physics B*, 22(18&19), 2924-2931.

Kim, S.W., Jung, H. D., Kang, M. H., Kim, H. E., Koh, Y. H., & Estrin, Y. (2013). Fabrication of Porous Titanium Scaffold with Controlled Porous Structure and Net-Shape Using Magnesium as Spacer. *Mater. Sci. Eng. C*, 33, 2808–2815.

Kotan, G., & Bor, A. S. (2007). Proudction and Characterization of High Porosity Ti-6Al-4V Foams by Space holder particle Technique In Powder Metallurgy. *Turkish Journal of Engineering and Environmental Sciences*, 31(3), 149-156.

Kwon, Y. S., Lee, H. T., & Kim, K. T. (1997). Analysis for Cold Die Compaction of Stainless-Steel Powder. *Journal of Engineering Materials and Technology*, 119(4), 366-373.

Kim, K. T., Lee, H. T., Kim, J. S., & Kwon, Y. S. (1997). Analysis for Die Compaction of Metal. *Powders Solid Mechanics and Its Applications*, 53, 403-413.

Kalpakjian, S., & Schmid. S. R. (2006). Manufacturing, Engineering and Technology. New Jersey, Upper Saddle River: Pearson Education.

Kang, S. J. L. (2005). Sintering: Densification, grain growth and microstructure. London: Elsevier Butterworth-Heinemann.

Krug, S., & Zachmann, S. (2009). Influence of Sintering Conditions and Furnace Technology on Chemical and Mechanical Properties of Injection Moulded 316L. *Powder Inject. Mould. Int.*, 3, 66-70.

Kacker, R. N., Lagergren, E. S., & Filliben, J. J. (1991). Taguchi's Orthogonal Arrays Are Classical Designs of Experiments. *Journal of Research of the National Institute of Standards and Technology*, 96(5), 577-591.

Kennedy, A. (2012). Porous Metals and Metal Foams Made from Powders. Powder Metallurgy, 31-46.

Li, B., Li, Z., & Lu, X. (2012). Effect of the macro-pore structure on the anodic polarization behavior of porous titanium. *Anti-Corrosion Methods and Materials*, 59, 57–62.

Liu, J., Yu, S., Zhu, X., Wei, M., Luo, Y., & Liu, Y. (2008). The compressive properties of closed-cell Zn-22Al foams. *Materials Letters*, 62, 683–685.

Li, B. Q., Wang, C. Y., & Lu, X. (2013). Effect of pore structure on the compressive property of porous Ti produced by powder metallurgy technique. *Materials and Design*, 50, 613–619.

Liu, P. S., & Liang, K. M. (2001). Review Functional Materials Of Porous Metals Made By P/M, Electroplating And Some Other Techniques. *Journal of Materials Science*, 36, 5059-5072.

Lumley, R., & Schaffer, G. (1996). The Effect of Solubility and Particle Size on Liquid Phase Sintering. *Scripta Materialia*, 35(5), 589-595.

Lund, J. A. (1982). Origins of Green Strength in Iron PIM Compacts. *International Journal of Powder Metallurgy*, 18(2), 1l7-127.

Li, B. Q., & Lu, X. (2011). The effect of pore structure on the electrical conductivity of titanium. *Transp Porous Med*, 87, 179–189.

Laptev, A., Bram, M., Buchkremer, H. P., & Stover, D. (2004). Study of Production Route for Titanium Parts Combining Very High Porosity and Complex Shape. *Powder Metallurgy*, 47, 85-92.

Li, C.F., Zhu, Z.G., & Liu, T. (2005). Microhardness of Pore Walls In Porous Titanium Prepared With Novel Powder Metallurgy. *Powder Metallurgy*, 48, 237–240.

Lin, Y. J., & Hwang, K. S. (2009). Effects of Powder Shape and Processing Parameters on Heat Dissipation of Heat Pipes with Sintered Porous Wicks. *Materials Transactions*, 50(10), 2427-2434.

Liu B., Wildman, R., Tuck, C., Ashcroft, I., & Hague,R. (2011). Investigation the Effect of Particle Size Distribution on Processing Parameters Optimisation in Selective Laser Melting Process. In: Twenty-second annual international solid freeform fabrication (sff) symposium: An Additive manufacturing conference.University of Texas, Austin. Unites States: Milliken.

Lindsley, B., Fillari, G., & Murphy, T. (2005). Effect of Composition and Cooling Rate on Physical Properties and Microstructure of Prealloyed P/M Steels. In C. Ruas & T. A. Tomlin (Eds.), Advances in Powder Metallurgy and Particulate Materials (p. 353). New Jersey, Princeton: Metal Powder Industries Federation.

Luo, Y., Yu, S., Liu, J., Zhu, X., & Luo, Y. (2010). Compressive property and energy absorption characteristic of open-cell SiCp/$AlSi_9Mg$ Composite Foams. *Journal of Alloys and Compounds,* 499, 227-230.

Lu, L., Lai, M. O., & Zhang, S. (1995). Fabrication of Ni^3Al Intermetallic Compound using Mechanical Alloying Technique. *Journal of Materials Processing Technology*, 48, 683-690.

Luk, S. H., Chan, F. Y., Davala, A. B., & Murphy, T. F. (1997, June 29-July 2). *Processing Experience of Green Strength Enhanced Material System*s. Paper presented at International Conference on Powder Metallurgy & Particulate Materials Chicago, United States of America.

Mustapha, M., Ismail, F., & Mama, O. (2011). Empirical Relationship between Relative Electrical Conductivity and Relative Density of the Al-Foam Fabricated through Pressure Assisted Sintering/Dissolution Process. IOP Conference Series: Materials Science and Engineering, 17(1), 1-19.

Manonukul, A., Muenya, N., Leaux, F., & Amaranan, S. (2010). Effects of replacing metal powder with powder space holder on metal foam produced by metal injection moulding. *Journal of Metals, Materials and Minerals*, 20(1), 529–535.

Matijasevic, B., & Banhart, J. (2006). Improvement of aluminium foam technology by tailoring of blowing agent. *Scripta Materialia*, 54, 503–508.

Mour, M., Das, D., Winkler, T., Hoenig, E., Mielke, G., Morlock, M. M., & Schilling, A. F. (2010). Review Advances in Porous Biomaterials for Dental and Orthopaedic Applications. *Materials*, 3, 2947-2974.

Mukai, T., Miyoshi, T., Nakano, S., Somekawa, H., & Higashi, K. (2006). Compressive response of a closed-cell aluminum foam at high strain rate. *Scripta Materialia*, 533-537.

Mittal, R., & Singh, D. (2012). Dry sliding wear behavior of spray formed ZrSiO4 reinforced Al-Si-Sn alloy. *Advanced Materials Letters*, 3(1), 38-43.

Mutlu, I., & Oktay, E. (2011). Production and Characterisation of Cr-Si-Ni-Mo Steel Foams. *Indian Journal of Engineering and Materials Sciences*, 18, 227-232.

Michailidis, N., Stergioudi, F., Tsouknidas, A., & Pavlidou, E. (2011). Compressive Response of Al-Foams Produced Via A Powder Sintering Process Based on A Leachable Space-Holder Material. *Materials Science and Engineering A*, 528, 1662–1667.

Murty, B. S., & Ranganathan, S. (1998). Novel materials synthesis by mechanical alloying/milling. *International Materials Reviews*, 43(3), 101-141.

Muhamad, N., Tatta, T. K., Muchtara, A., Sulong, A. B., & Yunna, H. S. (2012). Rheological Behaviour of Novel Feedstock for Manufacturing Porous Stainless Steel via (MIM). *Journal of Technology*, 59, 187-191.

Mustapha, F., Mustapha, M., Noorsal, K., Mamat, O., Hussain, P., Ahmad, F., Muhamad, N., Haris, S. N. (2010). Preliminary study on the fabrication of aluminium foam through pressure assisted sintering dissolution process. *Journal of Materials Processing Technology*, 210, 1598–1612.

Marcu Puscas, T., Signorini, M., Molinari, A., & Straffelini, G. (2003).Image analysis investigation of the effect of the process variables on the porosity of sintered chromium steels. *Materials characterization*, 50(1), 1-10.

Motz, C. and Pippan, R. (2011). Deformation Behaviour of Closed-cell Aluminium Foams in Tension. *Acta Materialia*, 49, 2463-2470.

MacAskilla, I. A., Hexemer Jr.b, R. L., Donaldsonb, I. W., & Bishop, D. P. (2010). Effects of Magnesium, Tin and Nitrogen on the Sintering Response of Aluminum Powder. *Journal of Materials Processing Technology*, 210, 2252-2260.

Michailidis, N., & Stergioudi, F. (2011). Establishment of process parameters for producing Al-foam by dissolution and powder sintering method. *Materials and Design*, 32, 1559-1564.

Niu, W., Gill, S., Dong, H., & Bai, C. (2010). A Two-Scale Model for Predicting Elastic Properties of Porous Titanium Formed With Space-Holders. *Comput. Mater. Sci.*, 50, 172–178.

Nesic, S., Krupp, U., & Michels, W. (2014). Monotonic and cyclic loading behavior of closed-cell aluminum foams and sandwich structures. *Procedia Materials Science*, 4, 269-273.

Nouri, A., Hodgson, P. D., & Wen, C. (2011). Effect of ball-milling time on the structural characteristics of biomedical porous Ti-Sn-Nb Alloy. *Materials and Design*, 47, 921-928.

Ohtaguchi, M., Muramatsu, Y., Wanikawa, S., Okada, H., & Abe, F. (2005). Gas Contamination due to Milling Atmospheres of Mechanical Alloying and Its Effect on Impact Strength. *Materials Transactions*, 46(3), 681- 686.

Ozan, S., & Bilhan, S. (2008). Effect of fabrication parameters on the pore concentration of the aluminum metal foam manufactured by powder metallurgy process. *International Journal of Advanced Manufacturing Technology*, 39, 257–260.

Olevsky, E. A., & Maximenko, A. L. (2004). Effective Diffusion Coefficients in Solid-State Sintering. *Acta Materialia*, 52(2004), 2953-2963.

Oh, I. H., Nomura, N., & Hanada, S. (2002). Microstructures and Mechanical Properties of Porous Titanium Compacts Prepared By Powder Sintering. *Mater. Trans.*, 43, 443–446.

Oh, I.H.,Nomura, N.,Masahashi, N., & Hanada, S. (2003). Mechanical Properties of Porous Titanium Compacts Prepared By Powder Sintering. *Scr. Mater.*, 49, 1197–1202.

Pieczonka, T., Schubert, T., Baunack, S., & Kieback, B. (2008). Dimensional Behaviour of Aluminum Sintered in Different Atmospheres. *Materials Science Engineering A*, 478, 251-256.

Pei-heng, Z., Long-jiang, D., Jian-liang, X., Di-fei, L., & Liang, C. (2005). A Study about Fe-Ni Mechanical Alloying Process by Dry and Wet Method. *Journal of Electronic Science and Technology of China*, 3(2), 164-167.

Paulin, I. (2014). Synthesis and Characterization of Al Foams Produced by Powder Metallurgy Route Using Dolomite and Titanium Hydride as a Space holder particles. *Materials and Technology*, 48, 943-947.

Paul, B., Verma, A., Bidaye, A. C., Hubli, R. C., & Suri, A. K. (2012). Optimization of Sintering Parameters of Submicron Cobalt Metal Powder Using Taguchi Method. *Journal of Metallurgical Engineering*, 1(1), 23-29.

Pachal, A. S., & Bagesar, A. (2013). Taguchi Optimization of Process Parameters in Friction Welding of 6061 Aluminum Alloy and 304 steel: A Review. *International Journal of Emerging Technology and Advanced Engineering*, 3(4), 229-233.

Qiao, J. C., Xi, Z. P., Tang, H. P., Wang, J. Y., & Zhu, J. L. (2008). Compressive Property and Energy Absorption of Porous Sintered Fiber Metals. *Materials Transactions*, 49(12), 2919-2921.

Rowsell, J. L. C., & Yaghi, O. M. (2004). Metal–organic frameworks: A new class of porous materials. Microporous and Mesoporous Materials, 73, 3–14.

Ruperez, E., Maneroa, J. M., Riccardi, K., Li, Y., Aparicio, C., & Gil, F. J. (2015). Development of tantalum scaffold for orthopedic applications produced by space-holder method. Materials and Design, 83, 112–119.

Rabiei, A., Vendra, L., Reese, N., Young, N., Neville, B. P. (2006). Processing and characterization of a new composite metal foam. Materials Transactions, 47(9), 2148-2153.

Ramezani, M., & Neitzert, T. (2012). Mechanical Milling of Aluminum Powder using Planetary Ball Milling Process. *Journal of Achievements in Materials and Manufacturing Engineering*, 55(2), 790-798.

Rafter, M., Ahmad, F. M., lbrahimz, S., & Hussin, R. (2014). Development of Stainless Steel (SS316L) Foam with Different Composition using Compaction Method. In: International Conference on X-Rays & Related Techniques in Research & Industry 2014 (ICXR120 14). Malaysia.

Roy, R. K. (2010). *A Premier on the Taguchi Method*. United States of America: Society of Manufacturing Engineers (SME).

Rajesh, A., & Venkatesh, P. J. (2014). Taguchi method and Pareto ANOVA: An approach for process parameters optimization in micro-EDM drilling. *International Journal of Scientific & Engineering Research*, 5(10), 38-42.

Ryan, G., Pandit, A., & Apatsidis, D. P. (2006). Fabrication methods of porous metals for use in orthopaedic applications. *Biomaterials*, 27, 2651-2670.

Raza, M. R., Sulong, A. B., Muhamad, N., Akhtar, M. N., & Rajabi, J. (2015). Effects of binder systemand processing parameters on formability of porous Ti/HA composite through powder injection molding. *Materials and Design*, 87, 386-392.

Smith, B. H., Szyniszewski, S., Hajjar, J. F., Schafer, B. W., & Arwade, S. R. (2010). Steel foam for structures: A review of applications, manufacturing and material properties. Journal of Constructional Steel Research, 71, 1-10.

Sukiman, N. L., Gupta, R. K., Buchheit, R. G., & Birbilis, N. (2014). Influence of microalloying additions on Al–Mg alloy. Part 1: Corrosion and electrochemical response. Corrosion Engineering, Science and Technology, 49(4), 254-262.

Surace, R., De Filippis, L. A. C., Ludovico, A. D., & Boghetic, G. (2010). Application of Taguchi method for the multi-objective optimization of aluminium foam manufacturing parameters. *International Journal of Materials Form*, 3, 1-5.

Surace, R., Bruno, S., De Filippis, L. A. C., & Ludovico, A. D. (2009). Multi-Objective Optimization of Aluminium Foam Manufacturing Parameters. *Int J simul model*, 8(2), 81-89.

Sobczak, J. (2003). High Porosity Media for Transportation-Selected Aspects. *Journal of KONES Internal Combustion Engines*, 10, 1-15.

Surace, R., De-Filippis, L. A. C., Ludovico, L. D., & Boghetich, G. (2009). Influence of Processing Parameters on Aluminium Foam Produced by Space holder particle Technique. *Materials and Design*, 30, 1878–1885.

Schaffer, G. B., Sercombe, T. B., & Lumley, R.N. (2001). Liquid phase sintering of aluminium alloys. *Materials Chemistry and Physics*, 67, 85–91.

Sercombe, T., & Schaffer, G. B. (1999). On The Use of Trace Additions of Sn To Enhance Sintered 2xxx Series Al Powder Alloys. *Materials Science and Engineering A: Structural Materials Properties Microstructure and Processing*, 268(1-2), 32-39.

Sanchez, F., Bolarin, A. M., Molera, P., Mendoza, J. E., & Ocampo, M. (2003). Relationship between particle size and manufacturing processing and sintered characteristics of iron powders. *Revista Latinoamericana de Metalurgia y Materiales*, 23(1), 35-40.

Sharma, M., Gupta, G. K., Modi, O. P., Prasad, B. K., & Gupta, A. K. (2011). Titanium Foam through Powder Metallurgy Route Using Acicular Urea Particles As Space holder particle. *Materials Letters*, 65, 3199–3201.

Senthil-Kumar, V., & Ahamed, H. (2011). A comparative study on the milling speed for the synthesis of nano-structured Al 6063 alloy powder by mechanical alloying. *Journal of Minerals and Materials Characterization and Engineering*, 10, 507-515.

Suryanarayana, C. (2001). Mechanical alloying and milling. *Progress in Materials Science*, 46 (2001), 1-184.

Shaw, L., Zawrah, M., Villegas, J., Luo, H., & Miracle, D. (2003). Effects of Process-Control Agents on Mechanical Alloying of Nanostructured Aluminum Alloys. *Metallurgical and Materials Transactions A*, 34A, 159-170.

Siebeck, S., Nestler, D., Podlesak, H., & Wielage, B. (2011, 21 August). *Influence of Milling Atmosphere on the High- Energy Ball-Milling Process of Producing Particle-Reinforced Aluminum Matrix Composites.* Paper presented at 18th International Conference on Composite Materials, Korea.

Sanchez, F., Bolarin, A., Coreno, J., Martinez, A., & Bas, J. A. (2001). Effect of the compaction process sequence on the axial density distribution of green compacts. *Powder Metallurgy*, 44(4), 1-5.

Spierings, A. B., Herres, N., & Levy, G. (2011). Influence of The Particle Size Distribution on Surface Quality and Mechanical Properties In Additive Manufactured Stainless Steel Parts. *Rapid Prototyping Journal*, 17(3), 195 - 202.

Sadighikia, S., Abdolhosseinzadeh, S., & Asgharzadeh, H. (2015). Production of high porosity Zn foams by powder metallurgy method. *Powder Metallurgy*, 58(1), 61-66.

Sercombe T. B. (1998). *Non Conventional Sintered Aluminum Powder Alloy*. Ph.D thesis, The University of Queensland, Australia.

Sercombe, T. B., & Schaffer, G. B. (1999). The Effect of Trace Elements on the Sintering of Al/Cu Alloys. Acta Materialia, 47(2), 689-697.

Sai, N. V. (2014). Fabrication and Characterization of Copper-Red Mud Particulate Composites Prepared by Powder Metallurgy Technique. *Jourdan Journal of Mechanical and Industrial Engineering*, 8(5), 313-321.

Surace, R., & Filippis, L. A. C. D. (2010). Investigation and Comparison of Aluminium Foams Manufactured by Different Techniques. *Advanced Knowledge Application in Practice*, 95-118.

Siemiaszko, D., Jozwiak, S., Czarnecki, M., & Bojar, Z. (2013). Influence of temperature during pressure-assisted induction sintering (PAIS) on structure and properties of the Fe40Al intermetallic phase. *Intermetallics*, 41, 16–21.

Siemiaszko, D., Kowalska, B., Jozwik, P., & Kwiatkowska, M. (2015). The Effect of Oxygen Partial Pressure on Microstructure and Properties of Fe40Al Alloy Sintered under Vacuum. *Materials*, 8, 1513-1525.

Sun, D. X., & Zhao, Y. Y. (2003). Static and Dynamic Energy Absorption of Al Foams Produced by a Sintering and Dissolution Process. *Metallurgical and Materials Transactions B*, 34(1), 69-74.

Tuncer, N., Arslan, G., Maire, E., & Salvo, L. (2011). Investigation of Spacer Size Effect on Architecture and Mechanical Properties of Porous Titanium. *Mater. Sci. Eng. A*, 530, 633–642.

Tang, P., & Puri, V. M. Methods for Minimizing Segregation: A Review. *Particul. Sci. Technol.*, 22, 321–337.

Travessa, D. N., Cardoso, K. R., Wolf, W., Jr, A. M. J., & Botta, W. J. (2012). The formation of quasicrystal phase in Al-Cu-Fe system by mechanical alloying. *Materials Research*, 15, 749-752.

Tingvall, C., Stigson, H., Erikson, L., Johansson, R., Krafft, M., & Lie, A. (2010). The properties of Safety Performance Indicators in target setting, projections and safety design of the road transport system. *Accident Analysis and Prevention*, 42, 372-376.

Tadayyon, G., Zebarjad, S. M., & Sajjadi, S. A. (2011). Effect of Mechanical Milling on the Thermal Behavior of Polyethylene Reinforced with Nano-sized Alumina. *International Polymer Processing*, 27, 355-360.

Torres, C. D. S., & Schaeffer, L. (2010). Effect of High Energy Milling on the Microstruture and Properties of WC-Ni Composite. Materials Research, 13(3), 293-298.

Torres, Y., Rodriguez, J. A., Arias, S., Echeverry, M., Robledo, S., Amigo, V., & Pavon, J. J. (2012). Processing, characterization and biological testing of porous titanium obtained by space-holder technique. Journal of Materials Science, 47(18), 6565-6576.

Torres, Y., Pavon, J. J., & Rodriguez, J. A. (2012). Processing and characterization of porous titanium for implants by using NaCl as space holder. *Journal of Materials Processing Technology*, 212, 1061-1069.

Uzun, A., & Turker, M. (2014). The Effect of Production Parameters on the Foaming Behavior of Spherical-shaped Aluminum Foam. *Materials Research*, 17(2), 311-315.

Umashankar, C., Jha, K., & Mahule, K. N. (2011). Aluminium Foam Fabrication by Powder Metallurgy Route. *Barcs New Letter.*, 332, 39-43.

Upadhyaya, G. S. (2002). Powder metallurgy technology. England: Cambridge Int Science Publishing.

Unal, R., & Dean, E. B. (1991, May 21-24). *Taguchi approach to design optimization for quality and cost: an overview*. Paper Presented at the Proceedings of the International Society of Parametric Analyst 13th Annual.

Verma, R. K., Mahesh N. S., & Anwar M. I. (2012). Numerical Analysis of Powder Compaction to Obtain High Relative Density in ‘601AB' Aluminum Powder. *SASTech-Technical Journal*, 11(1), 79-84.

Vilcekova, Z., Kasiarova, M., Domanicka, M., Hnatko, M., & Sajgalik, P. (2013). Influence of the Preparation of Si_3N_4 Based Foams on the Compressive Strength and Processing Flaws. *Powder Metallurgy Progress*, 13(3-4), 139-146.

Wang, B., & Zhang, E. (2008). On the compressive behavior of sintered porous coppers with low-to-medium porosities—Part II: Preparation and microstructure. International Journal of Mechanical Sciences, 50, 550-558.

Wang, X., Wu, J., Zhang, H., Zhang, Y., & Li, J. (2012). Effect of Copper Content on the Thermal Conductivity and Thermal Expansion of Al–Cu/Diamond Composites. *Materials and Design*, 39(2012), 87-92.

Wang, B. & Zhang, E. (2005). On The Compressive Behaviour of Sintered Porous Coppers with Low to Medium Porosities-Part I: Experimental Study. *International Journal of Mechanical Sciences*, 50, 550–558.

Wen C. E., Yamada Y., Shimojima K., Chino Y., Hosokawa, H., & Mabuchi, M. (2004). Compressability of Porous Magnesium Foam: Dependency on Porosity and Pore Size. *Materials Letters*, 58(3), 357-360.

Wen, C. E., Mabuchi, M., Yamada, Y., Shimojima, K., Chino, Y., & Asahina, T. (2001). Processing of Biocompatible Porous Ti and Mg. *Scripta Materialia*, 45, 1147-1153.

Wisutmethangoon, S., Nu-Young, P., Sikong, L., & Plookphol. T. (2008). Synthesis and characterization of porous titanium. *Songklanakarin Journal of Science and Technology*, 30(4), 509-514.

Wu, C. Y., Ruddy, O. M., Bentham, A. C., Hancock,B. C., Best, S. M., & Elliott, J. A. (2005). Modelling the Mechanical Behaviour of Pharmaceutical Powders during Compaction. *Powder Technology*, 152 (1), 107-117.

Weise, J., Salk, N., Jehring, U., Baumeister, J., Lehmhus, D., &. Bayoumi, M. A. (2013). Influence of Powder Size on Production Parameters and Properties of Syntactic Invar Foams Produced by Means of Metal Powder Injection Moulding. *Advanced Engineering Materials*, 15(3), 118-122.

Wysk, R. A., Niebel, B. W., Cohen, P. H., and Simpson, T. W. (2000). *Manufacturing Processes: Integrated Product and Process Design*. New York: McGraw Hill.

Wang, S., Wang, Q. H., Yang, X. L., Wang, L. Y., & Zhu, H. S. (2003). Properties of Silk Fibroin/Poly(ethylene glycol) 400 Blend Films. *Chinese Journal of Polymer Science*, 21(1), 87-91.

Wagih, A. (2014). Effect of milling time on morphology and microstructure of Al-Mg/Al_2O_3 nanocomposite powder produced by mechanical alloying. *International Journal of Advances in Engineering Sciences*, 4(2), 1-7.

Xiong, W., Yao, Z., Yuan, M., & Peng, Q. (2010). Effects of mechanical alloying on characteristics of nanocrystalline Fe–Cr–W–Ti–Y_2O_3 powders. *Journal of Nuclear Materials*, 403,198–203.

Xie, Z. K., Yamada, Y., & Banno, T. (2006). Mechanical Properties of Microporous Aluminum Fabricated by Powder Metallurgy. Japanese Journal of Applied Physics, 45(32), 864-865.

Yusoff, Z., & Jamaludin, S. B. (2011). The Influence of Particle Sizes and Compaction Pressure on Surface Hardness of Aluminum Composite Fabricated Via Powder Metallurgy. *Australian Journal of Basic and Applied Sciences*, 5(11), 133-140.

Yu, H., Guo, Z., Li, B., Yao, G., Luo, H., & Liu, Y. (2007). Research into the effect of cell diameter of aluminum foam on its compressive and energy absorption properties. *Material Science Engineering Part A*, 454–455, 542–546.

Yu, S., Liu, J., Luo, Y., & Liu, Y. (2007). Compressive behavior and damping property of ZA22/SiCp composite foams. Materials Science Engineering Part A, 457, 325-328.

Zhao, Y. Y., Fung, T., Zhang, L. P., & Zhang, F. L. (2005). Lost carbonate sintering process for manufacturing metal foams. Scripta Materialia, 52, 295–298.

Zhang, J., Zhao, G.-P., Lu, T.-J., & He, S.-Y. (2015). Strain rate behavior of closed-cell Al-Si-Ti foams: Experiment and numerical modeling. *Mechanics of Advanced Materials and Structures*, 22, 556–563.

Zhang, D. L., & Ying, D. Y. (2000). Solid-state reactions between Cu and Al during mechanical alloying and heat treatment. *Journal of Alloys and Compounds*, 311, 275-282.

Zi-li, L., Xi-qin, L., Ping, S., Xiu-rong, Z., Liang, M. (2010). Effect of ball-milling parameter on mechanical and damping properties of sintered Mg-Zr alloy. *Transactions of Nonferrous Metals Society of China*, 20, 2092-2095.

Zhang, S., Lu, L., & Lai, M. O. (1993). Cu-based shape memory powder preparation using the mechanical alloying technique. *Materials Science and Engineering A*, 171, 257-262.

Zuyan, L., Guoxian, L., & Erde, W. (1996). Effect of Milling Intensity on Structural Changes of Mixed Al-Fe-Ni Powders in Mechanical Alloying Process. *Transactions Nonferrous Metals Society of China*, 6(3), 143-149.

Zhang, Y. F., Lu, L., & Yap, S. M. (1999). Prediction of the Amount of PCA for Mechanical Alloying. *Journal of Materials Processing Technology*, 89-90, 260-265.

Zhang, J., Wu, L., Jing, D., & Ding, J. (2005). A Comparative Study of Porous Scaffolds With Cubic and Spherical Macropores. *Polymer*, 46, 4979–4985.

Zhao, Y.Y., Tao, X.F., & Xue, X.B. (2008) Manufacture and Mechanical Properties of Metal Matrix Syntactic Foams. In: Materials Science and Technology 2008, Pittsburgh.

Zhao, X., Sun, H., Lan, L., Huang, J., Zhang, H., & Wang, Y. (2009). Pore Structures of High-Porosity NiTi Alloys Made From Elemental Powders With NaCl Temporary Space-Holders. *Materials Letters*, 63, 2402–2404.

Zhao, Y., Han, F., & Fung, T. (2004). Optimisation of compaction and liquid-state sintering in sintering and dissolution process for manufacturing Al foams. *Materials Science and Engineering A*, 364, 117–125.

Zhao, Y., & Monaghan, L. E. (2008, June 8-June 12). *A Novel Manufacturing Method for Titanium Foam for Biomedical Applications*. Paper presented at 2008 World Congress on Powder Metallurgy and Particulate Materials, Washington, United States of America.

LIST OF APPENDICES

APPENDIX A - LIST OF PUBLICATIONS

1) Jamal, N. A., Tan, A. W., Yusof, F., Katsuyoshi, K., Hisashi, I., S. Singh & Anuar, H. (2016). Fabrication and Compressive Properties of Low to Medium Porosity Closed-Cell Porous Aluminum Using PMMA Space Holder Technique. *Materials*, 9, 1-13. (ISI Cited Paper)

2) Jamal, N. A., Farazila, Y., Ramesh, S., & H. Anuar.Role of mechanical alloying parameters on powder distribution of Al/Cu alloy and Al/Cu composite. *Materials Research Innovations*, 18, 1-4. (ISI Cited Paper)

APPENDIX B - LIST OF PAPERS PRESENTED

1) Jamal, N. A., Farazila, Y., Ramesh, S., & H. Anuar. (2014, November). *Preliminary study on development of porous aluminum*. Paper presented at the AUN-SEED/NET-Regional Conference on Materials Engineering, Kuala Lumpur.

2) Jamal, N. A., Farazila, Y., Ramesh, S., & H. Anuar. (2013, November). *Role of mechanical alloying parameters on powder distribution of Al/Cu alloy and Al/Cu composite*. Paper presented at the International Conference on the Science and Engineering of Materials (ICOSEM), Kuala Lumpur.